

PREDICTION OF FLOW DEPTH AND SEDIMENT DISCHARGE

IN OPEN CHANNELS

by

William R. Brownlie

Project Supervisor:

Norman H. Brooks
James Irvine Professor of
Environmental and Civil Engineering

Supported by

National Science Foundation
Grant Numbers ENG-77-10182 and CME 79-20311

W. M. Keck Laboratory of Hydraulics and Water Resources
Division of Engineering and Applied Science
California Institute of Technology
Pasadena, California

Report No. KH-R-43A

November 1981

ACKNOWLEDGEMENTS

A number of people have provided encouragement and assistance without which this work would not have been possible.

Special thanks to my advisor, Professor Norman H. Brooks, who believed in this project from the start and provided valuable advice and assistance throughout this project.

I would also like to thank Dr. Robert C. Y. Koh and Professor Vito A. Vanoni for all the assistance they have provided. It was a great joy to be able to call on Dr. Vanoni's vast experience in the field of sediment transport whenever I needed it. Also, without Dr. Koh's computer programs for statistical analysis and plotting, and his advice, this work would have been much more difficult.

A special thank you to Melinda Hendrix-Werts who typed most of the awful equations and to Joan Mathews who assisted. Thank you to Rayma Harrison and Gunilla Hastrup, in the library, who helped me locate many unusual references. Also thanks to Theresa Fall and Phil Dube for their assistance with the drafting of figures.

I also thank my loving wife Debbie who provided support when I needed it and assistance (particularly in assembling this report) whenever I asked.

This research was supported by the National Science Foundation Grant Numbers ENG-77-10182 and CME 79-20311.

PREFACE

In recent years, attempts have been made to develop numerical models for unsteady flows in channels with sediment transport. The work presented in Reports KH-R-43A and KH-R-43B was conducted to analyze two essential ingredients of any numerical model: the relationship between the hydraulic variables (slope, depth, and velocity), and the predictor of sediment concentration.

Report KH-R-43A presents a detailed analysis of the two components and examines their role in numerical modeling. Six hydraulic relationships and 13 sediment concentration predictors are examined and compared. New relationships are then developed which appear to be more accurate than the existing techniques. Finally, the new relationships are utilized in a numerical unsteady flow, moveable bed model which uses a four-point implicit finite difference solution scheme.

The data base utilized in the first report is presented in Report KH-R-438. The data base contains 7,027 records (5,263 laboratory records and 1,764 field records), in 77 data files. Not all records were used in the final analyses, but they have been included in an attempt to provide a historically complete set of alluvial channel observations.

The material presented in these reports is essentially the same as the thesis submitted by the author in partial fulfillment of the requirements for the degree of Doctor of Philosophy. A common list of references, with data sources separated from other references, has been included in both reports.

CONTENTS

<u>Chapter</u>	<u>Page</u>
1 INTRODUCTION	1
2 DEVELOPMENT OF A DATA BASE	7
3 REVIEW OF METHODS FOR CALCULATING FLOW DEPTH IN SAND-BED CHANNELS	12
3.1 Statement of Purpose	12
3.2 General Form of Velocity Equations	14
3.3 Fixed-Bed Friction Factors	15
3.4 Existing Stage Discharge Predictors	19
3.4.1 Alam, Cheyer, and Kennedy Analysis (1965)	21
3.4.2 Chu and Mostafa Analysis (1979)	23
3.4.3 Einstein and Barbarossa Analysis (1952)	27
3.4.4 Engelund Analysis (1967)	28
3.4.5 Garde and Ranga Raju Analysis (1970)	36
3.4.6 White, Paris, and Bettess Analysis (1979)	39
3.5 Summary	43
4 A PROPOSED METHOD FOR CALCULATING FLOW DEPTH IN SAND-BED CHANNELS	44
4.1 Dimensional Analysis	44
4.2 Formulation of a Pair of Equations	45
4.3 Determination of Flow Regime	55
4.4 Verification of Proposed Method	60
4.5 Comparison of Stage-Discharge Predictors	67
4.6 Summary and Conclusions	70
5 AN ANALYSIS OF METHODS FOR PREDICTING SEDIMENT CONCENTRATION	73
5.1 Selection of Available Techniques	73
5.2 Method of Analysis	76
5.3 Appraisal of Existing Techniques	84
5.3.1 Ackers and White Technique (1973)	85
5.3.2 Bagnold Technique (1966)	91
5.3.3 Bishop, Simons, and Richardson Technique (1965)	96

<u>Chapter</u>	<u>Page</u>
5.3.4 Einstein Technique (1950)	101
5.3.5 Engelund and Fredsoe Technique (1976)	106
5.3.6 Engelund and Hansen Technique (1967)	112
5.3.7 Graf Technique (1968)	117
5.3.8 Laursen Technique (1958)	122
5.3.9 Ranga Raju, Garde, and Bhardwaj Technique (1981)	127
5.3.10 Rottner Technique (1959)	133
5.3.11 Shen and Hung Technique (1971)	138
5.3.12 Toffaleti Technique (1968)	143
5.3.13 Yang Technique (1973)	148
5.4 Discussion	153
6 A NEW MEIHD FOR PREDICTING SEDIMENT CONCENTRATION	155
6.1 Expected Scatter in Sediment Concentration	155
6.2 Width and Depth Effects	157
6.3 Critical Velocity	159
6.4 Dimensional Analysis	163
6.5 Effects of a Nonrectangular Cross-Section	166
6.6 Comparison with Existing Methods	186
6.7 Summary	190
7 RECOMMENDATIONS FOR NUMERICAL MODEL DEVELOPMENT	192
7.1 Solutions to the Differential Equations	192
7.2 Recommendations for Future Work	204
7.3 Discussion	206
8 SUMMARY	208
8.1 Summary	208
8.2 List of Conclusions	210
LIST OF REFERENCES	213
Data Sources	217
LIST OF SYMBOLS	224
APPENDIX - Re-Examination of Nikuradse Roughness Data	228

LIST OF FIGURES

<u>Figure</u>		<u>Page</u>
1.1	Definition sketch for equations of motion.	3
3.1	Limits of smooth and fully rough flow, and initiation of motion from the Shields diagram in Vanoni (1975) .	17
3.2	Comparison of semilogarithmic and power law resistance equations.	18
3.3	Replot of Alam, Cheyer and Kennedy (1966) diagram for determining f'' .	22
3.4	Replot of Chu and Mostafa (1979) diagram for determining the dimensionless Manning coefficient, C_M .	26
3.5	Replot of Einstein and Barbarossa (1952) diagram for determining f'' .	29
3.6	Replot of Engelund (1967) diagram for determining τ_* .	32
3.7	Comparison of Engelund technique with data of: a) Guy et al. (1966), b) Mississippi R., Tarbert Landing, La. (Toffaletti, 1968), c) Williams (1970).	33
3.8	Replot of Ranga Raju (1970) diagram for determining densimetric Froude number, F_R .	37
3.9	Comparison of White et al. (1979) technique with laboratory data of Guy et al. (1966).	42
4.1	Relationship between dimensionless shear stress, τ_{*S} , and q_* and S, for lower flow regime (dune and ripple bed forms).	48
4.2	Relationship between τ_{*S} and q_* and S for upper flow regime (flat bed, antidunes, standing waves) and flat beds prior to initiation of motion.	50
4.3	Comparison of flow regimes -- solid lines represent best fit lines of data reduced to two variables by means of the lower regime values of the exponents x, y and z, dashed lines represent one standard deviation error bars.	54
4.4	Determination of flow regimes -- grain Froude number, F_g , plotted against slope, S.	57

<u>Figure</u>	<u>Page</u>	
4.5	Viscous effects on the transition from lower flow regime to upper flow regime.	58
4.6	Replot of Fig. 4.5, defining the viscous effects in terms of the desired independent variables.	61
4.7	Rating curves determined by the new technique, from average bed slope and average D_{50} and σ_g , from data plots of Dawdy (1961) for: a) Middle Loup River at St. Paul, Nebraska, b) Republican River at Stratton, Nebraska, c) Rio Grande near Bernalillo, New Mexico, and d) Pigeon Roost Creek near Byhalia, Mississippi.	62
4.8	Comparison of predicted vs. actual mean depth in the Sacramento River at Butte City, data given by Nakato (1981).	68
5.1	Typical error distributions for the Yang (1973) technique.	82
5.2a	Ratio of concentration calculated by the Ackers and White (1973) technique to observed concentration as a function of observed concentration, for laboratory data.	87
5.2b	Ratio of concentration calculated by the Ackers and White (1973) technique to observed concentration as a function of observed concentration, for field data,	89
5.3a	Ratio of concentration calculated by the Bagnold (1966) technique to observed concentration as a function of observed concentration, for laboratory data.	92
5.3b	Ratio of concentration calculated by the Bagnold (1966) technique to observed concentration as a function of observed concentration, for field data.	94
5.4a	Ratio of concentration calculated by the Bishop, Simons, and Richardson (1965) technique to observed concentration as a function of observed concentration, for laboratory data.	97
5.4b	Ratio of concentration calculated by the Bishop, Simons, and Richardson (1965) technique to observed concentration as a function of observed concentration, for field data.	99
5.5a	Ratio of concentration calculated by the Einstein (1950) technique to observed concentration as a function of observed concentration, for laboratory data.	102

<u>Figure</u>		<u>Page</u>
5.5b	Ratio of concentration calculated by the Einstein (1950) technique to observed concentration as a function of observed concentration, for field data.	104
5.6a	Ratio of concentration calculated by the Engelund and Fredsoe (1976) technique to observed concentration as a function of observed concentration, for laboratory data.	108
5.6b	Ratio of concentration calculated by the Engelund and Fredsoe (1976) technique to observed concentration as a function of observed concentration, for field data.	110
5.7a	Ratio of concentration calculated by the Engelund and Hansen (1967) technique to observed concentration as a function of observed concentration, for laboratory data.	113
5.7b	Ratio of concentration calculated by the Engelund and Hansen (1967) technique to observed concentration as a function of observed concentration, for field data.	115
5.8a	Ratio of concentration calculated by the Graf (1968) technique to observed concentration as a function of observed concentration, for laboratory data.	118
5.8b	Ratio of concentration calculated by the Graf (1968) technique to observed concentration as a function of observed concentration, for field data.	120
5.9a	Ratio of concentration calculated by the Laursen (1958) technique to observed concentration as a function of observed concentration, for laboratory data.	123
5.9b	Ratio of concentration calculated by the Laursen (1958) technique to observed concentration as a function of observed concentration, for field data.	125
5.10a	Ratio of concentration calculated by the Ranga Raju, Garde, and Bhardwaj (1981) technique to observed concentration as a function of observed concentration, for laboratory data.	129
5.10b	Ratio of concentration calculated by the Ranga Raju, Garde, and Bhardwaj (1981) technique to observed concentration as a function of observed concentration, for field data.	131
5.11a	Ratio of concentration calculated by the Rottner (1959) technique to observed concentration as a function of observed concentration, for laboratory data.	134

<u>Figure</u>	<u>Page</u>
5.11b	Ratio of concentration calculated by the Rottner (1959) technique to observed concentration as a function of observed concentration, for field data. 136
5.12a	Ratio of concentration calculated by the Shen and Hung (1971) technique to observed concentration as a function of observed concentration, for laboratory data. 139
5.12b	Ratio of concentration calculated by the Shen and Hung (1971) technique to observed concentration as a function of observed concentration, for field data. 141
5.13a	Ratio of concentration calculated by the Toffaleti (1968) technique to observed concentration as a function of observed concentration, for laboratory data. 144
5.13b	Ratio of concentration calculated by the Toffaleti (1968) technique to observed concentration as a function of observed concentration, for field data. 146
5.14a	Ratio of concentration calculated by the Yang (1973) technique to observed concentration as a function of observed concentration, for laboratory data. 149
5.14b	Ratio of concentration calculated by the Yang (1973) technique to observed concentration as a function of observed concentration, for field data. 151
6.1	Velocity, depth, and bed-material sediment concentration fluctuations, plotted as fraction of the respective mean values, for the ten highest discharge observations, Atchafalaya River, 1961 to 1965. 156
6.2	Williams (1970) data showing the effects of low values of w/d and d/D_{50} on sediment concentration. 160
6.3	Revised Shields curve, data from Vanoni (1965). 162
6.4	Laboratory sediment concentration as observed and as predicted by Eq. 6.9, as a function of $S^{1/3}F_g$. 167
6.5	Field sediment concentration as observed and as predicted by Eq. 6.9, as a function of $S^{1/3}F_g$. 174
6.6a	Ratio of concentration calculated from Eq. 6.8 or Eq. 6.9 technique to observed concentration as a function of observed concentration, for laboratory data. 180
6.6b	Ratio of concentration calculated from Eq. 6.8 or Eq. 6.9 technique to observed concentration as a function of observed concentration, for field data. 181

<u>Figure</u>		<u>Page</u>
6.7	Idealized nonrectangular channel,	183
6.8	Ratio of cross-sectionally integrated concentration calculated from mean depth, as a function of the value of exponent B in Eq. 6.14.	187
6.9	Comparison of methods for predicting sediment concentration.	189
7.1	Definition sketch for four-point implicit finite difference scheme.	194
7.2	Water surface profiles for model test reach for: (a) $t = 0$ to 60 minutes, and (b) $t = 60$ to 120 minutes.	200
7.3	Attenuation of inflow hydrograph; hydrographs shown at a one kilometer interval.	201
7.4	Sediment concentrations along model test reach for: (a) $t = 0$ to 60 minutes, and (b) $t = 60$ to 120 minutes.	202
7.5	Sediment concentration rating curves.	203

LIST OF TABLES

<u>Table</u>		<u>Page</u>
4.1	Error analysis of new method of predicting flow depth for laboratory and field data.	51
4.2	Range of data used in analysis.	52
4.3	Compilation of Stage-Discharge Predictors.	69
5.1	Methods of predicting sediment concentration analyzed in this report,	77
5.2a	Range of lab data used in the analyses of concentration predictors.	78
5.2b	Range of field data used in the analyses of concentration predictors,	79
5.3	Restrictions on input data,	80
5.4a	Ratio of predicted to observed concentration for Ackers and White (1973) method, for laboratory data.	88
5.4b	Ratio of predicted to observed concentration for Ackers and White (1973) method, for field data,	90
5.5a	Ratio of predicted to observed concentration for Bagnold (1966) method, for laboratory data.	93
5.5b	Ratio of predicted to observed concentration for Bagnold (1966) method, for field data.	95
5.6a	Ratio of predicted to observed concentration for Bishop, Simons, and Richardson (1965) method, for lab data.	98
5.6b	Ratio of predicted to observed concentration for Bishop, Simons, and Richardson (1965) method, for field data.	100
5.7a	Ratio of predicted to observed concentration for Einstein (1950) method, for laboratory data.	103
5.7b	Ratio of predicted to observed concentration for Einstein (1950) method, for field data.	105
5.8a	Ratio of predicted to observed concentration for Engelund and Fredsoe (1976) method, for laboratory data.	109

<u>Table</u>		<u>Page</u>
5.8b	Ratio of predicted to observed concentration for Engelund and Fredsoe (1976) method, for field data.	111
5.9a	Ratio of predicted to observed concentration for Engelund and Hansen (1967) method, for laboratory data.	114
5.9b	Ratio of predicted to observed concentration for Engelund and Hansen (1967) method, for field data.	116
5.10a	Ratio of predicted to observed concentration for Graf (1968) method, for laboratory data.	119
5.10b	Ratio of predicted to observed concentration for Graf (1968) method, for field data.	121
5.11a	Ratio of predicted to observed concentration for Laursen (1958) method, for laboratory data.	124
5.11b	Ratio of predicted to observed concentration for Laursen (1958) method, for field data.	126
5.12a	Ratio of predicted to observed concentration for Ranga Raju, Garde, and Bhardwaj (1981) method, for lab data.	130
5.12b	Ratio of predicted to observed concentration for Ranga Raju, Garde, and Bhardwaj (1981) method, for field data.	132
5.13a	Ratio of predicted to observed concentration for Rottner (1959) method, for laboratory data.	135
5.13b	Ratio of predicted to observed concentration for Rottner (1959) method, for field data.	137
5.14a	Ratio of predicted to observed concentration for Shen and Hung (1971) method, for laboratory data.	140
5.14b	Ratio of predicted to observed concentration for Shen and Hung (1971) method, for field data.	142
5.15a	Ratio of predicted to observed concentration for Toffaleti (1968) method, for laboratory data.	145
5.15b	Ratio of predicted to observed concentration for Toffaleti (1968) method, for field data.	147
5.16a	Ratio of predicted to observed concentration for Yang (1973) method, for laboratory data.	150
5.16b	Ratio of predicted to observed concentration for Yang (1973) method, for field data.	152

<u>Table</u>		<u>Page</u>
6.1	Atchafalaya River at Simmesport, Louisiana: top ten observations ranked by discharge, 1961 through 1965.	158
6.2	Ratio of predicted to observed concentration for the proposed new method for lab data.	178
6.3	Ratio of predicted to observed concentration for the proposed new method for field data.	179
6.4	Geometric mean and geometric standard deviation of the ratio of predicted to observed concentration for all methods, for laboratory and field conditions.	188
7.1	Rearrangement of flow depth predictors, Equation 4.10a and Equation 4.10b.	196

CHAPTER 1

INTRODUCTION

In the design and analysis of channels, one is often faced with the problem of determining the depth of flow and sediment concentration which occur in a channel with given bed slope, water discharge, and bed-material properties. The most fundamental problem can be stated as: given steady uniform flow, what depth and concentration can be expected? A more complex question is: given a nonsteady inflow discharge and concentration, what will be the time history of depth and concentration along the channel? This latter question requires solution of a set of differential equations which will include the possibility of scour and deposition along the channel. This report primarily focuses on the former question, but with a view toward ultimate solution of the latter, Only sand-bed channels are considered.

1.1 Differential Equations

The problem of modeling scour and deposition in unsteady nonuniform flows in a wide straight channel with a sand bed can be reduced to solving three partial differential equations with two constitutive relations, for a total of five unknowns. The equations can be written in different forms with different sets of unknowns. One possible set of unknown quantities consists of the mean flow velocity (u), the flow

depth (h), the **mean** sediment concentration (C), the friction slope (S), and the bed elevation (z) relative to some horizontal datum, which are all functions of the distance x along the channel and time t . The width is presently assumed to be constant and the flow and bed conditions uniform across the width. There are of course many field situations where this is not true, but this additional complexity will be set aside in this report.

The three conservation equations to be solved are (see Fig. 1.1), the momentum equation (Ponce et al., 1979)

$$\frac{\partial z}{\partial x} + \frac{\partial h}{\partial x} + \frac{u}{g} \frac{\partial u}{\partial x} - \frac{1}{g} \frac{\partial \psi}{\partial t} = -S \quad (1.1)$$

the continuity equation for water

$$\frac{\partial(hu)}{\partial x} + \frac{\partial h}{\partial t} = 0 \quad (1.2)$$

and, the continuity equation for sediment

$$(1 - \lambda) \frac{\rho_s}{\rho} \frac{\partial z}{\partial t} + \frac{\partial(Cuh)}{\partial x} + \frac{\partial(Ch)}{\partial t} = 0 \quad (1.3)$$

where λ = the porosity of bed sediment and ρ_s = mass density of sediment particles. Because there are five dependent variables, but only three equations so far, two more relations are needed for closure. These are the equation for the friction slope as a function of flow and sediment characteristics

$$S = \text{function of } (u, h, t, \dots) \quad (1.4)$$

and the sediment concentration relationship

$$C = \text{function of } (u, h, t, \dots) \quad (1.5)$$

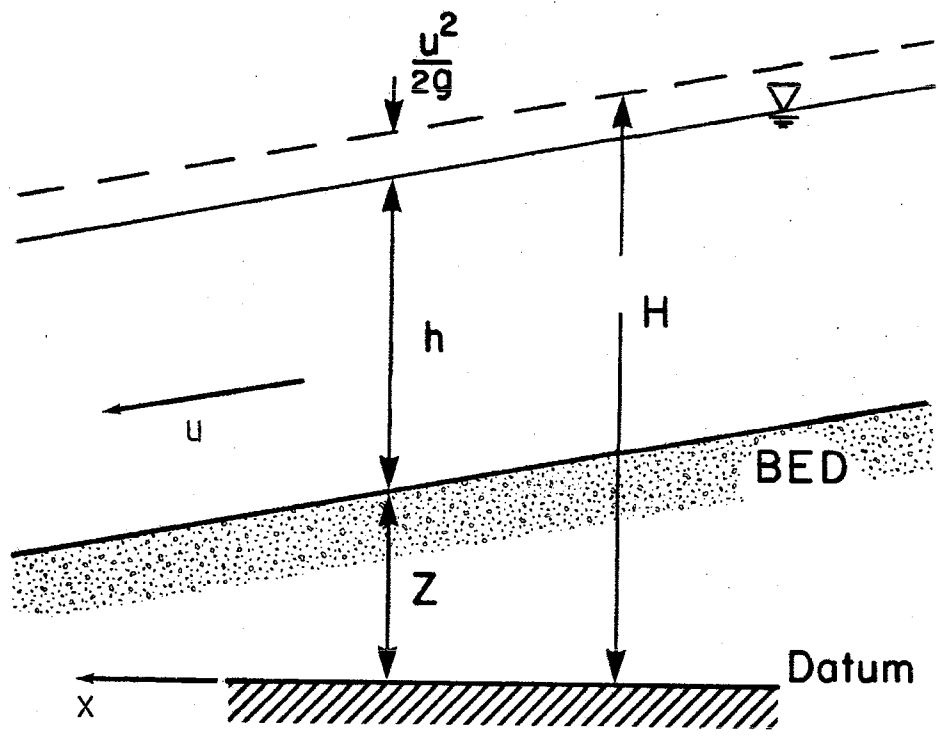


Figure 1.1 Definition sketch for equations of motion.

1.2 Previous Research

Probably the most widely used model for solving these equations is the Hydrologic Engineering Center (1976), HEC-6 model. The ingredients of the HEC-6 are generally considered the current state-of-the-art, although more recent work, such as that of Ponce et al. (1979) and Soni (1980) has brought about improvements which are not yet widely used in general engineering practice. The model of Chang (1976), for example, is founded on basically the same principles as the HEC-6 and shares some of the problems, although more recently improvements have been made on this model (Chang and Hill, 1981).

Since the HEC-6 represents a state-of-the-art model, it is worthwhile to discuss some problems that one might encounter for situations involving rapidly changing flows:

- (1) The "standard step method" (see e.g. Henderson, 1966) is used to solve for the hydraulic parameters. This technique is, strictly speaking, applicable only to steady nonuniform flow. The technique assumes that the $\partial u/\partial t$ and $\partial h/\partial t$ terms in Eqs. 1.1 and 1.2, respectively, are small and can be eliminated.
- (2) The hydraulic equations and the sediment equations are not coupled. For each step, first the hydraulic variables are solved, and then the sediment discharge and bed changes are calculated. Thus $\partial z/\partial x$ in Eq. 1.1 is taken as the initial value at the beginning of the time step.
- (3) The slope is defined by a Manning equation, and values of Manning n must be known or estimated at each cross-section.
- (4) The user is offered a choice of three sediment relationships (i.e. Eq. 1.5), but it is not clear what accuracy each provides, or why one should be selected over another.
- (5) Time is not included in any of the sediment transport relationships. Therefore, disregarding armoring, every flow

is assumed to be carrying the equilibrium concentration for a comparable steady, uniform flow, without any time lag for particle settling or resuspension or adjustment during transients or non-uniformities.

Despite its flaws, the HEC-6 model is very general in its capability of accepting complicated geometry and flow obstructions such as bridges. As such, it is tempting to apply it to a wide variety of channels and flow situations. It is the **writer's** belief that engineering models such as HEC-6 should be applied with great care to modeling applications involving rapidly varying flows, and that the results should be viewed with considerable skepticism.

1.3 Scope of Study

Having considered the problems involved in formulating a numerical model, we return to the problem of the formulation of the hydraulic and sediment concentration relationships. Solutions to the differential equations are meaningless without adequate formulations of these relationships. Rather than formulate these relationships as represented by Eqs. 1.4 and 1.5, a different approach will be taken, **which** will be more useful for steady uniform flow, and can be applied as an approximation for the unsteady case. For the uniform case, the assumption will be made that slope and unit discharge, $q = uh$, are known and one wishes to find depth and concentration.

In order to examine previous definitions of these relationships a large data base of both field and laboratory data was needed. The establishment of such a data base is discussed in Chapter 2. In Chapter

3 six existing formulations of the hydraulic relationship are analyzed to answer the question: can they be used to determine depth, given slope and unit discharge? The data base was then used to develop a new **formulation** of the hydraulic relationship, which is presented in Chapter 4. The data base was also used to examine existing definitions of Eq. 1.5 (Chapter 5) and to develop a new definition of this relationship (Chapter 6). Chapter 7 discusses solutions to the set of differential equations which utilize the new formulations, and presents recommendations for future work. A summary of the study and conclusions are presented in Chapter 8.

CHAPTER 2
DEVELOPMENT OF A DATA BASE

The analyses presented in this report required the establishment of the large data base of both laboratory and field data which is presented in Report KH-R-43B. The initial thought was that the data compendium of Peterson and Howells (1973) could be used to supply the required data. Unfortunately, in working with this data compendium, the writer discovered a significant number of errors. Furthermore, additional data were needed, particularly good field data.

Peterson and Howells (1973) are to be commended for taking the first step toward the development of a computerized data base. The task of locating data and reducing it to a common set of variables and units requires long hours of tedious work. The data collection of Peterson and Howells is essentially an update of the data collection of Johnson (1943). However, before any data set can be used with total satisfaction, all of the errors must be eliminated.

A careful, item-by-item check suggests that four types of errors were made in the preparation of the Peterson and Howells (1973) compendium:

- (1) Incorrect individual entries -- these entries usually have incorrectly ordered digits or misplaced decimal points.
- (2) Conversion errors -- errors made in converting the data to a standard format, typically involving conversion of transport rates to sediment concentrations.

- (3) Misinterpretation of data -- this error usually involved whole columns of data, and probably occurred as a result of confusing notation in the data source.
- (4) Source errors -- errors originating from incorrect original publication of data, discovered by checks on internal consistency.

Also encountered were omissions of entries such as bed form and the gradation parameter (geometric standard deviation of bed particle size), which could be determined from the original data sources, even though they were not explicitly stated.

The following is a description of some of the apparent errors that were encountered. In the data of Sato, Kikkawa, and Ashida (1958) the grain size given in centimeters was read as millimeters. Therefore the values of the median sediment size given by Peterson and Howells must all be multiplied by 10 to obtain the correct values for this data set. The Straub (1954, 1958) data set contains 3 concentration values which are a factor of 10 too high. For the data sets of Abdel-Aal and of Kalkanis (Abdel-Aal, 1969), and Vanoni and Hwang (1967), the values given for discharge are really flow velocity, and the slope and depth entries are interchanged. An incorrect interpretation of the transport rate of the Williams (1970) data as being given in dry unit weight per time instead of submerged weight resulted in an error of about 60 percent in the sediment concentration readings. The transport rate for the Indian Canal data (Chaudhry, Smith, and Vigil, 1970), given in metric tons, was read as English short tons, causing a 12 percent error in sediment concentration.

In the development of a new data base from the Peterson and Howells (1973) compendium, a few sets of data were omitted, while many others were added. The sets were omitted either because the data were not applicable (one set of data was for transport of sludge), or because important variables were unavailable (one set contained no slope measurements). The sets that were added included newer data (e.g. Willis, 1979) and a large quantity of field data, such as the Colorado River data (U.S. Bureau of Reclamation, 1958) and the Rio Grande (Nordin and Beverage, 1965) data.

At this point it is worthwhile to define a few terms related to sediment transport, as used in this report.

Sediment concentration is the ratio of the sediment discharge to the discharge of the water-sediment mixture, both expressed in terms of mass per unit time, usually given as parts per million (ppm). For practical reasons, the density of the water-sediment mixture is taken to be approximately equivalent to the density of the water. This approximation will cause errors of less than one percent for concentrations less than 16,000 ppm. In this thesis, the concentration is used as a depth- and time-averaged (i.e. mean) value, unless specified otherwise.

Sediment load or total sediment load is the material being transported. The sediment load can be divided into wash load and bed-material load. The wash load is the fine material of sizes which are not found in appreciable quantities on the bed, and is not considered to be dependent on the local hydraulics of the flow, As a

practical definition, the wash load is considered to be the fraction of the sediment load finer than 0,062 mm. The bed-material load is the material of sizes which are found in appreciable quantities on the bed. The bed-material load can be conceptually divided into the bed load (that portion of the load that moves near the bed) and the suspended load (that portion of the load that moves in suspension), although the division is not precise,

Sediment transport rate is equivalent to the sediment discharge, which is expressed as mass per unit time,

The concentrations given in the data set and predicted by the transport formulas are for the bed-material load, including both bed load and suspended load. From this point onward the term concentration will refer to the bed-material-load concentration. Under field conditions this quantity is very difficult to measure; often the bed load portion is left unmeasured and must be estimated. In some cases, such as for some of the data of Mahmood et al. (1979), the estimated portion of the load may represent 80 percent of the concentration. In the case of the NEDECO (1973) data, the sampling procedure included material as fine as 0.05 mm, instead of the usual cutoff of 0.062 mm. Neither of these data sets was used in the analyses of sediment transport formulas.

Ten variables, including bed form codes, are given for each observation. Bed form classifications are as given by Vanoni (1975, p. 160). Actual flume measurements, without adjustment for sidewall roughness, are given in the tables. (Sidewall corrections for

laboratory data have been used in the analyses that follow.)

While great care has been taken to reduce all data sets to common variables, in some cases it **was** not possible to achieve complete consistency between data sets. Space limitations do not permit a detailed account of all of the procedures and assumptions that were used to reduce each data set to common terms. Potential users of the data base are urged to consult the original sources of the data.

The data tabulations and description of the entries are given in Report KH-R-43B. The references for the data have been compiled separately from the literature references.

CHAPTER 3

REVIEW OF METHODS FOR CALCULATING FLOW DEPTH IN SAND-BED CHANNELS

The problem of determining the velocity and depth of flow for a given discharge of a river has long been a subject of interest to hydraulic engineers, and more recently to numerical modelers. A numerical model requires a logical scheme, whereby stage and velocity can be predicted for a channel of given dimensions, bed material, bed slope, discharge, and water temperature. For certain ranges of these parameters, multiple values of sediment discharge and flow depth may be possible, as discussed by Kennedy and Brooks (1965). However, the engineer is often faced with the problem of designing a channel to accommodate a given discharge with a given bed slope and an unknown sediment discharge. Therefore, this chapter considers the problem where sediment discharge is assumed to be unknown, and explores possible solutions for uniform flow depth as a function of discharge, bed slope, and bed-sediment and fluid properties. Later, the development of a model will require adaptation of such a relationship for unsteady, nonuniform flows.

3.1 Statement of Purpose

A technique is sought, whereby an engineer can directly calculate the uniform or normal flow depth of a channel with a given unit

discharge, and which can also be used in a numerical model for unsteady, nonuniform flows. Such a technique should:

1. Agree with experiences gained in both the laboratory and the field;
2. Include confidence limits or some statistical analysis of the input data to indicate expected errors;
3. Be easily adaptable to computer modeling applications which may require thousands or millions of depth of flow calculations;
4. Provide solutions for a wide range of independent variables.

Six techniques for predicting friction factor (which relates velocity to shear velocity) are examined for their usefulness as stage predictors in a moveable-bed river model. Each technique has been rearranged so that given unit discharge and slope, along with other independent variables, one can directly determine flow depth. The six schemes are those of Alam, Cheyer and Kennedy (1966); Chu and Mostafa (1979); Einstein and Barbarossa (1952); Engelund (1967); Garde and Ranga Raju (1977); and White, Paris and Bettess (1979). Although each technique has provided an important contribution to the field, none satisfies all of the criteria listed above. Therefore, a new technique is presented which does satisfy the four criteria.

The reader is referred to the report of the ASCE Task Force (1963) for an excellent historical review of the problem of predicting friction factors in open channels. Reviews of many friction factor predictors can be found in Vanoni (1975), Garde and Ranga Raju (1977), and Jansen, et al. (1979). It will be assumed that the the reader has some familiarity with these techniques.

3.2 General Form of Velocity Equations

Strickler (1923) listed 22 velocity formulas for open channels, whereby, as of 1914, stage could be predicted. Most of these equations are power laws relating mean flow velocity to different powers of hydraulic radius and hydraulic slope. Two formulas remain in wide useage today, the one attributed to Manning, $v = r^{2/3} S^{1/2} / n$ (metric units), and the Chezy equation, $v = C\sqrt{rS}$, where v is mean velocity, r is hydraulic radius, S is the slope of the hydraulic grade line, and n and C are known as the "Manning" and "Chezy" coefficients, respectively. Both of these empirical equations have dimensional coefficients which must be estimated for a given application.

A more modern formulation is based on dimensional analysis and the concept that the mean shear stress, $\tau = \rho g r S$, in which ρ is the density of the fluid, and g is gravitational acceleration, is proportional to $\frac{1}{2}\rho v^2$. This gives the Darcy-Weisbach equation:

$$v = \sqrt{\frac{8}{f}} \sqrt{g r S} = \sqrt{\frac{8}{f}} u_* \quad (3.1)$$

where u_* is known as the shear velocity. This equation is conceptually sound, and f is dimensionless.

A dimensionally consistent Manning-type equation can be created by defining friction factor in the following manner:

$$\frac{v}{u_*} = \sqrt{\frac{8}{f}} = a \left(\frac{r}{k_s} \right)^{1/6} \quad (3.2)$$

where a is a coefficient of proportionality and k_s is a measure of bed

roughness. If Eq. 3.2 holds, then Manning's n (metric units) can be defined by

$$n = \frac{k_s^{1/6}}{a\sqrt{g}} \quad (3.3)$$

After comparing the Manning and Darcy-Weisbach equations, the ASCE Task Force (1963) concluded that:

"At the present (1961) state of knowledge, if applied with judgement, both n and f are probably equally effective in the solution of practical problems."

This comment suggests that Eq. 3.2 may form a reasonable definition of friction factor, in many practical situations.

3.3 Fixed-Bed Friction Factors

Friction factors for turbulent flow in fixed-bed channels have their roots in the classic sand-roughened pipe experiments conducted by Nikuradse (1933). The fixed-bed concept may be generalized to include some rivers with gravel beds, which, although not strictly fixed, do not form dunes or bars in the manner of sand bed streams. The ASCE Task Force (1963) has reviewed this topic in some detail, and only a brief discussion, pertinent to the later derivations, is given here.

For high bed Reynolds numbers ($u_* k_s / \nu$), the data of Nikuradse, based on experiments with sand-roughened pipes give

$$\frac{1}{\sqrt{f}} = 2 \log \frac{2r}{k_s} + 1.74 = 2 \log \frac{14.8r}{k_s} \quad (3.4)$$

Here, pipe flow is analagous to channel flow with diameter replaced by 4 times the hydraulic radius. As discussed by the writer (1981), these data are the basis for the fully rough region of the Moody pipe friction diagram. The transitional region between smooth and fully rough conditions is defined by the magnitude of the bed Reynolds number:

$$\sqrt{10} < \frac{u_* k_s}{\nu} < 100 \quad (3.5)$$

As illustrated in Fig. 3.1, rough conditions include **most** flow depths one might encounter in gravel-bed channels.

Friction factors for bed Reynolds numbers less than 100 can be obtained from the diagram or equations given by the writer (1981), based on Nikuradse data; or from the Moody diagram (Streeter, 1971) or the Colebrook-White transition function, upon which it is based. The Nikuradse data show that friction factor decreases and then increases as Reynolds number decreases, while the Colebrook-White data show a corresponding steady increase in f , through the transition region. Therefore, the value of friction factor for a channel with a transitional Reynolds number cannot be determined with certainty.

An earlier equation, proposed by Strickler (1923), is based on data from gravel-bed rivers and fixed-bed channels. The equation, now known as the Manning-Strickler equation, is equivalent to Eq. 3.2 with $a = 7.66$ and with k_s defined as the mean gravel-particle size. The Manning-Strickler equation and the Nikuradse Eq. 3.4 are plotted in Fig. 3.2, along with the mean values of the fully rough Nikuradse data. Figure 3.2 shows that for the range of relative roughness used by

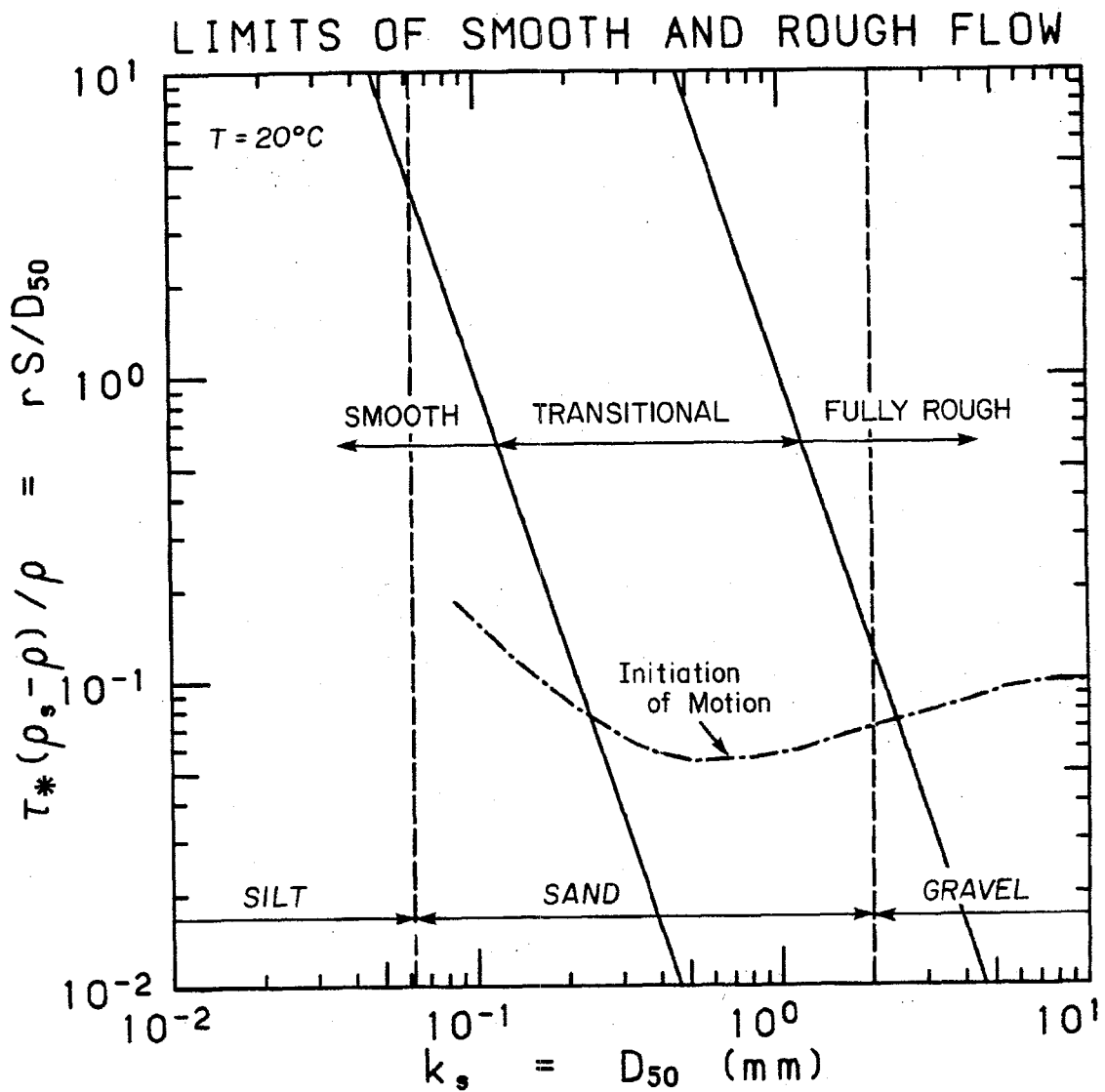


Figure 3.1 Limits of smooth and fully rough flow, and initiation of motion from the Shields diagram in Vanoni (1975), based on $T = 20^\circ\text{C}$, $\nu = 10^{-6} \text{ m}^2/\text{s}$.

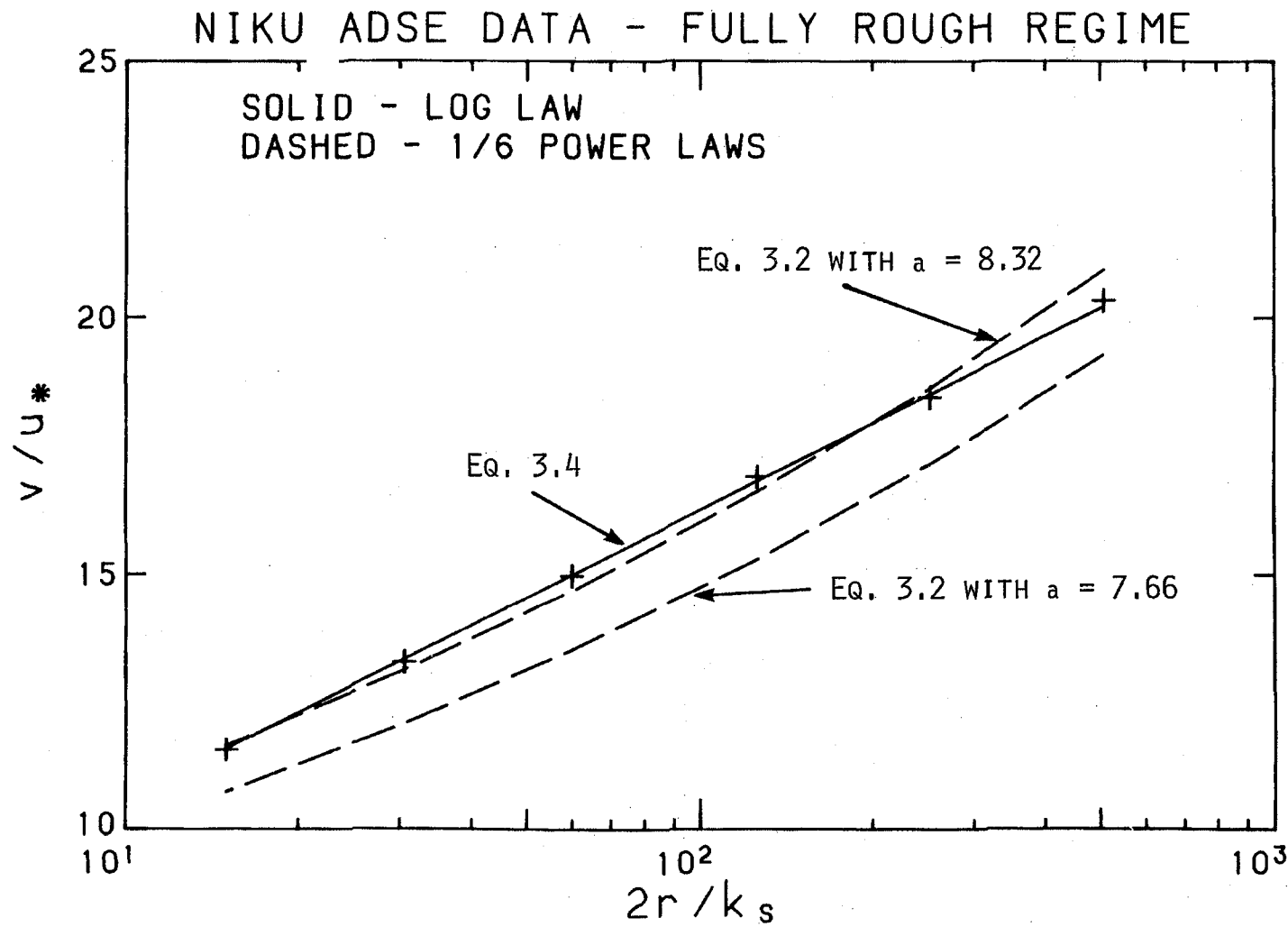


Figure 3.2 Comparison of semilogarithmic and power law resistance equations, with Nikuradse (1933) data in the fully rough regime (+).

Nikuradse, the semilogarithmic Eq. 3.4 is almost identical to the power law, Eq. 3.2, with $a = 8.32$.

Field data for very low values of relative roughness, r/k_s (e.g. flow over boulders) of Limerinos (1970) suggest that the semi-logarithmic form may be more appropriate than a simple power law, when one considers such extreme values of relative roughness. However, for low values of relative roughness, experiments of Bayazit (1976) of flow over hemispheres, suggest that the semi-logarithmic Eq. 3.4 is correct only when k_s is replaced by 2.5 times the diameter of the hemispheres. Therefore, whether due to the uncertainty in determining k_s , or to the differences between pipe and open channel resistance, it seems that a power law, such as Eq. 3.2, will give results of accuracy equivalent to Eq. 3.4, in many cases.

3.4 Existing Stage-Discharge Predictors

The six techniques discussed here have been reworked to directly answer the question: given unit discharge, slope, bed-material properties, and temperature, what will be the depth of flow, or hydraulic radius? The techniques have been selected on the basis of the following criteria: (1) they seem reasonable to the writer or have achieved some degree of acceptance, (2) they are dimensionally consistent, and (3) they are self-contained. The third criterion eliminates those techniques which require a knowledge of bed form, but do not specify how one would determine the bed form for a particular

flow condition.

Garde and Ranga Raju (1977) have considered stage-discharge, or friction factor predictors in two categories, those that divide resistance into grain resistance and form resistance, and those that do not. The divided approach assumes that friction factor, $f = f' + f''$, where f' is for flat-bed grain resistance and f'' is for the added resistance of bed forms. The quantity f' is usually determined from one of the fixed-bed relations previously discussed, by assuming either $S = S' + S''$ or $r = r' + r''$, and then replacing f by f' and S by S' or r by r' in the appropriate diagram or equations. While the divided and non-divided approaches represent different conceptualizations of the problem, the writer does not feel that either technique is clearly superior or more valid than the other. Therefore, here both the divided resistance approach and the singular approach are considered together,

At this point a few words about notation are worthwhile. Since none of the techniques discussed deal with channel width, it has been assumed that they apply to wide channels, for which hydraulic radius and mean flow depth are equivalent. For consistency, hydraulic radius has been substituted for flow depth in those cases where flow depth was used in the original analysis. Unit discharge is therefore defined as $q = vr$. For laboratory flume data, the sidewall correction of Vanoni and Brooks (1957) has been used to define a bed hydraulic radius which is equivalent to the mean depth of an infinitely wide channel with the same slope, velocity, and bed friction factor as the flume. Therefore, the subscript b , sometimes used on r and f to indicate that a sidewall

correction has been performed, has been omitted. Finally, with the exception of a few definitions, unique to individual authors, all notation has been converted to a **common** convention.

4.1 Alam, Cheyer and Kennedy Analysis (1965)

This technique is a divided-resistance approach, which assumes $S = S' + S^n$. The technique is similar to the more recent Alam and Kennedy (1969) version, except for the manner in which the grain friction factor is determined. The earlier technique is discussed here because the **grain** resistance is determined from a standard Moody diagram, and can easily be expressed in equation form, by the Colebrook-White equation. The diagrams for determining f'' for the two versions are nearly identical, therefore the discussion of the earlier analysis could be adapted to apply to the later version.

Using dimensional analysis, Alam, Cheyer and Kennedy (1966) created a diagram based on the following relations;

$$f'' = \text{funct} \left(\frac{r}{D_{50}}, \frac{v}{\sqrt{gD_{50}}} \right) \quad (3.6)$$

and the Colebrook-White equation,

$$\frac{1}{\sqrt{f''}} = -2 \log \left(\frac{D_{50}}{14.8r} + \frac{2.51}{\sqrt{f''} R} \right) \quad (3.7)$$

where $R \square 4q/v$ is Reynolds number.

A diagram (Fig. 3.3) can be constructed whereby, given q , S , R , g , and D_{50} one can determine r/D_{50} and f'' directly. Taking the product of the independent dimensionless groups in Eq. 3.6, and defining $q_* =$

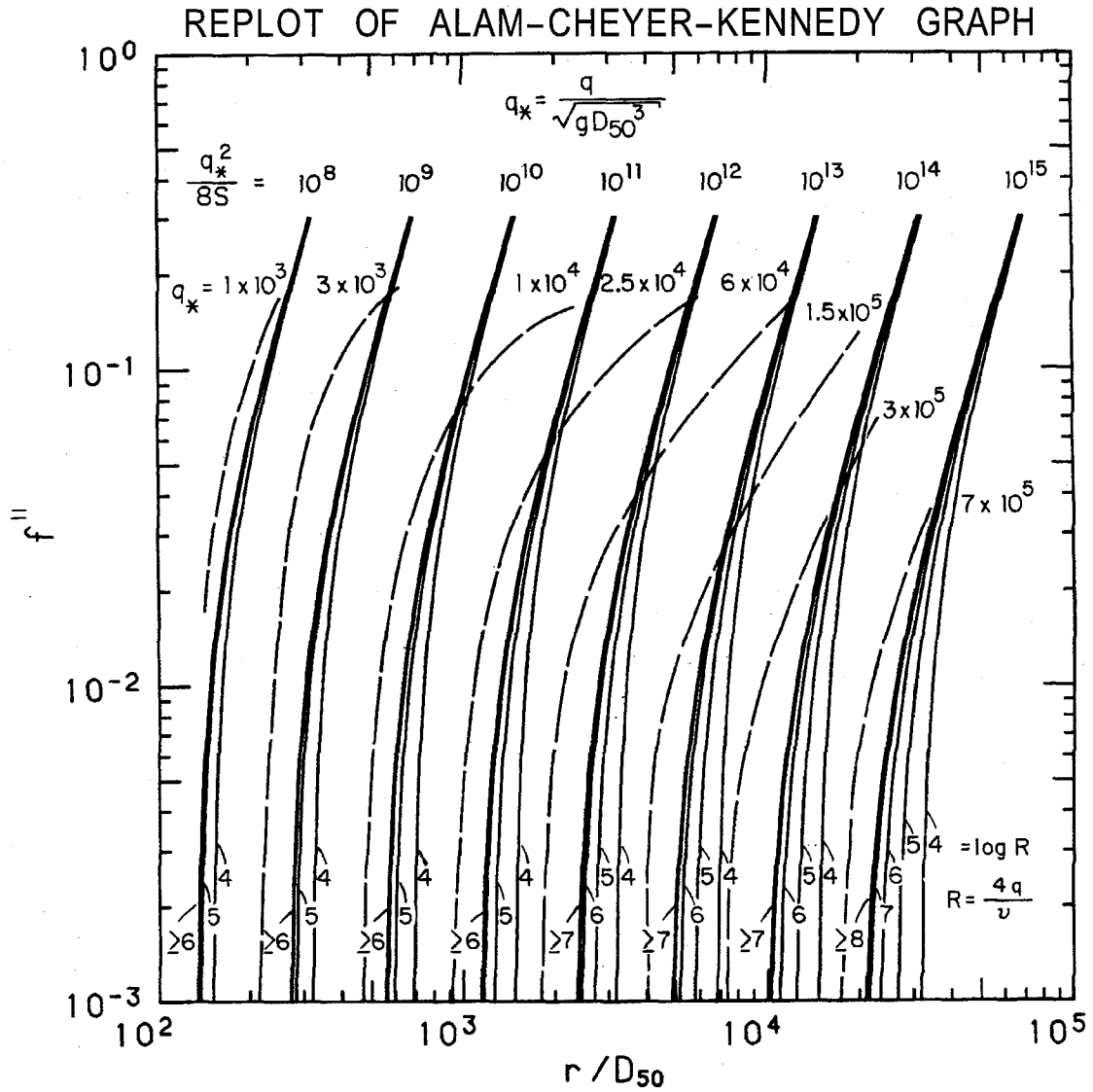


Figure 3.3 Replot of Alam, Cheyer and Kennedy (1966) diagram for determining f'' . Solid lines were determined from Eqs. 3.7 and 3.9. Dashed lines are from the original diagram in the form of Eq. 3.8.

$q/\sqrt{gD_{50}^3}$, yields

$$f'' = \text{funct } q_*, \left(\frac{r}{D_{50}} \right) \quad (3.8)$$

while the definition of friction factor yields

$$f'' = \frac{8S}{q_*^2} \left(\frac{r}{D_{50}} \right)^3 - f' \quad (3.9)$$

Figure 3.3 was created from Eqs. 3.8 and 3.9, where the relation described by Eq. 3.8 was taken from the Alam, Cheyer and Kennedy (1966, Fig. 12) diagram.

For the purposes at hand, there are several problems with the application of Fig. 3.3. 1) Computer coding would be difficult, and the resulting algorithm would undoubtedly be computationally slow. 2) For large and small values of q , on the diagram, the curves of constant q_* and constant $q_*^2/8S$ are nearly parallel, suggesting that there are virtually no solutions in these regions. 3) For large rivers, such as the Mississippi, q , may be larger than any values found on Fig. 3.3, which has exactly the same range of applicability as the original diagram of Alam, Cheyer and Kennedy.

3.4.2 Chu and Mostafa Analysis (1979)

The technique presented by Chu and Mostafa (1979) is essentially a mathematical expression of the graphical technique presented by Mostafa and McDermid (1971). The newer analysis allows a straightforward adaptation of the technique to numerical modeling applications. The analysis is based on the definition of a dimensionless Manning

As f'' approaches 0, q and $q_^2/8S$ are no longer independent.

coefficient, C_M , which is equivalent to the inverse of the Manning-Strickler a in Eq. 3.2, with $k_s = D_{50}$.

Using **nonlinear** curve fitting techniques, **Chu and Mostafa (1979)** developed the following equations

$$C_M = 0.037 \left(\frac{D_{50}}{\delta}\right)^{0.583} \cdot F^{-[0.228\left(\frac{D_{50}}{\delta}\right) + 0.785]} + 0.122 \quad (3.10a)$$

...for $\frac{D_{50}}{\delta} < 5$

and

$$C_M = 0.077 F^{-1.02} \quad \dots \text{for } \frac{D_{50}}{\delta} > 5 \quad (3.10b)$$

where $F = v/\sqrt{gr} =$ Froude number and $\delta = 11.6\nu/u_* =$ thickness of the laminar sublayer. A detailed description of the data used to derive the equations is not available. However, from **Mostafa and McDermid (1971, Figs. 2-F.12 and 2-F.13)**, the diagram corresponding to Eq. 3.10a shows about 100 measurements from 4 rivers and 44 runs from one set of laboratory data, while the diagram corresponding to Eq. 3.10b shows 28 measurements on gravel-bea canals from **Lane and Carlson (1953)**. The range or applicability of Eqs. 3.10 is apparently $0.122 < C_M < 0.45$ and $0.15 < F < 1.0$.

The following equations can be determined from the definitions of C_M and δ , with $R_g = \sqrt{gD_{50}^3}/\nu$:

$$C_M F^{10/9} = q_*^{1/9} S^{1/2} = \alpha \quad (3.11a)$$

and

$$\frac{D_{50}}{\delta} F^{1/3} = \frac{q_*^{1/3} R_g S^{1/2}}{11.6} = \beta \quad (3.11b)$$

where a and β are dimensionless groupings of q , S , D_{50} , v and g , as derived here. By combining Eqs. 3.10a and 3.11 b, one can obtain an equation for C_M in terms of F and β , and, along with Eq. 3.11a, one has a set of equations which define F and C_M in terms of a and β . Figure 3.4 was developed in this manner, and can be used to determine F and C_M , when D_{50}/δ is less than five.

An expression for F , for values of $D_{50}/\delta > 5$, can be determined by combining Eqs. 3.10b and 3.11a. In principle, the resulting equation,

$$F = 1.666 q_*^{1.220} S^{5.488} \times 10^{12} \quad (3.12)$$

in conjunction with Fig. 3.4, should complete the theory,

In reality, a simple example shows that this is not the case. To illustrate the point, we can consider the example where $S = 0.0005$, $D_{50} = 0.24$ mm, $T = 20^\circ$ C and $q = 1$ m²/s. The calculated values of the right sides of Eqs. 3.11a and 3.11b are 0.08 and 1.00, respectively, and from Fig. 3.4, $F = 0.31$ and $C_M = 0.30$, and from Eq. 3.11b, $D_{50}/\delta = 1.5$. Now, if we assume that we are considering a uniform river-flow problem, we may wish to increase the unit discharge, while holding all other independent variables constant. If q is increased to 8 m²/s, then the values of Eqs. 3.11a and 3.11b are increased to 0.10 and 2.00, respectively. An inspection of Fig. 3.4 indicates that no solution is available. We may suspect that Eq. 3.12 will now be applicable. However, substitution into this equation gives Froude number, $F = 16.7$, an unreasonable value, and calculation of D_{50}/δ indicates that this equation is not applicable either. This example illustrates a typical

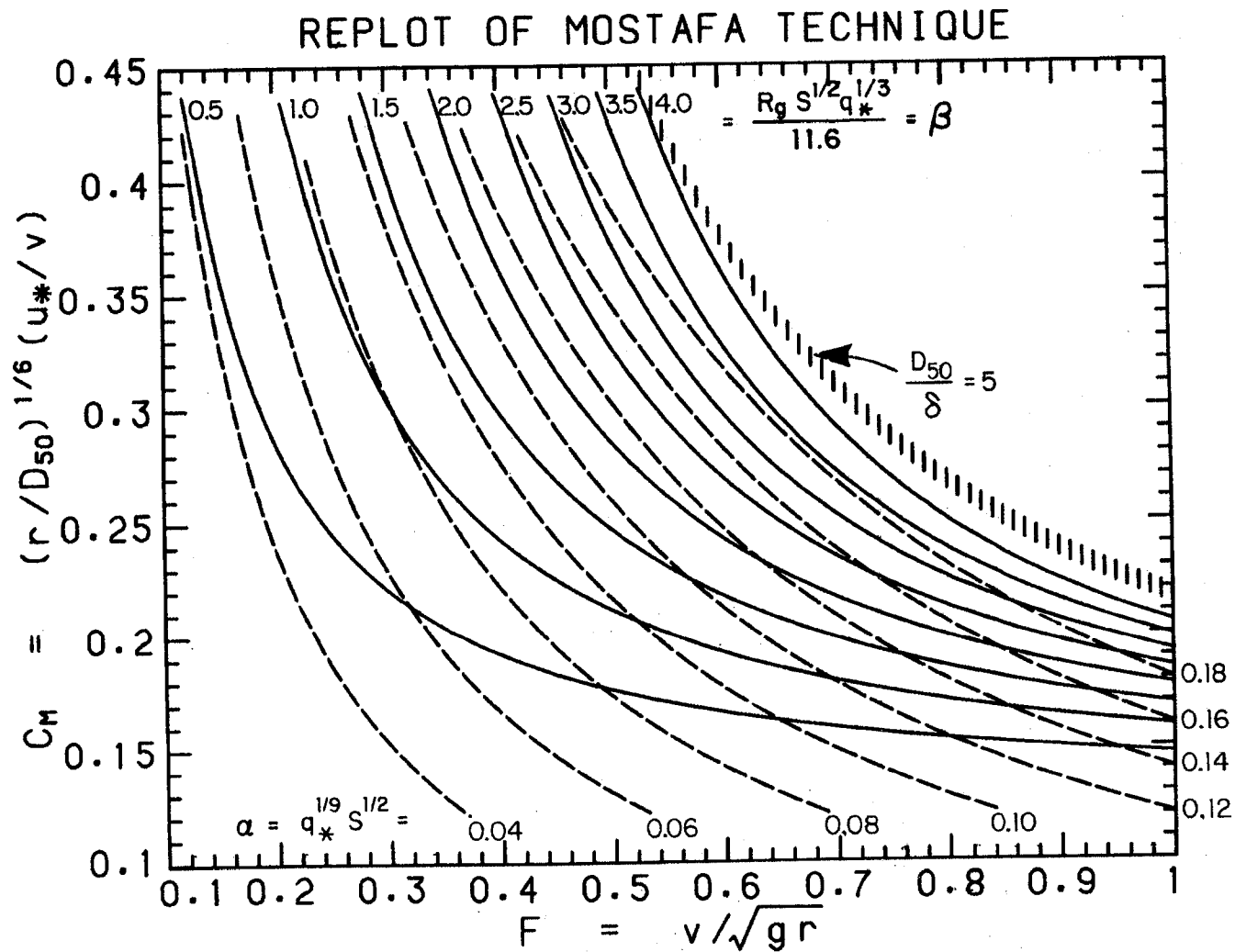


Figure 3.4 Replot of Chu and Mostafa (1979) diagram for determining the dimensionless Manning coefficient, C_M .

problem one might encounter for Froude numbers less than 0.5, since, in this region of Fig. 3.4, the solid and dashed curves are nearly parallel (this point was mentioned briefly in Vanoni, 1975, p.145).

3.4.3 Einstein and Barbarossa Analysis (1952)

The concept of a form-resistance diagram was developed by Einstein and Barbarossa (1952). Although the technique is now nearly 30 years old, it is still probably the most widely quoted of any existing techniques. The technique uses the divided hydraulic radius approach, i.e. $r = r' + r''$, $u_*' = \sqrt{gr'S}$.

When the grain roughness produces fully rough conditions, r' can be determined from the Manning-Strickler equation, in the form

$$\frac{v}{u_*'} = a \left(\frac{r'}{D} \right)^{1/6} = \sqrt{\frac{8}{f'}} \quad (3.13)$$

where $a = 7.66$. For those cases where grain roughness does not produce fully rough conditions, Einstein and Barbarossa presented a semilogarithmic equation with a term which must be determined graphically. This equation is in agreement with the Nikuradse (1933) data and may be replaced by the equations given by the writer (1981) which do not rely on any graphically determined terms. The simple form of Eq. 3.2 allows a clean analysis of the technique, while the semilogarithmic equation does not. Therefore, further discussion of the technique is restricted to fully rough conditions. This restriction is not too serious, since both equations yield similar values of r' , for most field conditions, even when the flow is not strictly fully rough,

The Einstein-Barbarossa (1952) diagram, is of the form

$$f'' = \text{funct} \left[\frac{D_{65}}{D_{35}} \left(\frac{\rho}{\rho_s - \rho} \right) S \cdot \frac{r'}{D_{65}} \right] \quad (3.14a)$$

and from Eq. 3.13 and the fact that $r^w = r - r'$, one can derive

$$f'' = \frac{8}{a^2} \left[\left(\frac{D_{50}}{D_{65}} \right)^{3/2} \frac{q_*}{a\sqrt{S}} \cdot \left(\frac{r'}{D_{65}} \right)^{-2} - \left(\frac{r'}{D_{65}} \right)^{-1/3} \right] \quad (3.14b)$$

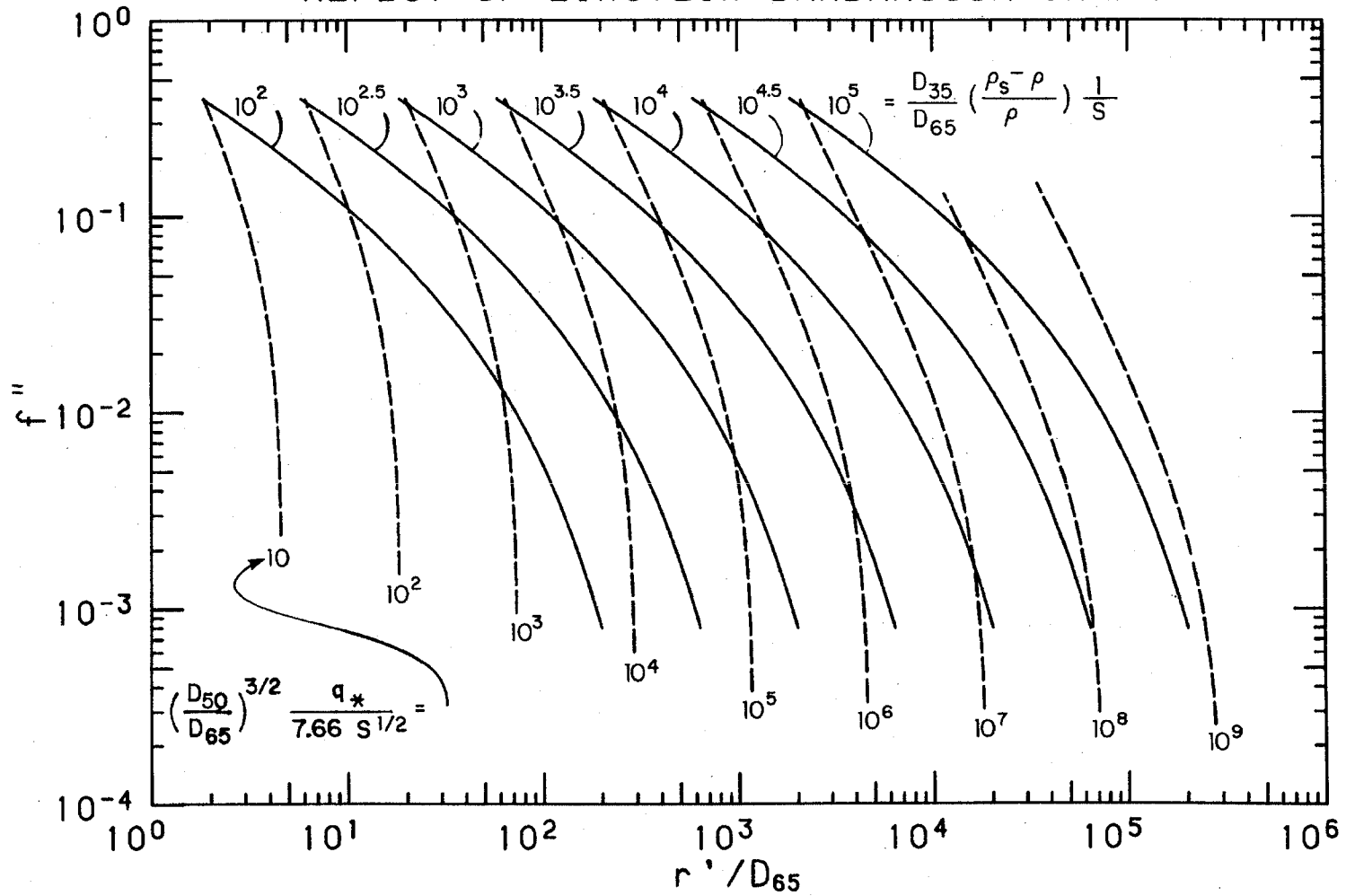
Figure 3.5 was created from Eqs. 3.14a and 3.14b.

As discharge varies, for a given channel with uniform flow (constant slope), the solution will move along the solid lines on Fig. 3.5. The diagram indicates that as discharge decreases, f'' increases monotonically. When f'' is about 0.17, regardless of any other variables, the dimensionless grain-shear stress $\tau_{*s}' = \rho r' S / (\rho_s - \rho) D_{35} = 0.062$, which is sometimes taken as the critical value for initiation of motion. Below this value f'' continues to increase as discharge is decreased, indicating high resistance, apparently from residual bedforms. Beyond the critical shear stress, about a twenty-fold increase in unit discharge causes the form resistance to steadily decrease to almost nothing, suggesting $f = f'$. A later comparison shows that for some channels this variation in f'' is too exaggerated.

3.4.4 Engelund Analysis (1967)

In principle, this technique is based on the divided slope approach, but in actualization, the divided hydraulic radius is used. The analysis is based on the assumption that S^n is the direct result of expansion losses that occur as a fluid flows over dunes. Furthermore,

REPLOTT OF EINSTEIN-BARBAROSSA GRAPH



Replot of Einstein and Barbarossa (1952) diagram for determining f''

it is assumed that $rS' = r'S$, thereby converting to a divided hydraulic radius approach. Definition of S' in such a manner is not in agreement with the concept of S' as defined in the introduction to the discussion of the various techniques. Verification of the analysis is based on laboratory data from runs using four different sands, published by Guy et al. (1966). In all, 148 runs are published (for these 4 sands), but it appears that about half this number were actually used by Engelund (1967).

The quantity r' is defined by

$$\frac{v}{u_*'} = 6 + 2.5 \ln \frac{r'}{2D_{65}} = 5.76 \log \frac{5.51r'}{D_{65}} \quad (3.15)$$

which agrees with the fully rough Nikuradse data and gives nearly the same results as Eq. 3.4. Once r' is determined, it is possible to determine τ_* by the empirical formulas for the lower flow regime (ripples and dunes):

$$\tau_* = 1.581\sqrt{\tau_*' - 0.06} \quad (3.16a)$$

and for the upper flow regime (plane bed, standing waves and antidunes):

$$\tau_* = \begin{cases} \tau_*' & \text{for } \tau_*' < 1 \quad (3.16b) \\ (1.425\tau_*'^{-1.8} - 0.425)^{-1/1.8} & \dots \text{for } \tau_*' > 1 \quad (3.16c) \end{cases}$$

Equations 3.16a and 3.16b are given by the author, while Eq. 3.16c was developed from the author's diagram (Engelund, 1967, p. 289). The equations for upper and lower flow regimes plot as discontinuous line segments with the transition occurring at about $\tau_*' = 0.55$.

Equations 3.16a-c can be represented in the general form

$$\tau_* = f \left[\frac{D_{65}}{D_{50}} \left(\frac{\rho}{\rho_s - \rho} \right) s \cdot \frac{r'}{D_{65}} \right] \quad (3.17a)$$

Also, rearrangement of Eq. 3.15 yields

$$\tau_* = \frac{\left(\frac{\rho}{\rho_s - \rho} \right) q_* \sqrt{\frac{D_{50}}{D_{65}} s}}{\sqrt{\frac{r'}{D_{65}} \left[6 + 2.51 \ln \left(\frac{1}{2} \frac{r'}{D_{65}} \right) \right]}} \quad (3.17b)$$

As for previous techniques, the desired graphical representation (Fig. 3.6) of the technique is now possible. Using Fig. 3.6, it is possible to directly determine τ_* and r'/D_{65} .

Equations 3.16a-c are easy to program and have been compared with three sets of data in Figs. 3.7a-c. Data of Guy et al. (1966) are shown in Fig. 3.7a, which includes almost all of the data used in the original analysis, plus additional data. Here, sands with fall diameter (not sieve diameter) D_{50} values of 0.19, 0.27, 0.28, 0.45 and 0.93 mm are plotted. Field data from the Mississippi River at Tarbert Landing, IA (Toffaletti, 1968), D_{50} about 0.25 mm, and laboratory data of Williams (1970), $D_{50} = 1.35$ mm, are plotted in Figs. 3.7b and 3.7c, respectively. (Note - Although Williams used many channel widths in his experiments, only data from the two widest channels are shown in Fig. 3.7c.)

The diagrams which comprise Fig. 3.7 suggest that more refinement of this technique would be necessary before general application could be recommended. Figure 3.7a shows that a few measurements in the chute-and-pool bed class have strongly influenced the vertical asymptote on the upper curve. Figure 3.7b suggests that more work is necessary in

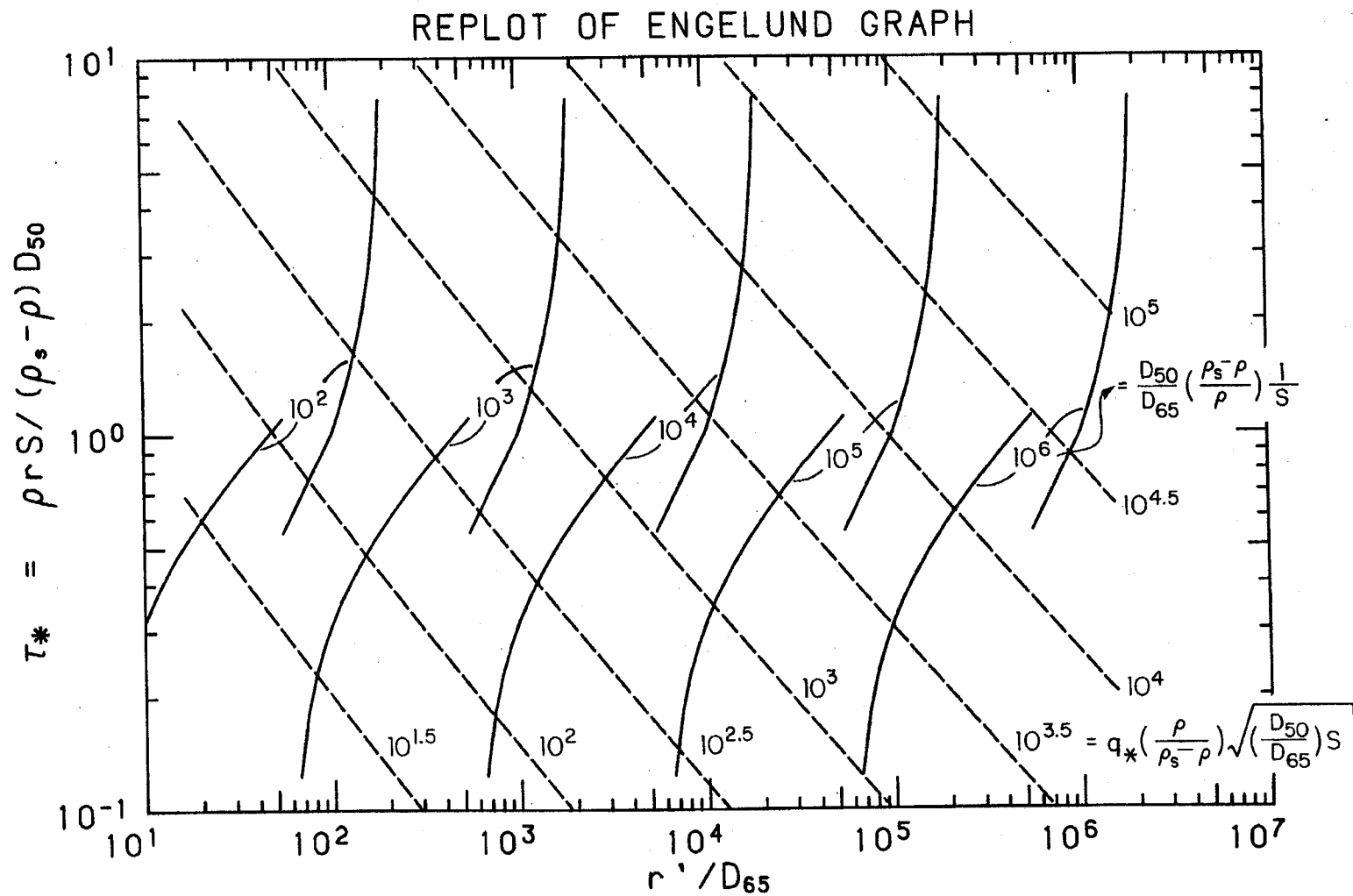


Figure 3.6 Replot of Engelund (1967) diagram determining

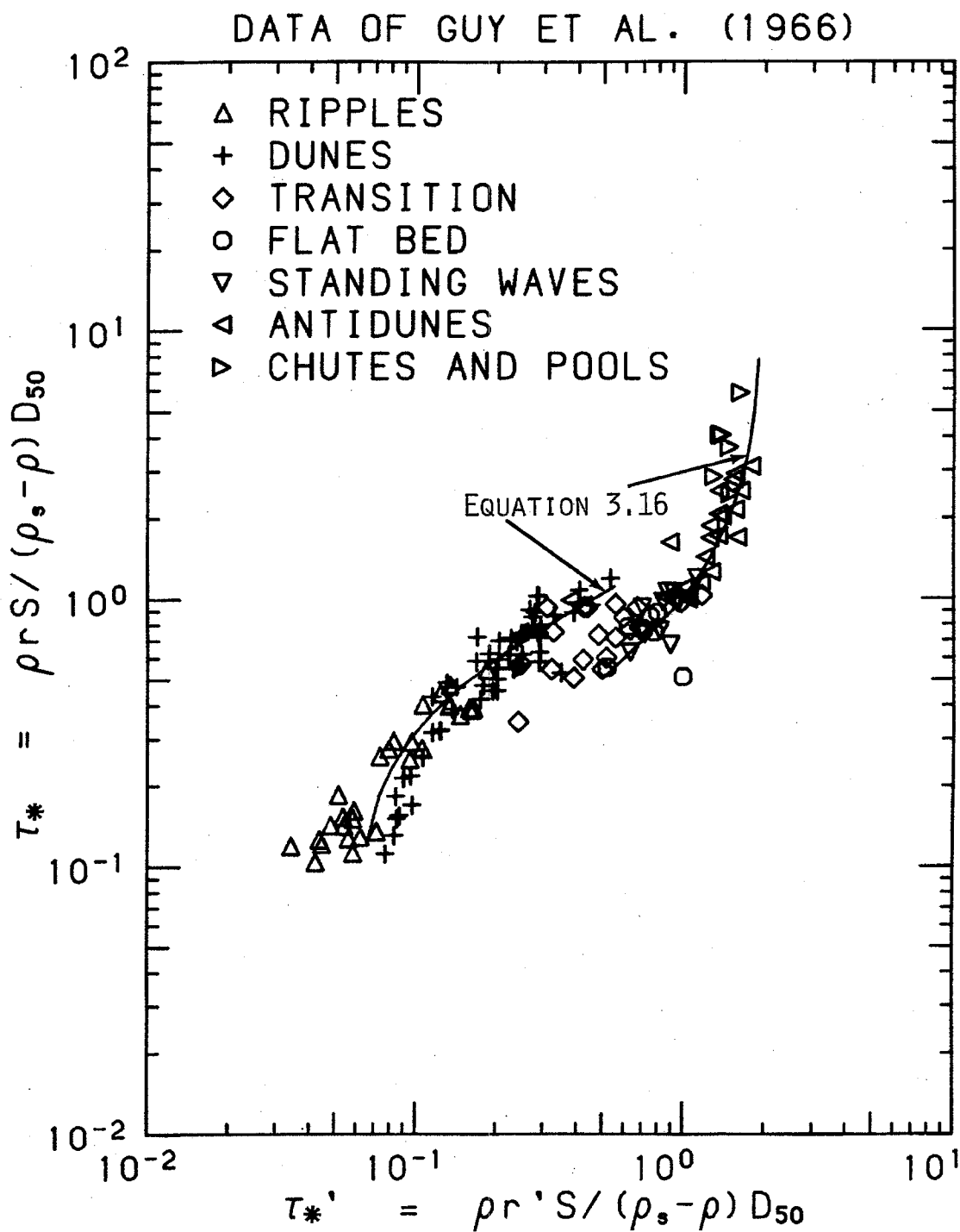


Figure 3.7a Comparison of Engelund technique with data of Guy et al. (1966).

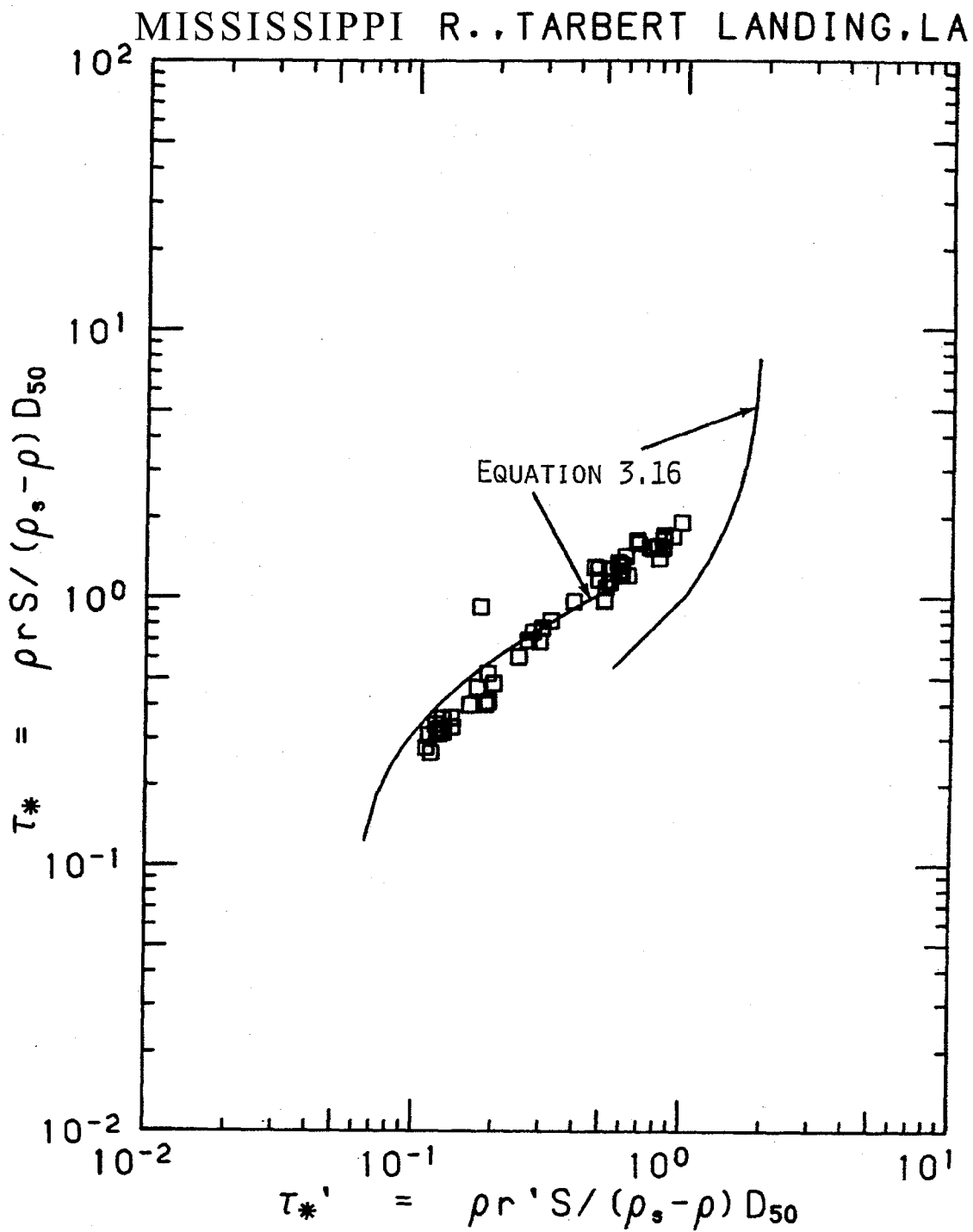


Figure 3.7b Comparison of Engelund technique with data for the Mississippi River, Tarbert Landing, Louisiana.

DATA OF WILLIAMS (1970)

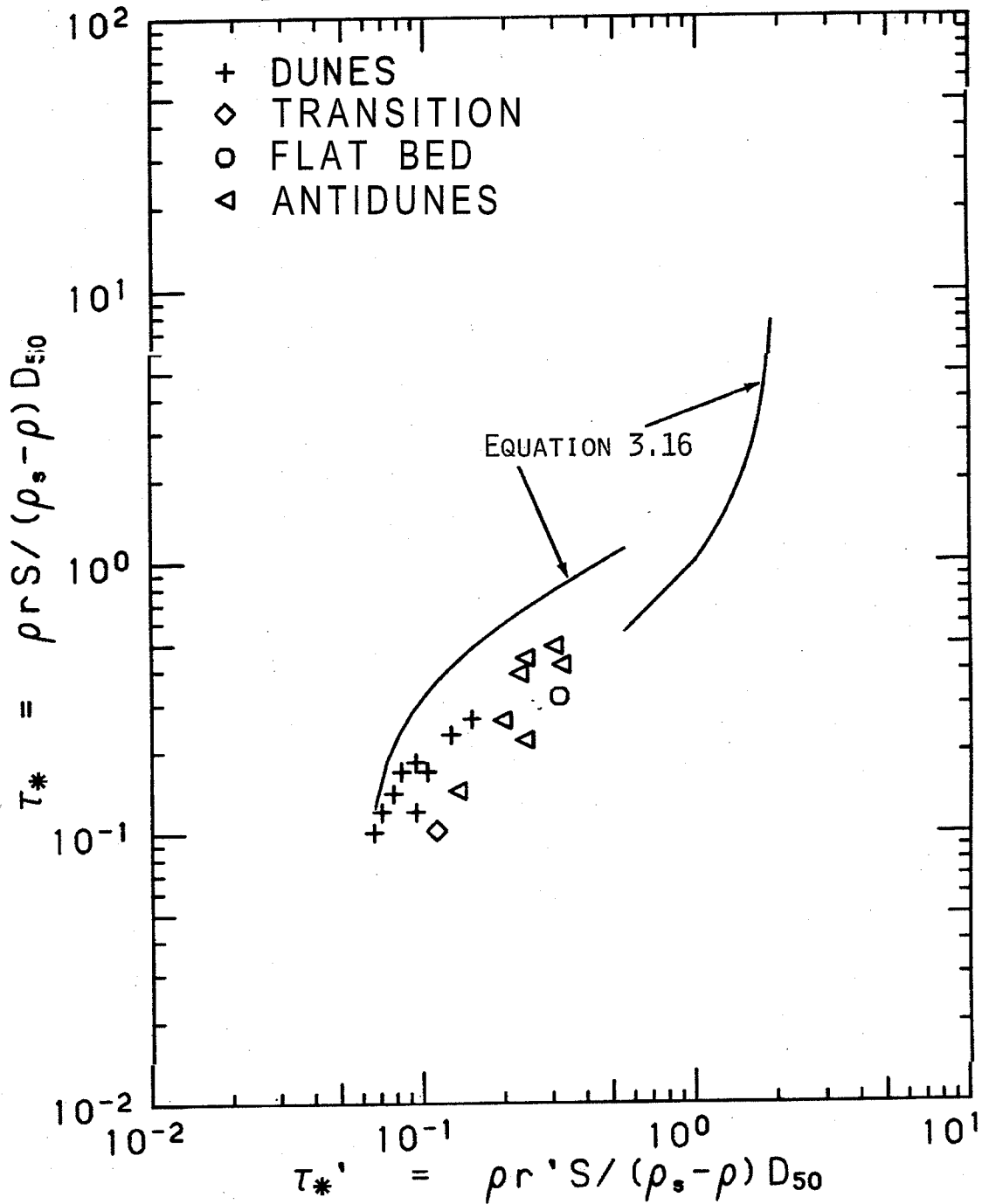


Figure 3.7c Comparison of Engelund technique with data of Williams (1970).

defining the transition region. The coarse sand data of Williams (1970), plotted in Fig. 3.7e, imply that the inclusion of some other variable may be necessary for certain ranges of data.

3.4.5 Garde and Ranga Raju Analysis (1970)

The original analysis for this technique was given by Garde and Ranga Raju (1966), later revised by Ranga Raju (1970), and summarized by Garde and Ranga Raju (1977). It is the revised version which is considered here. The technique does not employ the concept of divided resistance. In fact, the technique does not even require the calculation of a friction factor, per se.

Ranga Raju (1970) graphically presented a function of the form

$$K_1 F_R = K_1 q \sqrt{\frac{\rho}{(\rho_s - \rho) g r^3}} = f \left[K_2 \left(\frac{r}{D_{50}} \right)^{1/3} S \left(\frac{\rho}{\rho_s - \rho} \right) \right] \quad (3.18)$$

where K_1 and K_2 are functions of mean particle size and F_R , as defined here, is a modified Froude number. By multiplying the independent variable in Eq. 3.18 by the dependent variable raised to the 2/9 power, a relation represented by

$$K_1 F_R = f \left[(K_2 S) (K_1 q_*)^{2/9} \left(\frac{\rho}{\rho_s - \rho} \right)^{10/9} \right] \quad (3.19)$$

can be determined, which is plotted in Fig. 3.8.

Like the Engelund (1967) analysis, Fig. 3.8 suggests that an upper and a lower regime exist, separated by a transition zone. However, in contrast to the Engelund technique, in Fig. 3.8, the transition occurs as a continuous function. For a given bed material and slope, Froude

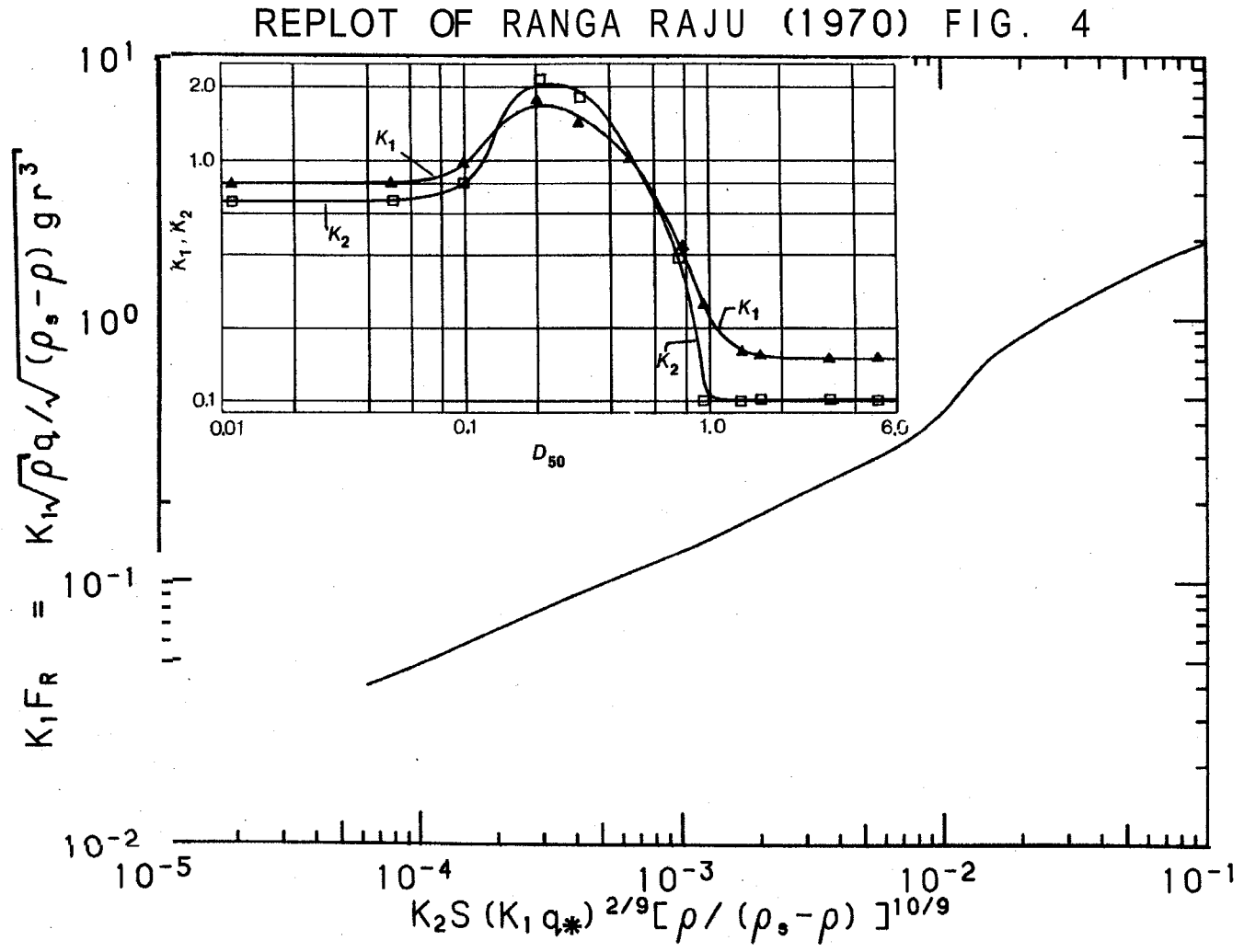


Figure 3.8 Replot of Ranga Raju (1970) diagram for determining densimetric Froude number, F_R .

number is a weak function of unit discharge, **i.e.** going to about the 0.10 power of unit discharge for both the upper and lower regimes, Therefore, for either of these regimes, a ten-fold increase in unit discharge causes only a 26 percent rise in Froude number.

Although Garde and Ranga Raju (1977) have not provided a rigorous statistical analysis of the data they used, they have given some indication of the expected accuracy of their technique, For 90 percent of the plotted data, they have stated that mean velocity ~~was~~ predicted to within 30 percent accuracy. Although a large body of data was used in the analysis, this is not an independent check of the technique, but merely a statement of the observed errors.

If the technique is to be adapted to numerical modelling applications, a specific function **must** be fitted to the curve in Fig. 3.8. The curve can be very closely approximated by three straight lines which, after rearranging, are represented by

$$V = b \frac{\sqrt{K_2}}{K_1} \left(\frac{r}{D_{50}}\right)^{1/6} \sqrt{grS} \quad (3.20)$$

$$\text{where } b = \begin{cases} 3.46 & \dots \text{for } K_1 F_R \leq 0.33 & (3.20a) \\ 3.46 + 6.73 \log(3K_1 F_R) & \dots \text{for } 1 > K_1 F_R > 0.33 & (3.20b) \\ 6.67 & \dots \text{for } K_1 F_R \geq 1 & (3.20c) \end{cases}$$

Equation 3.20 is similar to the Manning-Strickler Eq. 3.2, with the constant, a , replaced by a function of D_{50} . For $D_{50} > 1.5$ mm, Eq. 3.20c (upper flow regime) gives $a = 13.2$ (in Eq. 3.2), which is not too close to the value of $a = 7.66$ given by Strickler (1923).

If we consider only the lower regime, for a given channel, i.e. bed material and slope fixed (assuming uniform flow), two facts about Eq. 3.20a are evident. First, Manning's n is constant, and not a function of discharge. Second, transition begins when a certain Froude number is reached. This Froude number is not a function of slope, and depends only on K_1 , a function of D_{50} . The analysis presented in the next chapter suggests that Froude number varies slightly within a flow regime and that the transition is somewhat different than indicated here. Nevertheless, the work of Garde and Ranga Raju have provided important clues for the development of the new technique.

3.4.6 White, Paris and Bettess Analysis (1979)

As originally presented, this technique does not utilize the divided resistance concept, however, like the Engelund (1967) analysis, the dimensionless shear stress can be related to a dimensionless grain shear-stress. White, Paris and Bettess (1979) have provided both graphical and equational representations of their technique, as well as a statistical analysis of the errors.

The authors have given two versions of their technique; one using D_{35} of the parent bed material and one using D_{65} of the surface material. The **former** has greater accuracy and is more compatible with the other techniques discussed in this paper, and is therefore discussed here. For this version, a dimensionless grain size is defined by

$$D_{gr} = D_{35} \left[\frac{g(\rho_s - \rho)}{\rho v^2} \right]^{1/3} \quad (3.21)$$

which, in turn, is used to define the quantities

$$n = \begin{cases} 0 & \dots \text{ for } D_{gr} \geq 60 \\ 1.0 - 0.56 \log D_{gr} & \dots \text{ for } 1 \leq D_{gr} \leq 60 \end{cases} \quad (3.22a)$$

$$\text{and } A = \begin{cases} 0.17 & \dots \text{ for } D_{gr} \geq 60 \\ 0.23 D_{gr}^{-1/2} + 0.14 & \dots \text{ for } 1 \leq D_{gr} < 60 \end{cases} \quad (3.22b)$$

Utilizing a divided slope approach, it is possible to define a grain shear-velocity by

$$u_*' = \frac{v}{\sqrt{32} \log (10r/D_{35})} \quad (3.23)$$

and the corresponding dimensionless grain shear-stress as

$$\tau_*' = \frac{\rho u_*'^2}{g D_{35} (\rho_s - \rho)} = \frac{\rho r S'}{D_{35} (\rho_s - \rho)} \quad (3.24)$$

The dimensionless mean shear-stress is then $\tau_* = (u_*'/u_*'^2)^2 \tau_*'$. Using this definition, the White, Paris and Bettess (4979) method can be represented by

$$\tau_*' = \left[\frac{B(\sqrt{\tau_*} - A) + A}{\tau_*^{n/2}} \right]^{\frac{2}{1-n}} \quad (3.25)$$

where

$$B = 1.0 - 0.76[1.0 - e^{-(\log D_{gr})^{1.7}}] \quad (3.25a)$$

whereby, for a given value of D_{gr} , τ_*' is a continuous function of τ_* .

It is possible to present an analysis similar to the one given for the Engelund technique, relating hydraulic radius to unit discharge and slope. However the resulting diagram (analogous to Fig. 3.6), due to the added variable D_{gr} , would be too confusing to be of much use. It is

more appropriate to examine a specific example, as in Fig. 3.9. The data in Fig. 3.9, $D_{50} = 0.45$ mm and $D_{gr} = 10.1$, represent a portion of the data plotted in Fig. 3.7a. While the Engelund (1967) technique (see Fig. 3.7a) predicts reasonably well over the whole range of data, the White, Paris and Bettess (1979) technique (Fig. 3.9) does a better job in the dune range, but is otherwise a poor predictor. Comparisons with other sets of field and laboratory data verify the hypothesis that the present technique gives reasonable results only for flow over dunes. Under no circumstances does the technique describe upper and lower flow regimes.

The behavior displayed in Fig. 3.9 is partially explained by an examination of the way in which the technique was originally derived. The key lies in the empirical expression Eq. 3.25a, which was derived from a plot of average values of B , defined by a rearrangement of Eq. 3.25, against 47 values of D_{gr} . The average values of B were determined from 837 laboratory experiments with sand, collected from 16 investigators. Only Froude numbers less than or equal to 0.8 were used. The fact that average values were used would tend to reduce the scatter, while the fact that only low Froude numbers were used explains why only the lower flow regime is described. In testing the technique with an extended data set (also Froude numbers less than or equal to 0.8), the authors have stated that 89 percent of the total calculated friction factors were within a factor of two, while 44 percent were within 0.80 and 1.25 of the observed value,

TEST OF WHITE ET AL. TECHNIQUE

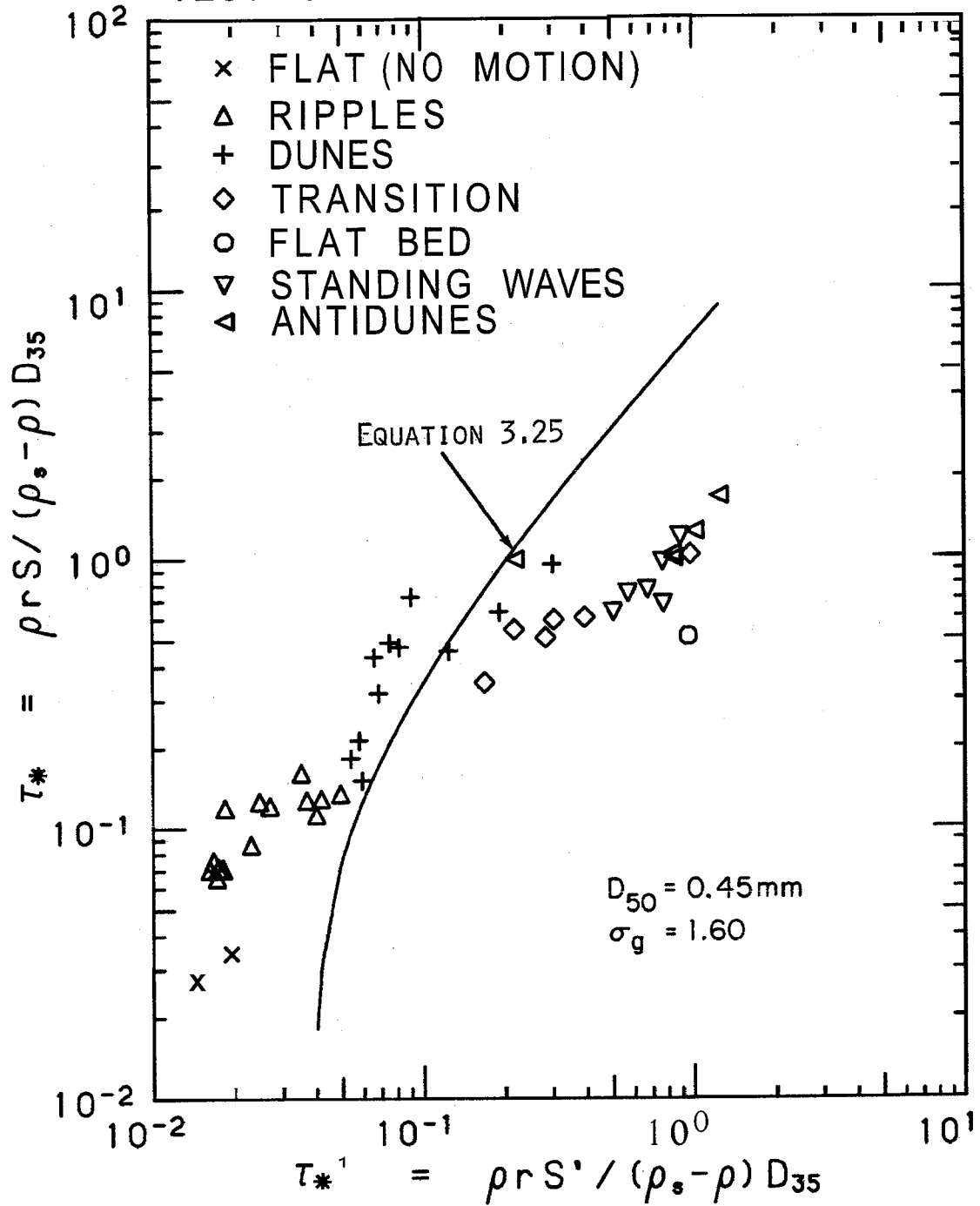


Figure 3.9 Comparison of White et al. (1979) technique with laboratory data of Guy et al. (1966).

3.5 Summary

In this chapter, six stage-discharge predictors have been discussed. Each technique provides some insight into the processes involved, and yet, no technique appears to provide a totally satisfactory analytical tool for the **numerical** modeller. The relation between shear stress and grain shear stress as defined by **Engelund** (1967) is perhaps the most satisfactory.

In Chapter 4, a new technique is proposed, which the writer believes does provide such a tool. Near the end of the chapter, a comparison is given for the proposed method and the techniques that have just been discussed.

The assumption was made in the analysis of the six techniques that they apply to wide channels, or that sidewall effects have been removed. Under this assumption the hydraulic radius, r , and mean flow depth, d , are equivalent. Alam, Cheyer, and Kennedy (1965); Einstein and Barbarossa (1952); and Garde and Ranga Raju (1970) actually used r in their analyses, while the others used mean flow depth, d , which was called r in the analysis.

CHAPTER 4

A PROPOSED METHOD FOR CALCULATING FLOW DEPTH IN SAND-BED CHANNELS

The foregoing analysis of available techniques indicates that none of those that are described satisfy the **four** desired attributes established in Chapter 3. Nevertheless, each of the analyses is useful and has provided inspiration for the derivation that follows. The proposed technique is easy to use and requires no iteration or graphical interpolation for wide channels. For laboratory channels $q = vr$ rather than $q = vd$, therefore, for some applications iteration may be required.

4.1 Dimensional Analysis

The particle sizes of ~~most~~ river sands are approximately log-normally distributed, by weight, therefore the sand can be described by two measures of grain size, D_{50} and σ_g , and its specific gravity, ρ_s . Adding the flow variables and the fluid variables gives

$$r = f(q, S, g, \rho, v, \rho_s, D_{50}, \sigma_g) \quad (4.1)$$

Using the π -theorem, the 9 variables in Eq. 4.1 can be arranged into 6 dimensionless groups in the form

$$\frac{rS}{D_{50}} = \frac{(\rho_s - \rho)}{\rho} \tau_* = f(q_*, S, \sigma_g, R, \frac{\rho_s - \rho}{\rho}) \quad (4.2)$$

where $q_* = q/\sqrt{gD_{50}^3}$ and $R = 4q/\nu$.

Since we are primarily interested in fully **rough** flow, R is expected to be of secondary importance. Preliminary tests on large bodies of data have verified this conclusion. Furthermore, since only sand is under consideration, $(\rho_s - \rho)/\rho$ will be constant, and can be put aside. Therefore, Eq. 4.2 can be reduced to

$$\frac{(\rho_s - \rho)}{\rho} \tau_* = f(q_*, S, \sigma_g) \quad (4.3)$$

4.2 Formulation of a Pair of Equations

We are now ready to develop a specific relationship which can be generally described by Eq. 4.3. It is assumed that, to a first approximation, the flow resistance in a channel will be determined by the largest scale of bed roughness. Then, for flow over a dune bed, we might expect friction factor to be defined by a semilogarithmic equation similar to Eq. 3.4, but with k_s replaced by a measure of equivalent dune roughness, k_d . As shown in Fig. 3.2, this equation can be approximated by the power law, Eq. 3.2. Replacement of k_s in Eq. 3.2 by k_d , after considerable rearrangement, yields

$$\left(\frac{\rho_s - \rho}{\rho}\right) \tau_* = a^{-0.6} \left(\frac{k_d S}{D_{50}}\right)^{0.1} (q_* S)^{0.6} \quad (4.4)$$

If the particle sizes of a bed material are log-normally distributed, by weight, then any given size fraction can be related to the mean size, D_{50} , by

$$D_s = \sigma_g^z D_{50} \quad (4.5)$$

where z is the number of standard deviations from the mean and the subscript "s" refers to the percent by weight of particles which are smaller than the given size. For example, if $z=1$, since the distribution is log-normal, $D_s = D_{84}$, and 84 percent of the particles in a sample, by weight, are finer than D_{84} . We can now define a dimensionless shear stress based on this particle size by $\tau_{*s} = \tau_*/\sigma_g^z$. For non-uniform bed materials, we can replace τ_* in Eq. 4.4 by τ_{*s} , thereby normalizing the bed shear-stress by some particle diameter other than D_{50} .

One variable appears in Eq. 4.4, k_d , the measure of dune roughness, which is not included in the independent variables listed in Eq. 4.1. Therefore, k_d should, in fact, be a dependent variable. Since this variable appears in the equation raised to the 0.1 power, only large changes in k_d will be important, and an exact definition is not a critical factor in obtaining sufficient accuracy in the prediction of τ_* . Assuming that k_d/D_{50} is proportional to the product of undetermined powers of q , and S , upon substitution into Eq. 4.4 (also recalling the definition of τ_{*s}), yields

$$\left(\frac{\rho_s - \rho}{\rho}\right) \tau_{*s} = w(q_* S)^x S^y \sigma_g^z \quad (4.6)$$

where w , x , y and z are constants to be fitted empirically. If the dependence of k_d/D_{50} on q_* and S is fairly weak, x is expected to be approximately equal to 0.6 and y is expected to be approximately equal to 0.1.

It is possible to represent Eq. 4.6 in a reasonably simple diagram by rearranging it as (with $\tau_{*S} = \tau_* / \sigma_g^z$)

$$\left(\frac{\rho_* - \rho}{\rho}\right) \tau_{*S} = w(q_* S^{1+\frac{y}{x}})^x \quad (4.7)$$

which can be represented by a straight line on a log-log plotting scale. Lower regime (ripple and dune) data, from laboratory flumes, rivers and canals, gathered from 22 sources, were used to fit the coefficients. By taking the logarithms of both sides of Eq. 4.6, the coefficients w , x , y and z were determined by multiple regression. The data and the best fit line are shown in Fig. 4.1. Because nearly 900 runs were used in the analysis, only every third point is plotted. The values of w , x , y and z are 0.3724, 0.6539, 0.09188 and 0.1050, respectively, with a multiple correlation coefficient, $R = 0.992$, indicating excellent agreement.

A similar analysis can be performed for the flat bed regime. In this case, the largest roughness scale of the bed should be some measure of the bed material. Therefore, k_d in Eq. 4.4 will be replaced by some D_s , and we can again derive an equation with the form of Eq. 4.6. The coefficients will take on new values, and this time the values of x and y should be almost identical to 0.6 and 0.1, respectively. Furthermore, if the Strickler equation is approximately correct with the value $a=8.32$ (see Fig. 3.2), then w should be about 0.28.

A regression analysis identical to the one performed for dune and ripple data was performed for flat bed or upper regime data. This data includes flat beds, before and after initiation of motion, standing waves and antidunes. The same 22 data sources have again been used,

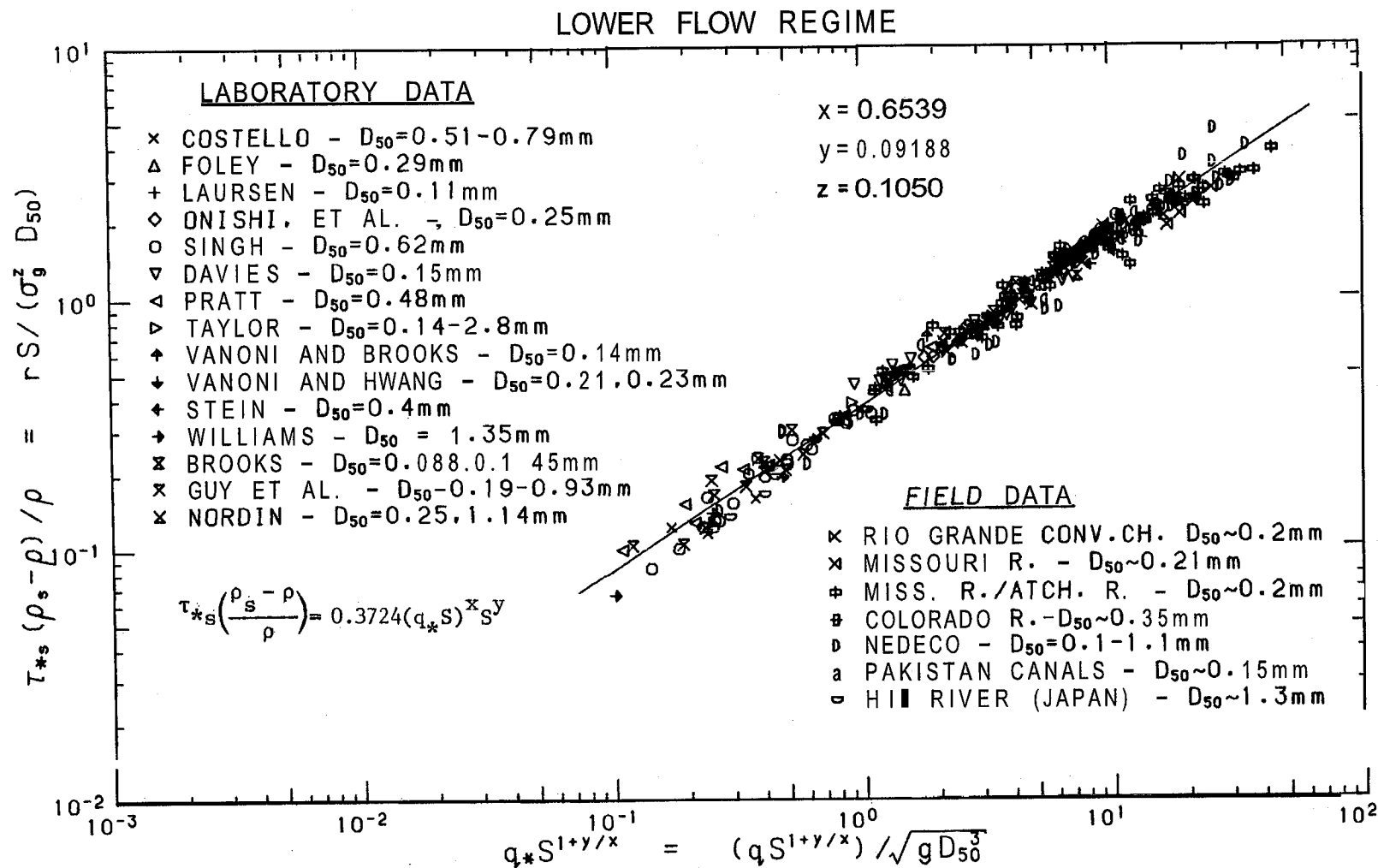


Figure 4.1 Relationship between dimensionless shear stress, τ_{*s} and q_* and S , for lower flow regime (dune and ripple bed forms).

although not all contain data for these bed classes. The values of w , x , y and z are now 0.2836, 0.6248, 0.08750 and 0.08013, respectively, with a cross-correlation coefficient, $R = 0.999$. Note that, indeed, w , x , and y are close in value to 0.28, 0.6, and 0.1, respectively. The data and best fit line are plotted in Fig. 4.2.

An error analysis of the regression procedure is given, by data source, in Table 4.1. **The errors are quite small, especially when one** considers the accuracy of the data. For example, Guy et al. (1966) have indicated that errors in slope measurements may be as high as 15–20 percent, while errors in depth measurements may be on the order of 5 percent. This range of errors is probably typical of many of the data sets.

The data used in this analysis were selected from a pool of data collected from over 70 sources which was assembled in connection with this study. The 22 sources that were finally used in the analysis were selected because they covered a wide range of the desired variables, and because the data seemed to be carefully collected and **documented**. Only laboratory data with bed form observations have been included. For field data, this restriction would have been too limiting, and where bed form was not given, only observed flows which could logically be assumed to have dune beds were selected. The ranges of important variables are given in Table 4.2. Since only sand beds are being considered, median particle-sizes were generally limited to values between 0.062 mm to 2.0 mm, although a few runs at 2.8 mm were included. To avoid samples with large amounts of gravel or fine material, geometric standard deviations

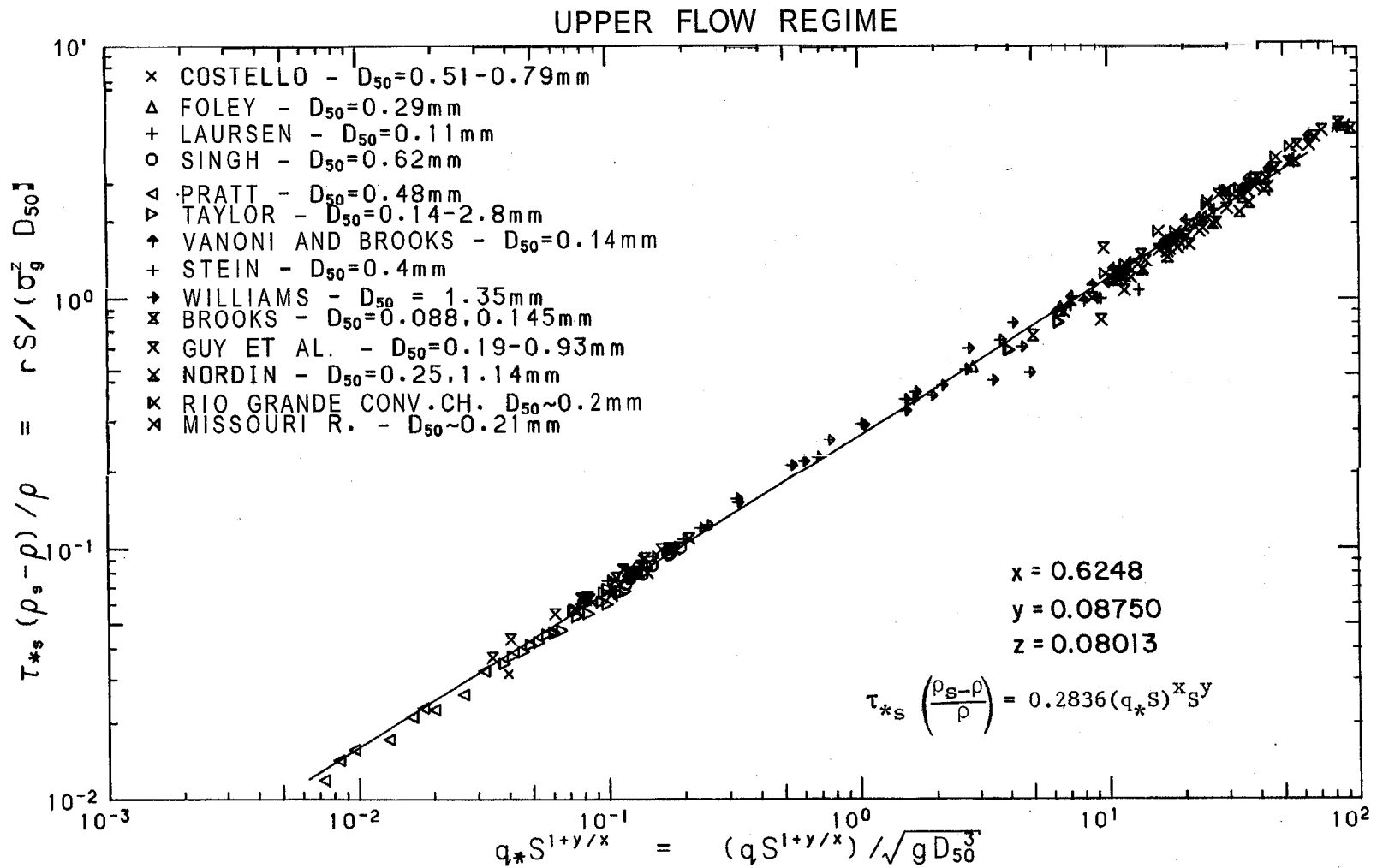


Figure 4.2 Relationship between τ_{*s} and q_* and S , for upper flow regime (dune and ripple bed forms).

Table 4.1
Error Analysis of New Method for Laboratory and Field Data

Source	Lower Regime			Upper Regime		
	Number of Records	Average % Error in τ_*	Standard Deviation of Errors	Number of Records	Average % Error in τ_*	Standard Deviation of Errors
<u>Laboratory Data</u>						
1 Costello (1974)	8	12.6%	12.7%	8	-2.6%	9.2%
2 Foley (1975)	1	12.5	-	3	1.1	1.9
3 Laursen (1958)	10	0.1	10.0	1	32.8	-
4 Onishi, Jain, & Kennedy (1972)	12	-0.8	6.9	0	-	-
5 Singh (1960)	62	6.9	11.0	12	0.1	2.2
6 Davies (1971)	34	-1.4	10.7	0	-	-
7 Pratt (1970)	37	-6.7	7.6	9	5.1	4.9
8 Taylor (1971)	12	0.0	7.0	25	5.5	5.0
9 Vanoni & Brooks (1957)	12	7.3	9.8	3	3.0	4.2
10 Vanoni & Hwang (1967)	6	-1.0	5.9	0	-	-
11 Stein (1965)	20	2.5	13.9	24	-2.6	5.6
12 Williams (1970)	14	15.0	7.9	29	-1.9	13.2
13 Brooks (1957)	2	-6.7	0.7	2	7.2	2.7
14 Guy, Simons, & Richardson (1966)	97	-1.0	9.9	65	0.3	9.9
15 Nordin (1976)	17	-0.9	8.5	13	6.0	7.0
<u>Field Data</u>						
16 Rio Grande Conveyance Channel, New Mexico	9	-6.4	6.7	12	-9.5	3.9
17 Mississippi & Atchafalaya Rivers ¹	233	0.6	11.8	0	-	-
18 Colorado River at Taylor's Ferry, AZ	30	-6.8	4.5	0	-	-
19 Missouri River near Omaha, Nebraska	11	22.0	5.0	1	-3.7	-
20 NEDECO ² - So. Amer. river data	96	6.7	17.6	0	-	-
21 ACOP ³ - Pakistan Canals	148	-3.6	7.4	0	-	-
22 Hii River, Japan, 5 stations	23	6.0	9.3	0	-	-
All sources	894	0.7	12.1	207	0.4	9.5

¹Mississippi River at Tarbert Landing, LA, and at St. Louis, MO, and the Atchafalaya River at Simmespot, IA.

²Data collected by Netherlands Engineering Consultant (NEDECO) on the Rio Magdalena and the Canal del Dique, Columbia, S.A., 10 stations each.

³ACOP - Alluvial Channels Observation Project data from 14 study reaches on 5 canals.

Table 4.2

Range of Data Used in Analysis

Variable	Minimum	Maximum
Median particle size, D_{50} (mm)	0.088	2.8
Unit discharge, q ($m^3/s/m$) [Discharge Q (m^3/s)]	0.012 [0.0032]	40 [22,000]
Slope, S	3.0×10^{-6}	3.7×10^{-2}
Hydraulic radius, r (m)	0.025	17
Temperature, T ($^{\circ}C$)	0	63
<u>Also:</u>		
Width-to-depth ratio, w/d	Greater than or equal to 4	
Geometric standard deviation of particle sizes, σ_g	Less than or equal to 5	

were restricted to values between 1 and 5, with no exceptions.

The present analysis was undertaken to develop a means of predicting hydraulic radius, which for wide channels is equivalent to mean depth. To avoid sidewall effects in laboratory data, only experiments with width to depth ratios, w/d , greater than 4 were considered. The sidewall correction suggested by Vanoni and Brooks (1957) was used to calculate the hydraulic radius of the bed, which is equivalent to the mean depth of a flow in a wide channel with the same slope, mean velocity, and bed friction factor. For most of the field data, only mean depth, and not hydraulic radius, was available. For consistency, mean depth was used in place of hydraulic radius for all field data, but w/d was restricted to values greater than 20, *i.e.* wide channels. Values of both hydraulic radius and mean depth were published for the Mississippi River at St. Louis, by Jordan (1965). A comparison of 56 measurements made during the years 1950 through 1954 indicates that hydraulic radius was 3.8 percent lower than mean depth, with a standard deviation of less than 1 percent. Therefore, the two are very closely correlated, and the difference is within the factor of uncertainty of the analysis.

The difference between the upper and the lower regime is illustrated in Fig. 4.3. Best fit lines are shown for each regime, with a one standard deviation error range indicated by dashed lines. In order to draw the two lines on the same plot, a best fit of the upper regime data was performed on the data after they were reduced to two dimensionless groups, using the regression coefficients for the lower

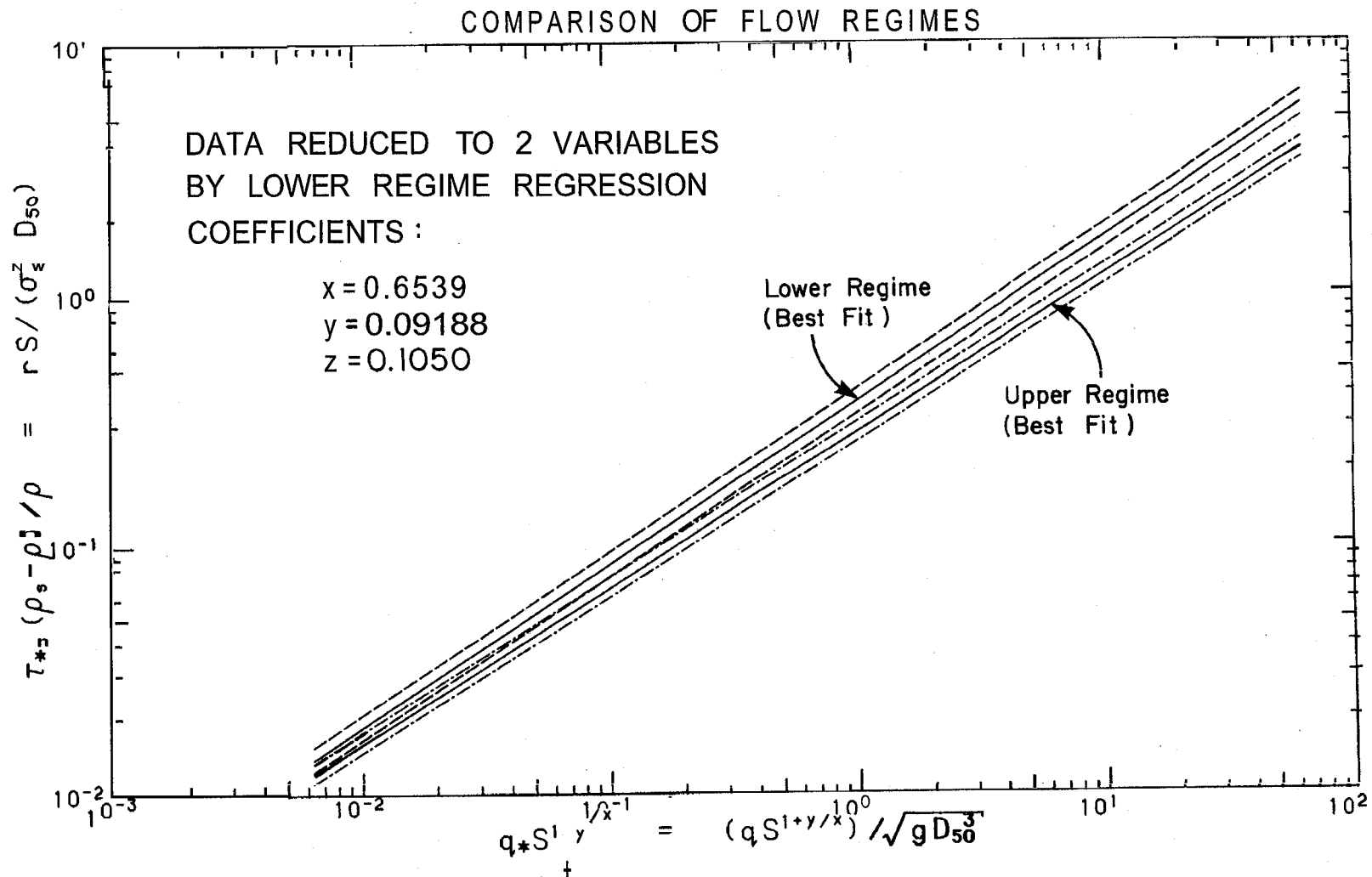


Figure 4.3 Comparison of flow regimes - solid lines represent best fit lines of data reduced to two variables by means of the lower regime values of the exponents x , y and z , dashed lines represent one standard deviation error bars.

regime, in the form of Eq. 4.7. The resulting upper regime line in Fig. 3.3 has only a slightly lower correlation coefficient than the line shown in Fig. 3.2. For a value of 10 on the abscissa of Fig. 3.3, a channel with a given slope would have an r value, in the lower regime, 36 percent larger than in the upper regime. At a value of 0.1 on the abscissa this difference would be only 18 percent.

4.3 Determination of Flow Regime

So far, for a given set of independent variables, there are two possible solutions for r , one for the upper regime, and one for the lower regime. A way of deciding which flow regime to expect is needed. From the dimensional analysis, neglecting $(\rho_s - \rho)/\rho$, the flow regime should be determinate given four independent dimensionless groups. These groups need not be the same as those used in Eq. 4.2. For a given flow regime, the mean velocity and hydraulic radius can be calculated, and can therefore be used in the new dimensionless groups.

Deformation of the bed must be a function of the forces on the particles which make up the bed. After consideration of many possible dimensionless groups, the following four were selected as indicators of flow regime:

$$F_g, \frac{D_{50}}{\delta}, S, \sigma_g$$

F_g is the grain Froude number, defined as $\sqrt{\rho} v / \sqrt{(\rho_s - \rho)g D_{50}}$, representing the square root of the ratio of drag forces on a particle

to its weight. The second parameter, D_{50}/δ , is the ratio of the mean grain size to the thickness of the laminar sublayer, and is defined by $u'_* D_{50}/11.6\nu$. The variable u'_* , the shear velocity, is assumed to be equivalent to u_* as defined by Eq. 4.6 with the upper regime coefficients, for a flow with a given slope and unit discharge. Of the final two dimensionless parameters, only slope has been used in the actual analysis, since the effects of σ_g are believed to be small, and few data are available on its impact on transition.

The flow regime relationship between F_g and S is illustrated in Fig. 4.4. The first point that is immediately obvious from Fig. 4.4 is that beyond a slope of $S = 0.006$, only upper regime flow exists. For lower values of slope, an approximate dividing line can be defined by

$$F_g = F'_g = 1.74 S^{-1/3} \quad (4.8)$$

The overlap along this line indicates that an additional variable will be needed to improve the definition of the transition zone.

In Fig. 4.5, values of F_g/F'_g for transition data with $S < 0.006$ are plotted against D_{50}/δ . Division of F_g by F'_g eliminates the bias that would be introduced by slope alone. Included with the data sets used previously is the set of data of Hill et al. (1969) which was collected for the purpose of defining the transition between the flow regimes. To include all of this data, it was necessary to waive the requirement that width-to-depth ratio be larger than four, which was adhered to for all other data sets. The transition region can be defined by the equations

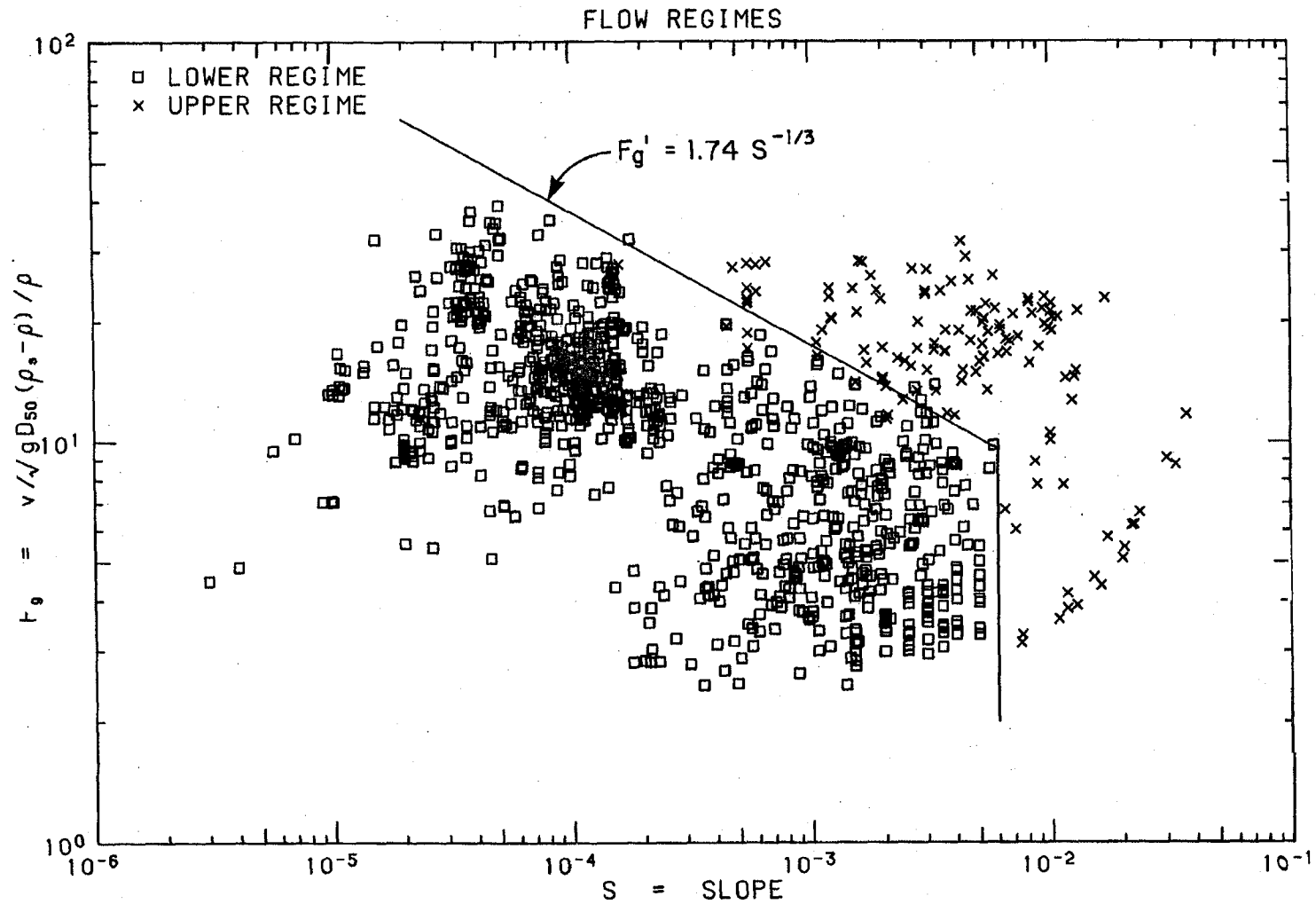


Figure 4.4 Determination of flow regimes - grain Froude number, F_g , plotted against slope, S . This diagram generally agrees with the more detailed diagrams given by Vanoni (1974).

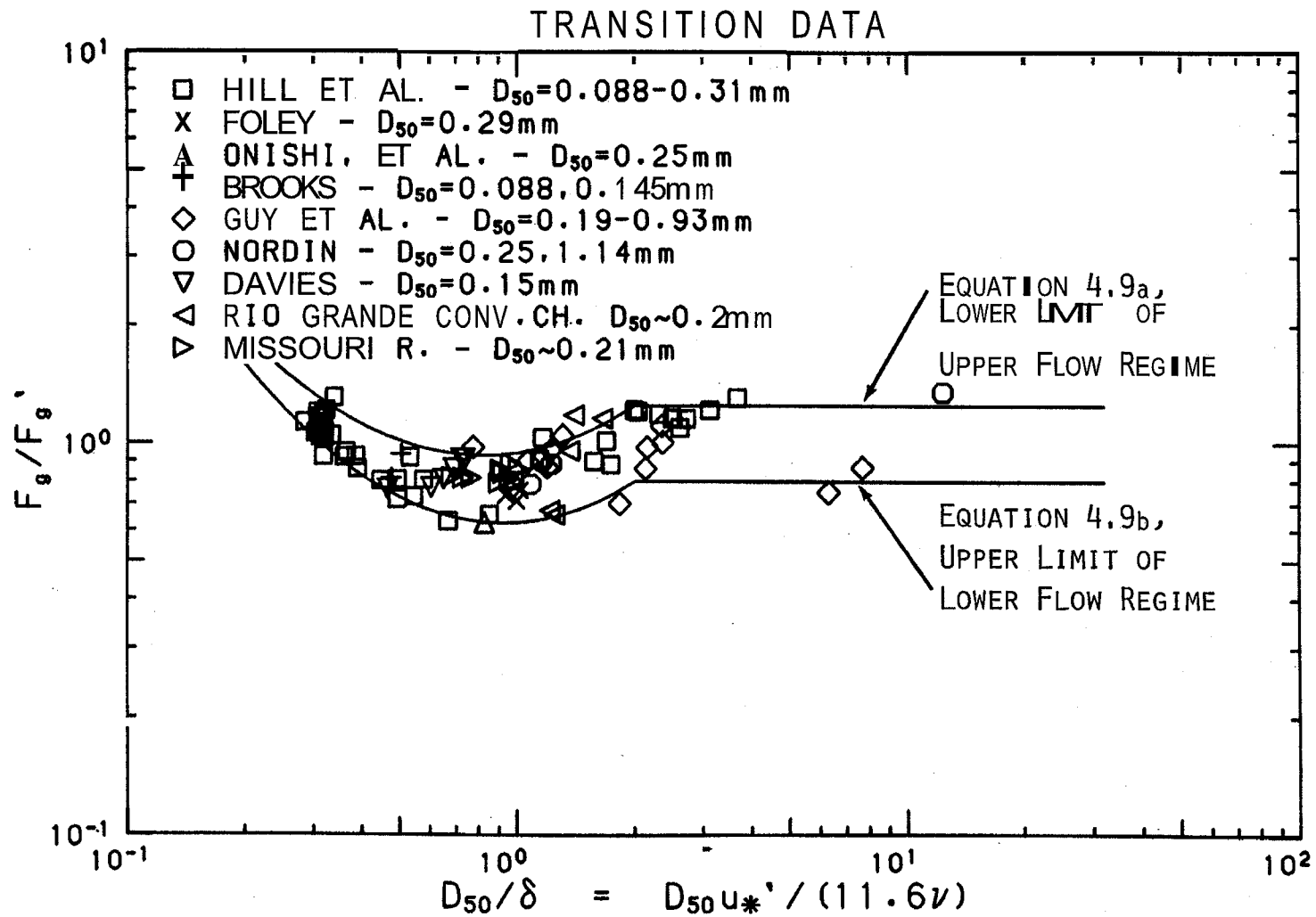


Figure 4.5 Viscous effects on the transition from lower flow regime to upper flow regime.

for the lower limit of the upper flow regime:

$$\log \frac{F_g}{F_g'} = \begin{cases} -0.02469 + 0.1517 \log \frac{D_{50}}{\delta} + 0.8381(\log \frac{D_{50}}{\delta})^2 & \dots \text{for } \frac{D_{50}}{\delta} < 2 \\ \log 1.25 & \dots \text{for } \frac{D_{50}}{\delta} \geq 2 \end{cases} \quad (4.9a)$$

and, for the upper limit of the lower flow regime:

$$\log \frac{F_g}{F_g'} = \begin{cases} -0.2026 + 0.07026 \log \frac{D_{50}}{\delta} + 0.9330(\log \frac{D_{50}}{\delta})^2 & \dots \text{for } \frac{D_{50}}{\delta} < 2 \\ \log 0.8 & \dots \text{for } \frac{D_{50}}{\delta} \geq 2 \end{cases} \quad (4.9b)$$

Between these values lies the transition regime. The value $D_{50}/\delta = 0.2$ is the lower limit of all data used in the present analysis.

By using Figs. 4.4 and 4.5 and the equations for mean shear stress for the upper and lower flow regimes, it is possible to determine which flow regime will exist for a set of independent variables. To do this it is necessary to calculate F_g' from Eq. 4.8, D_{50}/δ , and values of F_g from Eq. 4.6, using regression coefficients for both the upper and lower regimes. It is now possible to locate two points on Fig. 4.5, one for the upper regime and one for the lower regime. Three conditions are possible. The most likely condition is that only one of the two points will fall in its correct zone, in which case this flow regime is expected. A second possibility is that neither point will fall in the correct region, in which case neither solution is valid. This condition will be clarified later. Finally, for some low values of D_{50}/δ , both points will lie in their correct region of the diagram, in which case multiple solutions are possible. As formulated, this condition will be rare since, in general, the ratio of upper and lower

regime values of F_g will be less than the width of the transition zone.

To facilitate calculation of the mean velocities at which transition will take place for a particular channel with uniform flow, a final transition diagram was created (Fig. 4.6). By using the resistance equation for upper regime flow, it is possible to eliminate flow variables as input in the definition of the transition zone. Using channel variables combined with Eq. 4.9a, and, assuming transition takes place with an approximately constant value of D_{50}/δ , Eq. 4.9b. The resulting diagram, Fig. 4.6, can be used to determine the maximum flow velocity in the lower regime and the minimum velocity in the upper regime, given values of D_{50} , σ_g , S and temperature. The variable R_g in Fig. 4.6 is the grain Reynolds number, $\sqrt{gD_{50}^3}/\nu$.

4.4 Verification of Proposed Method

A method has been described which can be used either graphically or numerically to determine a rating curve or to determine depth of flow for a specific condition. It now remains to be tested for some data which have not been used in the development of the technique.

Dawdy (1961) presented data for several rivers with discontinuous rating curves, of which four sets are shown in Figs. 4.7a-d. Given S , D_{50} and σ_g , and assuming water temperature = 20° C, it is possible to derive average rating curves for the upper and lower regimes, and define an approximate transition zone, from the preceding analysis. Given the fact that the input data are of only one or two digit accuracy, the

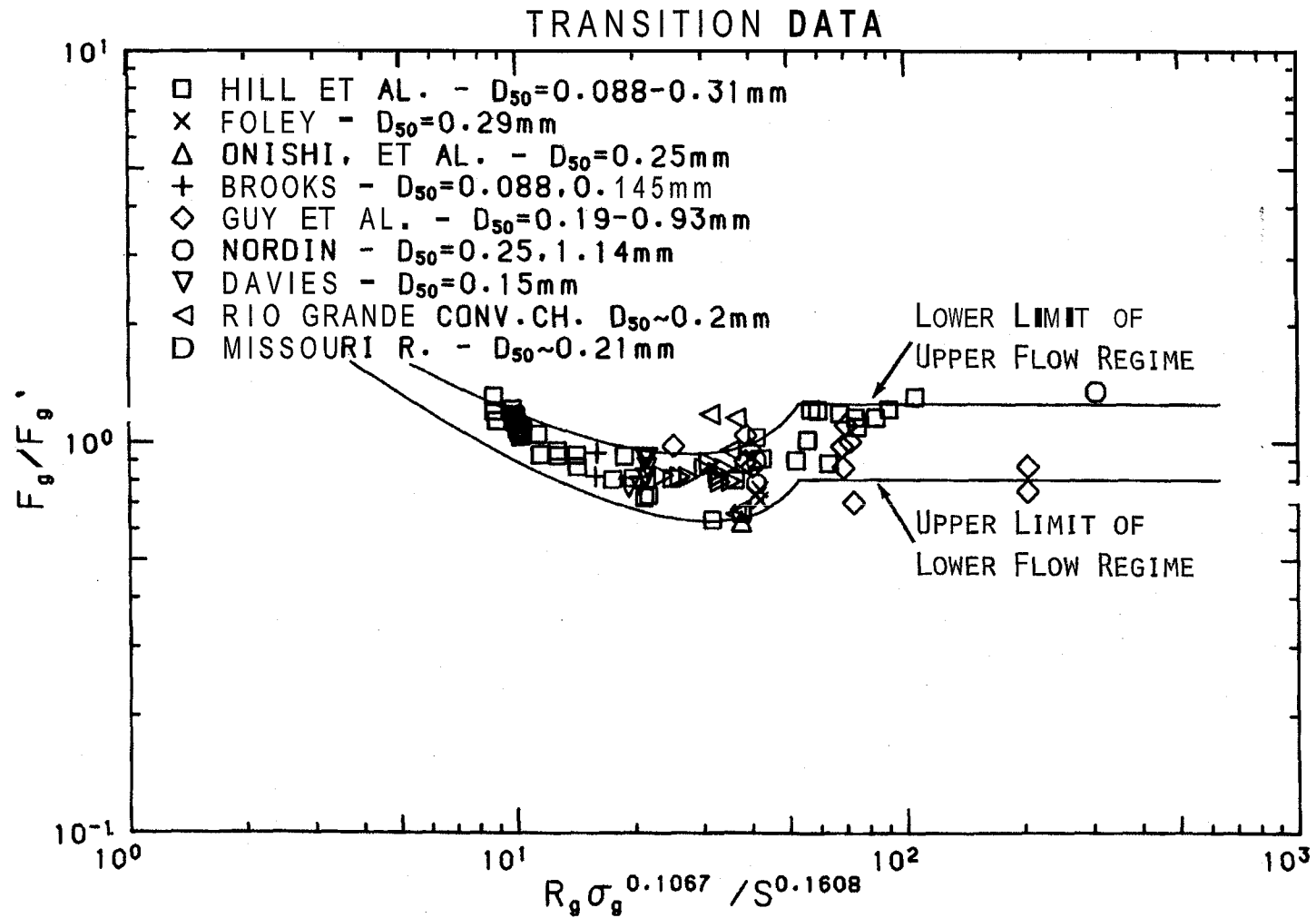


Figure 4.6 Replot of Fig. 4.5, defining the viscous effects in terms of the desired independent variables.

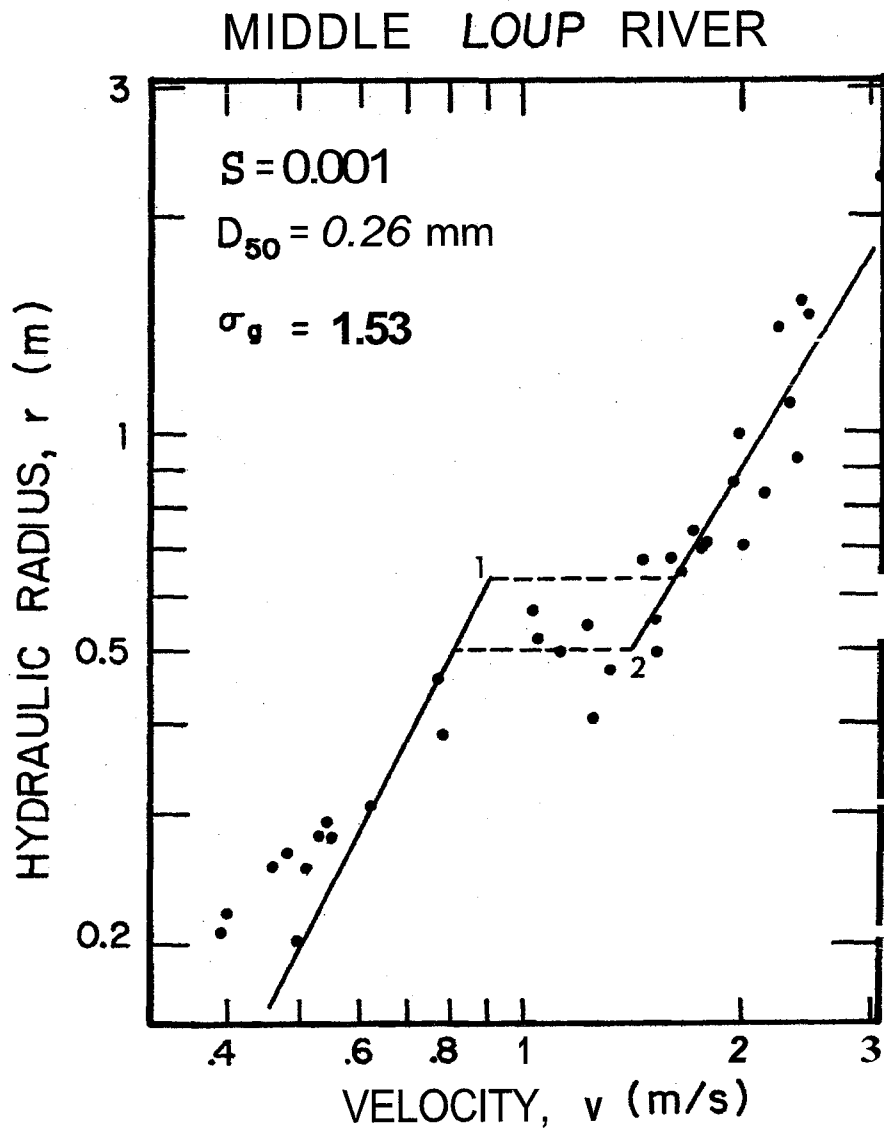


Figure 4.7a Rating curves determined by the new technique, from average bed slope and average D_{50} and σ_g , for data plots of Dawdy (1961) for Middle Loup River at St. Paul, Nebraska.

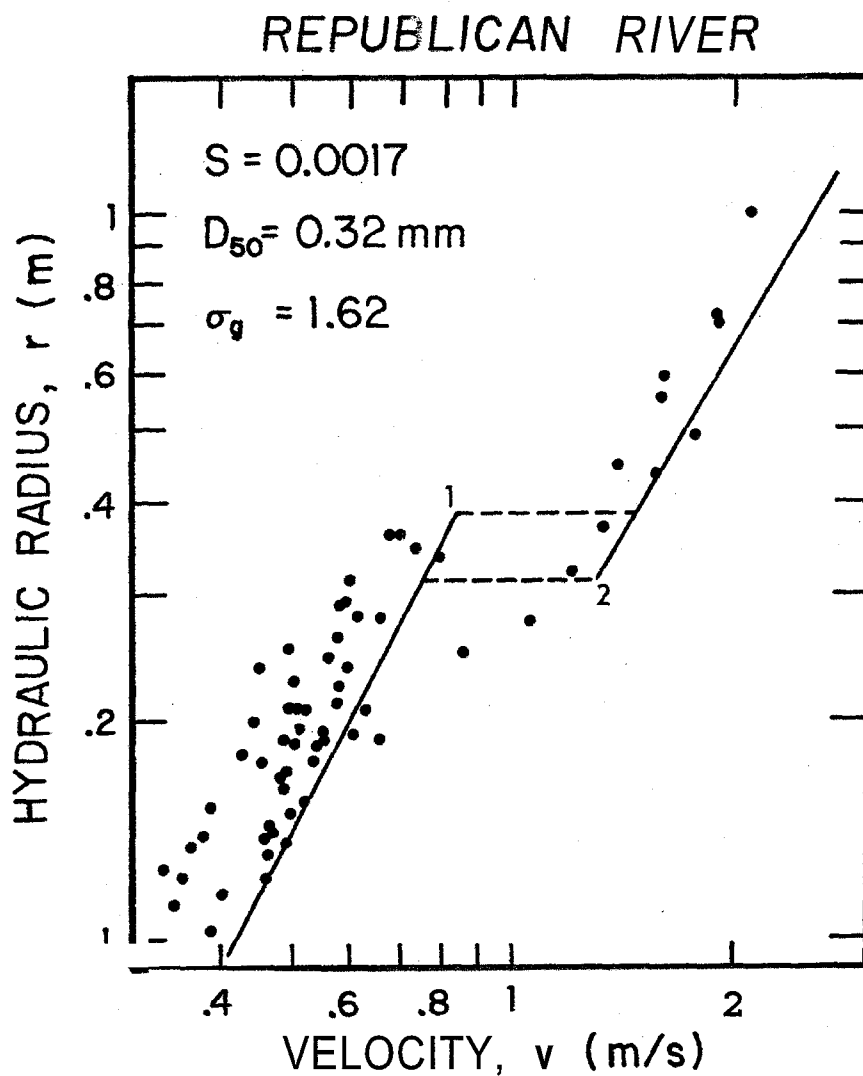


Figure 4.7b Rating curves determined by the new technique, from average bed slope and average D_{50} and σ_g , for data plots of Dawdy (1961) for Republican River at Stratton, Nebraska.

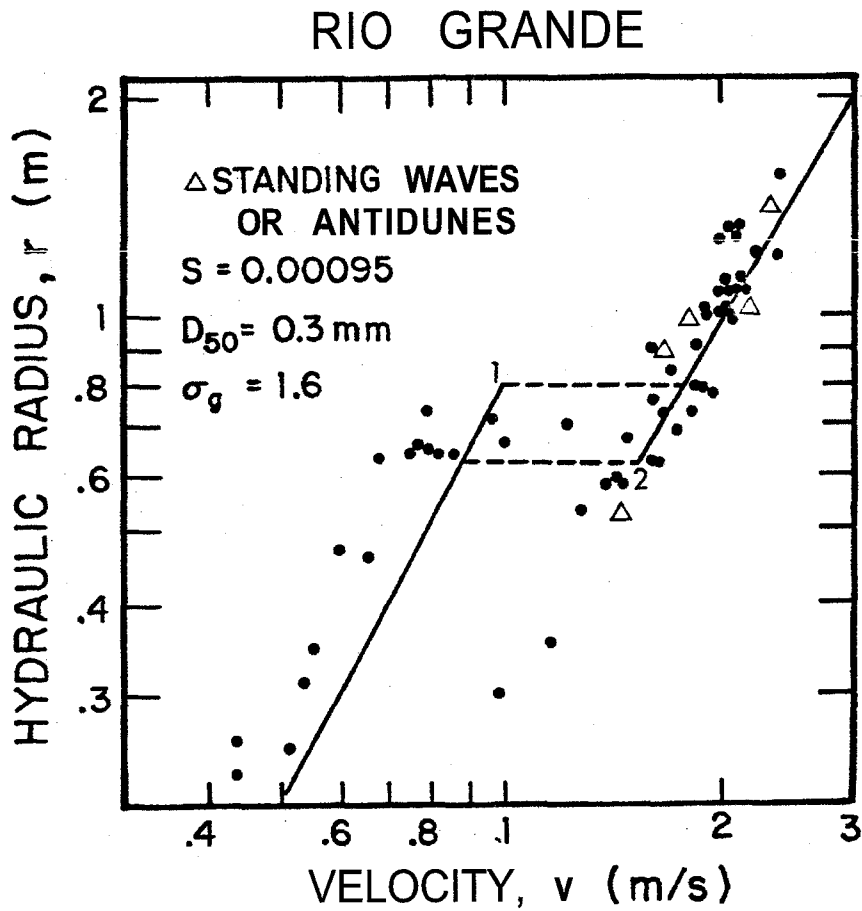


Figure 4.7c Rating curves determined by the new technique, from average bed slope and average D_{50} and σ_g , for data plots of Dawdy (1961) for Rio Grande near Bernalillo, New Mexico.

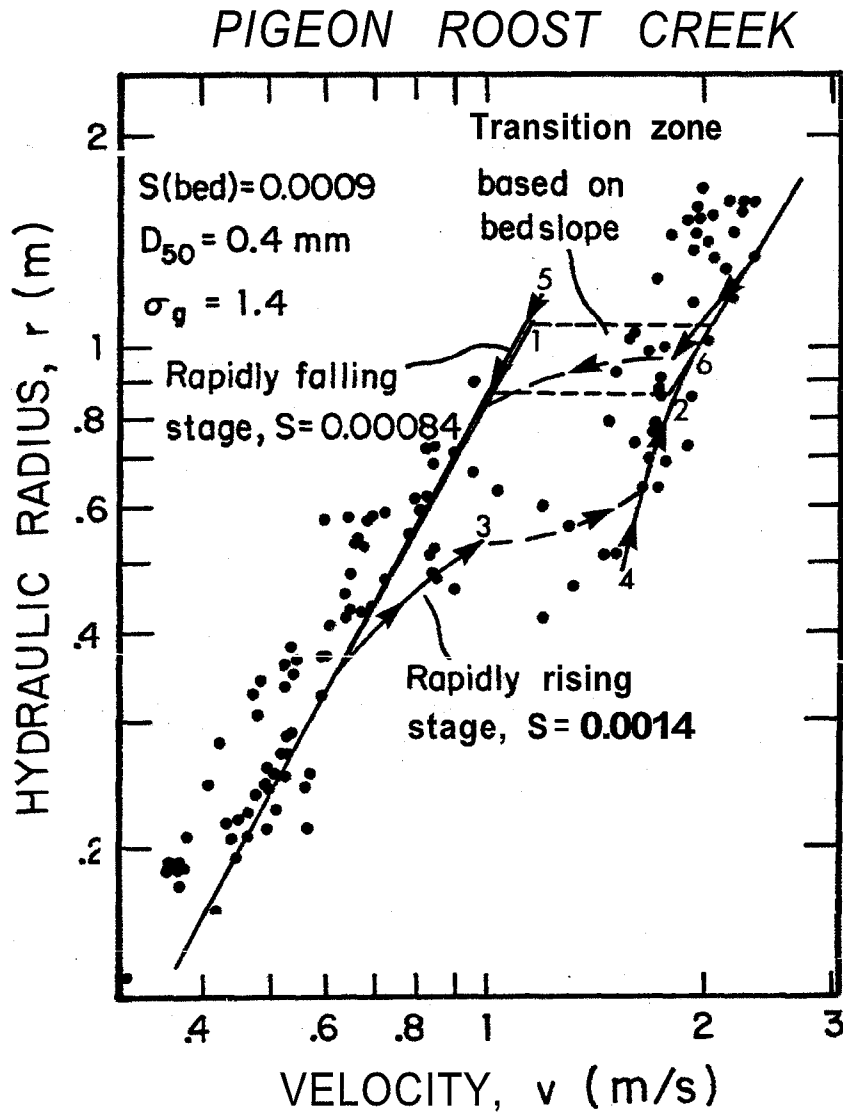


Figure 4.7d Rating curves determined by the new technique, from average bed slope and average D_{50} and σ_g , for data plots of Dawdy (1961) for Pigeon Roost Creek near Byhalia, Mississippi.

curves shown in Fig. 4.7 are quite reasonable. At 20°C , viscous effects are not important, and the location of the transition zone is based only on the slope, which is taken to equal the bed slope, and D_{50} (marked as points 1 and 2 on the diagrams). This method works reasonably well, except on Pigeon Roost Creek (Fig. 4.7d).

In an examination of discontinuous rating curves on Pigeon Roost Creek, Colby (1960) did some energy slope calculations. He found that on a nearby station with a bed slope of 0.0011 (compared to 0.0009 for the station in Fig. 4.7d), the energy slope rose to 0.0017 during a rapid rise in stage, and decreased to 0.00103 during a rapid gage-height recession. If the station under consideration underwent proportional changes in energy slope, then, by Eq. 4.9b, during a rapidly rising stage the transition zone would be defined by points 3 and 4 (Fig. 4.7d). The transition zone for the falling stage would be defined by points 5 and 6. Dashed lines indicate hypothetical paths of transition. These "dynamic" transitions fit the data much better than the uniform flow transition.

The depth of flow during transition has not been discussed, and yet in a numerical model one is required to calculate flow depth for all conditions. According to Eqs. 4.9a and 4.9b, the depth of flow at the lower limit of the upper flow regime, and the depth at the upper limit of the lower regime will be approximately the same. A reasonable estimate of flow depth during a gradual transition may be the average of the two depths. Alternatively, one might suspect that transition will take place along a line of constant depth, as indicated by the dashed

lines of Figs. 4.7a-c. In this case, during a gradual rise in discharge, the depth would reach the upper limit of the lower regime and remain constant during transition, and for a gradual decrease in discharge, the depth would reach the lower limit of the upper regime and remain constant. During a rapid transition, not only will the energy slope vary, but a certain amount of time will be required for the growth and decay of bed forms. Clearly more data are needed before we can fully understand the exact nature of the transition.

Figure 4.8 is a plot of predicted mean depth as a function of measured mean depth for the Sacramento River at Butte City (USGS station 11389000), for data given by Nakato (1981). The range of flow conditions prove to be well within the lower regime, and therefore the lower regime equation has been used. The mean error is 4.8 percent, with a standard deviation of 6.0 percent. The data range is: $s = 0.000099$ to 0.000288 , $D_{50} = 0.40$ to 6.3 mm and $\sigma_g = 1.40$ to 9.53 , with the grain parameters ranging beyond the limits used in the development of the technique. Data are also available for the Sacramento River at Colusa, but sidewall effects are too significant for the technique to produce reasonable results.

4.5 Comparison of Stage-Discharge Predictors

A rigorous statistical comparison of techniques is not given here; instead some sample calculations for two rivers are presented in Table 4.3. The two channels are the Rio Granae Conveyance Channel and the

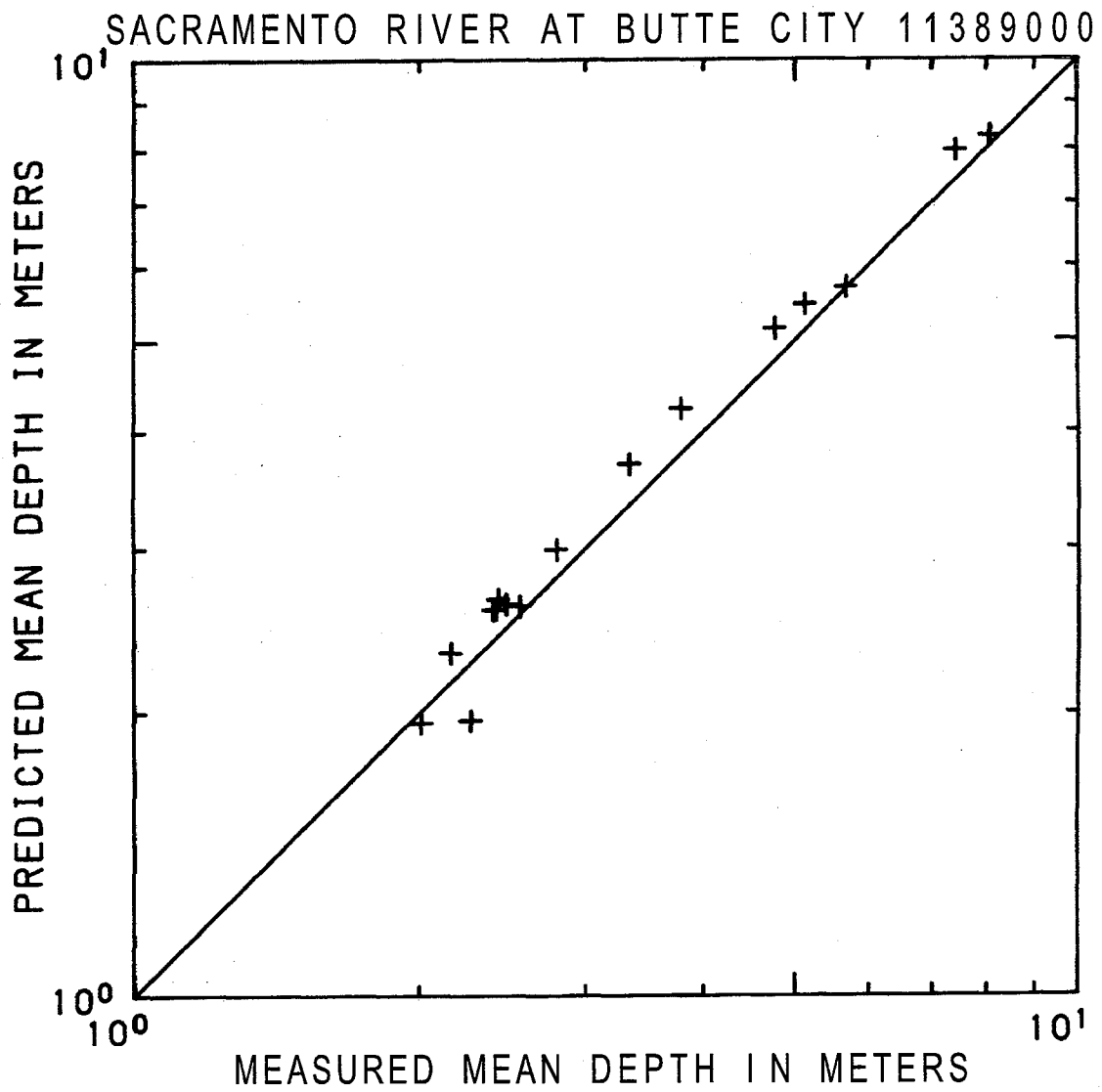


Figure 4.8 Comparison of predicted vs. actual mean depth in the Sacramento River at Butte City, data given by Nakato (1981).

Table 4.3
Comparison of Stage-Discharge Predictors

q Unit Discharge m ² /s	d Mean Depth ¹ m	S x 1000 Slope	D50 Median Bed Size mm	σg Geometric Standard Deviation Bed Mat ¹	T Temp. °C	Predicted Mean Depth ¹ , m (% Error)						
						Alam et al.	Chu, Mostafa	Einstein, Barbarossa	Engelund	Garde Ranga Raju	White et al.	New Method ²
						Rio Grande Conveyance Channel						
0.225	0.403	0.50	0.25	1.48	20	0.50 (25%)	0.36 (-10%)	0.47 (18%)	0.35 (-13%)	0.46 (14%)	0.39 (-1%)	0.41 (2%)
0.693	0.769	0.55	0.19	1.40	11	0.61 (-21%)	0.58 (-25%)	0.57 (-26%)	0.55 (-29%)	0.80 (4%)	0.79 (3%)	0.82 (7%)
2.01	1.19	0.60	0.23	1.36	13	0.99 (-17%)	1.29 (10%)	0.94 (-21%)	1.13 (-5%)	1.60 (34%)	1.52 (28%)	1.10 (-7%)
						Mississippi River, Tarbert Landing, LA						
4.74	7.59	0.0183	0.31	1.66	21	NS ³	NS	17 (124%)	8.2 (8%)	7.1 (-7%)	7.4 (-3%)	7.1 (-7%)
10.4	10.7	0.0266	0.25	1.81	24	NS	NS	17 (59%)	11 (4%)	11 (4%)	12 (8%)	11 (1%)
26.0	16.7	0.0382	0.30	1.63	18	NS	NS	19 (14%)	12 (-26%)	18 (6%)	19 (17%)	18 (7%)

69

1. For the channels under consideration, it is assumed that $d = r$.
2. The Rio Grande record at $q = 2.01 \text{ m}^2/\text{s}$ is an upper regime flow, all others are lower regime.
3. NS: No solution for the given combination of independent variables.

Mississippi River at Tarbert Landing, Louisiana. The **former** is a channel with typical depths of 1 meter, and the latter with typical depths of 10 to 20 meters. For both channels, the lowest, highest, and median discharges of the available record are given.

The results are considerably varied, Both the Alam-Cheyer-Kennedy and Chu-Mostafa techniques were not applicable to the deeper river. The poorest results were obtained from the Einstein-Barbarossa technique. The Engelund technique gave good results, except when the wrong flow regime was predicted, as for the second Rio Grande and third Mississippi values. The Garde-Ranga **Raju** and White-Paris-Bettess techniques did very well, except for the last Rio Grande flow, which had a flat bed.

4.6 Summary and Conclusions

An analysis of existing schemes **for** predicting flow depth in sand bed streams and rivers has indicated that no existing technique satisfies the criteria established in the introduction to this paper. A new technique has been presented which does satisfy these criteria. The technique solves for flow depths and mean velocities for the upper and lower flow regimes and determines limits of the mean velocity for each regime.

For wide channels, with $d = r$, flow depth for the lower flow regime can be determined from:

$$\frac{rS}{D_{50}} = 0.3724 (q_* S)^{0.6539} S^{0.09188} \sigma_g^{0.1050} \quad (4.10a)$$

and for the upper flow regime, from:

$$\frac{rS}{D_{50}} = 0.2836 (q_* S)^{0.6248} S^{0.08750} \sigma_g^{0.08013} \quad (4.10b)$$

Either equation can be rearranged into a dimensionally consistent power law equation which can be directly substituted for a Manning equation in a numerical model. For flow situations involving both regimes, a transition mechanism is required. The nature of this mechanism has not as yet been explored.

Neglecting viscous effects, the upper and lower transitional velocities can be determined from the slope and the median grain size. For slopes greater than 0.006, only upper regime flow is expected. For slopes less than 0.006, the maximum velocity of the lower regime can be determined from $F_g = 0.8F'_g$, and the minimum velocity of the upper regime from $F_g = 1.25F'_g$, where F'_g is from Eq. 4.8.

When temperature effects are important the transition values of F_g must be determined from Eqs. 4.9a and 4.9b or Fig. 4.5. For a given S , R_g , and a_g , F_g can also be determined from Fig. 4.6. Depending on the ratio of the median grain size to the thickness of the laminar sublayer, any change in temperature may either increase, decrease or have no influence on the transitional velocities. The maximum temperature effect is about a 25 percent change in the velocities of the limits of the flow regimes.

A review of the extensive literature on alluvial channels suggests that, in spite of the volume, little is known about the transition from the lower flow regime to the upper flow regime. Carefully collected

data are needed to better understand both slowly varying and rapidly varying transitions. Although the new technique includes a definition of the transition limits, the writer feels that more information is needed to improve the definition of these limits.

CHAPTER 5

AN ANALYSIS OF METHODS FOR PREDICTING SEDIMENT CONCENTRATION

Having considered the problem of predicting flow depth in a channel, attention is now turned to the problem of predicting sediment concentration. Throughout this century dozens of techniques, or "sediment transport formulas," have been proposed. Early efforts were hampered by a poor understanding of the mechanics of turbulence and sediment entrainment, poor data, and the absence of computers. While the mechanics are still not well understood, at least it is possible to readily analyze the large amounts of data that are now available. In this chapter, 13 techniques for predicting sediment concentration in a channel are analyzed using both field and laboratory data.

In the discussion that follows, the wash load or fine-material load is not considered. Therefore, the bed-material load is taken to be equivalent to the total load, which can be divided into a bed load and a suspended load.

5.1 Selection of Available Techniques

The available techniques for calculating sediment concentration are widely varied. They range from simple equations to complicated procedures involving many calculations. The techniques selected for analysis in this chapter likewise cover a wide range of computational expediency.

Probably the most computationally complex procedure is still the Einstein (1950) total load function. To begin the procedure, the bed material is divided into size fractions. An integration over the flow depth is required for each size fraction. The integrand is the product of the suspended load equation (Vanoni, 1975, p. 76):

$$\frac{C(y)}{C_a} = \left(\frac{d-y}{y} \frac{a}{d-a} \right)^z \quad (5.1)$$

where C_a is a reference concentration at elevation a , and the velocity distribution (Vanoni, 1975, p. 75):

$$v(y) = \frac{2.3u_*'}{k} \log \frac{y}{d} + v_{\max} \quad (5.2)$$

where k = von Karman's constant and has a mean value of 0.4 for clear water.

Einstein (1950) uses the values $z = w_i / 0.4u_*'$ and $a = 2D_{s1}$, where w_i and D_{s1} are the fall velocity and mean grain diameter, respectively, of a size fraction." The reference concentration is determined from the empirical "bed load function" which relates a dimensionless bed load transport rate to a dimensionless grain shear stress. A full description of the procedure, including the various correction factors, is given by Vanoni (1975, pp. 195-201).

Several investigators have attempted to modify or adapt either all or parts of the Einstein (1950) procedure. In the development of his procedure, Toffaleti (1968) used many of Einstein's concepts and a large amount of newer data. Engelund and Fredsoe (1976) derived an analytical bed load equation and used Einstein integrals for the suspended load.

In this case u_' can be defined from Eq. 3.13.

These techniques are appealing because they rely on what is known of the mechanics of the processes involved. However, our current understanding of the processes is still incomplete, and the derivations of these techniques include various assumptions.

Other investigators have relied heavily on dimensional analysis. This approach usually avoids the problem of dividing the bed-material load into a bed load component and a suspended load component. Typically, sediment concentration or a dimensionless transport rate is related to several other dimensionless parameters. One of these parameters usually varies strongly with discharge and can therefore be considered as the principal variable. Examples of principal variables are the mobility number of Ackers and White (1973), a parameter combining shear stress and grain shear stress, and the unit stream power used by Yang (1973), v_s/w , where w is particle fall velocity.

When the formulation of a technique is based primarily on dimensional analysis, the data base becomes extremely important. A technique would be useless if it were based on faulty or insufficient data. Although large amounts of data are now available, the quality of the data is not uniform, primarily because of the difficulty involved in making sediment concentration measurements.

In this chapter, 13 techniques were selected for analysis. It is hoped that the presentation here will complement the excellent appraisal of 15 methods given by White, Milli, and Crabbe (1973). Eight of the 10 best methods as appraised by White, Milli, and Crabbe (1973) have been included here. Of the best ten methods, the two that have not been

included here are a modified version of the Bishop, **Simons** and Richardson (1965) technique (which has been included) and the bea load portion of the Einstein (1950) procedure, which has not been considered apart from the total load procedure. Also included are three newer methods, plus two other techniques which have achieved some degree of acceptance. A list of the 13 techniques is given in Table 5.1 .

5.2 Method of Analysis

One of the most important aspects of an appraisal of existing techniques is the data base. For this analysis approximately 1000 records from 31 sets of laboratory and field data have been selected from the larger data bank. Data sets with sand bed channels were selected on the basis of accuracy and range of important parameters. After performing a sidewall correction (Vanoni and Brooks, 1957) on all records, the data were filtered to remove various biases, thus leaving the approximately 1000 records.

The data sets used and ranges of **important** variables are listed in Tables 5.2a and 5.2b. The numerical filters or **restrictions** on the ranges of certain parameters are given in Table 5.3. More explanation of why some of these filters were selected is given in the next chapter, section 6.2.

The number of records for each data set listed in Tables 5.2a and 5.2b is the number available for analysis. For some formulas, certain combinations of variables may be beyond the **explicitly** derived range of

Table 5.1

Methods of Predicting Sediment Concentration
Analyzed in this Report

<u>Investigator</u>	<u>Date</u>	<u>Graded Sediment</u>	<u>Bed Load and Suspended Load Separate</u>	<u>Dimensional Homogeneity</u>
Ackers and White	1973	No	No	Yes
Bagnold	1966	No	Yes	Yes
Bishop, Simons, and Richardson	1965	Yes	No	Yes
Einstein	1950	Yes	Yes	Yes
Engelund and Fredsoe	1976	No	Yes	Yes
Engelund and Hansen	1967	No	No	Yes
Graf	1968	No	No	Yes
Laursen	1958	Yes	No	Yes
Ranga Raju, Garde, and Bhardwaj	1981	No	No	Yes
Rottner	1959	No	No	Yes
Shen and Hung	1971	No	No	No
Toffaletti	1968	Yes	Yes	No
Yang	1973	No	No	Yes

Table 5.2a

Range of Laboratory Variables

Source	Code	No.	Velocity(m)		Depth(m)		Slope X 1000		D ₅₀		Concentration(ppm)	
			Min.	Max.	Min.	Max.	Min.	Max.	Min.	Max.	Minimum	Maximum
Barton & Lin (1955)	BAL	26	0.226	1.093	0.091	0,256	0.440	2.100	0.180	0.180	19.00	3776.00
Brooks (1957)	BRO	6	0.373	0,617	0,047	0.060	2.400	3,500	0.088	0.145	1200.00	5300.00
Costello (1974)	COS	11	0.403	0,503	0.140	0,156	0,450	1,010	0,600	0,790	10.95	102.08
Davies (1971)	DAV	69	0.244	0.792	0,076	0,305	0.248	2.670	0.150	0,150	11.30	1760.00
Foley (1975)	FOL	9	0.388	0.806	0,035	0,047	3.740	10.540	0,290	0,290	845.34	10254.39
Guy et al.(1966)	GUY1	27	0.317	1.445	0.149	0.332	0.430	5.820	0.190	0.190	29.00	26600.00
Guy et al.(1966)	GUY2	47	0,318	1.505	0.091	0,344	0.450	8.200	0,270	0.280	12.00	28700.00
Nordin (1976)	NOR1	22	0.561	2.017	0,238	0,585	0.470	4.490	0.250	0.250	73.00	17200.00
Nordin (1976)	NOR2	11	0,524	1.843	0.256	0,359	0.740	5.770	1.140	1,140	33.00	2920.00
Onishi et al.(1976)	OJK	14	0.338	0,585	0,075	0.135	1.090	2.670	0.250	0.250	66.79	3355.67
Pratt (1970)	IRA	25	0,254	0.701	0.076	0.305	0,282	2,870	0.479	0,479	11.63	560.00
Singh (1960)	SIN	20	0.277	0.442	0,076	0.104	1,000	3.000	0,620	0,620	35.70	454.00
Stein (1965)	STE	44	0,514	1.841	0.091	0.302	2,010	16,950	0.399	0.399	640.00	39293.00
Straub (1954,58)	STR	21	0.356	0,835	0.035	0.222	0.950	7.347	0.163	0,191	423.00	12600.00
Taylor (1971)	TAY	12	0,390	0.878	0.079	0.143	1.010	2.090	0,228	0,228	100.27	2269.74
Vanoni, Brooks(1957)	VAB	14	0,234	0.771	0.062	0.169	0.700	2.800	0.137	0.137	37.00	3000.00
Vanoni, Hwang (1967)	VAH	6	0.319	0,558	0.176	0,238	0.642	1.303	0.206	0,206	31.00	1490.00
Williams (1970)	WM	5	0.539	0.669	0.204	0.222	0.912	2.140	1.349	1.349	31.13	196.10
Willis (1972)	WLS	77	0.358	1.572	0,104	0,302	0,269	2,040	0.100	0,100	102.00	19399.99
Znamenskaya (1963)	ZNA	14	0.224	0.925	0.040	0,123	1.660	8,000	0.180	0.800	150.00	3240.00
All Laboratory Data		480	0.224	2.017	0.035	0.585	0,269	16.950	0,088	1.349	10.95	39263.00

Table 5.2b

Range of Field Variables

River	Code	No.	Velocity(m)		Depth(m)		Slope X 1000		D ₅₀		Concentration(ppm)	
			Min.	Max.	Min.	Max.	Min.	Max.	Min.	Max.	Minimum	Maximum
Atchafalaya River	ATC	63	0.574	2.028	6.401	14.752	0.010	0.051	0.086	0.303	12.52	567.34
Colorado River	COL	30	0.663	1.001	1.134	3.139	0.147	0.333	0.273	0.400	78.30	412.70
Hii River, Japan	HII	22	0.630	0.803	0.202	0.493	0.840	1.660	1.330	1.440	116.31	552.86
Middle Loup River	MID	38	0.593	1.125	0.247	0.412	0.928	1.572	0.215	0.436	437.76	2444.00
Miss. R., St. Louis	COE1	111	0.621	2.423	4.663	17.282	0.025	0.134	0.163	1.129	11.70	511.71
Miss. R., Tarbert	COE2	53	0.625	1.609	6.736	16.429	0.018	0.043	0.165	0.346	12.07	261.68
Mountain Creek	MOU	75	0.366	0.652	0.108	0.272	1.360	1.790	0.899	0.899	26.76	686.10
Niobrara River	NIO	40	0.625	1.271	0.398	0.588	1.136	1.799	0.212	0.359	392.00	2750.00
Red River	RED	29	0.407	1.140	2.999	7.376	0.066	0.082	0.094	0.217	20.92	499.75
Rio Grande Conv, Ch.	RGC	8	0.805	1.518	0.923	1.512	0.530	0.800	0.180	0.280	674.00	2695.00
RioGrande, Bernalillo	RGR	50	0.441	2.384	0.305	1.463	0.740	0.930	0.197	0.424	315.00	5830.00
All Field Data		519	0.366	2.423	0.108	17.282	0.010	1.799	0.086	1.440	11.70	5830.00

Table 5.3

Restrictions on Input Data

Parameter	Symbol	Restriction	Reason
Median grain size, mm	D_{50}	$0.062 \leq D_{50} \leq 2.0$	Sand only
Geometric standard deviation of bed particles	σ_g	$\sigma_g < 5$	Eliminate bimodal distributions
Width to depth ratio	w/d	$w/d > 4$ (Lab Data)	Reduce sidewall effects
Relative roughness	r/D_{50}	$r/D_{50} > 100$	Eliminate shallow water effects
Concentration, ppm	C	$C > 10$	Accuracy problems associated with low concentration

the technique. In other cases, certain combinations of variables will lead to non-definable expressions, such as a negative number raised to a non-integer power. Furthermore, calculated concentrations lower than 1 ppm are not included in statistical analyses. Therefore, for some formulas the actual number of records given in the analyses may be considerably less than that indicated in Tables 5.2a and 5.2b.

Some formulas require separate calculations for individual bed-material size fractions. In these cases, the bed material has been divided into 5 size fractions based on the values of D_{50} and σ_g , and the assumption that the size distribution of the bed particles is log-normal. Divisions were located at the 6.7, 31.0, 69.0, and 93.3 percentile values.

Selection of a technique for analysis of a transport formula is not a simple matter. After consideration of a number of possible analysis variables, the ratio of calculated to observed concentration was selected. This variable was also used by White, Milli, and Crabbe (1973) in their appraisal of formulas.

It was found that for a given formula, the ratio of the calculated to the observed concentration is nearly log-normally distributed for many data sets. Figures 5.1a and 5.1b are log-probability plots of this ratio for the Yang (1973) technique. On this type of graph a log-normal distribution plots as a straight line.

A parameter that is log-normally distributed can be described by its geometric mean and geometric standard deviation. The geometric mean and geometric standard deviation are the **antilogs** of the mean and

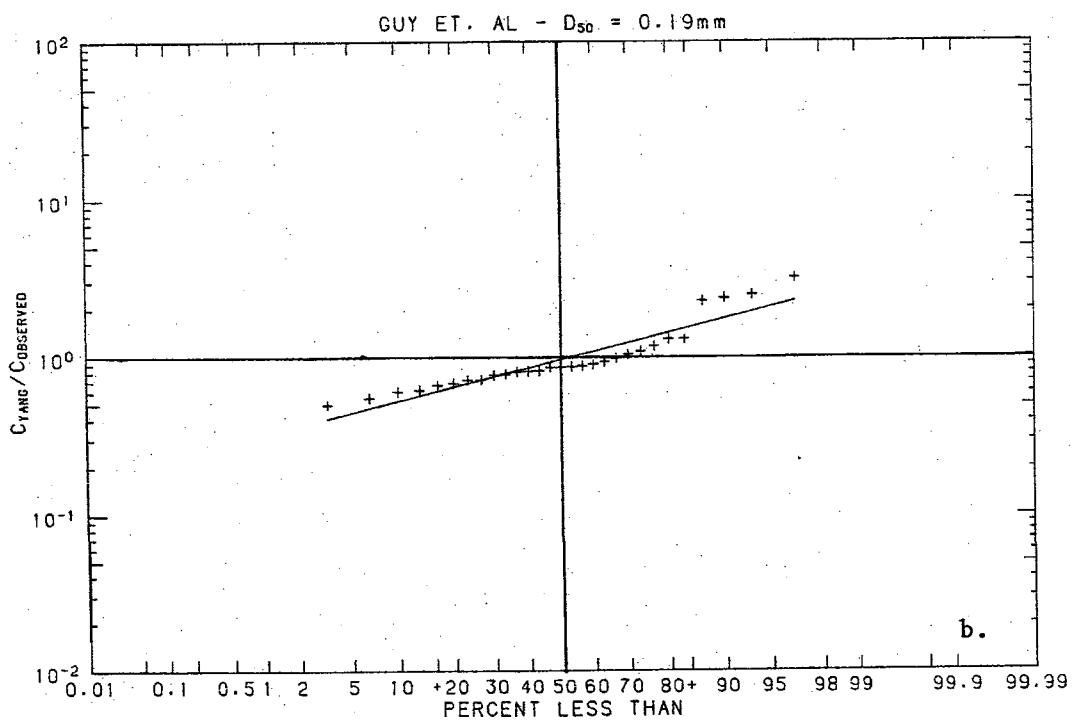
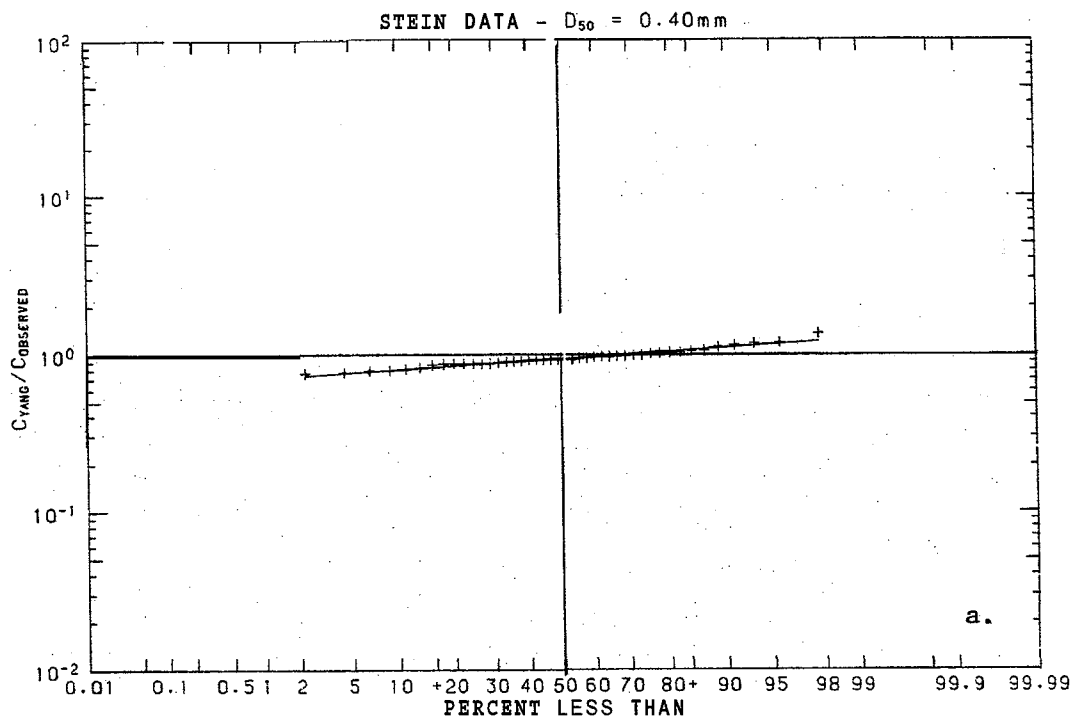


Figure 5.1 Typical error distributions for the Yang (1973) technique.

standard deviation, respectively, of the logarithms of the values of the parameter. If a parameter is log-normally distributed its median value will be equivalent to its geometric mean. Furthermore, the eighty-fourth percentile value can be determined by the product of the geometric mean and the geometric standard deviation, and the sixteenth percentile value will be the quotient of the geometric mean divided by the geometric standard deviation.

For the ratio of calculated to observed concentration, geometric mean and geometric standard deviation values of 1 would indicate perfect agreement. The geometric standard deviation will be greater than or equal to 1, while the geometric mean can be greater than or less than 1, depending on whether the formula tends to over-predict or under-predict.

For each formula, two tables of statistics are given, one for laboratory data and one for field data. Each table gives the geometric mean and geometric standard deviation (abbreviated **Geo.Mean** and **Geo.S.D.**, respectively) for the ratio of calculated to observed values of concentration for each data set. The data sets are listed by the codes in Tables 5.2a and 5.2b. The tables include estimates of the sixteenth and eighty-fourth percentile values, calculated from the geometric mean and geometric standard deviation, assuming a log-normal distribution. The minimum, median, and maximum values of the ratio are also given for each data set. The last line in each table gives the statistics for all of the data included in the table.

The analysis of each formula includes two plots of the ratio of calculated to observed concentration versus observed concentration, one

for lab data and one for field data. Each data set is plotted with a different plotting symbol. Dashed lines show the geometric mean value of the plotted data, and dash-dotted lines show the approximate sixteenth and eighty-fourth percentile values.

5.3 Appraisal of Existing Techniques

The following is an analysis of the 13 techniques for predicting sediment concentration listed in Table 5.1. For each technique, a brief summary is presented along with the figures and tables which can be used to evaluate the performance of the technique. The summaries do not include complete descriptions of all techniques. In conjunction with the reviews of methods given by Vanoni (1975) and White, Milli, and Crabbe (1973), however, the reader can obtain a complete understanding of the workings of all the techniques discussed here. (Page number references for the latter report refer to the first volume, unless otherwise specified.)

The equations give the mean concentration in terms of ~~mass~~ per unit mass, i.e. mass of sediment to mass of water-sediment mixture, with the exception of the technique of Shen and Hung (1971). This technique, which is not dimensionally homogeneous, is given in its original form where concentration is given in ppm by mass. To convert to parts per million, all other concentrations must be multiplied by 1,000,000.

5.3.1 Ackers and White Technique (1973)

The Ackers and White (1973) method is based on a combination of grain shear stress and shear stress. The basic concentration equation is

$$C = c \frac{\rho_s}{\rho} \frac{D_{50}}{r} \left(\frac{v}{u_*'} \right)^n \left[\frac{F_{gr}}{A} - 1 \right]^m \quad (5.3)$$

where F_{gr} is the mobility number defined by

$$F_{gr} = \frac{u_*'^n u_*'^{1-n}}{\sqrt{g D_{50} \left(\frac{\rho_s - \rho}{\rho} \right)}} \quad (5.4)$$

and u_*' is given by

$$u_*' = \frac{v}{\sqrt{32} \log \frac{10r}{D_{50}}} \quad (5.5)$$

The quantities n , A , m , and c are functions of D_{gr} which is defined by

$$D_{gr} = \left[\sqrt{\frac{\rho_s - \rho}{\rho}} R_g \right]^{2/3} \quad (5.6)$$

where $R_g = \sqrt{g D_{50}^3} / v$ is the grain Reynolds number.

When $D_{gr} > 60$ the four coefficients are:

$$n = 0.0$$

$$A = 0.17$$

$$m = 1.5$$

$$c = 0.025$$

and for $60 \geq D_{gr} \geq 1$:

$$n = 1 - 0.56 \log D_{gr}$$

$$A = \frac{0.23}{\sqrt{D_{gr}}} + 0.14$$

$$m = \frac{9.66}{D_{gr}} + 1.34$$

$$\log c = 2.86 \log D_{gr} - (\log D_{gr})^2 - 3.53$$

The results of the analysis for laboratory data are given in Fig. 5.2a and Table 5.4a, and for field data, the results are given in Fig. 5.2b and Table 5.4b.

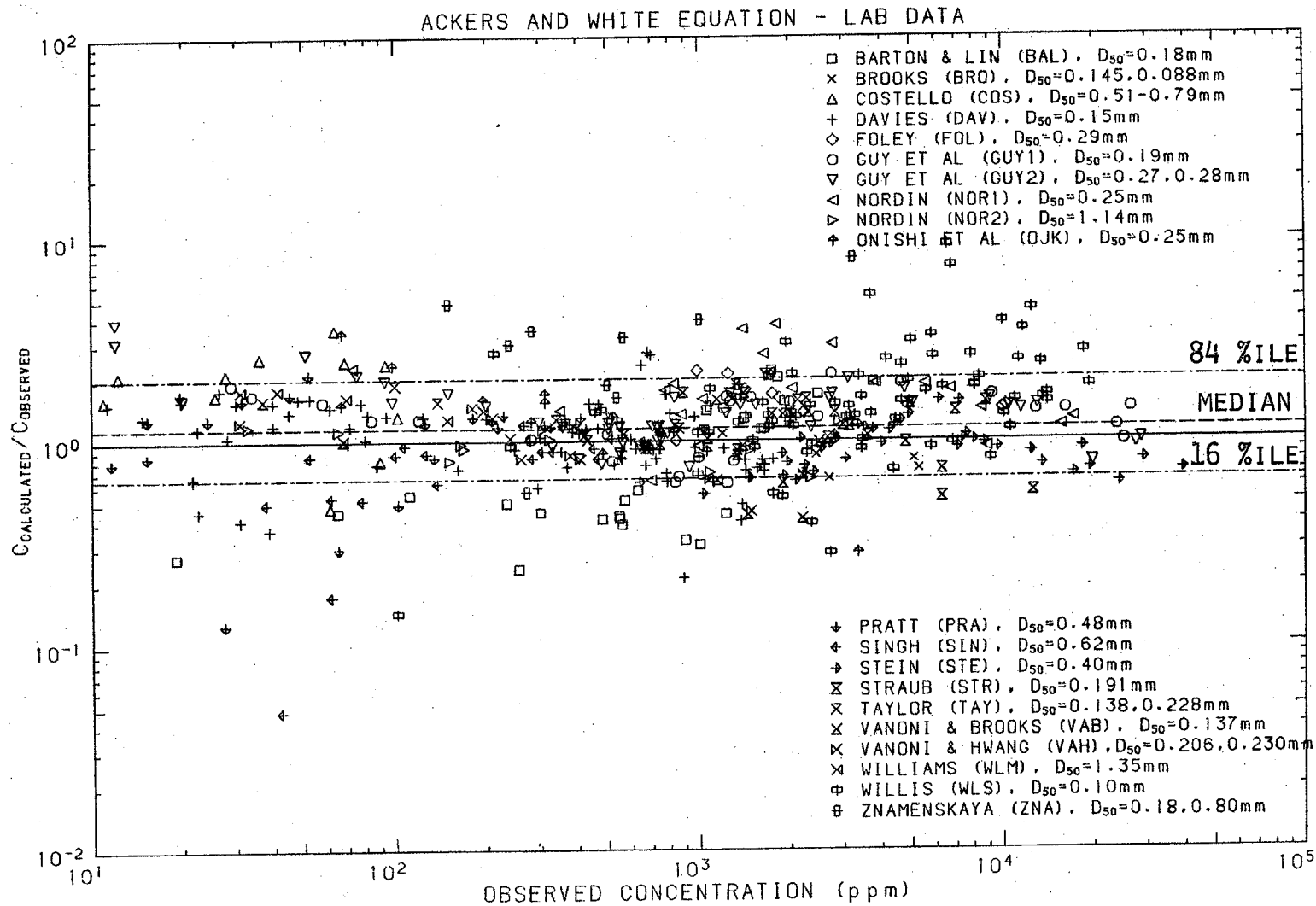


Figure 5.2a Ratio of concentration calculated by the Ackers and White (1973) technique to observed concentration as a function of observed concentration, for laboratory data.

Table 5.4a

Ratio of Predicted to Observed Conc. for Ackers and White Method - Lab Data

Data Set	Number	Geo.Mean	Geo.S.D.	Minimum	16 %ile	Median	84 %ile	Maximum
BAL	26	0.719	2.035	0.237	0.353	0.513	1.464	2.199
BRO	6	0.881	1.276	0.649	0.690	0.810	1.124	1.336
COS	11	1.699	1.735	0.474	0.979	2.117	2.948	3.561
DAV	69	0.986	1.579	0.214	0.625	0.926	1.557	2.730
FOL	9	1.588	1.253	1.005	1.267	1.609	1.990	2.203
GUY1	27	1.236	1.412	0.618	0.875	1.397	1.745	2.106
GUY2	47	1.347	1.429	0.741	0.943	1.352	1.925	3.919
NOR1	22	1.659	1.546	0.640	1.073	1.766	2.565	3.745
NOR2	11	0.950	1.227	0.649	0.774	0.971	1.165	1.234
OJK	14	1.226	1.745	0.281	0.702	1.252	2.138	3.415
PRA	25	1.034	1.782	0.128	0.580	1.210	1.843	2.131
SIN	19	0.652	2.110	0.048	0.309	0.861	1.375	1.203
STE	44	0.881	1.288	0.548	0.684	0.914	1.134	1.570
STR	21	1.104	1.379	0.524	0.801	1.169	1.523	1.719
TAY	12	1.361	1.255	0.956	1.085	1.276	1.707	1.887
VAB	14	0.880	1.510	0.414	0.583	0.941	1.330	1.593
VAH	6	0.883	1.455	0.450	0.607	0.824	1.286	1.468
WLM	5	1.569	1.140	1.282	1.376	1.638	1.788	1.788
WLS	77	1.487	1.889	0.145	0.787	1.464	2.808	9.277
ZNA	14	2.161	1.944	0.564	1.111	1.867	4.200	7.966
All	479	1.150	1.758	0.048	0.654	1.180	2.022	9.277

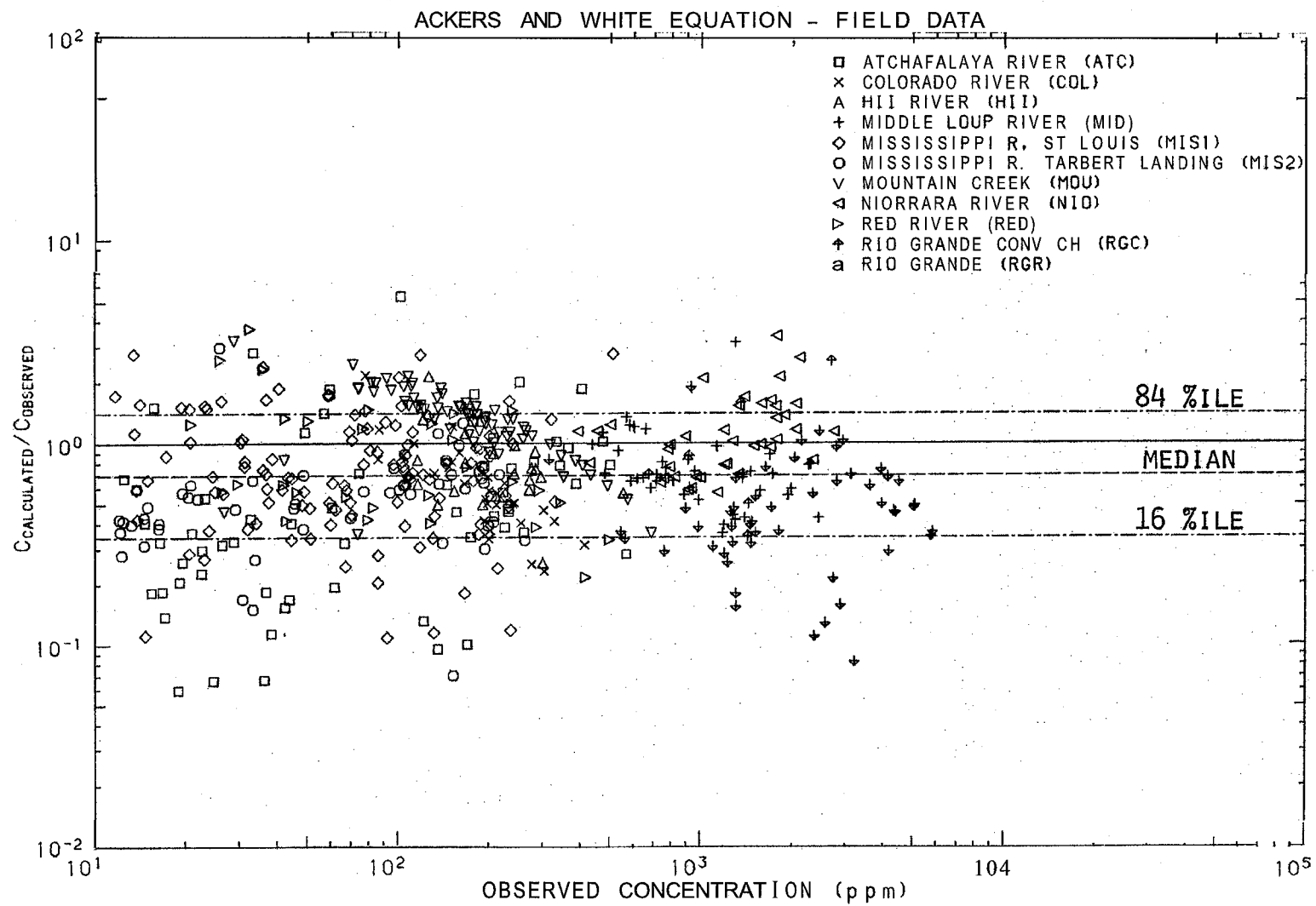


Figure 5.2b Ratio of concentration calculated by the Ackers and White (1973) technique to observed concentration as a function of observed concentration, for field data,

Table 5.4b

Ratio of Predicted to Observed Conc. for Ackers and White Method - Field Data

Data Set	Number	Geo.Mean	Geo.S.D.	Minimum	16 %ile	Median	84 %ile	Maximum
ATC	63	0.461	2.618	0.060	0.176	0.459	1.207	5.348
COL	30	0.591	1.608	0.232	0.367	0.566	0.950	2.172
HII	22	0.719	1.503	0.256	0.478	0.683	1.081	2.148
MID	38	0.718	1.500	0.359	0.478	0.676	1.077	3.152
MIS1	111	0.701	1.971	0.109	0.356	0.704	1.382	2.768
MIS2	53	0.519	1.770	0.071	0.293	0.547	0.919	2.983
MOU	75	1.253	1.498	0.356	0.836	1.327	1.877	3.226
NIO	40	1.072	1.521	0.570	0.705	1.021	1.631	3.380
RED	29	0.795	1.931	0.217	0.412	0.633	1.535	3.692
RGC	8	0.852	1.789	0.348	0.477	0.784	1.525	2.543
RGR	50	0.427	1.846	0.083	0.231	0.457	0.789	1.897
All	519	0.694	2.027	0.060	0.343	0.701	1.407	5.348

5.3.2 Bagnold Technique (1966)

The total load equation can be expressed in terms of concentration as

$$C = \left(\frac{\rho_s - \rho}{\rho_s} \right) \frac{u_*^2}{gr} \left[\frac{e_b}{t_g \psi_o} + 0.01 \frac{v}{w_m} \right] \quad (5.7)$$

where e_b is the bed load transport efficiency, $t_g \psi_o$ is a measure of dynamic friction, and w_m is the mean fall velocity of the bed particles. The quantities e_b and $t_g \psi_o$ can be evaluated from the graphs given by Bagnold (1966) or the equations given by White, Milli, and Crabbe (1973, pp 22-26).

The results of the analysis for laboratory data are given in Fig. 5.3a and Table 5.5a, and for field data, the results are given in Fig. 5.3b and Table 5.5b.

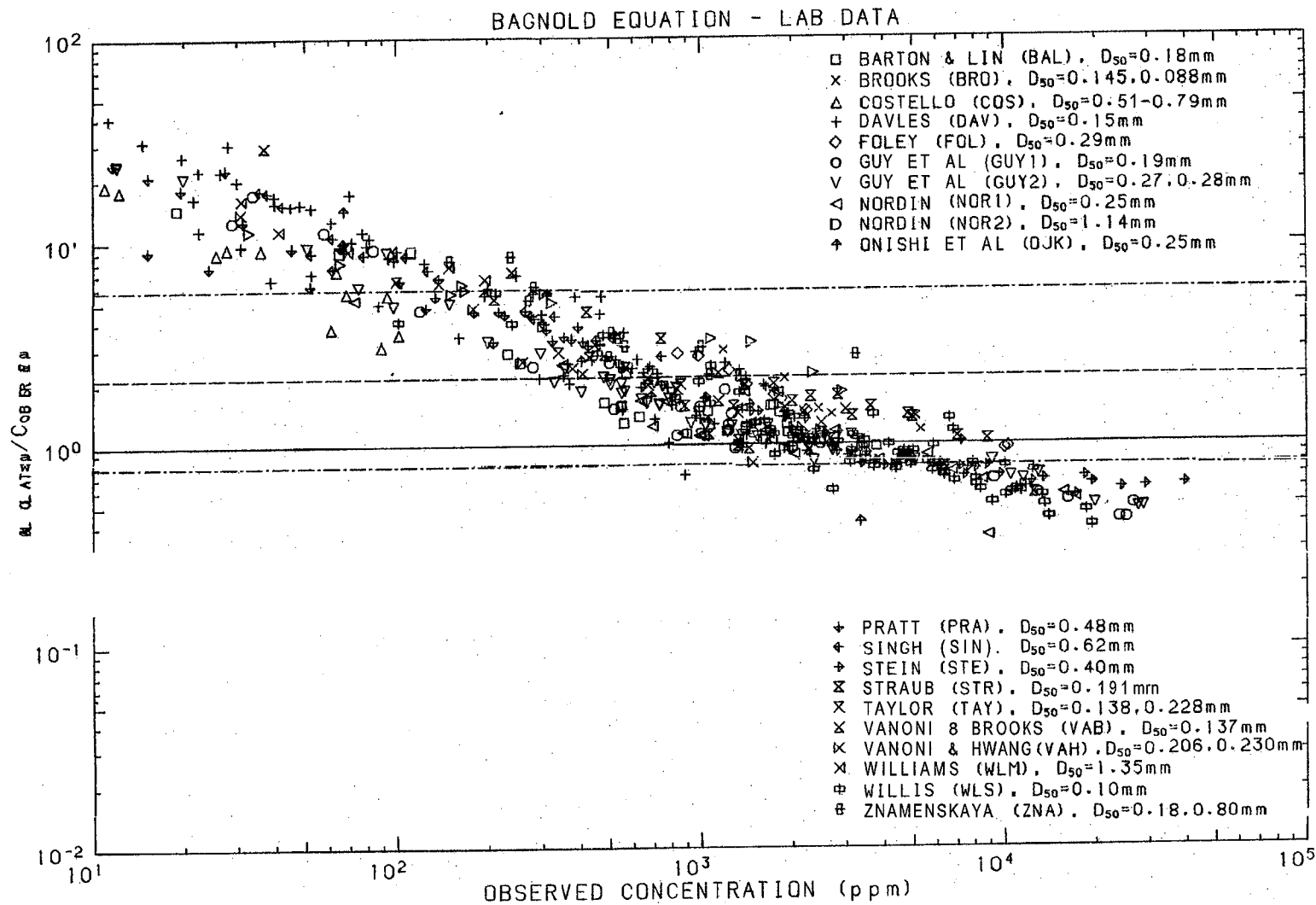


Figure 5.3a Ratio of concentration calculated by the Bagnold (1966) technique to observed concentration as a function of observed concentration, for laboratory data.

Table 5,511

Ratio of Predicted to Observed Concentration for Bagnold Method - Lab Data

Data Set	Number	Geo.Mean	Geo.S. D.	Minimum	16 %ile	Median	84 %ile	Maximum
BAL	26	1.836	2.040	0.968	0.900	1.436	3.747	14.537
BRO	6	1.654	1.363	1.170	1.213	1,405	2.255	2.914
COS	11	7.099	1.795	3.068	3.955	7.251	12.742	18.960
DAV	69	4.371	2.822	0.711	1.549	2.855	12.337	40.504
FOL	9	1.723	1.463	0.940	1.177	1.750	2.521	2.813
GUY1	27	1.556	2.773	0.418	0.561	1.171	4.315	17.180
GUY2	47	1.851	2.561	0.469	0.723	1.688	4.739	24.007
NOR1	22	1.132	1.755	0.349	0.645	1.105	1.987	5.187
NOR2	11	4.636	1.681	1.811	2.758	5.591	7.794	11.208
OJK	14	3.517	2.443	0.409	1.439	3.428	8.591	14.187
FRA	25	6,186	1.975	2.416	3.132	4.752	12.218	24.259
SIN	20	6.41 0	1.767	2.725	3.627	6.633	11.329	17.856
STE	44	0.938	1.378	0.547	0.681	0.873	1.292	1.931
SIR	21	1.371	1.595	0.562	0.860	1.376	2.187	4,512
TAY	12	2.191	1.785	0.932	1.227	1.970	3.912	6.472
VAB	14	2.607	2.586	0.955	1.008	1.637	6.742	29,216
VAH	6	3.013	2.352	0.813	1.281	2,403	7.089	13.817
WLM	5	9.620	1.371	6.587	7.017	9.036	13.187	16,137
WLS	77	0.992	1.677	0.390	0.591	0.953	1.664	5.643
ZNA	14	3.322	1.740	0.967	1.909	3.025	5.781	8,486
All	480	2,155	2.718	0.349	0.793	1.693		40.504

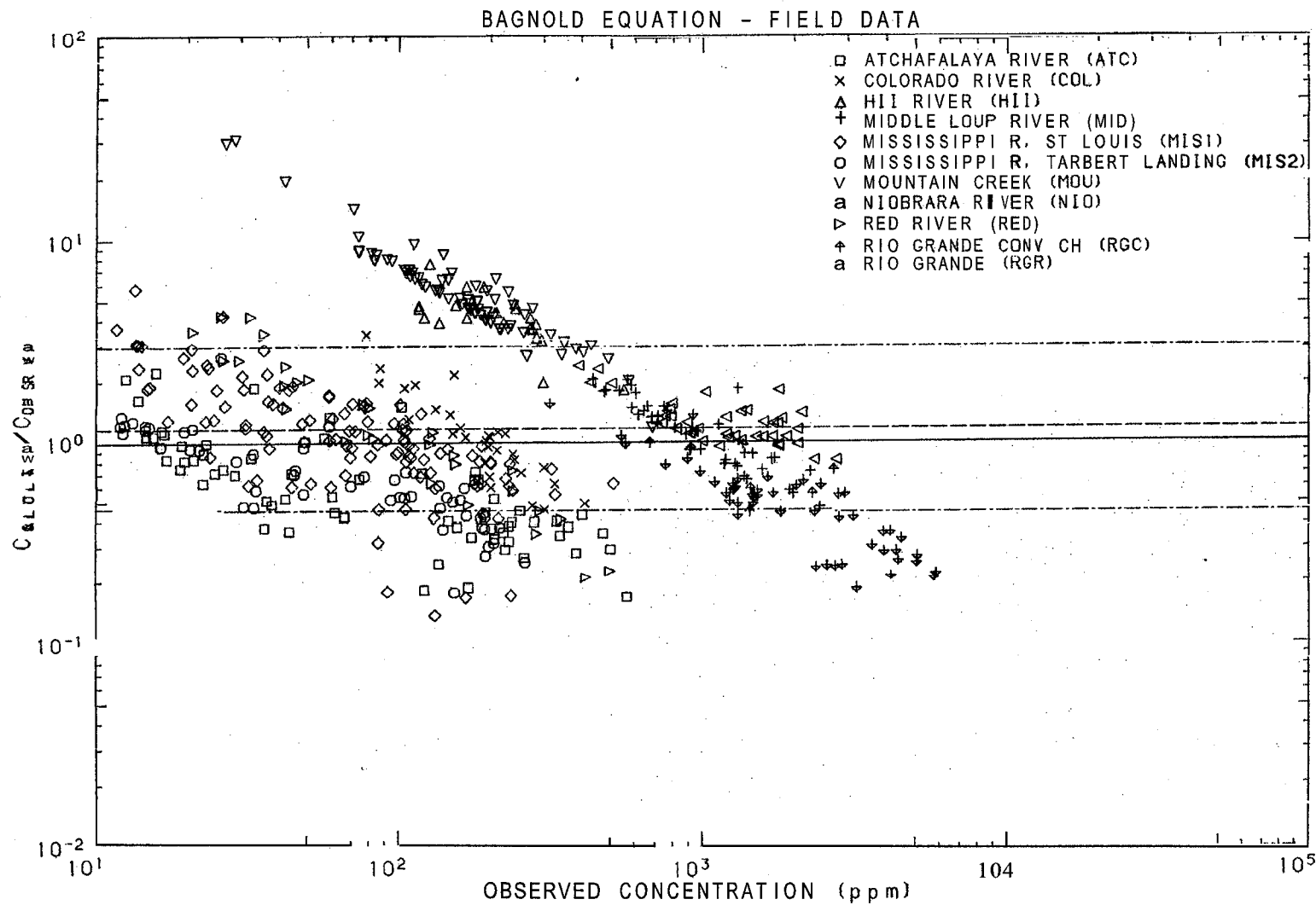


Figure 5.3b Ratio of concentration calculated by the Bagnold (1966) technique to observed concentration as a function of observed concentration, far field data,

Table 5.5b

Ratio of Predicted to Observed Concentration for Bagnold Method - Field Data

Data Set	Number	Geo.Mean	Geo.S.D.	Minimum	16 %ile	Median	84 %ile	Maximum
ATC	63	0.579	1.793	0.172	0.323	0.532	1.039	2.245
COL	30	1.057	1.615	0.468	0.654	1.061	1.706	3.382
HII	22	4.032	1.361	1.808	2.964	4.102	5.486	7.553
MID	38	1.103	1.490	0.478	0.740	1.144	1.643	2.057
MIS1	111	1.065	1.886	0.141	0.565	1.041	2.009	5.764
MIS2	53	0.645	1.676	0.182	0.385	0.599	1.080	2.656
MOU	75	5.306	1.669	1.182	3.179	4.995	8.856	30.725
NIO	40	1.248	1.286	0.815	0.971	1.172	1.605	2.394
RED	29	1.135	2.266	0.215	0.501	1.101	2.511	4.234
RGC	8	0.741	1.324	0.455	0.559	0.728	0.981	0.998
RGR	50	0.467	1.627	0.190	0.287	0.514	0.760	1.567
ALL	519	1.173	2.537	0.141	0.462	1.059	2.975	30.725

5.3.3 Bishop, Simons, and Richardson Technique (1965)

White, Milli, and Crabbe (1973) have evaluated both the original version of this technique and a modified version. Although the modified version tested slightly better, it is the original version that is evaluated here.

The development of the technique was based on a modification of the probabilistic approach used by Einstein (1950) to develop his bed load function. Here the total load transport rate, rather than just the bed load transport rate, is related to a dimensionless grain shear stress. A complete description of the application of the technique is given by White, Milli, and Crabbe (1973).

The results of the analysis for laboratory data are given in Fig. 5.4a and Table 5.6a, and the results for field data are given in Fig. 5.4b and Table 5.6b.

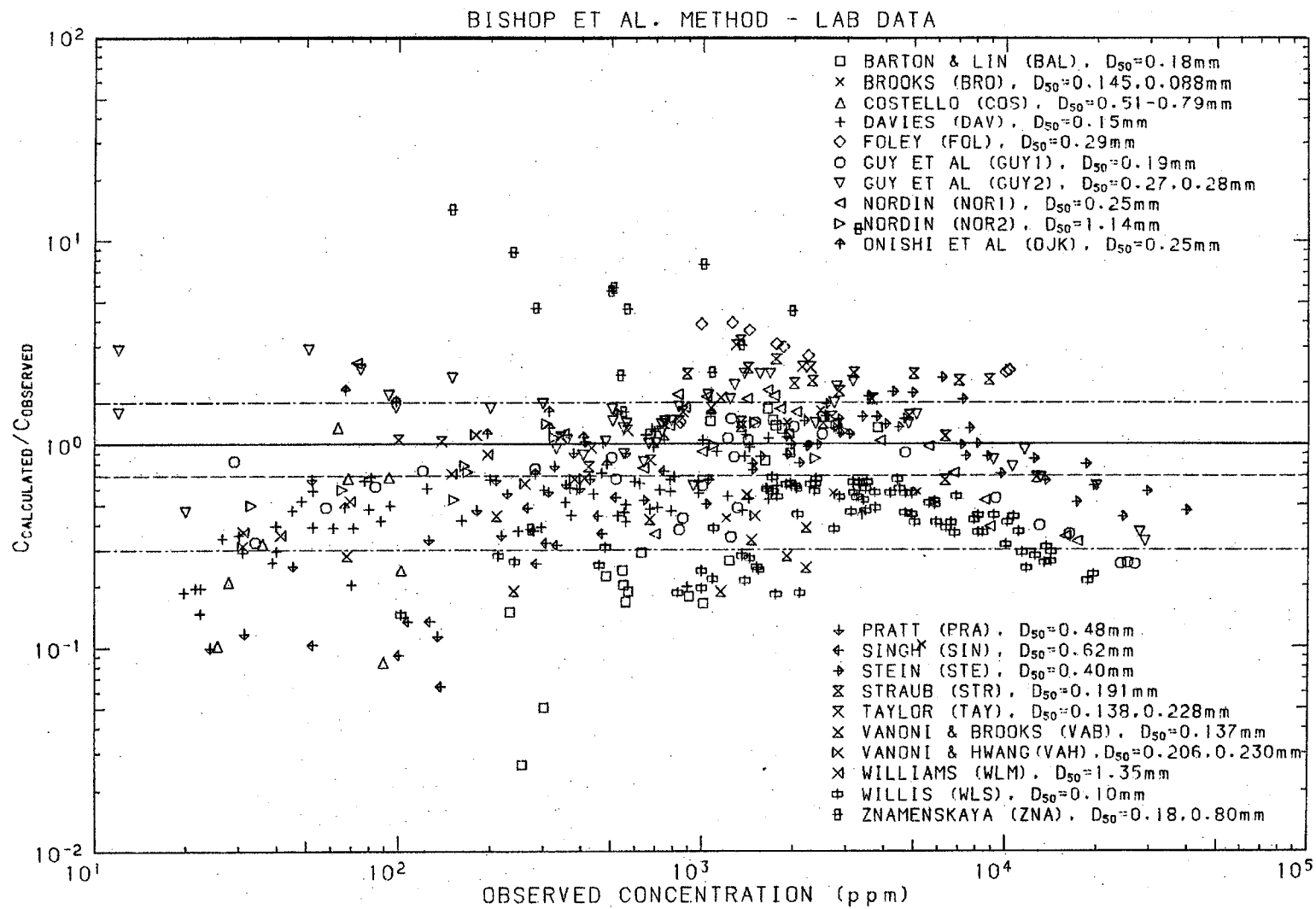
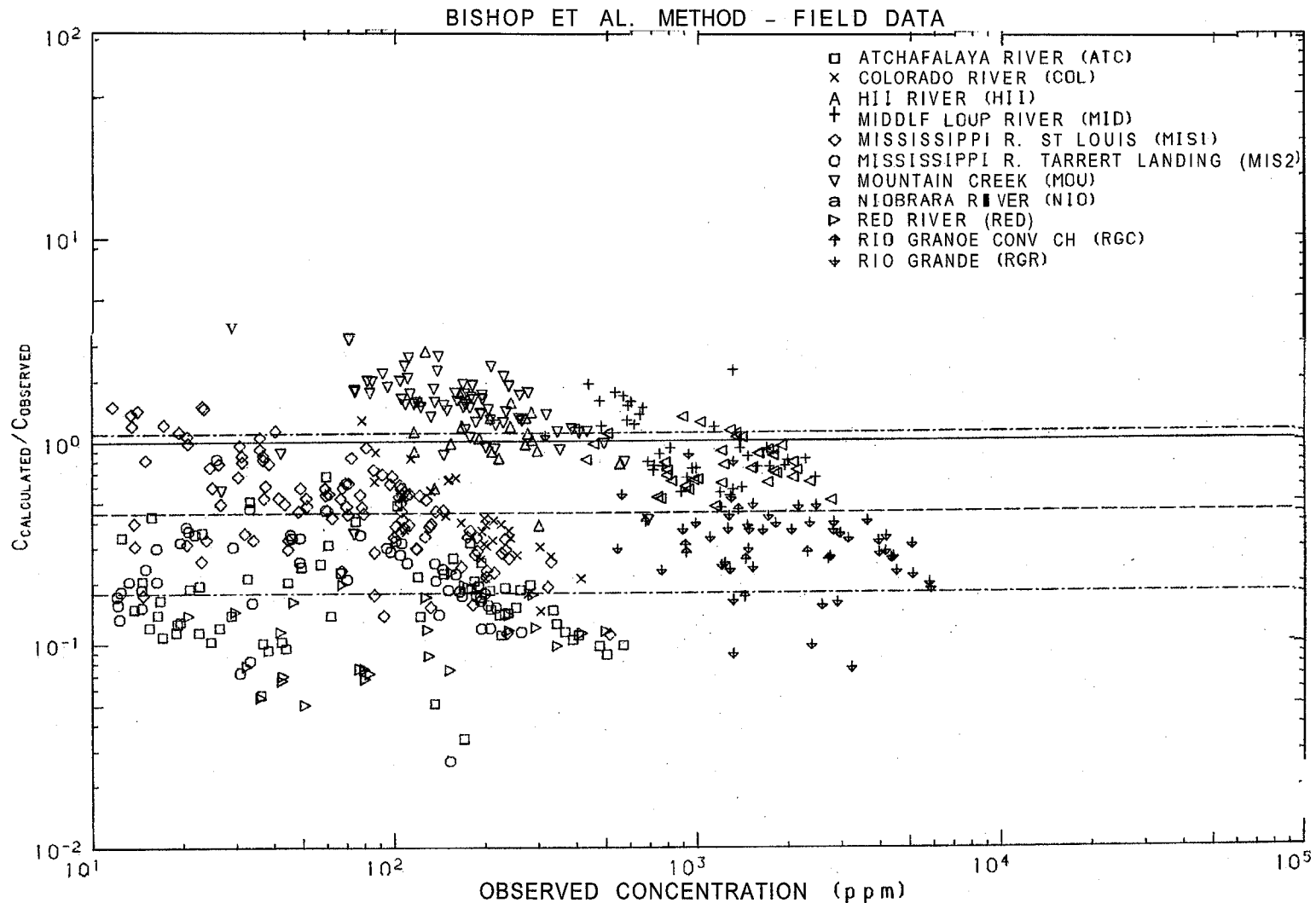


Figure 5.4a Ratio of concentration calculated by the Bishop, Simons, and Richardson (1965) technique to observed concentration as a function of observed concentration, for laboratory data.

Table 5.6a

Ratio of Predicted to Observed Conc. for Bishop et al. Method - Lab Data

Data Set	Number	Geo.Mean	Geo.S.D.	Minimum	16 %ile	Median	84 %ile	Maximum
BAL	23	0.402	3.110	0.026	0.129	0.292	1.250	1.488
BRO	6	0.547	2.387	0.102	0.229	0.570	1.307	1.455
COS	8	0.306	2.419	0.084	0.126	0.239	0.739	1.201
DAV	66	0.508	1.592	0.147	0.319	0.523	0.809	1.185
FOL	9	2.740	1.395	1.276	1.965	2.969	3.821	3.915
GUY1	27	0.606	1.679	0.255	0.361	0.622	1.018	1.330
GUY2	47	1.232	1.619	0.331	0.760	1.292	1.994	2.887
NOR1	22	0.994	1.808	0.331	0.549	1.128	1.797	2.476
NOR2	11	0.841	1.383	0.497	0.608	0.847	1.163	1.273
OJK	14	1.030	1.507	0.444	0.683	1.080	1.552	1.832
PRA	18	0.444	2.046	0.099	0.217	0.580	0.908	1.027
SIN	14	0.248	2.069	0.064	0.120	0.31 _H	0.513	0.736
STE	44	0.972	1.471	0.436	0.661	0.991	1.429	2.108
STR	21	1.522	1.486	0.662	1.025	1.65 _H	2.262	2.586
TAY	12	1.480	1.579	0.831	0.938	1.16 _p	2.337	3.205
VAB	12	0.406	1.929	0.187	0.210	0.336	0.782	1.683
VAH	6	0.596	1.479	0.315	0.403	0.638	0.882	1.113
WLM	5	0.534	1.433	0.355	0.373	0.523	0.766	0.890
WLS	77	0.397	1.498	0.144	0.265	0.438	0.595	0.684
ZNA	14	3.998	2.464	0.381	1.622	4.584	9.851	14.094
ALL	456	0.695	2.300	0.026	0.302	0.666	1.599	14.094



- ATCHAFALAYA RIVER (ATC)
- × COLORADO RIVER (COL)
- △ HII RIVER (HII)
- † MIDDLE LOUP RIVER (MID)
- ◇ MISSISSIPPI R. ST LOUIS (MIS1)
- MISSISSIPPI R. TARRANT LANDING (MIS2)
- ▽ MOUNTAIN CREEK (MOU)
- ⊠ NIobrARA RIVER (NIO)
- △ RED RIVER (RED)
- ⊕ RIO GRANDE CONV CH (RGC)
- ⊕ RIO GRANDE (RGR)

Figure 5.4b Ratio of concentration calculated by the Bishop, Simons, and Richardson (1965) technique to observed concentration as a function of observed concentration, for field data,

Table 5.6b

Ratio of Predicted to Observed Conc. for Bishop et al. Method - Field Data

Data Set	Number	Geo.Mean	Geo.S.D.	Minimum	16 %ile	Median	84 %ile	Maximum
ATC	63	0.163	1.716	0.034	0.095	0.148	0.279	0.675
COL	30	0.394	1.617	0.146	0.244	0.368	0.637	1.275
HII	22	1.075	1.474	0.384	0.729	1.035	1.585	2.767
MID	38	0.928	1.484	0.469	0.626	0.811	1.378	2.225
MIS1	111	0.472	1.760	0.111	0.268	0.493	0.830	1.504
MIS2	53	0.211	1.692	0.027	0.125	0.205	0.356	0.824
MOU	75	1.454	1.476	0.351	0.985	1.531	2.146	3.593
NIO	40	0.777	1.292	0.474	0.601	0.762	1.004	1.317
RED	27	0.106	1.509	0.050	0.071	0.115	0.160	0.228
RGC	8	0.291	1.323	0.170	0.220	0.281	0.385	0.458
RGR	50	0.307	1.654	0.076	0.186	0.329	0.508	1.069
All	517	0.443	2.488	0.027	0.178	0.454	1.102	3.593

5.3.4 Einstein Technique (1950)

A thumbnail sketch of this technique is given in section 5.1, which is briefly reviewed here. The bed-load transport rate is calculated from the grain shear stress for each size fraction of the bed material. The suspended load for each size fraction can then be calculated by integration of the product of Eqs. 5.1 and 5.2, over the depth. The total load concentration is the sum of the concentrations for each size fraction.

The details of the technique are given by Vanoni (1975, pp. 195-201). Analytical representations of the various graphical factors are given by White, Milli, and Crabbe (1973, pp. 15-18).

The results of the analysis for laboratory data are given in Fig. 5.5a and Table 5.7a, and the results for field data are given in Fig. 5.5b and Table 5.7b.

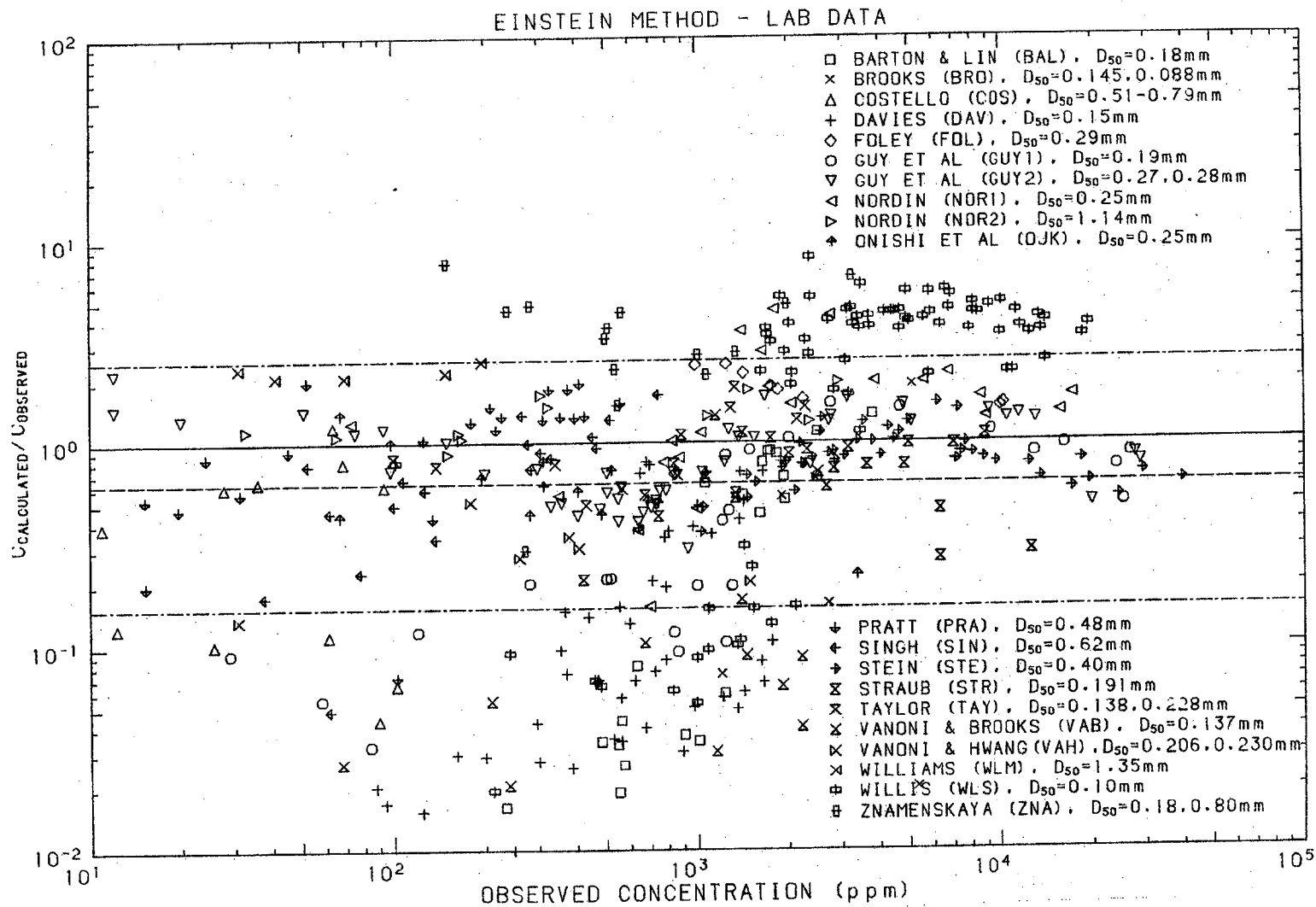


Figure 5.5a Ratio of concentration calculated by the Einstein (1950) technique to observed concentration as a function of observed concentration, for laboratory data.

Table 5.7a

Ratio of Predicted to Observed Concentration for Einstein Method - Lab Data

Data Set	Number	Geo.Mean	Geo.S.D.	Minimum	16 %ile	Median	84 %ile	Maximum
BAL	21	0.174	4.900	0.016	0.036	0.446	0.854	1.362
BRO	6	0.233	4.532	0.020	0.051	0.161	1.058	1.908
COS	11	0.260	2.991	0.044	0.087	0.391	0.777	1.204
DAV	46	0.098	3.381	0.005	0.029	0.074	0.330	0.802
FOL	9	1.683	1.429	0.698	1.178	1.795	2.405	2.422
GUY1	26	0.340	2.935	0.033	0.116	0.412	0.997	1.547
GUY2	47	0.816	1.607	0.302	0.507	0.769	1.311	2.230
NOR1	22	1.305	2.205	0.157	0.592	1.394	2.877	4.518
NOR2	11	1.313	1.276	0.878	1.029	1.257	1.676	1.968
OJK	14	0.595	1.520	0.222	0.391	0.578	0.905	1.388
PRA	22	0.914	2.218	0.071	0.412	1.267	2.028	2.015
SIN	18	0.590	2.318	0.049	0.255	0.742	1.367	1.715
STE	44	0.811	1.368	0.364	0.593	0.810	1.109	1.554
STR	21	0.661	1.609	0.214	0.411	0.764	1.063	1.114
TAY	12	0.884	1.512	0.494	0.585	0.784	1.337	1.859
VAB	12	0.091	3.377	0.021	0.027	0.064	0.308	1.358
VAH	6	0.273	1.515	0.136	0.181	0.275	0.414	0.513
WLM	5	2.261	1.068	2.117	2.117	2.223	2.415	2.519
WLS	77	1.689	4.571	0.020	0.369	3.585	7.717	8.182
ZNA	14	2.997	2.160	0.298	1.388	3.265	6.474	7.737
All	444	0.628	4.059	0.005	0.155	0.797	2.551	8.182

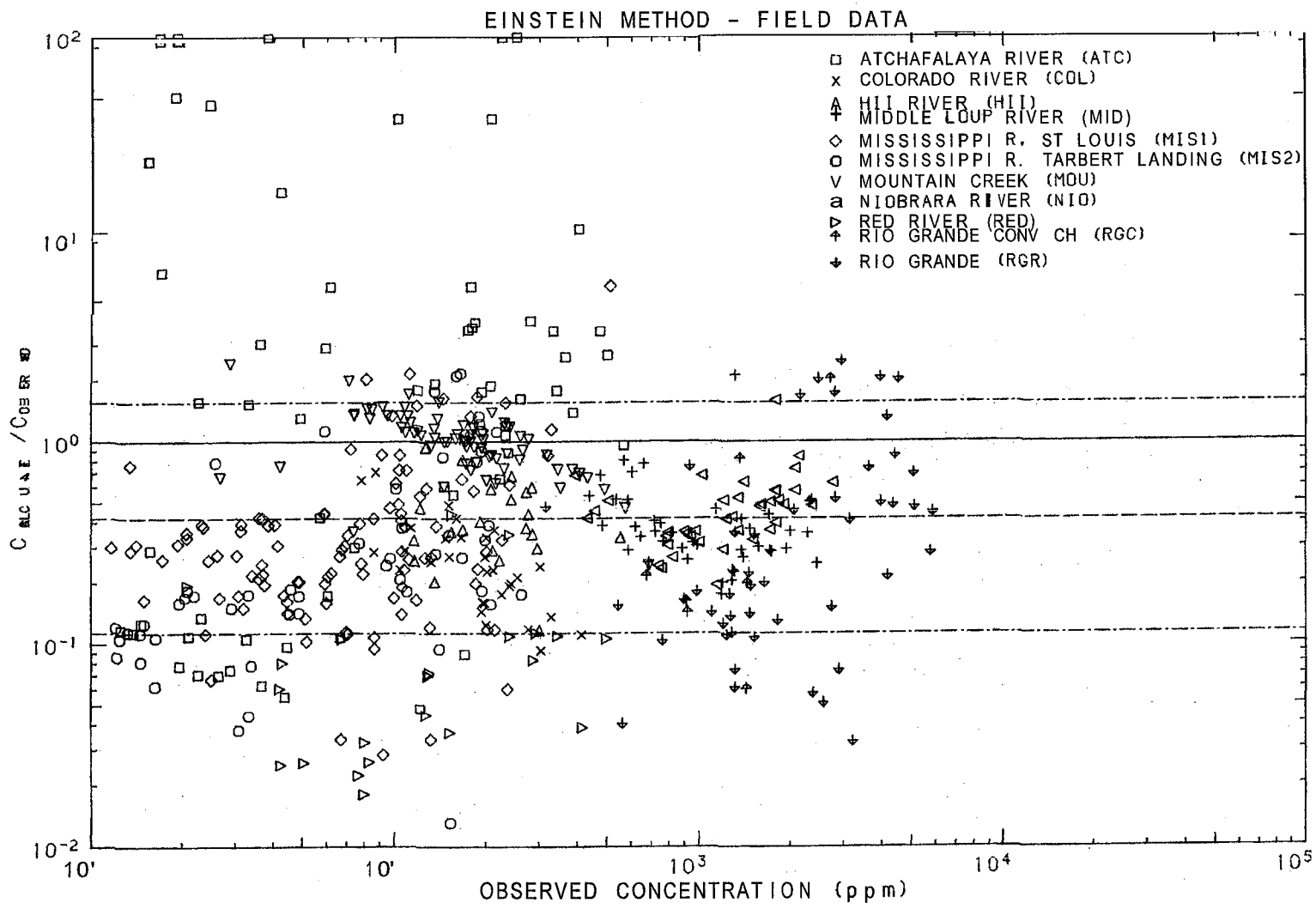


Figure 5.5b Ratio of concentration calculated by the Einstein (1950) technique to observed concentration as a function of observed concentration, for field data,

Table 5.7b

Ratio of Predicted to Observed Concentration for Einstein Method - Field Data

Data Set	Number	Geo.Mean	Geo.S.D.	Minimum	16 %ile	Median	84 %ile	Maximum
ATC	62	1.521	10.121	0.048	0.150	1.571	15.395	233.312
COL	30	0.240	1.640	0.093	0.146	0.234	0.394	0.708
HII	22	0.393	1.586	0.117	0.248	0.370	0.624	0.940
MID	38	0.374	1.578	0.176	0.237	0.355	0.591	2.119
MIS1	106	0.315	2.447	0.028	0.129	0.289	0.772	6.002
MIS2	52	0.241	2.948	0.013	0.082	0.182	0.710	2.167
MOU	75	0.973	1.434	0.245	0.679	1.026	1.395	2.427
NIO	40	0.442	1.465	0.196	0.302	0.427	0.648	1.591
RED	23	0.075	2.718	0.018	0.028	0.072	0.204	1.045
RGC	8	0.291	2.835	0.060	0.103	0.201	0.826	2.027
RGR	50	0.279	2.988	0.033	0.094	0.226	0.835	0.500
All	506	0.420	3.719	0.013	0.113	0.373	1.562	233.312

Table 5.7b

Ratio of Predicted to Observed Concentration for Einstein Method - Field Data

Data Set	Number	Geo.Mean	Geo.S.D.	Minimum	16 %ile	Median	84 %ile	Maximum
ATC	62	1.521	10.121	0.048	0.150	1.571	15.395	233.312
COL	30	0.240	1.640	0.093	0.146	0.234	0.394	0.708
HII	22	0.393	1.586	0.117	0.248	0.370	0.624	0.940
MID	38	0.374	1.578	0.176	0.237	0.355	0.591	2.119
MIS1	106	0.315	2.447	0.028	0.129	0.289	0.772	6.002
MIS2	52	0.241	2.948	0.013	0.082	0.182	0.710	2.167
MOU	75	0.973	1.434	0.245	0.679	1.026	1.395	2.427
NIO	40	0.442	1.465	0.196	0.302	0.427	0.648	1.591
RED	23	0.075	2.718	0.018	0.028	0.072	0.204	1.045
RGC	8	0.291	2.835	0.060	0.103	0.201	0.826	2.027
RGR	50	0.279	2.988	0.033	0.094	0.226	0.835	2.500
All	506	0.420	3.719	0.013	0.113	0.373	1.562	233.312

5.3.5 Engelund and Fredsoe Technique (1976)

This technique utilizes an analytical expression for the bed-load transport rate plus the Einstein (1950) integrals for calculation of the suspended load transport rate.

The first step in the procedure is the calculation of u_*' from Eq. 3.15, from which $\tau_*' = \rho u_*'^2 / g(\rho_s - \rho) D_{50}$ can be determined. Given τ_*' , the quantity p can be determined from

$$p = \left[1 + \frac{0.51 \frac{\pi}{6}}{\tau_*' - 0.05} \right]^{-1/4} \quad (5.8)$$

Then, the dimensionless bed load transport rate is given by

$$\phi_B = 5p (\sqrt{\tau_*'} - 0.7\sqrt{0.05}) \quad (5.9)$$

Next, the volumetric bed concentration is determined from

$$c_b = \frac{0.65}{(1 + 1/\lambda_b)^3} \quad (5.10)$$

where

$$\lambda_b = \left[\frac{\tau_*' - 0.05 - 0.51 \frac{\pi}{6} p}{0.027 \frac{\rho_s}{\rho} \tau_*'} \right]^{1/2} \quad (5.11)$$

Finally, the suspended load transport rate is determined from

$$\phi_s = 11.6 \sqrt{\tau_*'} c_b 2 \left[I_1 \ln \frac{12r}{D_s} + I_2 \right] \quad (5.12)$$

where D_s is the fall diameter, and I_1 and I_2 are the Einstein integrals, which are given both graphically and analytically by Vanoni (1975, pp. 196-198). And the total concentration by mass is given by

$$C = \frac{\rho_s}{\rho q} \sqrt{\left(\frac{\rho_s - \rho}{\rho} \right) g D_s^3} (\phi_B + \phi_s) \quad (5.13)$$

Although the writer believes that the equations presented here are correct, Eqs. 5.8 and 5.12 are slightly altered from their original presentation. The changes are suggested by a careful review of the derivation given by Engelund and Fredsoe (1976).

For analysis purposes, the fall diameter has been taken to be equivalent to D_{50} .

The results of the analysis for laboratory data are given in Fig. 5.6a and Table 5.8a, and for field data, the results are given in Fig. 5.6b and Table 5.8b.

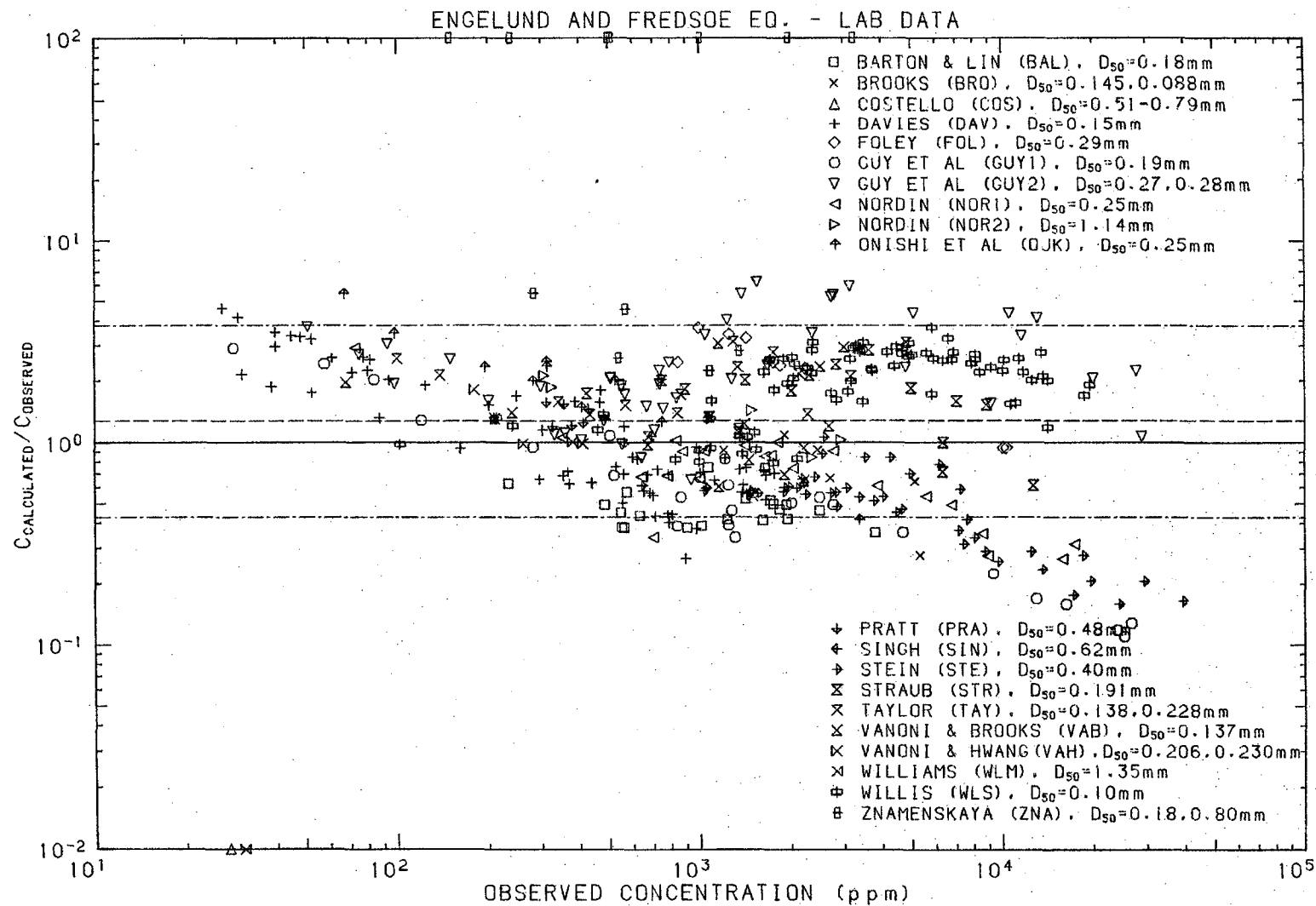


Figure 5.6a Ratio of concentration calculated by the Engelund and Fredsoe (1976) technique to observed concentration as a function of observed concentration, for laboratory data.

Table 5.8a

Ratio of Predicted to Observed Conc. for Engelund and Fredsoe Eq. - Lab Data

Data Set	Number	Geo.Mean	Geo.S.D.	Minimum	16 %ile	Median	84 %ile	Maximum
BAL	21	0.475	1.228	0.361	0.387	0.463	0.583	0.751
BRO	6	0.691	1.567	0.277	0.441	0.667	1.083	1.089
COS	0	1.000	1.000	0.000	1.000	1.089	1.000	0.000
DAV	61	1.042	2.005	0.268	0.520	0.756	2.090	4.601
FOL	9	2.198	1.616	0.942	1.360	2.465	3.553	3.671
GUY1	26	0.500	2.388	0.110	0.209	0.502	1.194	2.899
GUY2	44	2.206	1.748	0.653	1.262	2.055	3.857	6.192
NOR1	22	0.675	1.719	0.267	0.393	0.683	1.160	2.911
NOR2	6	1.364	1.374	0.844	0.992	1.309	1.874	2.122
OJK	13	1.754	1.824	0.417	0.961	2.004	3.198	5.434
PRA	8	1.306	1.152	1.002	1.134	1.249	1.505	1.574
SIN	1	2.030	1.000	2.030	2.030	2.030	2.030	2.030
STE	44	0.464	1.600	0.159	0.290	0.560	0.742	1.064
STR	21	1.617	1.520	0.614	1.064	1.787	2.457	3.086
TAY	12	1.776	1.354	1.066	1.311	1.580	2.405	3.126
VAB	13	1.255	1.715	0.604	0.732	1.230	2.153	3.064
VAH	5	0.995	1.462	0.546	0.681	0.990	1.455	1.814
WLM	0	1.000	1.000	0.000	1.000	1.814	1.000	0.000
WLS	77	1.952	1.499	0.790	1.303	2.231	2.926	3.686
ZNA	13	39.289	11.446	1.911	3.432	155.198	449.703	1290.333
All	402	1.274	2.972	0.110	0.429	1.210	3.785	1290.333

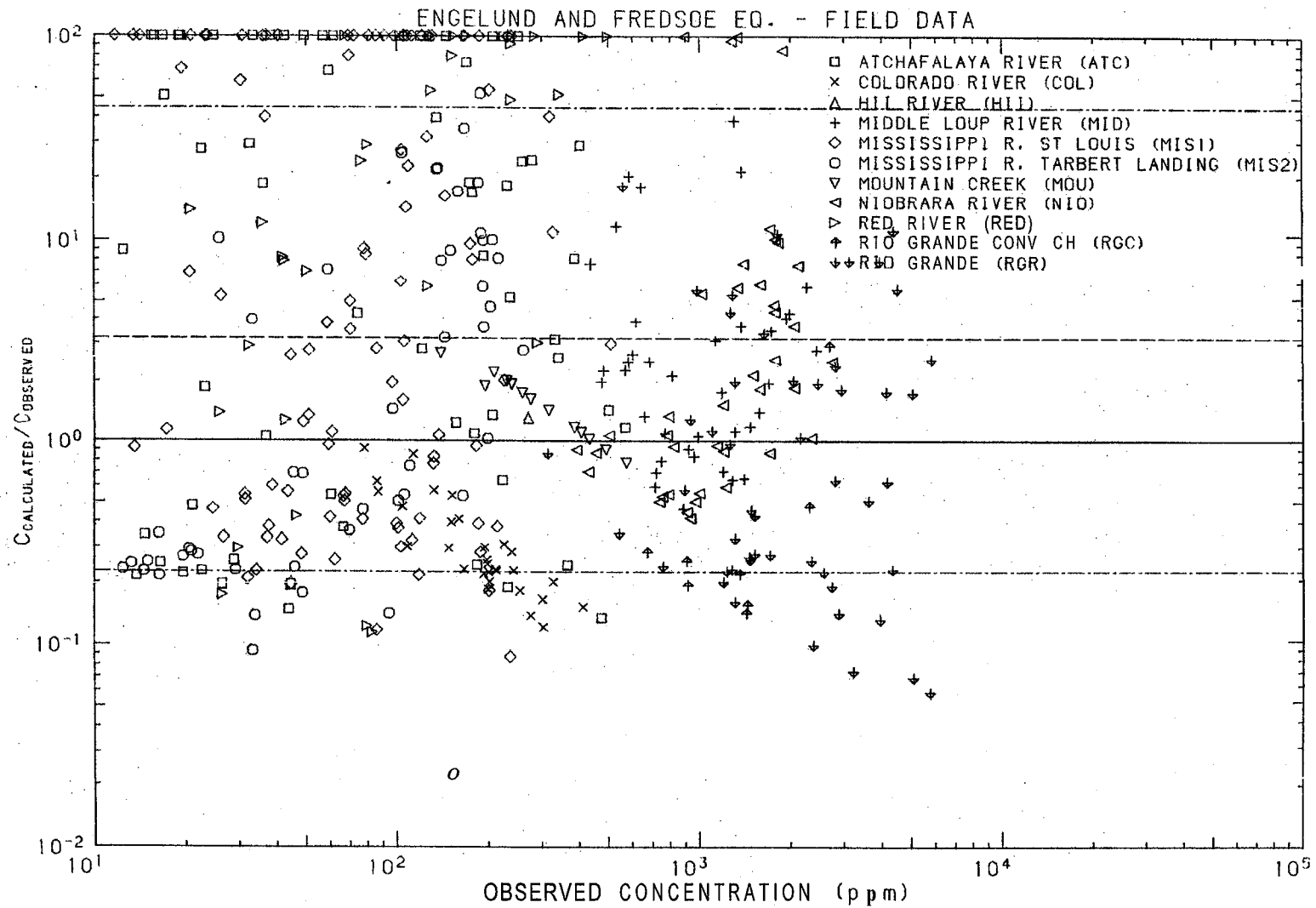


Figure 5.6b Ratio of concentration calculated by the Engelund and Fredsoe (1976) technique to observed concentration as a function of observed concentration, for field data.

Table 5.8b

Ratio of Predicted to Observed Conc. for Engelund and Fredsoe Eq. - Field Data

Data Set	Number	Geo.Mean	Geo.S.D.	Minimum	16 %ile	Median	84 %ile	Maximum
ATC	63	10.406	20.421	0.134	0.510	8.888	212.514	2252.931
COL	30	0.291	1.673	0.121	0.174	0.248	0.487	0.914
HII	1	1.293	1.000	1.293	1.293	1.293	1.293	1.293
MID	38	2.333	2.953	0.465	0.790	2.060	6.888	38.363
MIS1	102	9.964	25.624	0.086	0.389	3.783	255.309	5788.821
MIS2	48	1.395	6.763	0.023	0.206	0.694	9.433	52.154
MOU	14	1.483	1.415	0.777	1.048	1.586	2.098	2.679
NIO	40	2.528	4.796	0.417	0.527	1.491	12.125	148.858
RED	29	14.133	14.651	0.115	0.965	14.074	207.068	2167.521
RGC	8	0.314	2.492	0.142	0.126	0.221	0.783	2.911
RGR	50	0.750	4.354	0.057	0.172	0.574	3.266	18.183
ALL	423	3.179	14.026	0.023	0.227	1.694	44.591	5788.821

5.3.6 Engelund and Hansen Technique (1967)

This technique is one of the simplest to use of all the methods analyzed. Yet it is one of the most effective. The technique can be reduced to the single equation:

$$c = 0.05 \left(\frac{\rho_s}{\rho_s - \rho} \right) \left(\frac{vS}{\sqrt{\left(\frac{\rho_s - \rho}{\rho} \right) g D_{50}}} \right) \tau_*^{1/2} \quad (5.14)$$

where $\tau_* = \rho r s / (\rho_s - \rho) D_{50}$.

The results of the analysis for laboratory data are given in Fig. 5.7a and Table 5.9a, and the results for field data are given in Fig. 5.7b and Table 5.9b.

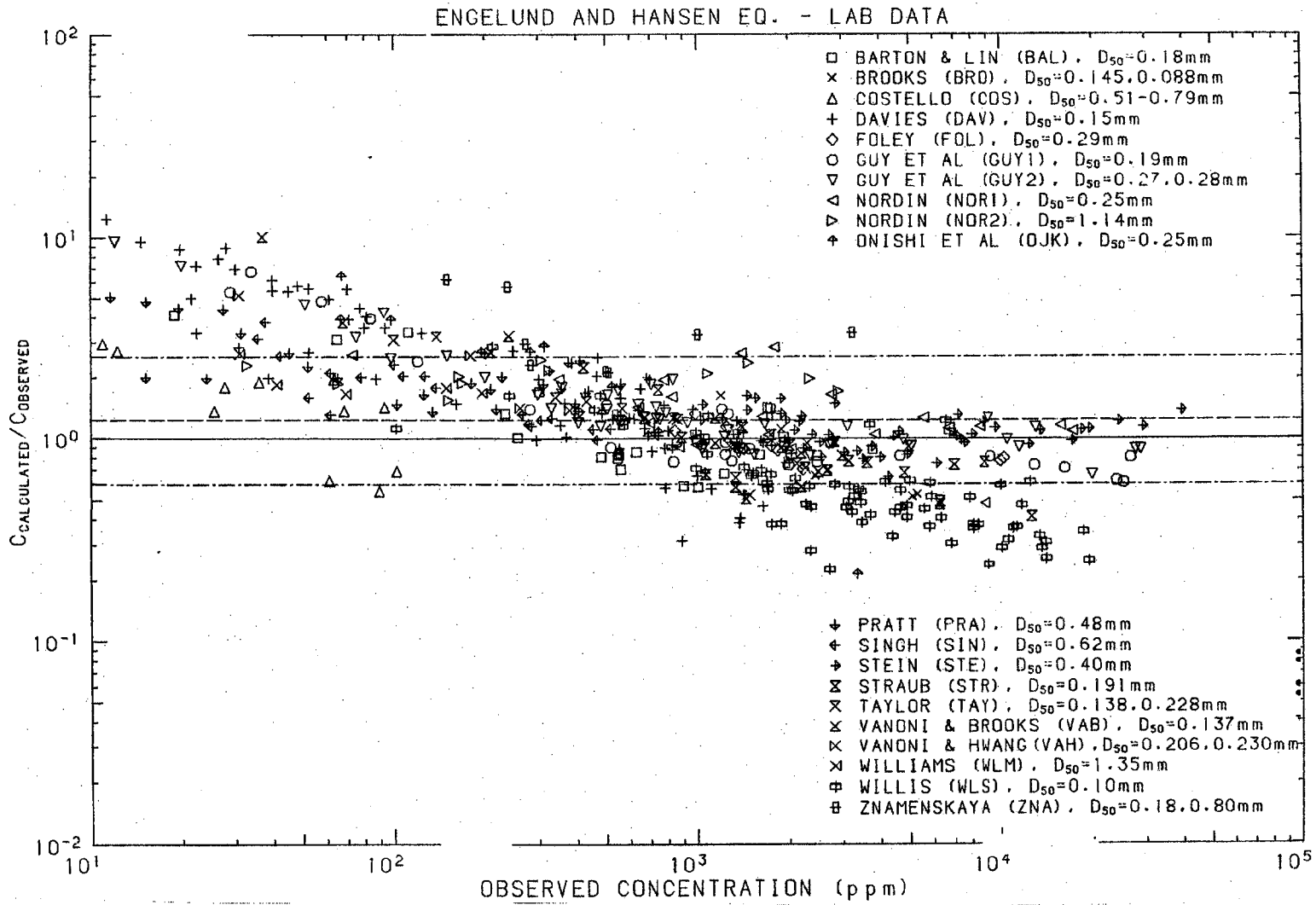


Figure 5.7a Ratio of concentration calculated by the Engelund and Hansen (1967) technique to observed concentration as a function of observed concentration, for laboratory data.

Table 5.9a

Ratio of Predicted to Observed Conc. for Engelund and Hansen Method - Lab Data

Data Set	Number	Geo.Mean	Geo.S.D.	Minimum	16 %ile	Median	84 %ile	Maximum
BAL	26	1.081	1.660	0.578	0.651	0.897	1.794	4.132
BRO	6	0.784	1.513	0.520	0.518	0.657	1.186	1.635
COS	11	1.380	1.728	0.553	0.799	1.431	2.384	2.950
DAV	69	1.960	2.386	0.315	0.822	1.768	4.676	12.380
FOL	9	0.931	1.213	0.706	0.767	0.890	1.129	1.329
GUY1	27	1.199	1.967	0.608	0.610	0.903	2.359	6.768
GUY2	47	1.503	1.849	0.663	0.813	1.251	2.779	9.620
NOR1	22	1.305	1.508	0.481	0.865	1.164	1.967	2.846
NOR2	11	2.024	1.143	1.555	1.771	2.031	2.313	2.458
OJK	14	1.775	2.307	0.215	0.769	1.806	4.095	6.412
PRA	25	2.225	1.465	1.362	1.519	2.001	3.260	5.064
SIN	20	1.626	1.463	0.985	1.112	1.323	2.378	3.794
STE	44	1.087	1.240	0.648	0.877	1.087	1.348	1.638
STR	21	0.816	1.478	0.414	0.552	0.765	1.206	2.247
TAY	12	1.330	1.584	0.717	0.839	1.268	2.107	3.197
VAB	14	1.360	2.252	0.509	0.604	0.949	3.063	10.073
VAH	6	1.622	2.006	0.530	0.808	1.387	3.253	5.183
WLM	5	1.899	1.185	1.666	1.602	1.788	2.251	2.645
WLS	77	0.549	1.639	0.227	0.335	0.523	0.900	2.857
ZNA	14	1.965	1.933	0.761	1.017	2.123	3.798	6.186
ALL	480	1.236	2.064	0.215	0.599	1.151	2.552	12.380

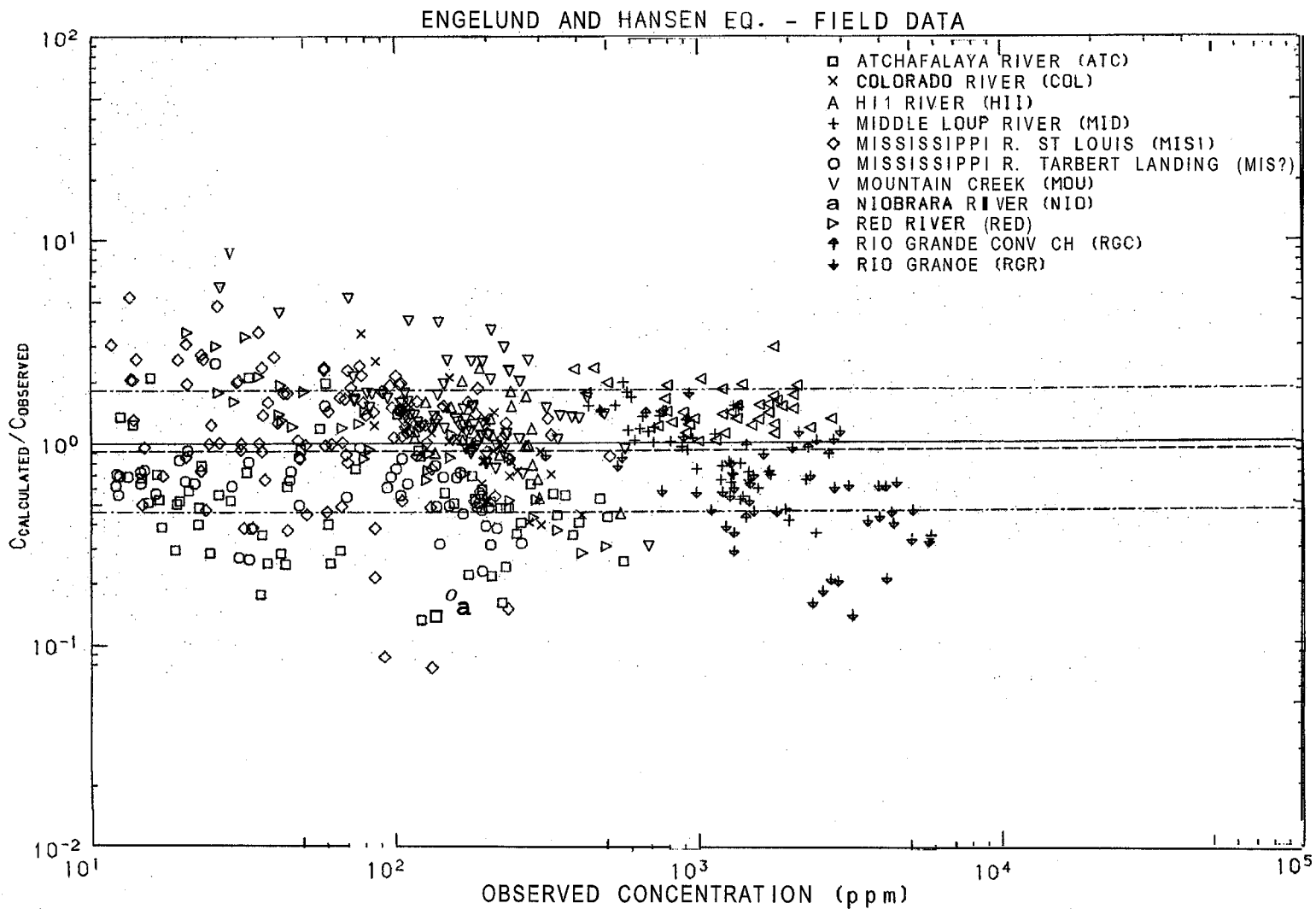


Figure 5.7b Ratio of concentration calculated by the Engelund and Hansen (1967) technique to observed concentration as a function of observed concentration, for field data.

Table 5.9b

Ratio of Predicted to Observed Conc. for Engelund and Hansen Method - Field Data

ta Set	Number	Geo.Mean	Geo.S.D.	Minimum	16 %ile	Median	84 %ile	Maximum
ATC	63	0.484	1.869	0.133	0.259	0.506	0.905	2.114
COL	30	0.981	1.659	0.395	0.591	0.979	1.627	3.462
HII	22	1.107	1.501	0.450	0.738	1.069	1.663	2.339
MID	38	0.937	1.533	0.356	0.611	1.005	1.436	1.986
MIS1	111	1.125	2.056	0.077	0.547	1.235	2.312	5.286
MIS2	53	0.576	1.543	0.178	0.373	0.618	0.889	2.478
MOU	75	1.528	1.674	0.308	0.913	1.379	2.558	8.655
NIO	40	1.497	1.266	1.016	1.183	1.429	1.895	2.947
RED	29	1.035	1.933	0.285	0.535	1.108	2.000	3.532
RGC	8	1.024	1.463	0.427	0.700	0.971	1.499	1.490
RGR	50	0.529	1.714	0.139	0.309	0.579	0.907	1.759
All	519	0.916	1.997	0.077	0.459	0.998	1.830	8.655

5.3.7 Graf Technique (1968)

Like the method of Engelund and Hansen (1967), the Graf* method is very easy to use. However, the test results for the latter method are much less favorable than for the former method. Likewise, the Graf technique can be reduced to a single equation:

$$C = 10.39 \left(\frac{\rho_s}{\rho_s - \rho} \right) \left(\frac{u_* D_{50}}{q} \right) \tau_*^{2.02} \quad (5.15)$$

As White, Milli, and Crabbe (1973) have indicated, Graf was not specific about which grain diameter should be used. As suggested by Eq. 5.15, D_{50} has been used here.

The results of the analysis for laboratory data are given in Fig. 5.8a and Table 5.10a, and the results for field data are given in Fig. 5.8b and Table 5.10b.

*The technique developed by Graf in 1968 is described in Graf, 1971.

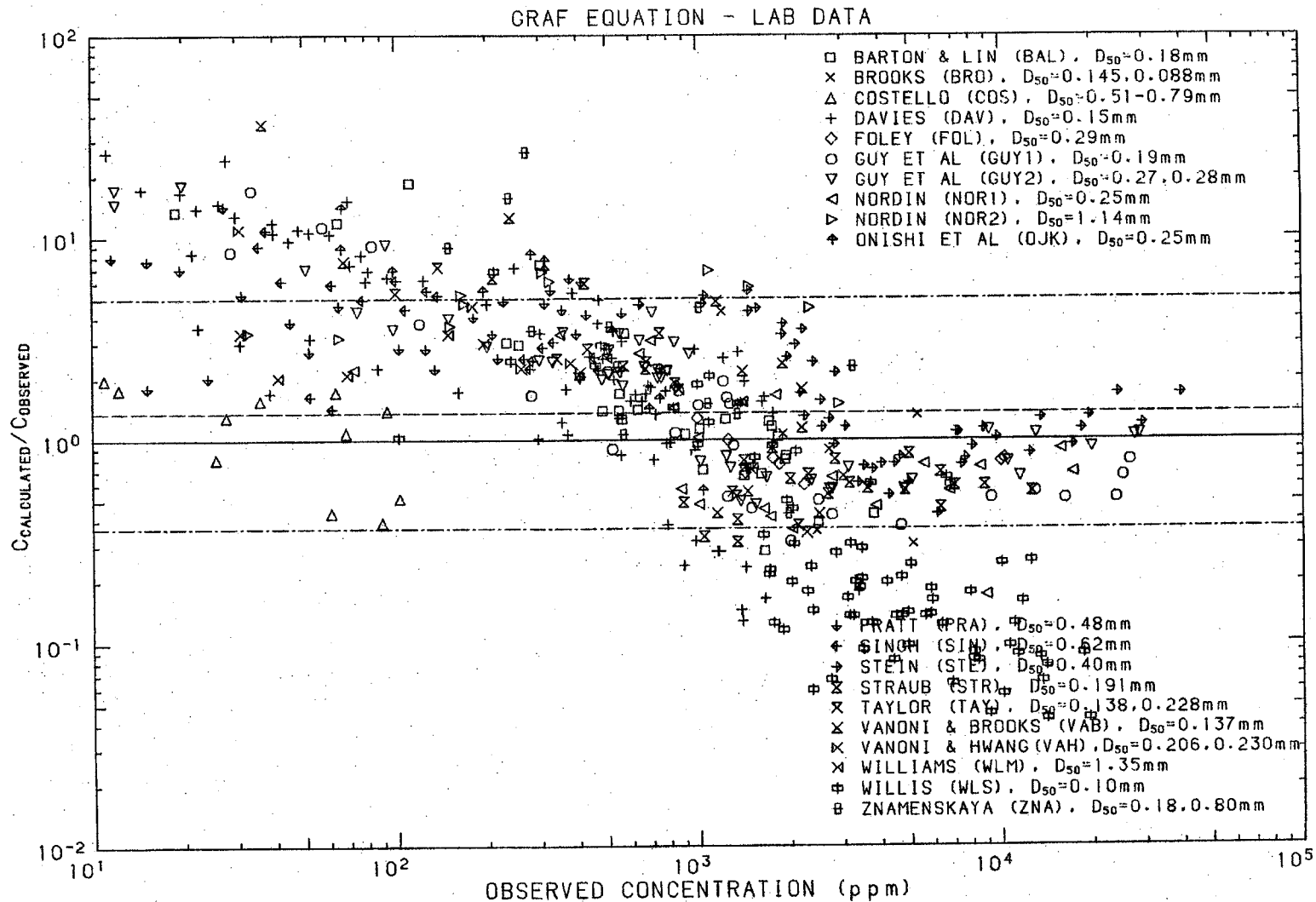


Figure 5.8a Ratio of concentration calculated by the Graf (1968) technique to observed concentration as a function of observed concentration, for laboratory data.

Table 5.10a

Ratio of Predicted to Observed Concentration for Graf Method - Lab Data

Data Set	Number	Geo.Mean	Geo.S.D.	Minimum	16 %ile	Median	84 %ile	Maximum
BAL	26	1.550	2.861	0.284	0.542	1.232	4.435	18.573
BRO	6	0.919	2.413	0.308	0.381	0.892	2.218	4.337
COS	11	1.027	1.762	0.392	0.583	1.299	1.810	1.990
DAV	69	2.600	3.560	0.129	0.730	2.531	9.257	26.242
FOL	9	0.897	1.388	0.599	0.646	0.805	1.245	1.848
GUY1	27	1.264	2.983	0.317	0.424	0.934	3.770	17.051
GUY2	47	1.852	2.550	0.479	0.726	2.029	4.723	18.148
NOR1	22	0.901	2.159	0.172	0.417	0.735	1.945	3.318
NOR2	11	4.359	1.524	1.505	2.860	4.727	6.642	6.886
OJK	14	3.120	3.217	0.179	0.970	3.433	10.036	14.016
PRA	25	4.231	1.599	1.818	2.646	4.243	6.764	14.209
SIN	20	3.591	1.737	1.426	2.067	2.863	6.237	10.864
STE	44	1.447	1.981	0.433	0.731	1.161	2.866	5.490
SIR	21	0.702	1.943	0.315	0.362	0.598	1.364	5.971
TAY	12	1.554	2.641	0.349	0.589	1.902	4.104	7.150
VAB	14	2.368	3.622	0.431	0.654	2.177	8.577	36.395
VAH	6	2.743	2.289	0.714	1.198	2.262	6.277	10.974
WLM	5	2.706	1.249	2.034	2.166	3.007	3.380	3.380
WLS	77	0.248	3.121	0.043	0.079	0.188	0.773	6.833
ZNA	14	2.948	2.881	0.432	1.023	2.305	8.493	26.385
All	480	1.260	3.696	0.043	0.260	1.503		36.395

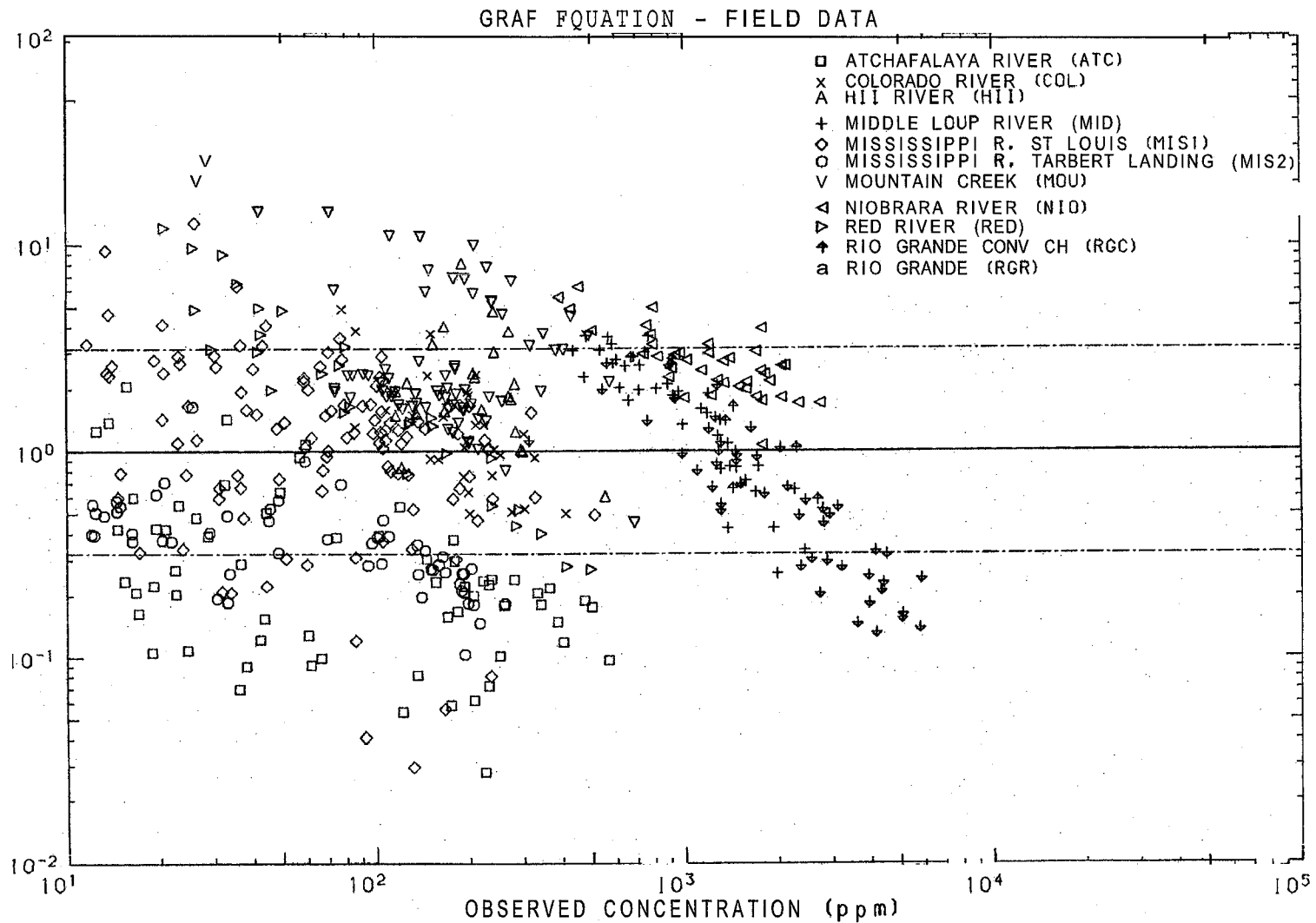


Figure 5.8b Ratio of concentration calculated by the Graf (1968) technique to observed concentration as a function of observed concentration, for field data,

Table 5.10b

Ratio of Predicted to Observed Concentration for Graf Method - Field Data

Data Set	Number	Geo.Mean	Geo.S.D.	Minimum	16 %ile	Median	84 %ile	Maximum
ATC	63	0.235	2.392	0.028	0.098	0.224	0.561	2.069
COL	30	1.265	1.809	0.501	0.699	1.213	2.288	4.887
HII	22	1.980	1.809	0.605	1.094	1.844	3.581	8.077
MID	38	1.490	2.022	0.258	0.737	1.854	3.013	3.607
MIS1	111	1.076	2.728	0.029	0.394	1.224	2.935	12.743
MIS2	53	0.347	1.624	0.104	0.214	0.363	0.564	1.644
MOU	75	2.682	2.148	0.453	1.249	2.017	5.762	25.596
NIO	40	2.643	1.430	1.068	1.848	2.582	3.780	6.215
RED	29	1.806	2.829	0.270	0.638	1.644	5.109	12.079
RGC	8	1.445	1.807	0.585	0.800	1.400	2.610	2.842
RGR	50	0.570	2.245	0.133	0.254	0.583	1.279	2.664
ALL	519	1.005	3.124	0.028	0.322	1.235	3.140	25.596

5.3.8 Laursen Technique (1958)

For the Laursen (1958) method, the particle size distribution is divided into n size fractions, p_i , which have mean size D_{si} and fall velocity w_i . The concentration is calculated from

$$c = 0.01 \sum_{i=1}^n p_i \left(\frac{D_{si}}{r} \right)^{7/6} \left[\frac{v^2}{58 Y_c D_{si} g \left(\frac{\rho_s - \rho}{\rho} \right)} \left(\frac{D_{50}}{r} \right)^{1/3} - 1 \right] \cdot f \left(\frac{u_*}{w_i} \right) \quad (5.16)$$

The value of Y_c is obtained from

$$Y_c = \begin{cases} 0.04 & \dots\dots D_{si}/\delta > 0.1 \\ 0.08 & \dots\dots 0.1 \geq D_{si}/\delta > 0.03 \\ 0.03 & \dots\dots D_{si}/\delta \leq 0.03 \end{cases} \quad (5.17)$$

where $\delta = 11.6\nu/u_*$ is the thickness of the laminar sublayer.

The function $f(u_*/w_i)$ was given graphically by Laursen (1958).

For this analysis, the following equation was fitted to the curve:

$$f \left(\frac{u_*}{w_i} \right) = \begin{cases} 3.988 + 0.250X & \dots\dots\dots \frac{u_*}{w_i} > 200 \\ -2.430 + 8.271X - 3.370X^2 + 0.476X^3 & \dots\dots 200 \geq \frac{u_*}{w_i} > 20 \\ 0.785 + 2.220X & \dots\dots\dots 20 \geq \frac{u_*}{w_i} > 2.8 \\ 1.162 + 0.767X + 1.014X^2 + 0.784X^3 & \dots\dots 2.8 \geq \frac{u_*}{w_i} > 0.2 \\ 1.025 + 0.245X & \dots\dots\dots \frac{u_*}{w_i} \leq 0.2 \end{cases} \quad (5.18)$$

where $X = \log(u_*/w_i)$.

The results of the analysis for laboratory data are given in Fig. 5.9a and Table 5.11a, and for field data, the results are given in Fig. 5.9b and Table 5.11b.

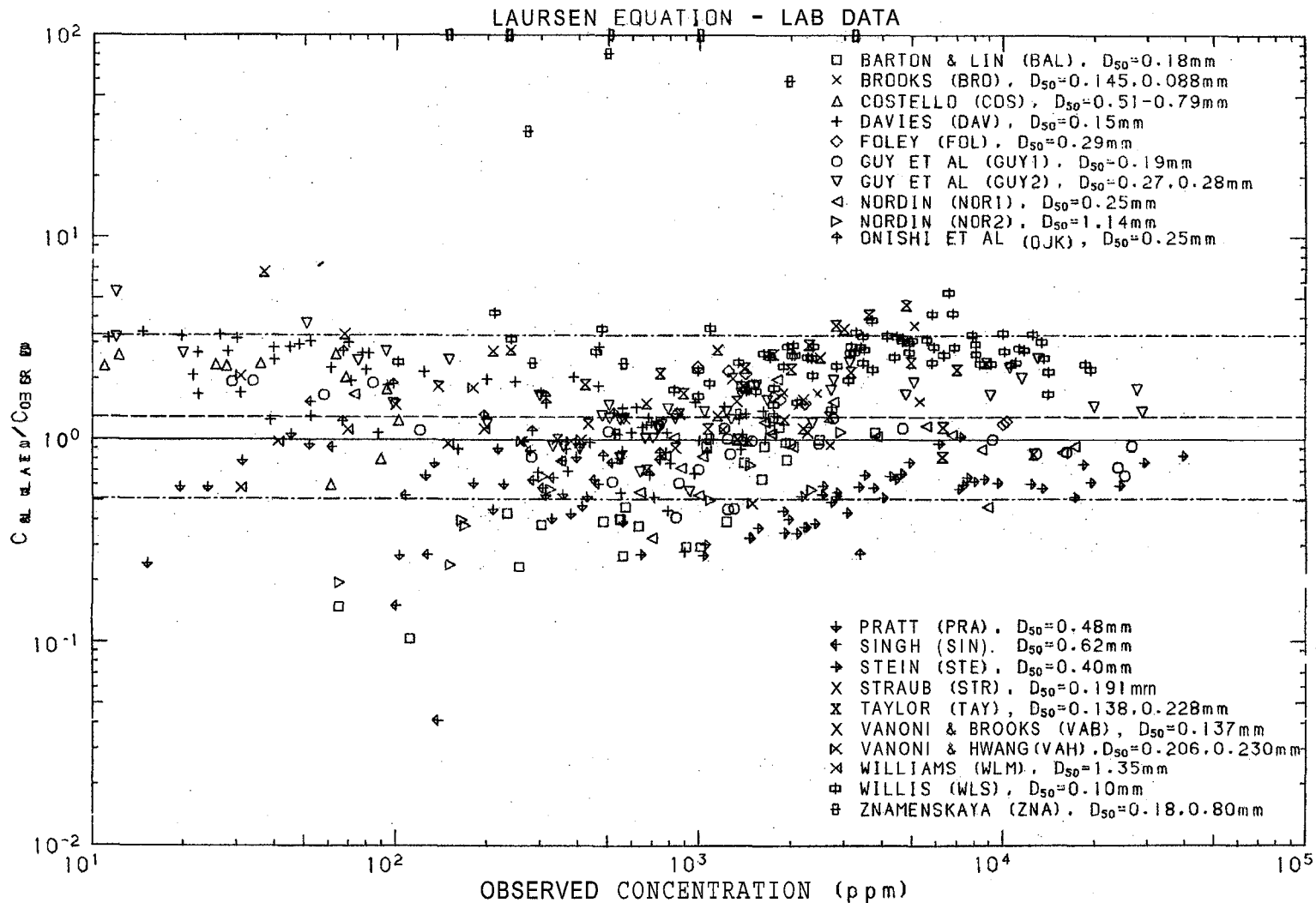


Figure 5.9a Ratio of concentration calculated by the Laursen (1958) technique to observed concentration as a function of observed concentration, for laboratory data,

Table 5.11a

Ratio of Predicted to Observed Concentration for Laursen Method - Lab Data

Data Set	Number	Geo.Mean	Geo.S.D.	Minimum	16 %ile	Median	84 %ile	Maximum
BAL	25	0.505	1.931	0.104	0.262	0.434	0.976	1.288
BRO	6	1.607	1.536	0.937	1.047	1.544	2.469	3.654
COS	11	1.738	1.619	0.598	1.073	2.298	2.814	2.637
DAV	69	1.439	1.723	0.280	0.835	1.346	2.479	3.402
FOL	9	1.630	1.262	1.193	1.292	1.580	2.056	2.279
GUY1	27	0.924	1.502	0.414	0.645	0.956	1.388	1.944
GUY2	47	1.539	1.536	0.556	1.002	1.458	2.363	5.336
NOR1	22	0.925	1.536	0.328	0.603	0.922	1.421	1.987
NOR2	10	0.478	1.633	0.195	0.283	0.503	0.781	1.091
OJK	14	1.090	1.693	0.274	0.644	1.110	1.845	2.732
PRA	21	0.562	1.451	0.245	0.387	0.584	0.816	1.068
SIN	15	0.524	2.362	0.041	0.222	0.637	1.238	1.540
STE	44	0.526	1.377	0.268	0.382	0.574	0.724	1.035
STR	21	1.884	1.644	0.821	1.146	2.160	3.098	4.627
TAY	12	1.276	1.329	0.709	0.960	1.282	1.695	2.007
VAB	14	2.111	1.673	0.988	1.262	1.849	3.531	6.698
VAH	6	1.098	1.605	0.486	0.684	0.983	1.762	2.064
WLM	5	0.929	1.280	0.578	0.726	0.979	1.190	1.135
WLS	77	2.599	1.286	1.412	2.020	2.645	3.344	5.328
ZNA	14	16.793	9.401	0.811	1.786	33.648	157.865	249.272
All	469	1.296	2.532	0.041	0.512	1.250	3.281	249.272

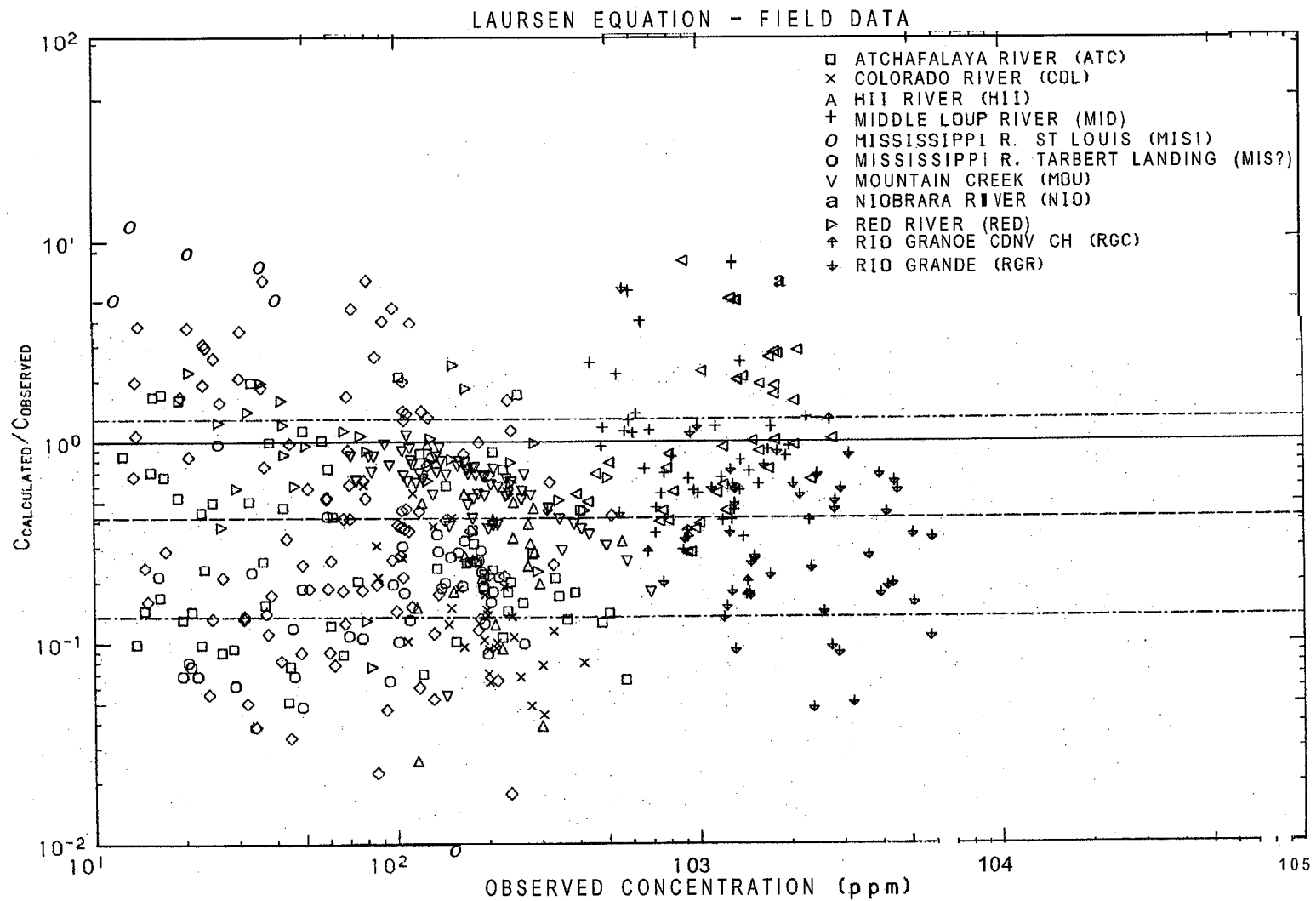


Figure 5.9b Ratio of concentration calculated by the Laursen (1958) technique to observed concentration as a function of observed concentration, for field data.

Table 5.11b

Ratio of Predicted to Observed Concentration for Laursen Method - Field Data

	Number	Geo.Mean	Geo.S.D.	Minimum	16 %ile	Median	84 %ile	Maximum
ATC	63	0.294	2.622	0.051	0.112	0.236	0.770	2.104
COL	30	0.138	1.942	0.044	0.071	0.115	0.268	0.610
HII	21	0.239	2.326	0.026	0.103	0.286	0.556	0.970
MID	38	0.935	2.061	0.293	0.454	0.840	1.927	7.601
MIS1	111	0.487	4.191	0.018	0.116	0.431	2.040	11.999
MIS2	42	0.146	2.172	0.009	0.067	0.181	0.317	0.973
MOU	71	0.575	1.551	0.055	0.371	0.654	0.892	1.077
NIO	40	1.079	2.385	0.284	0.453	0.894	2.574	8.260
RED	29	0.775	2.154	0.077	0.360	0.863	1.670	2.406
RGC	8	0.372	1.800	0.173	0.207	0.338	0.670	1.284
RGR	50	0.331	2.383	0.048	0.139	0.338	0.788	5.786
All	503	0.420	3.098	0.009	0.135	0.457	1.300	11.999

5.3.9 Ranga Raju, Garde, and Bhardwaj Technique (1981)

This is the most recently developed technique discussed. According to this method, the dimensionless transport rate, Φ , is determined from

$$\Phi = 60 \tau_*' \left(\frac{\tau_{o'}}{\tau_*'} \right)^{-3m} \quad (5.19)$$

in the range

$$0.05 \leq \tau_*' \left(\frac{r'}{r} \right)^{-m} \leq 1.0 \quad (5.20)$$

The quantity r' is defined from

$$r' = \left[\frac{vD_{50}^{1/6}}{7.66 \sqrt{gS}} \right]^{3/2} \quad (5.21)$$

which is the Strickler equation.

The exponent m is given by

$$m = \begin{cases} 0 & \dots \dots \dots \frac{u_*'}{w} \leq 0.5 \\ 0.2 \frac{u_*'}{w} - 0.10 & \dots \dots \frac{u_*'}{w} > 0.5 \end{cases} \quad (5.22)$$

The concentration can be determined from

$$C = \frac{\rho_s}{\rho q} \sqrt{\left(\frac{\rho_s - \rho}{\rho} \right) g D_{50}^3} \Phi \quad (5.23)$$

Equation 5.23 is slightly altered from the authors' equation by the removal of a factor of \sqrt{g} from the right side. As written here, Eq. 5.23 is dimensionless and conforms with the standard definition of Φ . The writer believes that there was a typesetting error in the original publication.

The results of the analysis for laboratory data are given in Fig. 5.10a and Table 5.12a, and for field data, the results are given in Fig. 5.10b and Table 5.12b.

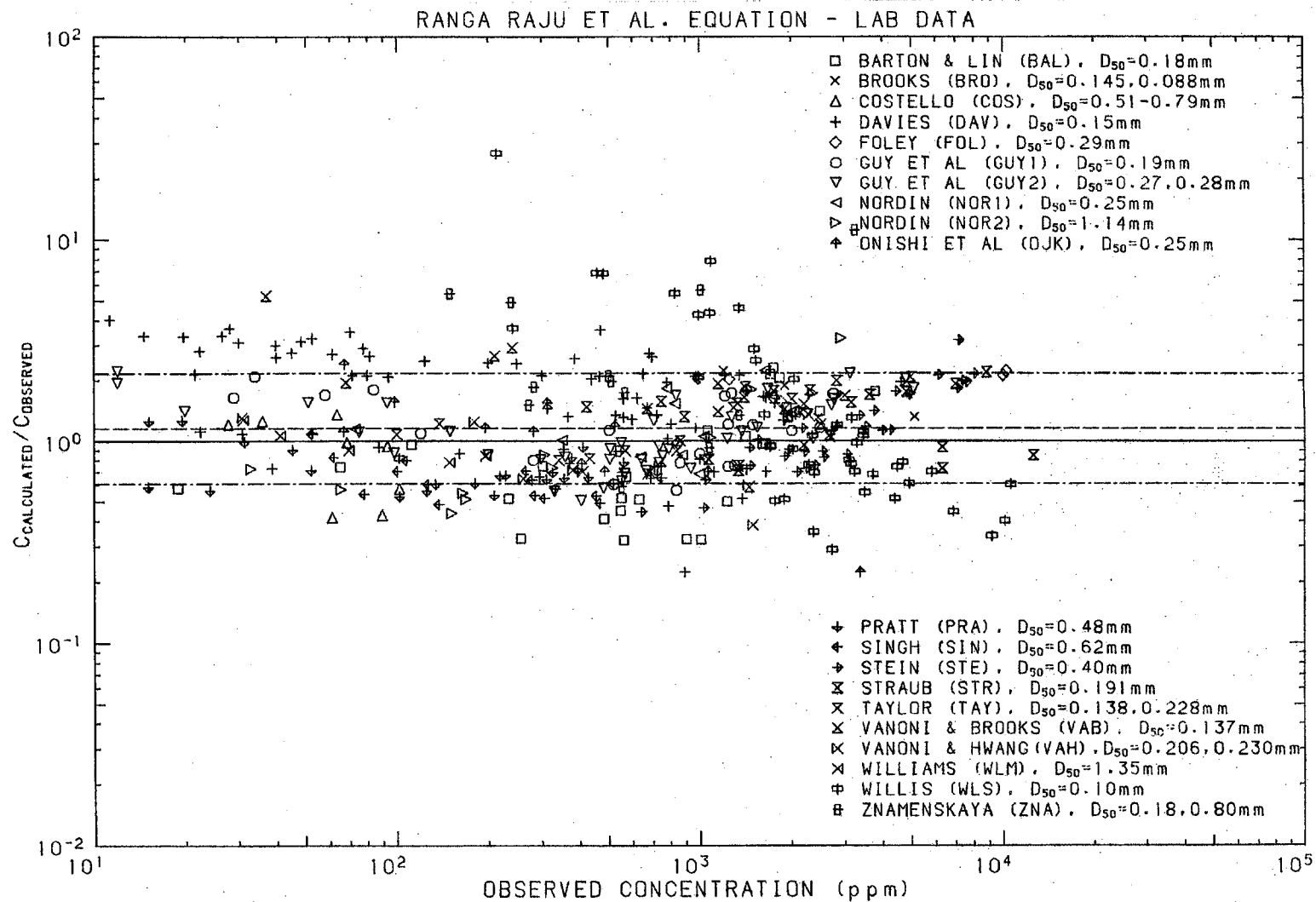


Figure 5.10a Ratio of concentration calculated by the Ranga Raju, Garde, and Bhardwaj (1981) technique to observed concentration as a function of observed concentration, for laboratory data.

Table 5.12a

Ratio of Predicted to Observed Conc. for Ranga Raju et al, Method - Lab Data

Data Set	Number	Geo.Mean	Geo.S.D.	Minimum	16 %ile	Median	84 %ile	Maximum
BAL	26	0.782	1.847	0.323	0.423	0.744	1.444	2.312
BRO	5	1.499	1.318	1.039	1.137	1.322	1.976	2.233
COS	8	0.817	1.573	0.418	0.519	0.944	1.286	1.358
DAV	69	1.608	1.832	0.224	0.878	1.959	2.946	4.035
FOL	9	1.706	1.281	0.974	1.331	1.795	2.185	2.233
GUY1	20	1.138	1.468	0.569	0.775	1.134	1.671	2.094
GUY2	40	1.067	1.480	0.507	0.721	0.981	1.580	2.236
NOR1	12	1.168	1.448	0.685	0.807	1.057	1.692	2.238
NOR2	11	0.908	1.820	0.438	0.499	0.736	1.652	3.249
OJK	14	0.967	1.729	0.224	0.559	1.119	1.671	2.413
PRA	22	0.723	1.276	0.530	0.567	0.672	0.923	1.267
SIN	16	0.631	1.234	0.484	0.512	0.608	0.779	1.084
STE	34	1.143	1.570	0.445	0.728	1.131	1.795	3.180
SIR	21	1.362	1.456	0.711	0.935	1.576	1.983	2.203
TAY	12	1.061	1.293	0.685	0.820	1.003	1.372	1.539
VAB	14	1.671	1.646	0.590	1.015	1.529	2.750	5.292
VAH	6	0.769	1.519	0.383	0.507	0.705	1.169	1.315
WLM	5	0.961	1.192	0.784	0.806	0.903	1.145	1.218
WLS	45	1.237	2.664	0.290	0.464	0.939	3.296	26.822
ZNA	14	2.087	2.223	0.591	0.939	1.741	4.640	11.093
A11	403	1.160	1.882	0.224		1.115		26.822

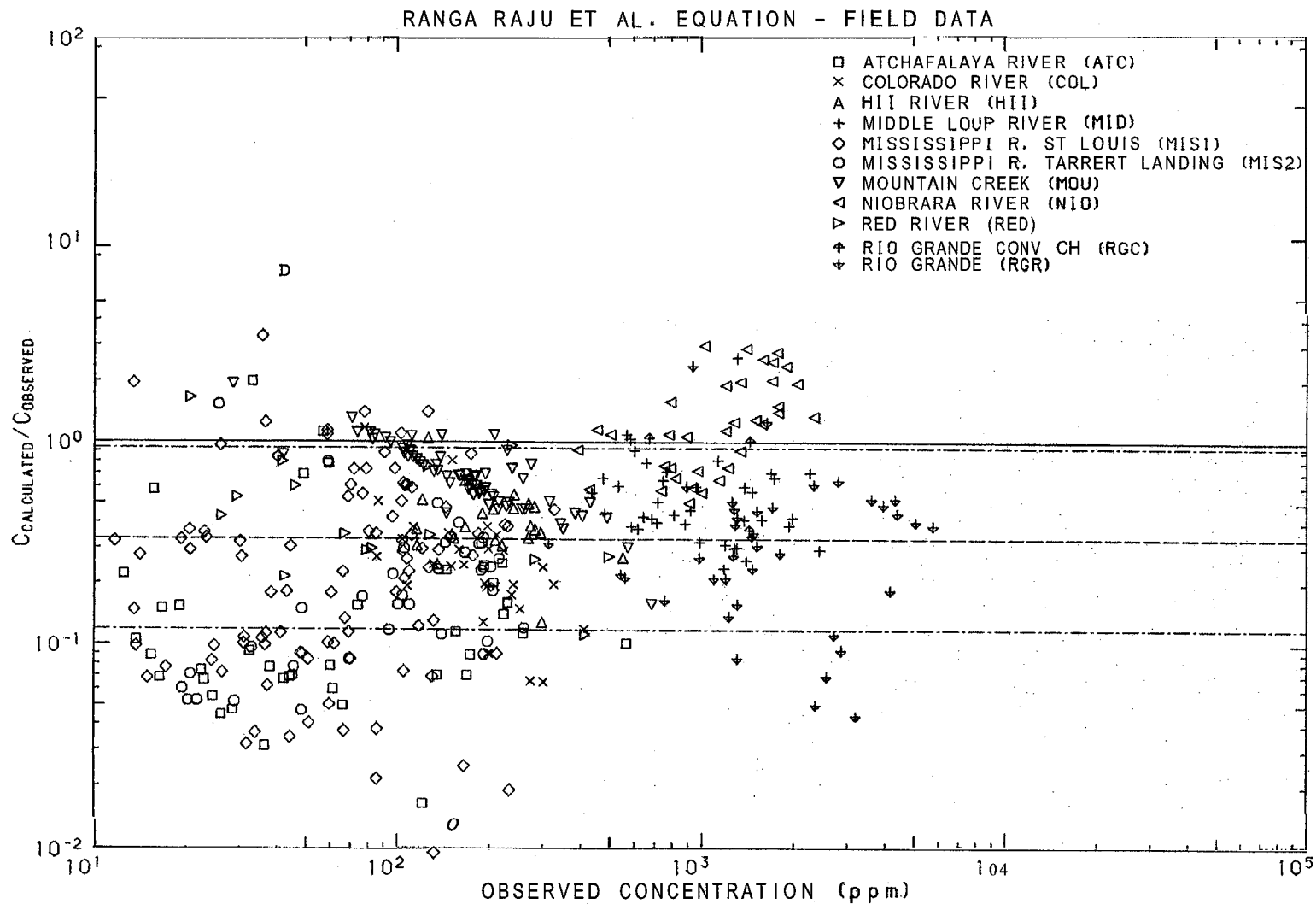


Figure 5.10b Ratio of concentration calculated by the Ranga Raju, Garde, and Bhardwaj (1981) technique to observed concentration as a function of observed concentration, for field data,

Table 5.12b

Ratio of Predicted to Observed Conc. for Ranga Raju et al. Method - Field Data

Data Set	Number	Geo.Mean	Geo.S.D.	Minimum	16 %ile	Median	84 %ile	Maximum
ATC	39	0.125	2.635	0.017	0.047	0.102	0.328	1.986
COL	30	0.228	1.888	0.066	0.121	0.242	0.431	1.172
HII	22	0.389	1.477	0.129	0.264	0.372	0.575	1.042
MID	38	0.515	1.585	0.238	0.325	0.443	0.817	2.610
MIS1	96	0.218	3.121	0.009	0.070	0.270	0.679	3.301
MIS2	39	0.159	2.398	0.013	0.066	0.171	0.381	1.528
MOU	73	0.667	1.449	0.158	0.460	0.674	0.967	1.933
NIO	35	1.195	1.693	0.502	0.706	1.154	2.022	2.982
RED	16	0.505	2.534	0.113	0.199	0.352	1.279	7.059
RGC	3	0.732	1.623	0.369	0.451	1.013	1.189	1.050
	39	0.288	2.229	0.045	0.129	0.316	0.642	2.372
	430	0.333	2.813	0.009	0.118	0.381	0.936	7.059

5.3.10 Rottner Technique (1959)

The Rottner (1959) technique is a simple equation which was based on dimensional analysis. Concentration is a function of a relative roughness, D_{50}/r , and a modified Froude number, F_D , in the form:

$$C = \frac{\rho_s}{\rho F_D} \left\{ \left[0.667 \left(\frac{D_{50}}{r} \right)^{2/3} + 0.140 \right] F_D - 0.778 \left(\frac{D_{50}}{r} \right)^{2/3} \right\}^3 \quad (5.24)$$

where $F_D = \frac{v}{\sqrt{\left(\frac{\rho_s - \rho}{\rho} \right) g r}}$

The results of the analysis for laboratory data are given in Fig. 5.11a and Table 5.13a, and for field data, the results are given in Fig. 5.11b and Table 5.13b.

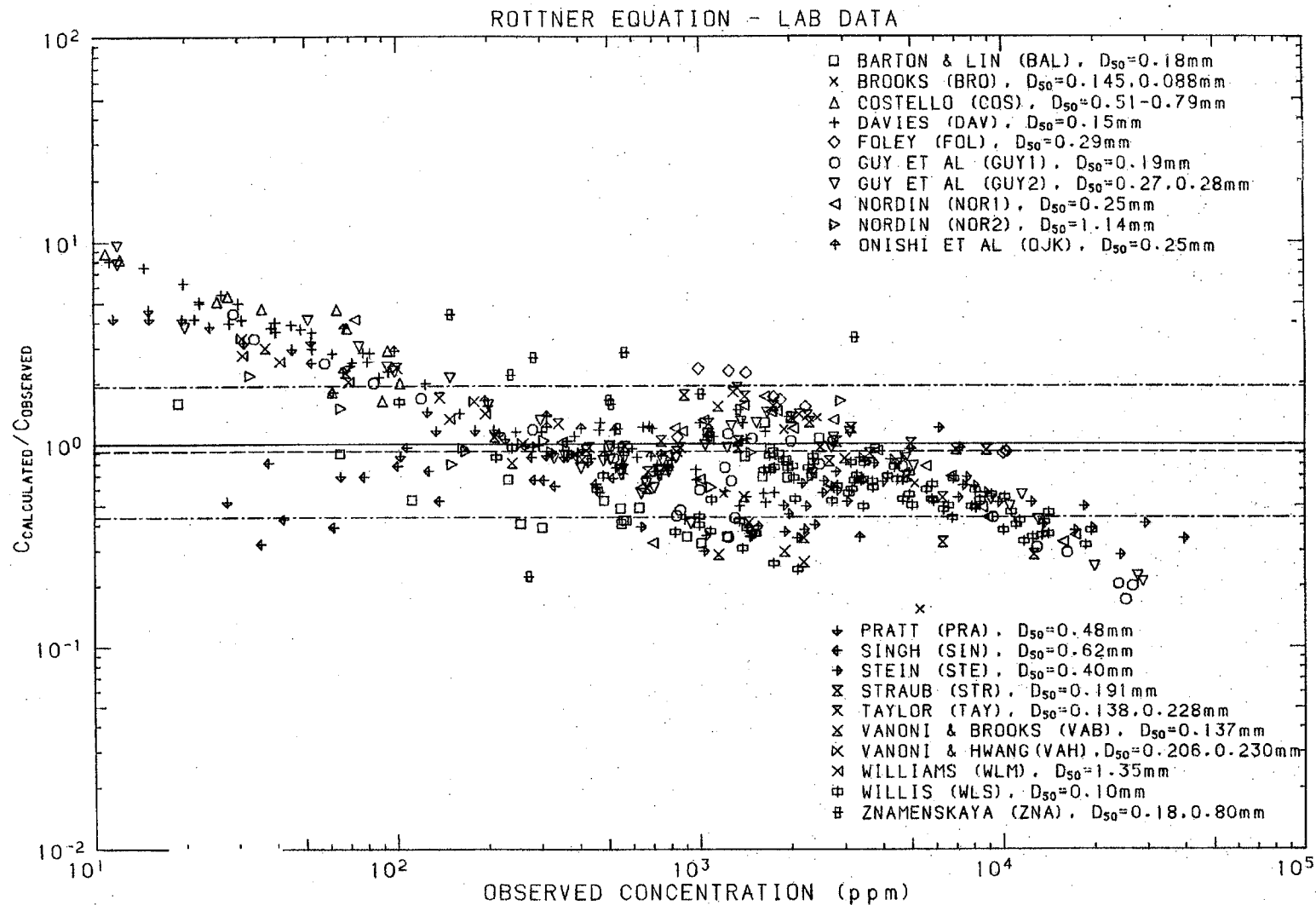


Figure 5.11a Ratio of concentration calculated by the Rottner (1959) technique to observed concentration as a function of observed concentration, for laboratory data.

Table 5.13a

Ratio of Predicted to Observed Concentration for Rottner Method - Lab Data

Data Set	Number	Geo.Mean	Geo.S.D.	Minimum	16 %ile	Median	84 %ile	Maximum
BAL	26	0.644	1.558	0.326	0.413	0.672	1.004	1.596
BRO	6	0.611	2.020	0.153	0.302	0.598	1.235	1.340
COS	11	3.835	1.737	1.627	2.209	4.614	6.660	8.771
DAV	69	1.505	2.155	0.428	0.698	1.172	3.242	8.052
FOL	9	1.525	1.433	0.899	1.064	1.644	2.186	2.340
GUY1	27	0.735	2.272	0.171	0.323	0.773	1.670	4.413
GUY2	47	0.979	2.165	0.210	0.452	0.850	2.119	9.599
NOR1	22	0.898	1.834	0.327	0.490	0.927	1.647	4.122
NOR2	11	1.028	1.438	0.612	0.715	0.921	1.478	2.174
OJK	14	1.251	1.755	0.347	0.713	1.169	2.195	3.731
PRA	25	1.451	1.978	0.522	0.734	1.134	2.870	4.623
SIN	20	0.724	1.574	0.323	0.460	0.679	1.140	2.508
STE	44	0.531	1.420	0.286	0.374	0.518	0.754	1.198
STR	21	0.938	1.572	0.286	0.597	1.003	1.474	1.736
TAY	12	1.281	1.407	0.729	0.910	1.255	1.804	2.365
VAB	14	0.707	2.106	0.263	0.336	0.607	1.490	2.982
VAH	6	1.072	1.940	0.384	0.553	0.866	2.080	3.345
WLM	5	1.925	1.348	1.325	1.428	2.020	2.594	2.749
WLS	77	0.549	1.396	0.242	0.393	0.564	0.766	1.613
ZNA	14	1.581	1.992	0.224	0.793	1.567	3.149	4.370
ALL	480	0.920	2.101	0.153	0.438	0.847	1.932	9.599

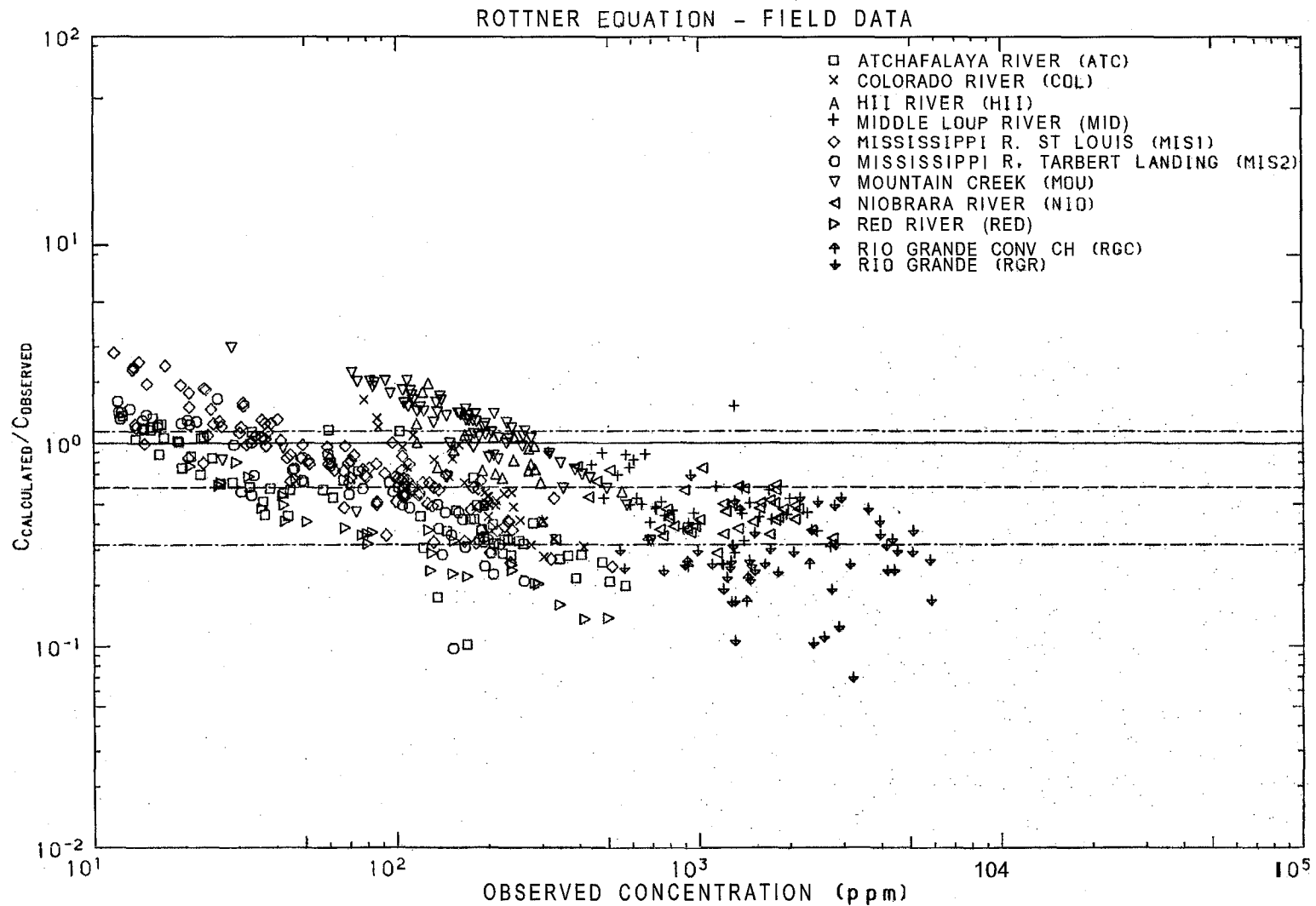


Figure 5.11b Ratio of concentration calculated by the Rottner (1959) technique to observed concentration as a function of observed concentration, for field data,

Table 5.13b

Ratio of Predicted to Observed Concentration for Rottner Method - Field Data

Data Set	Number	Geo.Mean	Geo.S.D.	Minimum	16 %ile	Median	84 %ile	Maximum
ATC	63	0.526	1.787	0.102	0.294	0.539	0.939	1.362
COL	30	0.606	1.553	0.277	0.390	0.545	0.941	1.634
HII	22	0.892	1.425	0.413	0.626	0.816	1.272	1.963
MID	38	0.503	1.441	0.253	0.349	0.474	0.725	1.525
MIS1	111	0.778	1.676	0.248	0.464	0.749	1.305	2.792
MIS2	53	0.611	1.893	0.097	0.323	0.595	1.158	1.652
MOU	75	1.187	1.475	0.331	0.805	1.241	1.751	2.980
NIO	40	0.464	1.257	0.289	0.369	0.460	0.584	0.764
RED	29	0.347	1.644	0.136	0.211	0.359	0.570	0.805
RGC	8	0.271	1.332	0.166	0.203	0.256	0.361	0.466
RGR	50	0.271	1.623	0.070	0.167	0.263	0.439	0.908
All	519	0.603	1.904	0.070	0.317	0.596	1.149	2.980

5.3.11 Shen and Hung Technique (1971)

Shen and Hung (1971) developed a single equation using advanced curve fitting techniques. The equation does not use dimensionless parameters and the units are in the English system. The equation for C in ppm by mass is:

$$\log C = a_0 + a_1 X + a_2 X^2 + a_3 X^3 \quad (5.25)$$

where

$$X = v^{a_4} S^{a_5} w^{a_6} \quad (5.26)$$

The quantities v and w are the flow velocity and fall velocity of the median sediment particle, respectively, in ft/s. The coefficients are:

$$\begin{aligned} a_0 &= -107404.46 \\ a_1 &= 324214.75 \\ a_2 &= -326309.59 \\ a_3 &= 109503.87 \\ a_4 &= 0.00750189 \\ a_5 &= 0.00428802 \\ a_6 &= -0.00239974 \end{aligned}$$

which have been rounded to 8 significant figures.

The results of the analysis for laboratory data are given in Fig. 5.12a and Table 5.14a, and for field data, the results are given in Fig. 5.12b and Table 5.14b.

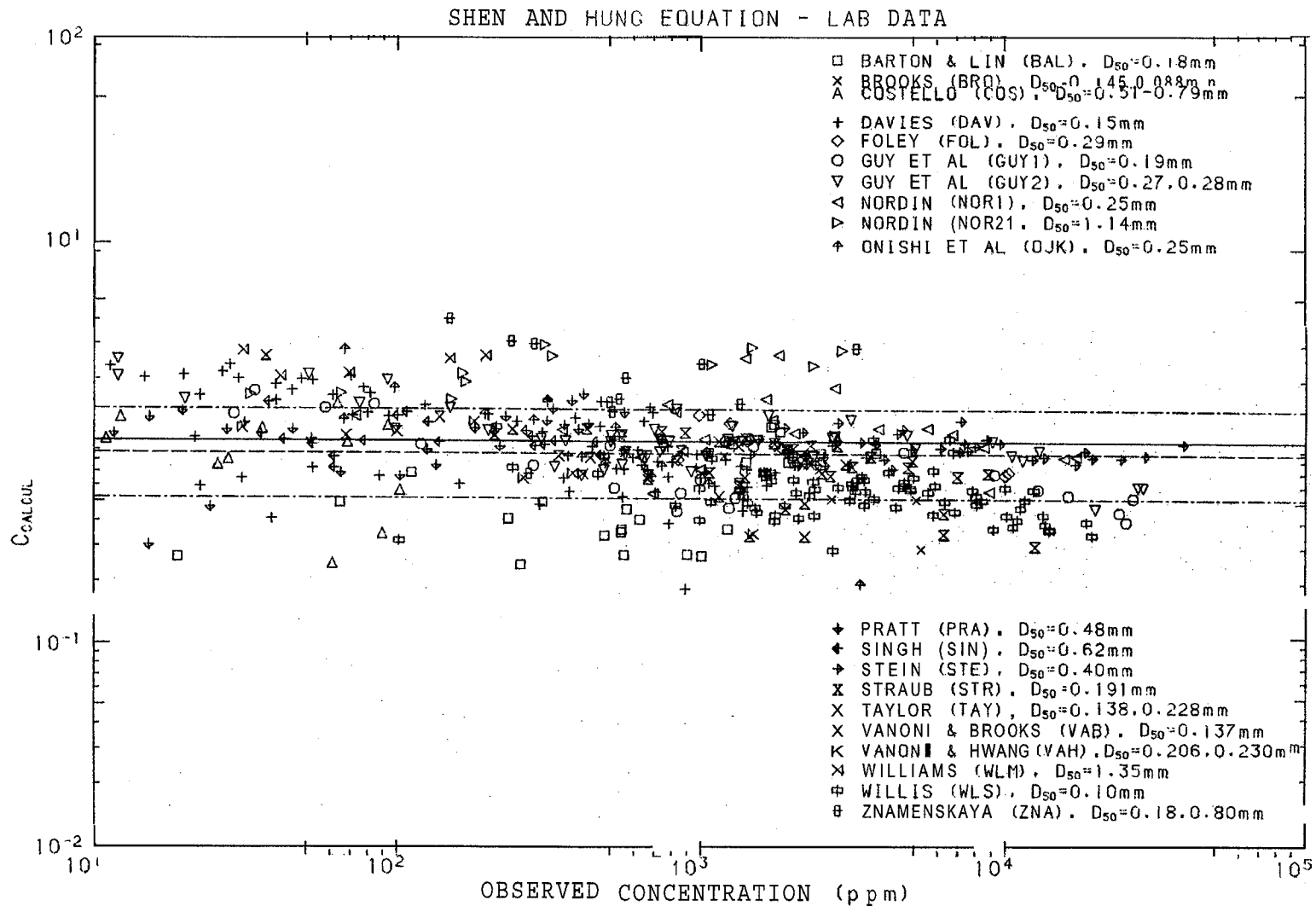


Figure 5.12a Ratio of concentration calculated by the Shen and Hung (1971) technique to observed concentration as a function of observed concentration, for laboratory data,

Table 5.14a

Ratio of Predicted to Observed Conc. for Shen and Hung Method - Lab Data

Data Set	Number	Geo.Mean	Geo.S.D.	Minimum	16 %ile	Median	84 %ile	Maximum
BAL	26	0.536	1.658	0.245	0.323	0.495	0.889	1.221
BRO	6	0.599	1.472	0.296	0.407	0.521	0.881	0.936
COS	11	0.797	1.720	0.247	0.463	0.984	1.371	1.520
DAV	69	0.966	1.682	0.186	0.574	0.861	1.624	2.353
FOL	9	0.916	1.247	0.685	0.735	0.928	1.143	1.347
GUY1	27	0.774	1.485	0.404	0.522	0.771	1.150	1.746
GUY2	47	1.027	1.391	0.468	0.738	1.009	1.429	2.497
NOR1	22	1.133	1.488	0.552	0.761	1.101	1.685	2.657
NOR2	11	2.226	1.246	1.588	1.787	2.350	2.773	2.977
OJK	14	1.018	1.843	0.197	0.553	1.175	1.877	2.794
PRA	25	1.039	1.461	0.303	0.711	1.145	1.518	1.698
SIN	20	1.039	1.185	0.732	0.877	1.005	1.231	1.542
STE	44	0.910	1.152	0.703	0.790	0.899	1.048	1.273
STR	21	0.741	1.424	0.306	0.520	0.753	1.055	1.151
TAY	12	0.899	1.180	0.673	0.762	0.850	1.061	1.307
VAB	14	0.727	1.688	0.341	0.431	0.665	1.227	2.607
VAH	6	0.737	1.520	0.351	0.485	0.692	1.120	1.248
WLM	5	2.411	1.124	2.063	2.145	2.534	2.711	2.782
WLS	77	0.551	1.309	0.291	0.421	0.566	0.721	1.175
ZNA	14	1.740	1.648	0.690	1.056	1.555	2.869	4.029
All	480	0.866	1.656	0.186	0.523	0.858	1.435	4.029

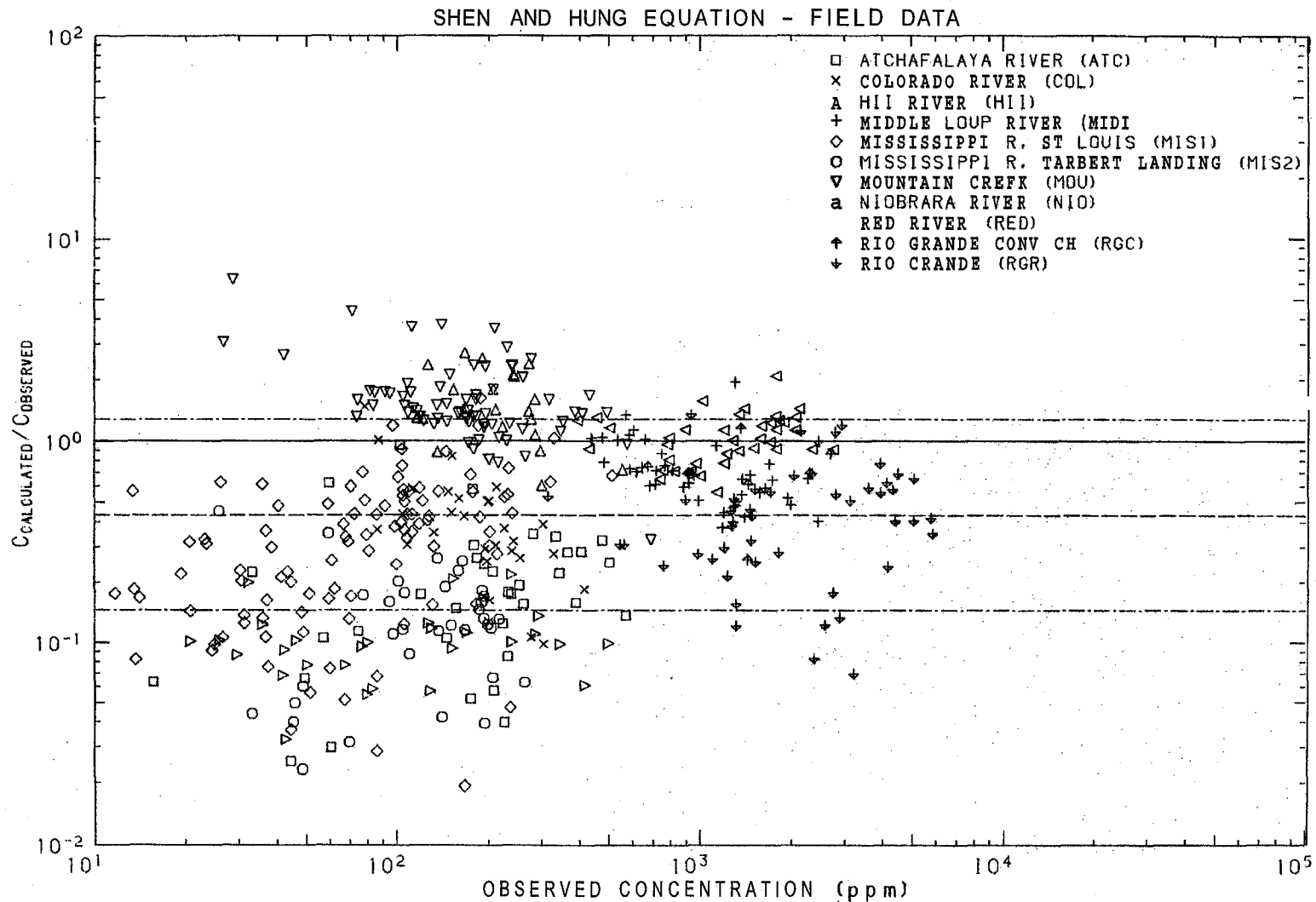


Figure 5.12b Ratio of concentration calculated by the Shen and Hung (1971) technique to observed concentration as a function of observed concentration, for field data.

Table 5.14b

Ratio of Predicted to Observed Conc. for Shen and Hung Method - Field Data

Data Set	Number	Geo.Mean	Geo.S.D.	Minimum	16 %ile	Median	84 %ile	Maximum
ATC	35	0.161	2.271	0.025	0.071	0.175	0.366	0.959
COL	30	0.347	1.844	0.099	0.188	0.354	0.640	1.475
HII	22	1.441	1.490	0.605	0.967	1.400	2.148	2.710
MID	38	0.698	1.418	0.376	0.492	0.677	0.990	1.951
MIS1	100	0.280	2.339	0.019	0.120	0.333	0.654	1.619
MIS2	34	0.112	2.019	0.023	0.055	0.122	0.225	0.455
MOU	75	1.516	1.547	0.327	0.980	1.398	2.345	6.290
NIO	40	1.013	1.317	0.559	0.769	1.005	1.334	2.089
RED	28	0.096	1.499	0.033	0.064	0.099	0.144	0.219
RGC	8	0.667	1.492	0.260	0.447	0.693	0.996	1.153
RGR	50	0.399	1.927	0.070	0.207	0.431	0.768	1.353
ALL	460	0.432	2.973	0.019	0.145	0.511	1.284	6.290

5.3.12 Toffaleti Technique (1968)

Toffaleti (1968) used the Einstein (1950) method as an inspiration for the development of this technique. Since the technique is quite complex, a full description is not given here. Full descriptions of the method can be found in Vanoni (1975, pp. 209-213) and White, Milli, and Crabbe (1973, pp. 35-41).

The principal similarity between the Einstein and Toffaleti techniques is the use of an empirical equation to determine a bed load concentration from which the suspended load concentration can be determined. For the Toffaleti technique, the suspended zone is divided into an upper, middle, and lower zone. For each zone the integral of the product of the concentration equation and the velocity equation has been replaced by an explicit function. These functions were developed for the English system of measurement, and are not dimensionally homogeneous.

Large amounts of field and laboratory data were used to determine the empirical coefficients. Much of the data used in the analysis here were actually used by Toffaleti (1968) in the original development of the technique. The Mississippi River and Atchafalaya River data were in fact obtained from **this** source.

The results of the analysis for laboratory data are given in Fig. 5.13a and Table 5.15a, and the results for field data are given in Fig. 5.13b and Table 5.15b.

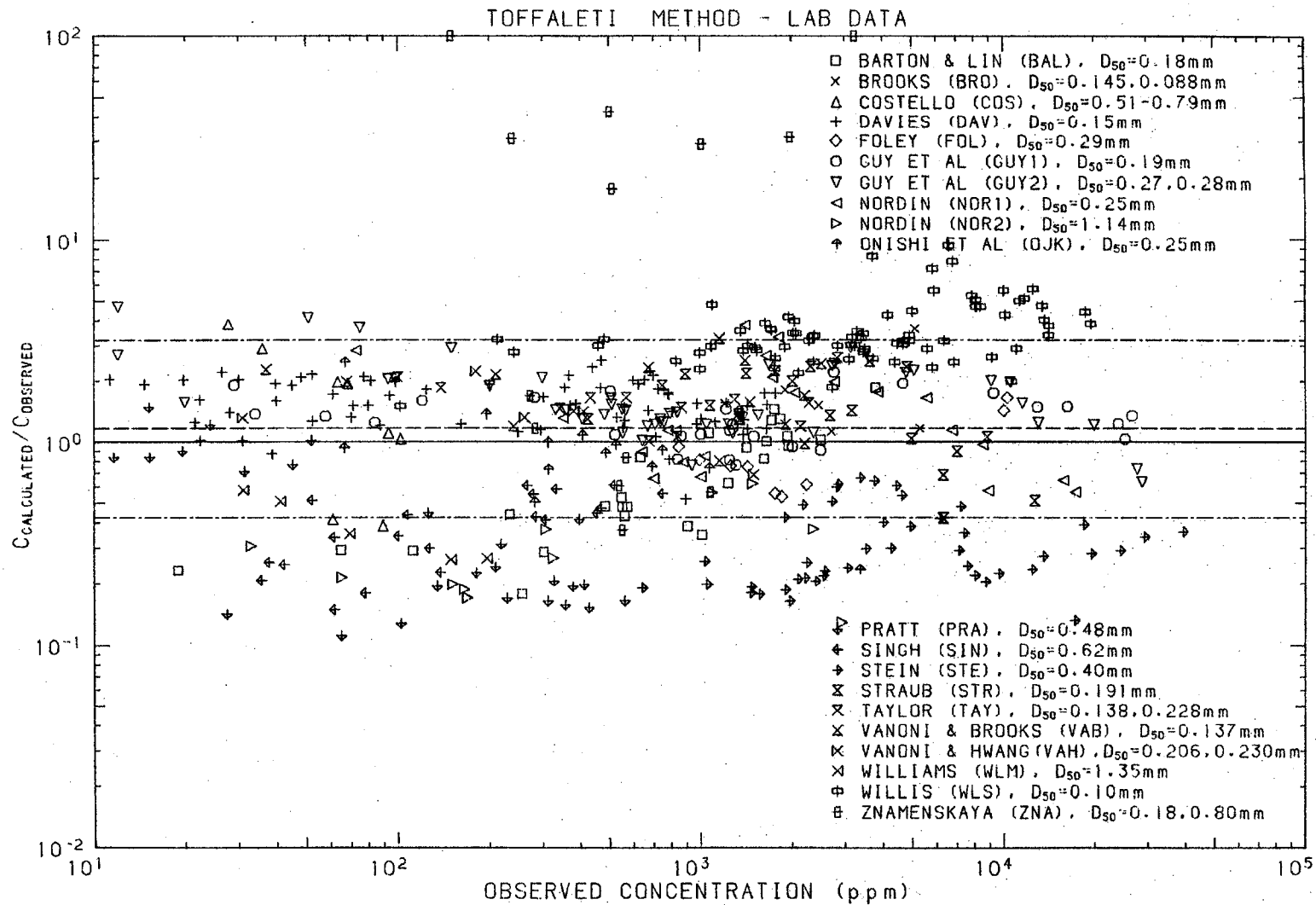


Figure 5.13a Ratio of concentration calculated by the Toffaletti (1968) technique to observed concentration as a function of observed concentration, for laboratory data.

Table 5.15a

Ratio of Predicted to Observed Concentration for Toffaleti Method - Lab Data

Data Set	Number	Geo. Mean	Geo. S.D.	Minimum	16 %ile	Median	84 %ile	Maximum
BAL	26	0.614	1.854	0.178	0.331	0.531	1.139	1.857
BRO	6	1.648	1.478	1.123	1.115	1.512	2.435	3.641
COS	8	1.291	2.207	0.385	0.585	1.105	2.850	3.833
DAV	69	1.533	1.328	0.522	1.154	1.547	2.035	2.540
FOL	9	0.830	1.452	0.535	0.572	0.757	1.205	1.656
GUY1	27	1.273	1.321	0.765	0.964	1.245	1.682	2.210
GUY2	47	1.599	1.521	0.634	1.051	1.430	2.432	4.683
NOR1	22	1.274	1.774	0.565	0.718	1.138	2.260	3.792
NOR2	11	0.276	1.607	0.130	0.171	0.268	0.443	0.621
OJK	14	0.907	1.721	0.235	0.527	0.911	1.562	2.484
PRA	25	0.326	2.229	0.111	0.146	0.226	0.727	1.483
SIN	20	0.362	1.525	0.149	0.237	0.413	0.553	0.610
STE	44	0.298	1.523	0.133	0.195	0.274	0.453	0.664
SIR	21	1.411	1.663	0.423	0.848	1.427	2.347	2.610
TAY	12	1.468	1.230	1.008	1.193	1.477	1.805	2.089
VAB	13	1.746	1.491	0.803	1.171	1.990	2.604	3.256
VAH	6	1.323	1.413	0.687	0.937	1.324	1.870	2.240
WLM	5	0.374	1.382	0.263	0.270	0.353	0.517	0.577
WLS	77	3.445	1.392	1.502	2.474	3.226	4.797	9.367
ZNA	14	6.065	7.915	0.367	0.766	1.687	48.002	123.929
All	476	1.166	2.749			1.312	3.206	123.929

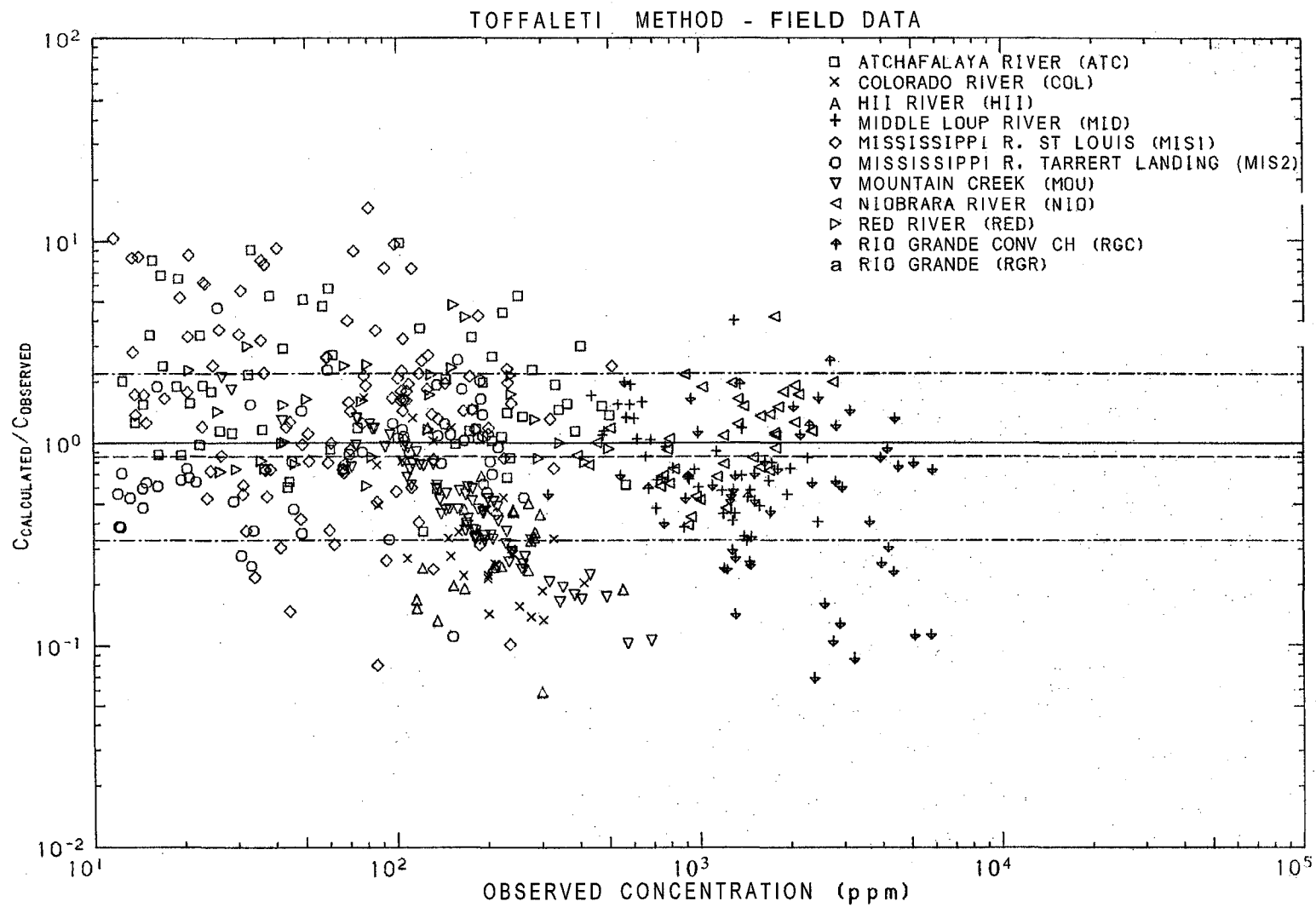


Figure 5.13b Ratio of concentration calculated by the Toffaleti (1968) technique to observed concentration as a function of observed concentration, for field data,

Table 5.15b

Ratio of Predicted to Observed Concentration for Toffaleti Method - Field Data

Data Set	Number	Geo.Mean	Geo.S.D.	Minimum	16 %ile	Median	84 %ile	Maximum
ATC	63	1.761	2.166	0.365	0.813	1.543	3.814	9.800
COL	30	0.358	1.966	0.134	0.182	0.301	0.704	1.666
HII	22	0.283	1.861	0.059	0.152	0.245	0.526	1.182
MID	38	0.817	1.682	0.348	0.486	0.745	1.375	4.028
MIS1	111	1.461	2.806	0.080	0.521	1.559	4.101	14.510
MIS2	53	0.809	1.919	0.111	0.422	0.808	1.554	4.649
MOU	75	0.483	1.866	0.102	0.259	0.471	0.902	2.107
NIO	40	1.042	1.650	0.393	0.632	1.047	1.720	4.194
RED	29	1.418	1.714	0.612	0.827	1.429	2.430	4.801
RGC	8	0.856	1.910	0.329	0.448	0.676	1.635	2.536
RGR	50	0.465	2.304	0.069	0.202	0.551	1.071	1.996
All	519	0.854	2.572	0.059	0.332	0.816	2.196	14.510

5.3.13 Yang Technique (1973)

This technique is based primarily on dimensional analysis. The principal variable is the dimensionless unit stream power, vS/w . Concentration is obtained from

$$\log C = a_1 + a_2 \log \left(\frac{vS}{w} - \frac{v_{cr}S}{w} \right) \quad (5.27)$$

where

$$a_1 = -0.565 - 0.286 \log \frac{wD_{50}}{v} - 0.457 \log \frac{u_*}{w}$$

$$a_2 = 1.799 - 0.409 \log \frac{wD_{50}}{v} - 0.314 \log \frac{u_*}{w}$$

and w is fall velocity.

The critical velocity is determined from

$$v_{cr} = \begin{cases} 2.05 \dots \dots \dots \frac{u_* D_{50}}{v} \geq 70 \\ \frac{2.5}{\log \left(\frac{u_* D_{50}}{v} \right) - 0.06} \dots \dots \dots 1.2 < \frac{u_* D_{50}}{v} < 70 \end{cases} \quad (5.28)$$

As written here, the concentration is given in mass per unit mass. To convert to ppm, 6 should be added to the right side of Eq. 5.27.

The results of the analysis for laboratory data are given in Fig. 5.14a and Table 5.16a, and for field data, the results are given in Fig. 5.14b and Table 5.16b.

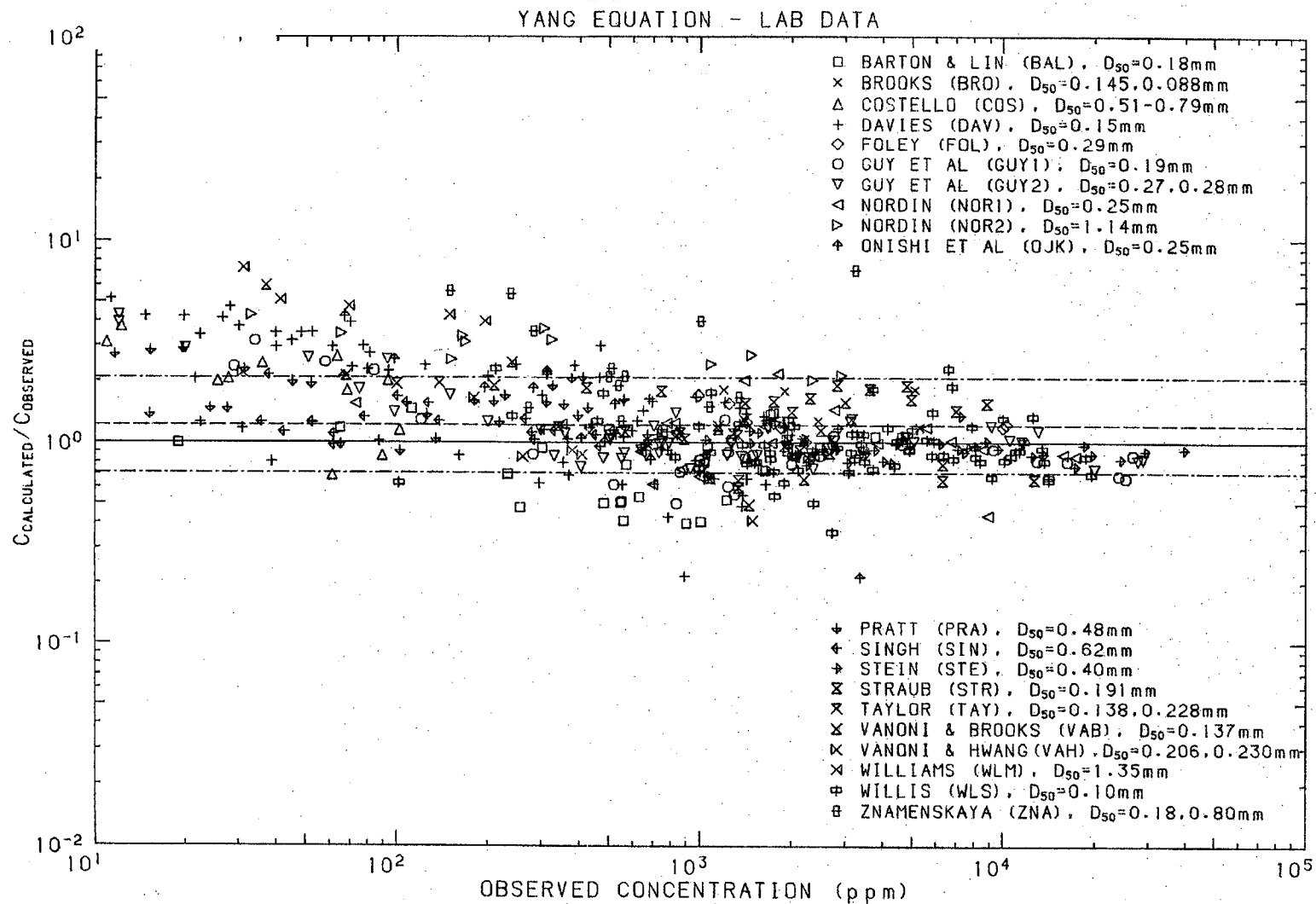


Figure 5.14a Ratio of concentration calculated by the Yang (1973) technique to observed concentration as a function of observed concentration, for laboratory data.

Table 5.16a

Ratio of Predicted to Observed Concentration for Yang Method - Lab Data

Data Set	Number	Geo. Mean	Geo. S.D.	Minimum	16 %ile	Median	84 %ile	Maximum
BAL	26	0.766	1.499	0.398	0.511	0.778	1.148	1.462
BRO	6	1.446	1.255	1.037	1.152	1.275	1.815	1.815
COS	11	1.827	1.653	0.688	1.105	2.014	3.019	3.735
DAV	69	1.486	1.957	0.217	0.759	1.385	2.909	5.158
FCL	9	1.258	1.164	1.007	1.081	1.225	1.464	1.698
GUY1	27	0.979	1.585	0.499	0.618	0.865	1.551	3.162
GUY2	47	1.137	1.511	0.734	0.753	1.011	1.718	4.285
NOR1	22	1.019	1.440	0.434	0.708	0.993	1.468	2.174
NOR2	11	2.915	1.249	2.024	2.334	3.120	3.640	4.266
OK	14	1.351	2.027	0.214	0.666	1.550	2.738	4.194
PRA	25	1.649	1.347	0.909	1.225	1.590	2.222	2.896
SIN	20	1.245	1.213	0.958	1.027	1.157	1.510	2.150
STE	44	0.943	1.124	0.759	0.839	0.928	1.060	1.353
SIR	21	1.198	1.519	0.596	0.789	1.429	1.820	1.904
TAY	12	1.165	1.281	0.844	0.909	1.108	1.492	1.956
VAB	14	1.347	1.795	0.490	0.751	1.163	2.418	5.968
VAH	6	1.004	1.707	0.411	0.588	0.873	1.713	2.204
WLM	5	4.955	1.238	3.966	4.004	4.730	6.132	7.329
WLS	77	0.945	1.369	0.359	0.690	0.906	1.294	2.299
ZNA	14	2.462	1.781	1.093	1.383	2.102	4.384	7.110
ALL	480	1.215	1.710	0.214		1.094	2.078	7.329

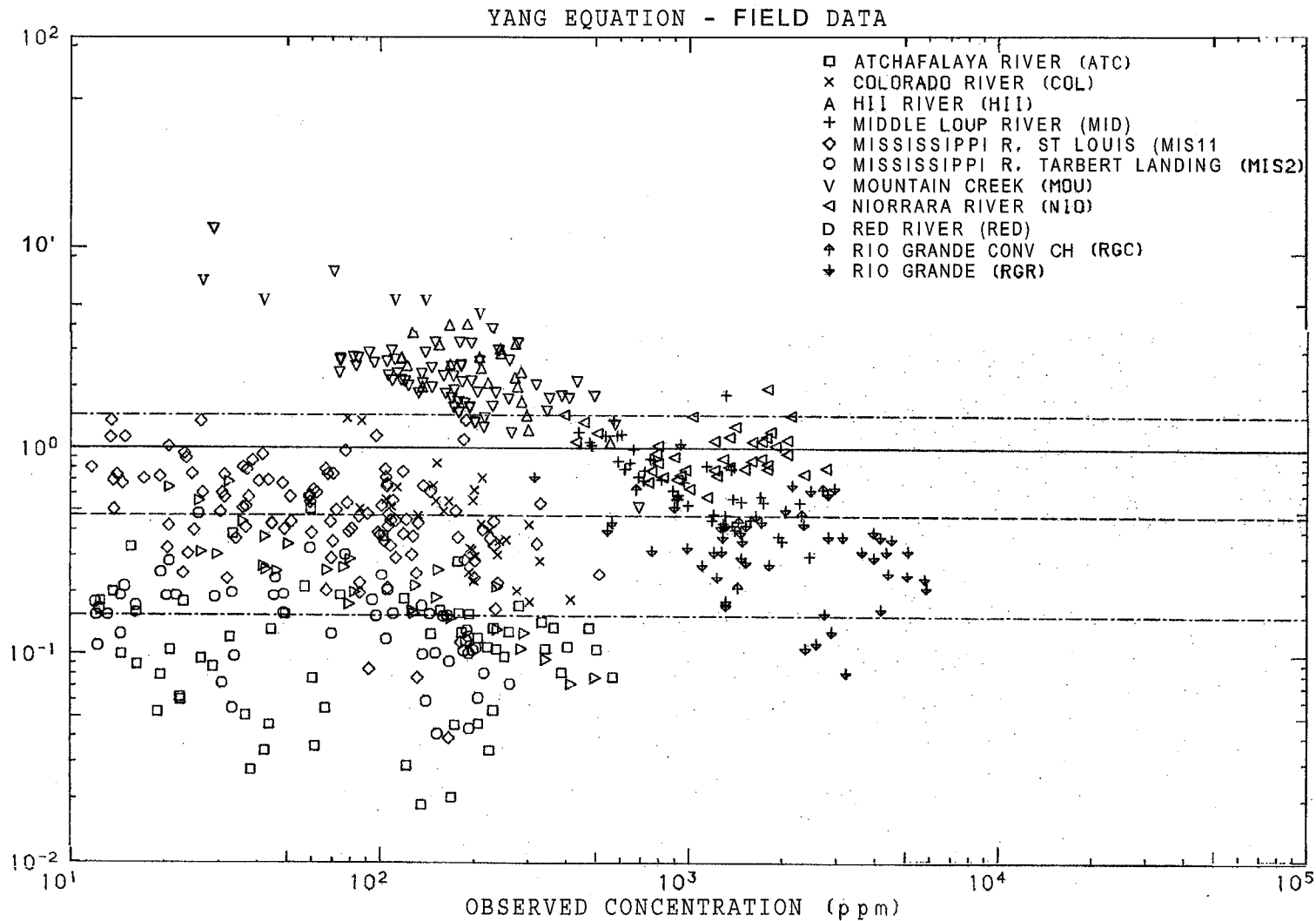


Figure 5.14b Ratio of concentration calculated by the Yang (1973) technique to observed concentration as a function of observed concentration, for field data.

Table 5.16b

Ratio of Predicted to Observed Concentration for Yang Method - Field Data

Data Set	Number	Geo.Mean	Geo.S.D.	Minimum	16 %ile	Median	84 %ile	Maximum
ATC	57	0.099	2.045	0.019	0.049	0.106	0.203	0.505
COL	30	0.437	1.657	0.179	0.264	0.428	0.724	1.390
HII	22	2.395	1.410	1.066	1.699	2.504	3.376	4.003
MID	38	0.685	1.512	0.301	0.453	0.685	1.036	1.829
MIS1	111	0.468	1.791	0.039	0.261	0.488	0.838	1.361
MIS2	53	0.139	1.638	0.041	0.085	0.154	0.228	0.480
MOU	75	2.286	1.566	0.519	1.460	2.130	3.579	11.646
NIO	40	0.951	1.293	0.583	0.735	0.897	1.229	1.955
RED	29	0.223	1.760	0.072	0.126	0.253	0.392	0.683
RGC	8	0.509	1.452	0.211	0.351	0.565	0.740	0.793
RGR	50	0.325	1.650	0.082	0.197	0.332	0.536	1.054
All	513	0.471	3.077	0.019	0.153	0.477	1.451	11.646

5.4 Discussion

In the analysis of the 13 techniques, thousands of statistics are presented and over 10,000 points are plotted in the 26 graphs. This mountain of information is somewhat overwhelming. However, all of the information has been provided for a purpose.

The figures help identify trends in the data that are not evident from the tables. For example, the Bagnold (1966) relation displays a distinctive trend in Fig. 5.3a. The trend suggests that, for the laboratory data, the predicted concentration tends to be near 1000 ppm regardless of the observed concentration. Similar but less distinctive trends are observed for the Graf (1968) equation (Fig. 5.8a) and the Rottner (1959) equation (Fig. 5.11a). Of course, excessive scatter in the figures also clearly indicates the poor performance of a technique.

The tables have been presented in an effort to evaluate the behavior of the techniques under various combinations of conditions. For example, the Yang (1973) equation tends to over-predict for the two sets of data with coarse sand, the Williams data and the Nordin data (WLM and NOR2, respectively, in Table 5.16a). On the other hand, it tends to under predict for deep river data such as the Atchafalaya River and the Mississippi River (ATC and MIS2, respectively, in Table 5.16b). Analogous behaviour can be seen for many of the techniques.

A comparison of all the techniques, including the proposed new method is given in Table 6.4 near the end of the next chapter.

In general, the newer methods which were fitted to large amounts of data have performed the best. Of the methods discussed here, the Ackers and White (1973) performed best for the laboratory data, while Engelund and Hansen (1967) did slightly better for the field data.

CHAPTER 6

A NEW METHOD FOR PREDICTING SEDIMENT CONCENTRATION

In the previous chapter, 13 methods for predicting mean sediment concentration in a channel were analyzed. Each method exhibited considerable scatter. The best methods gave reasonable results for the laboratory data, but were less satisfactory for the field data. Probably only a limited amount of field data were available when the various techniques were being developed.

In this chapter, a new equation for predicting mean sediment concentration is proposed. It is based solely on dimensional analysis and a best fit of the available data used in the analysis of existing techniques. The form of the equation has been intentionally kept as simple and easy to use as possible, under the assumption that a certain amount of scatter is inevitable and cannot be eliminated by increasing the complexity of the relationship or the analysis.

6.1 Expected Scatter in Sediment Concentration

To illustrate the amount of expected scatter, the top ten available discharge records for the Atchafalaya River at **Simmesport**, Louisiana have been analyzed. The observations, made between 1961 and 1965, have a maximum discharge of 14,200 m³/s and a minimum discharge of 10,200 m³/s. Figure 6.1 shows the velocity, depth and bed-material

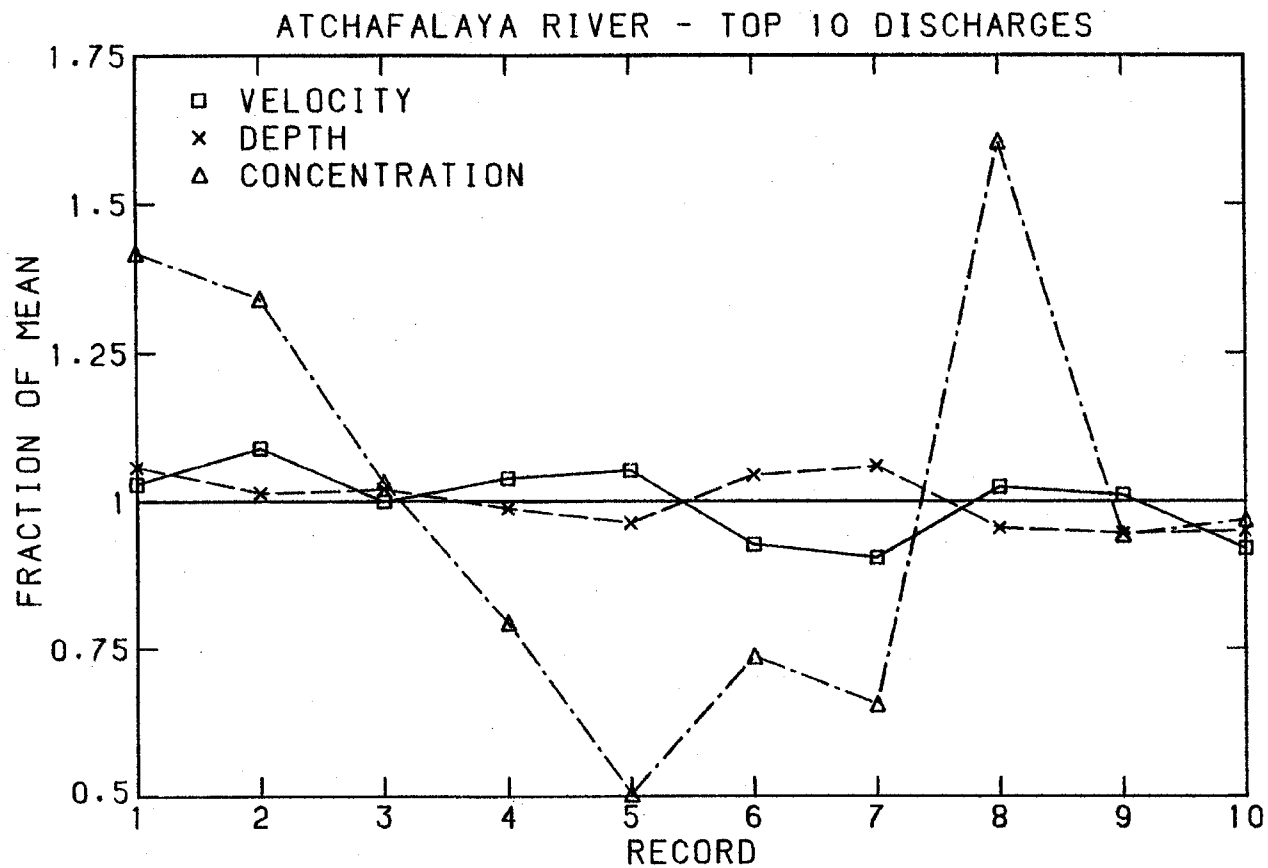


Figure 6.1 Velocity, depth, and bed-material sediment concentration fluctuations, plotted as fraction of the respective mean values, for the ten highest discharge observations, 1961 to 1965.

concentration, plotted as fraction of the respective mean values, for the ten records. The scatter in the sediment concentration is much larger than the fluctuations in velocity and depth. In fact, the range in the sediment concentration is greater than a factor of three.

The statistics of some of the hydraulic and sediment variables for the ten observations are given in Table 6.1. The fluctuations in concentration C , expressed as standard deviation as percent of the mean, are larger than the fluctuations in any of the other variables. For the narrow range of conditions, concentration is shown to be virtually uncorrelated with any of the given variables, with the exception of a weak, **probably** spurious, negative correlation with a_g .

Large fluctuations in sediment concentration over a narrow range of hydraulic and bed-material conditions are not unique to the Atchafalaya River. Therefore, the best that can be hoped for in predicting concentration from cross-sectional averaged hydraulic and bed material properties, is an accurate estimate of the expected value and an indication of the range of variations of concentration.

6.2 Width and Depth Effects

For the laboratory data, a sidewall correction has been used to adjust the hydraulic radius to **eliminate** the effects of the flume walls. If sediment concentration is correlated with velocity, however, the sidewall correction will be of little use. The laboratory experiments of Williams (1970), conducted in flumes with different widths, have been

TABLE 6.1

Atchafalaya River at Simmesport, Louisiana
 Top Ten Observations Ranked by Discharge
 1961 through 1965

Variable	Mean	Standard Deviation	Standard Deviation as % of Mean	R ² Correlation between Concentration, C, and Given Variable
v (m/s)	1.86	0.110	5.89	0.04
w (m)	467	15.7	3.35	0.04
d (m)	13.9	0.597	4.29	0
S x 10 ⁵	4.79	0.261	5.45	0
D ₅₀ (mm)	0.216	0.0415	19.2	0
σ_g	1.57	0.176	11.2	0.19
T (°C)	17.4	2.81	16.2	0
C (ppm)	353	119	33.7	1

used to examine the possible sidewall effects, plus effects of errors induced by very shallow depths.

The results of all Williams (1970) experiments with concentrations greater than 10 parts per million by weight are plotted in Fig. 6.2a. The dimensionless group plotted along the abscissa was determined from the analysis which follows later in this chapter. The data plotted in Fig. 6.2a exhibit a large amount of scatter. In Fig. 6.2b only width-to-depth ratios greater than four have been plotted, and the scatter has been greatly reduced. In Fig. 6.2c, the restriction that d/D_{50} be greater than 50 has been added, resulting in a greater reduction of scatter.

Throughout this report a width-to-depth ratio of 4 has been used as the lower limit in all analyses. Also, the relative roughness, defined by r/D_{50} , was limited to values greater than 100. These restrictions, along with a lower limit of 10 ppm for concentration, reduced the Williams (1970) data from 177 observations to 5 observations for the purposes of this report.

6.3 Critical Velocity

The "critical" shear stress at which motion begins on the bed can be determined from a Shields diagram, such as given by Vanoni (1975, p. 96). By combining the Shields diagram with the analysis presented in Chapter 4, the critical velocity of a channel can be determined.

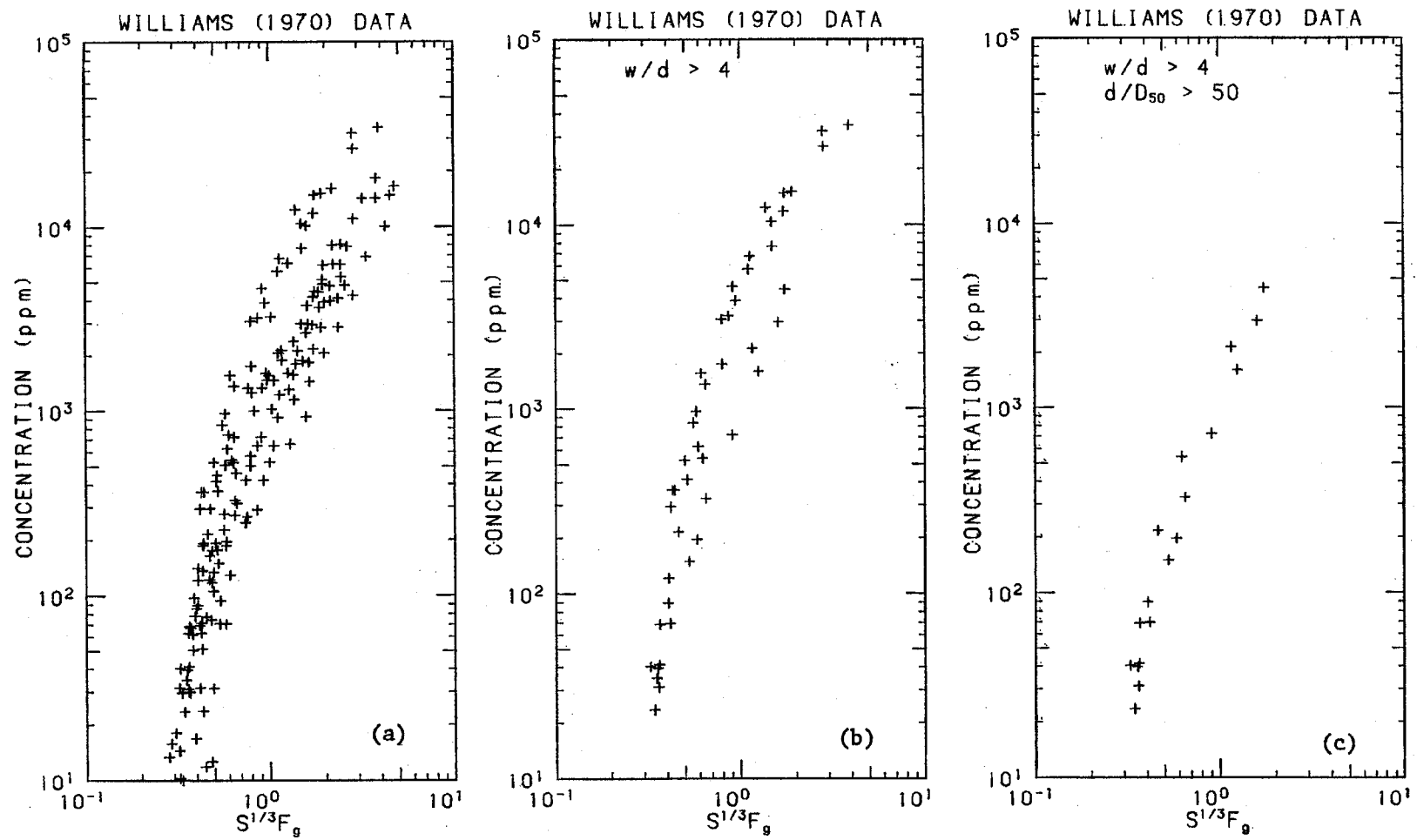


Figure 6.2 Williams (1970) data showing the effects of low values of w/d and d/D_{50} on sediment concentration.

The Shields diagram has the form

$$\tau_* = f\left(\frac{u_* D_{50}}{v}\right) \quad (6.1)$$

which can easily be transformed into the form

$$\tau_* = f(R_g) \quad (6.2)$$

The transformed Shields curve, plotted in Fig. 6.3, can be approximated

by

$$\tau_{*0} = 0.22Y + 0.06(10)^{-7.7Y} \quad (6.3)$$

$$\text{where } Y = \left(\sqrt{\frac{\rho_s - \rho}{\rho}} R_g\right)^{-0.6}$$

The original Shields data (Vanoni, 1965) are also plotted in Fig. 6.3.

Gessler (1971) has suggested that the Shields Diagram as given by Vanoni (1975) is for dune covered beds. If this is the case, then the lower regime Eq. 4.10a should be useful in relating shear stress to velocity. Rearrangement of Eq. 4.10a for critical conditions gives an equation for the grain Froude number:

$$F_{g0} = 4.596 \tau_{*0}^{0.5293} \sigma_g^{-0.1405} \sigma_g^{-0.1606} \quad (6.4)$$

from which velocity can be determined, where $F_g = v \sqrt{g D_{50} (\rho_s - \rho) / \rho}$.

Given slope, water temperature, and bed-material properties, it is possible to determine the critical grain Froude number, and hence velocity, from Eqs. 6.3 and 6.4.

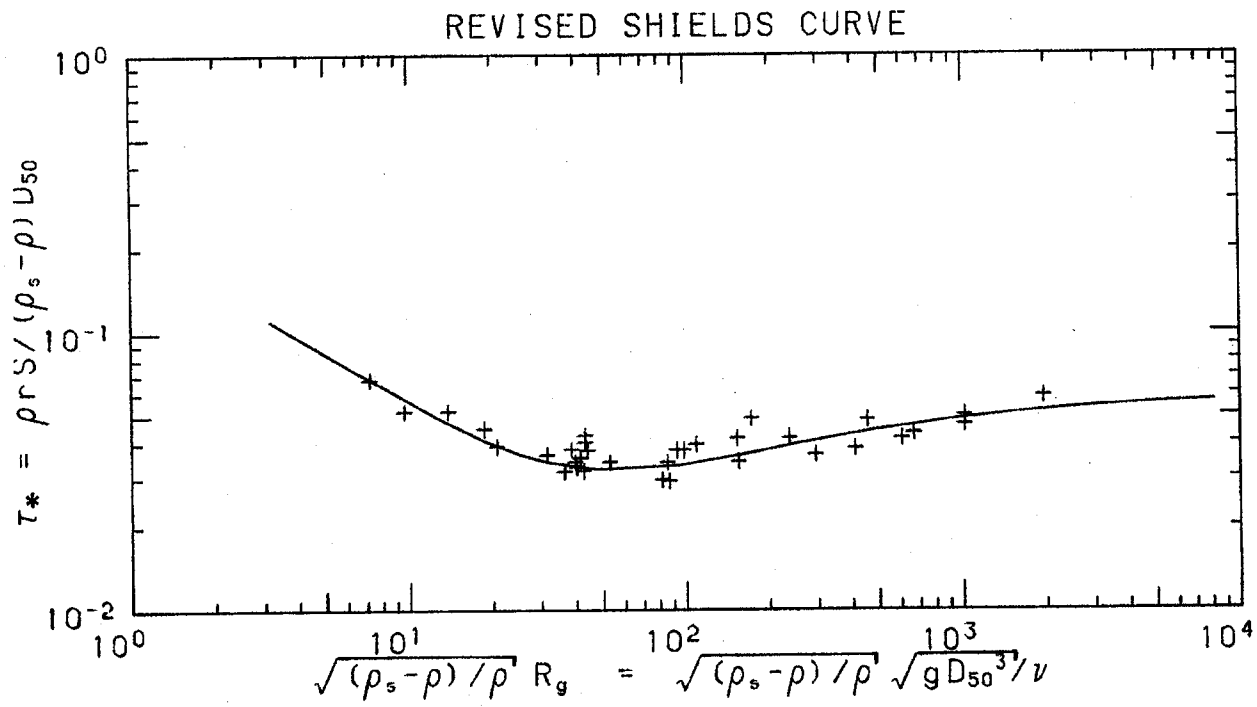


Figure 6.3 Revised Shields curve, data from Vanoni (1965).

6.4 Dimensional Analysis

Were a dimensional analysis is presented which is **analogous** to the one presented in Chapter 4. In this **case**, the dependent variable is sediment concentration instead of hydraulic radius.

If Eq. 4.1 is correct then a relationship for sediment concentration should have the general **form**

$$C = f(q, S, g, \rho, v, \rho_s, D_{50}, \sigma_g) \quad (6.5)$$

The eight independent variables can be rearranged into five dimensionless groups:

$$C = f\left(q_*, S, \sigma_g, R, \frac{\rho_s^{-p}}{\rho}\right) \quad (6.6)$$

From the analysis in Chapter 4, given the independent dimensionless groups in Eq. 6.6, multiple values of flow depth are possible. It is logical to assume that multiple values of sediment concentration are also possible. From the method in Chapter 4, q_* can be used to calculate F_g , the grain Froude number and r/D_{50} , the relative **roughness**. It is therefore assumed that for a given **discharge**, q , either r and v are known or can be calculated from the method in Chapter 4. Also, the Reynolds number, R , can be combined with other dimensionless groups to produce the grain Reynolds number, R_g . Now Eq. 6.6 can be replaced by

$$C = f\left(F_g, \frac{r}{D_{50}}, S, \sigma_g, R_g, \frac{\rho_s^{-p}}{\rho}\right) \quad (6.7)$$

where the following definitions apply:

$$\text{Grain Froude number, } F_g = \frac{v}{\sqrt{\left(\frac{\rho_s \rho}{\rho}\right) g D_{50}}}$$

$$\text{Grain Reynolds number, } R_g = \frac{v g D_{50}^3}{\nu}$$

In Eq. 6.7, F_g , r/D_{50} and S cannot all be specified independently, but all three have been used in the analysis to avoid the multiple value problem discussed in Chapter 4.

During the course of the investigation, it was noticed that the field data tended to have slightly higher sediment concentrations than laboratory data for similar ranges of dimensionless groups. To compensate for such a disparity, a dummy variable was used to flag field data and allow for a different sediment concentration for a field observation with the same dimensionless parameters as a laboratory observation. A possible cause for this disparity is discussed in section 6.5.

Multiple regression analysis was used to develop an equation with the general form of Eq. 6.7. The resulting equation is:

$$C = 7115 c_F \left(F_g - F_{g0} \right)^{1.978} S^{0.6601} \left(\frac{r}{D_{50}} \right)^{-0.3301} \quad (6.8)$$

where c_F is the coefficient for field data given by

$c_F = 1$ for laboratory data, and

$c_F = 1.268$...for field data.

F_{g0} is the critical grain Froude number determined from Eq. 6.3 and

Eq. 6.4. For identical independent dimensionless groups, the concentration for field data is on the average 26.8 percent higher than for lab data. The multiple correlation coefficient, $R = 0.955$ ($R^2 = 0.912$).

The parameters on the right side of Eq. 6.7, and its specific definition, Eq. 6.8, were arrived at through an iterative procedure. An attempt was made to combine the best features of the Ackers and White (1973), Engelund and Hansen (1967), and Yang (1973) techniques. Both Engelund and Hansen (1967) and Yang (1973) used the product of velocity and slope in their relationships. In each case the effect of slope seemed too great. Both Ackers and White (1973) and Yang (1973) effectively have critical velocity terms (the term A in the Ackers and White relationship acts like a critical value of their mobility number). From the present analysis, the most successful combination resulting in Eq. 6.8 was a velocity minus critical velocity term ($F_g - F_{g0}$), slope, and a depth term (r/D_{50}).

The data set used in the analysis is identical to the set of data used to examine the existing relationships. The data sources are listed in Tables 5.2a and 5.2b, and the restrictions or filters imposed on certain parameters are given in Table 5.3.

All dimensionless groups in Eq. 6.7 are independently required for the calculation of concentration, with the exception of $(\rho_s - \rho) / \rho$, which is a constant for sand-bed channels. If F_g and r/D_{50} are not known (i.e. if velocity and depth are not known independent of discharge) they can be determined if q_* is known, by the method proposed in Chapter 4.

However, some of the dimensionless groups enter only in the definition of the critical grain Froude number,

A simple rearrangement of Eq. 6.8 allows a reasonable graphical representation of the analysis. The approximation of Eq. 6.8 by:

$$C = 7100c_F \left(S^{1/3} F_g - S^{1/3} F_{g0} \right)^2 \left(\frac{r}{D_{50}} \right)^{-1/3} \quad (6.9)$$

allows sediment concentration to be plotted as a function of grain Froude number times slope to the 1/3 power. The predicted concentration cannot, however, be plotted as a line since both the critical grain Froude number and the relative roughness will vary with each observation. For most data sets these variations will not be too large and therefore plots of each data set should show little scatter. Plots of this type are shown in Figs. 6.4a-t for laboratory data, and in Figs. 6.5a-k for field data.

A statistical analysis of the ratio of predicted concentration to observed concentration is given in Tables 6.2 and 6.3. The individual ratios for laboratory data are plotted in Fig. 6.6a and for field data in Fig. 6.6b. The results seem quite reasonable when one considers the amount of scatter in the source data, as illustrated by Fig. 6.1.

6.5 Effects of a Nonrectangular Cross-Section

One principle difference between laboratory and field observations is that the laboratory channels tend to be much more rectangular in cross-section than river channels. For irregular channels, the

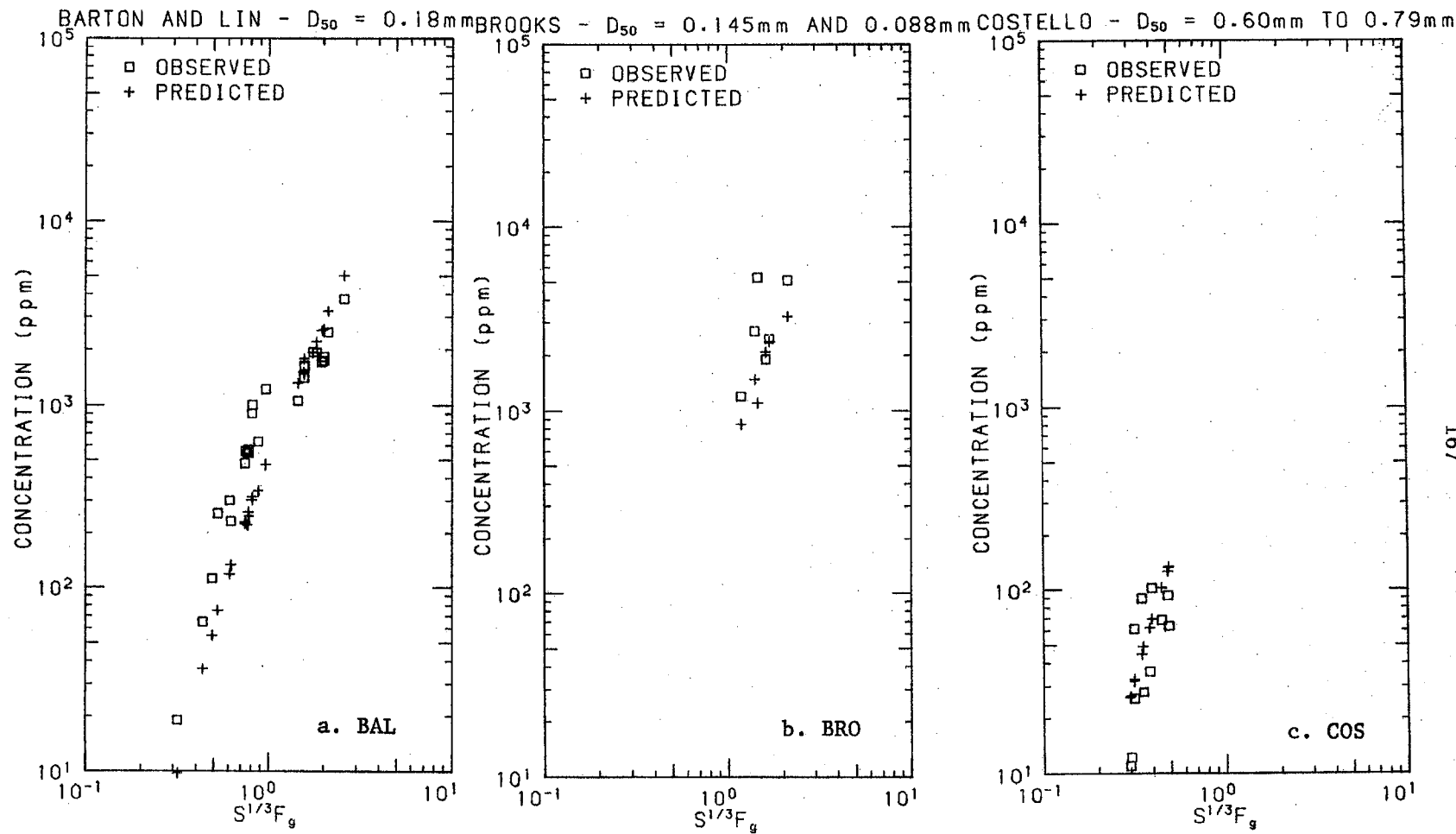


Figure 6.4 Laboratory sediment concentration as observed and as predicted by Eq. 6.9, as a function of $S^{1/3}F_g$, where $\bar{F}_g = v/\sqrt{gD_{50}(\rho_s - \rho)}/\rho$. Data set codes from Table 5.1 are given in the lower right corner of each plot.

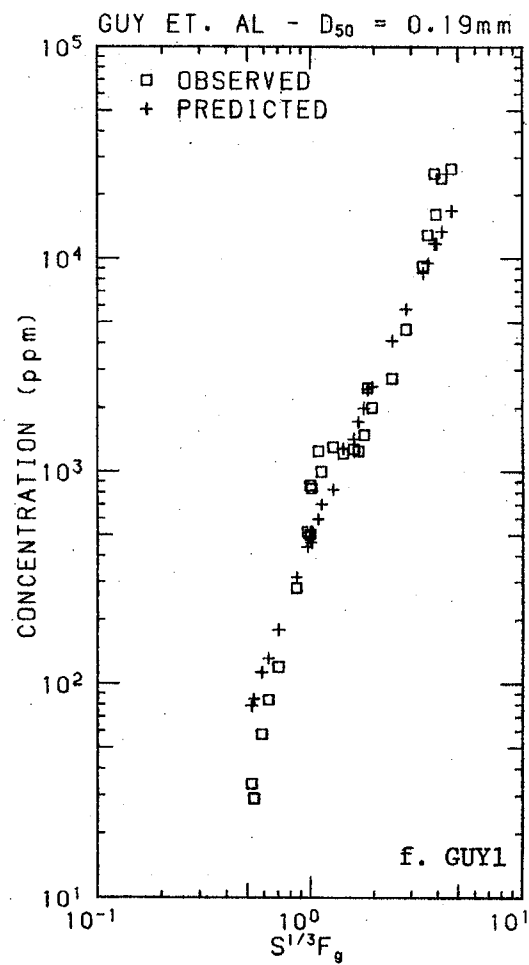
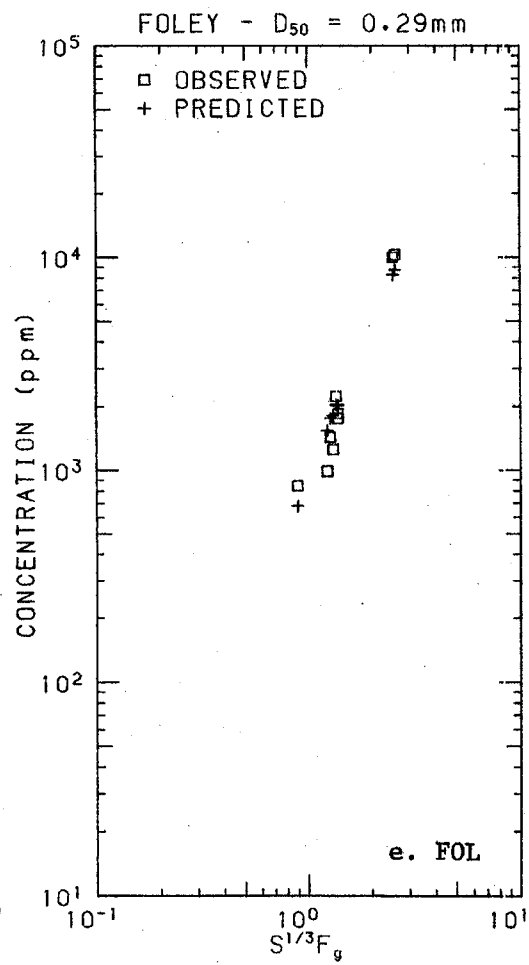
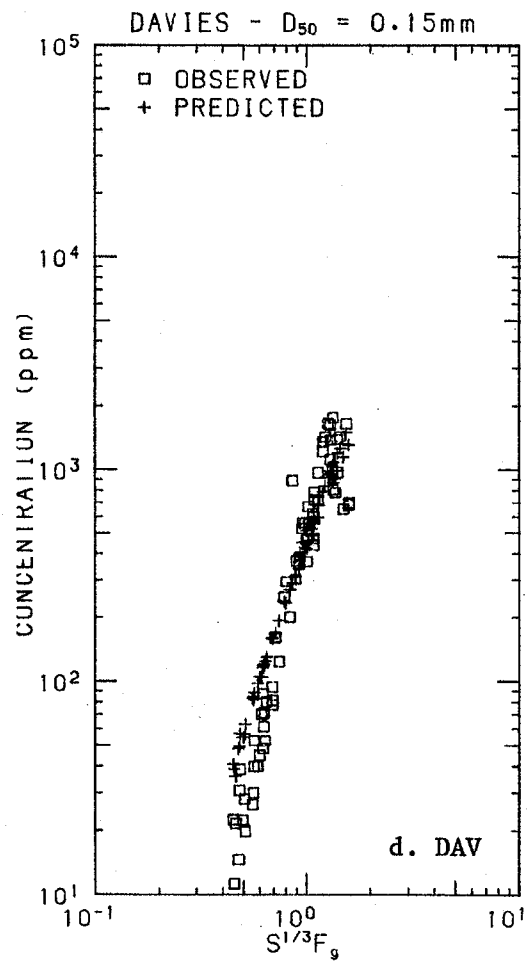
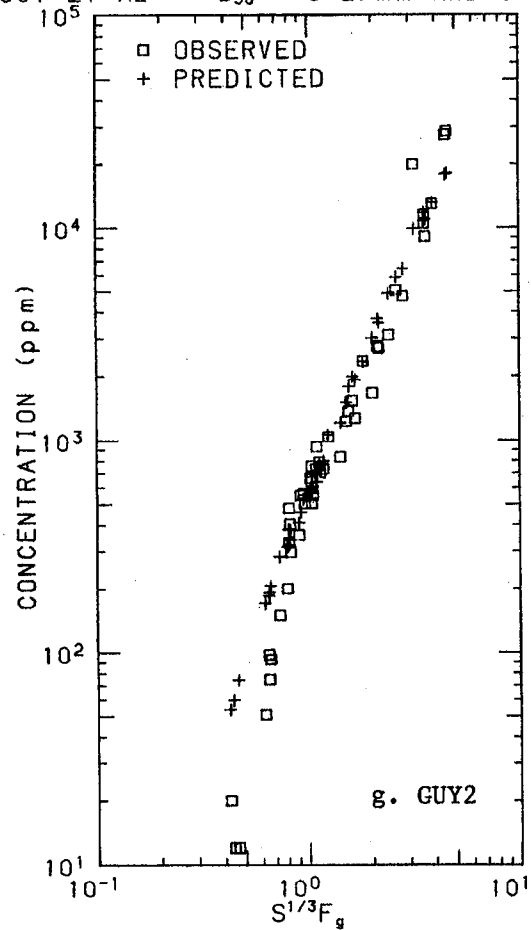
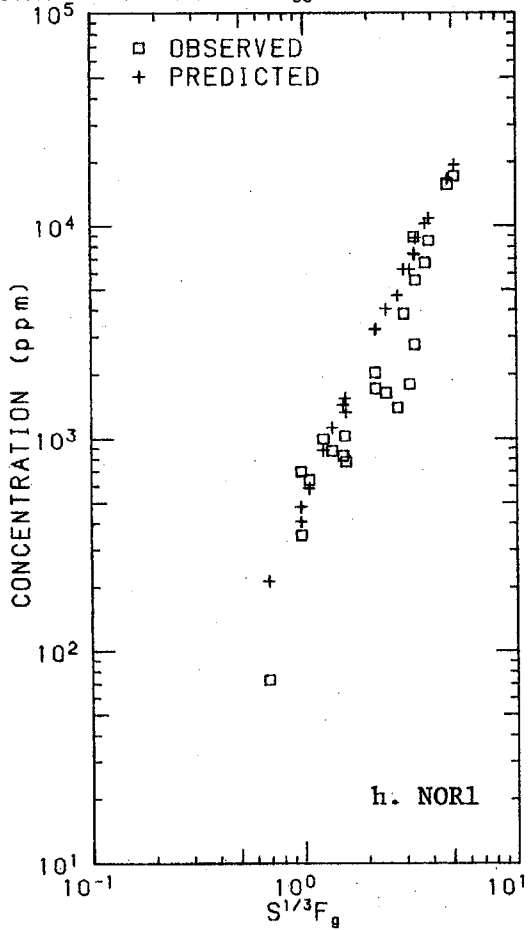


Figure 6.4 continued

GUY ET AL. - $D_{50} = 0.27\text{mm}$ AND 0.28mm



NORDIN - $D_{50} = 0.25\text{mm}$



NORDIN - $D_{50} = 1.14\text{mm}$

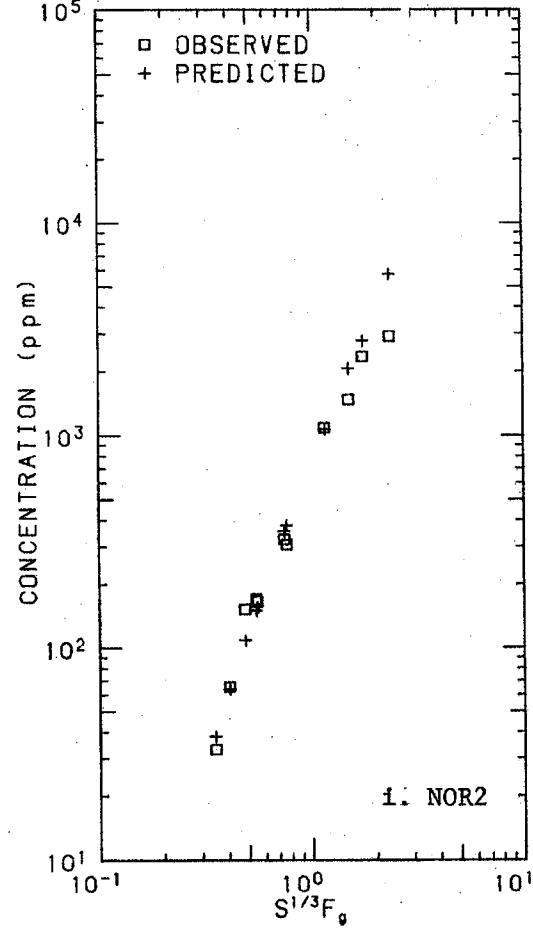


Figure 6.4 continued

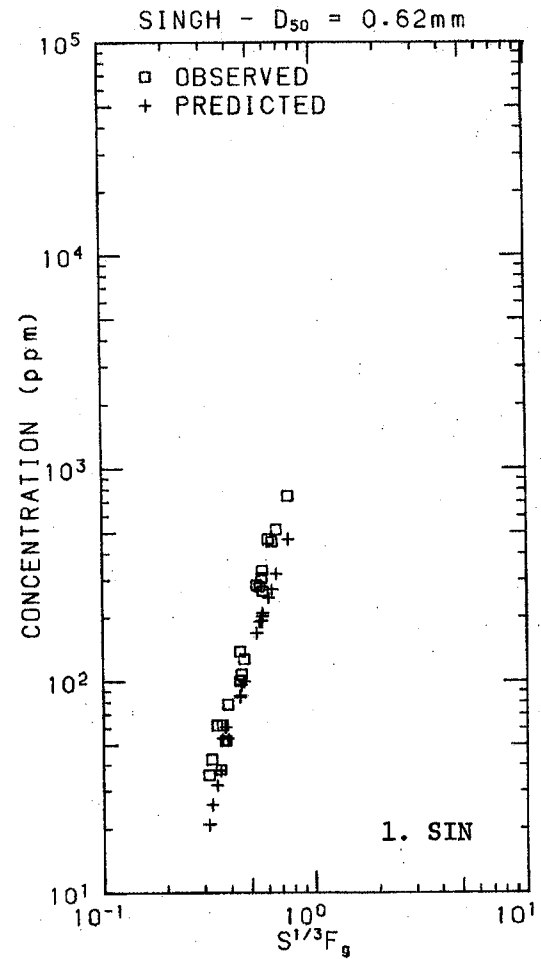
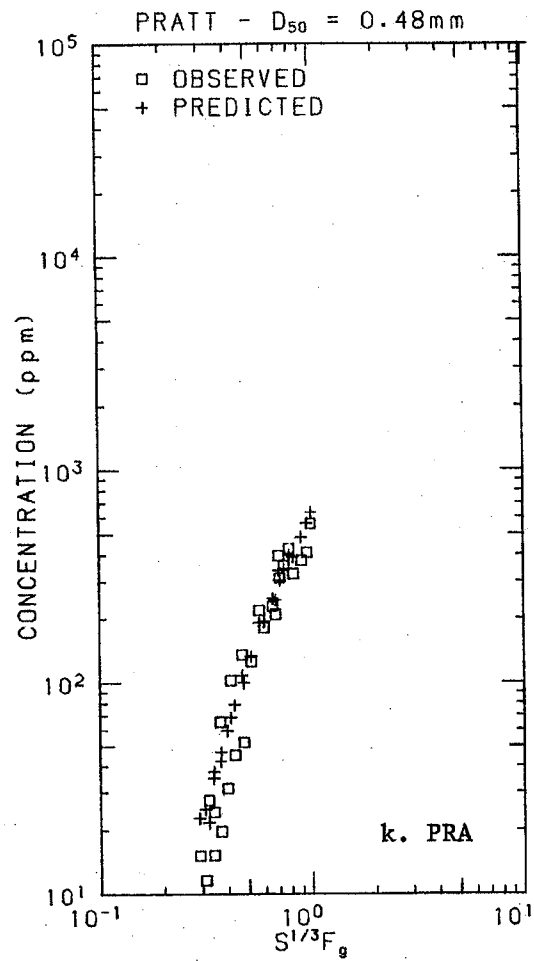
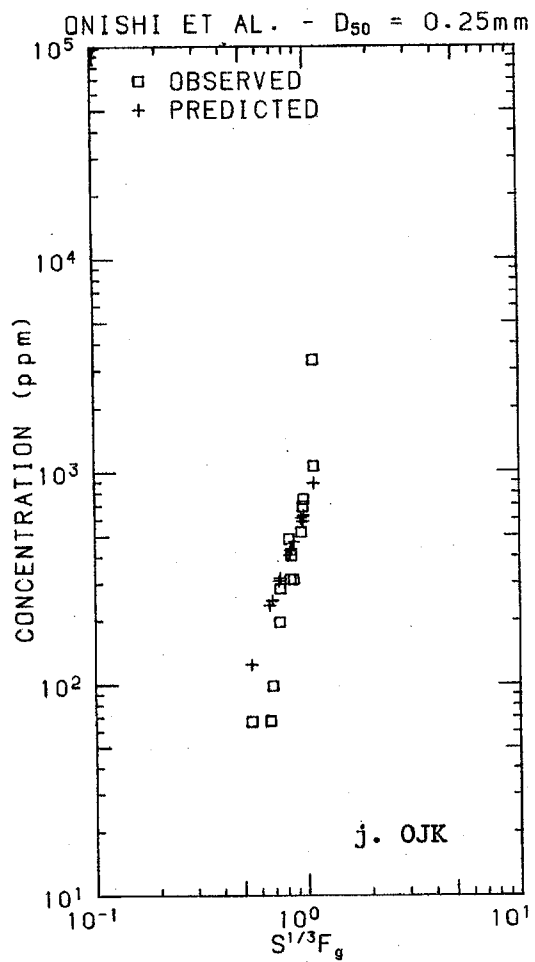


Figure 6.4 continued

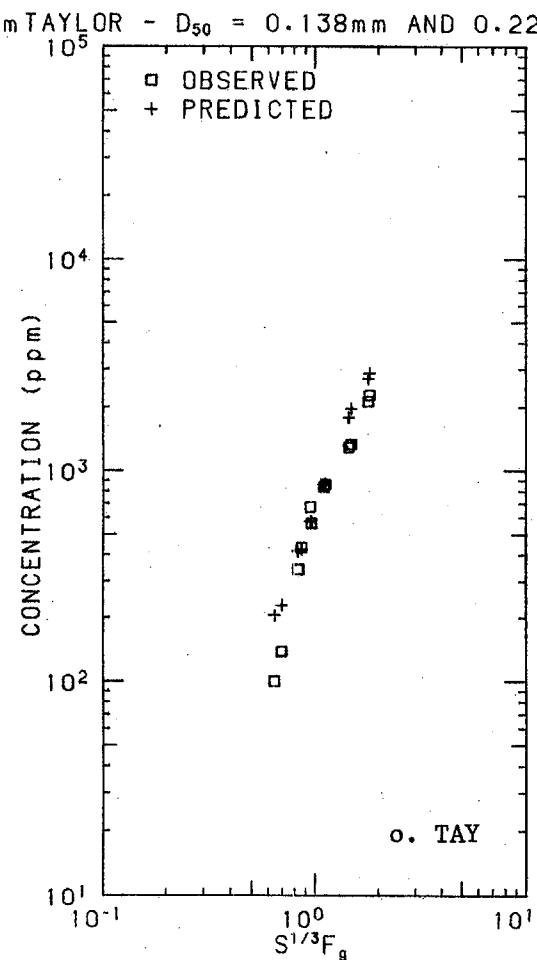
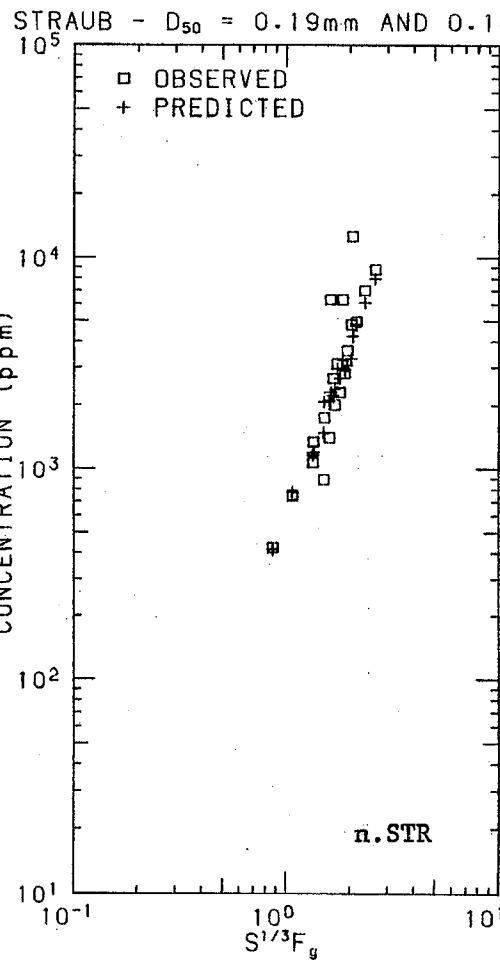
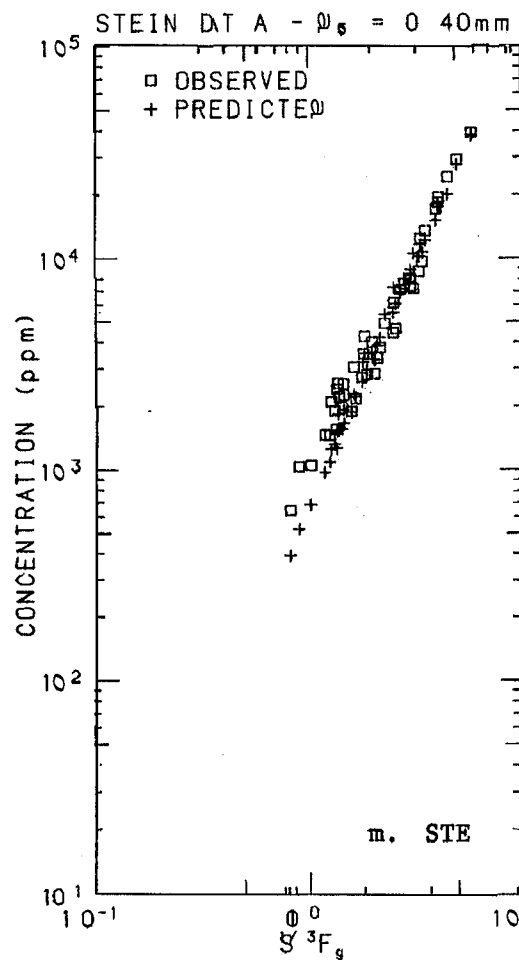


Figure 6.4 continued

VANONI AND BROOKS - $D_{50} = 0.137$ VANONI AND HWANG - $D_{50} = 0.206, 0.230$

WILLIAMS - $D_{50} = 1.35 \mu m$

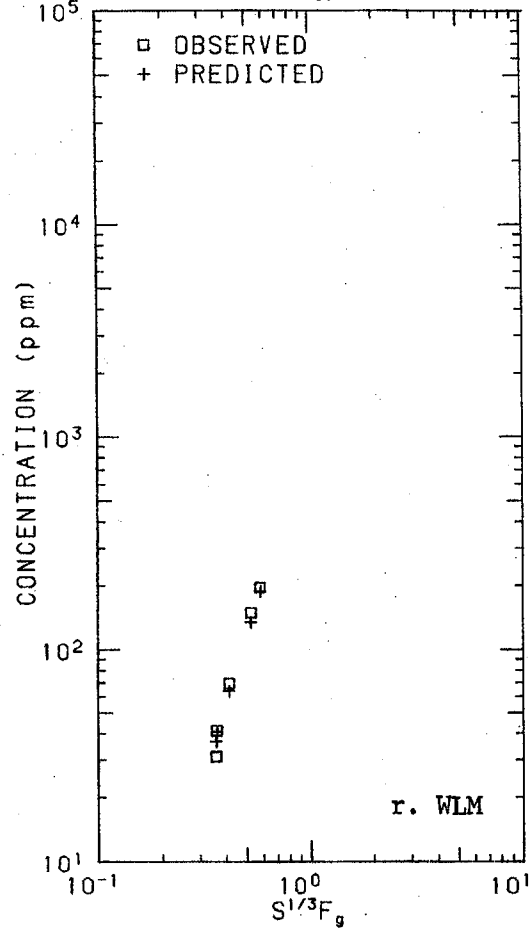
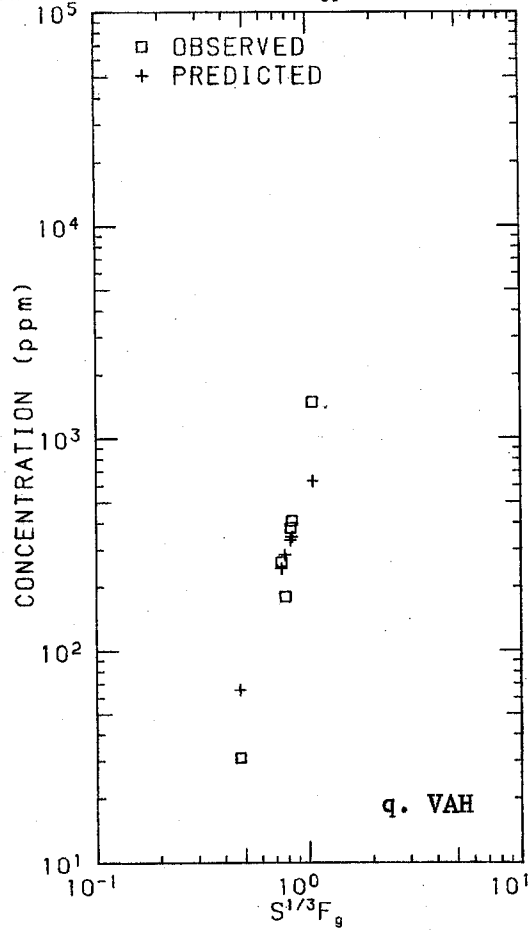
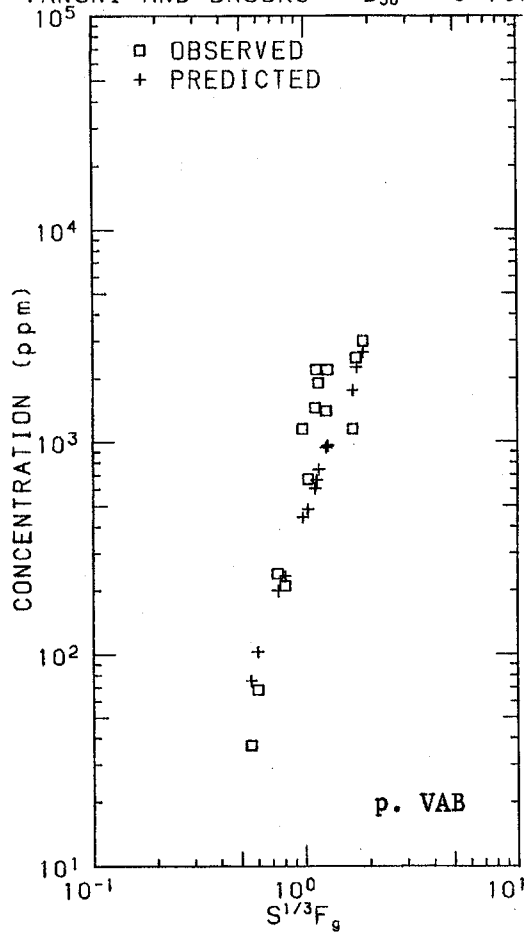


Figure 6.4 continued

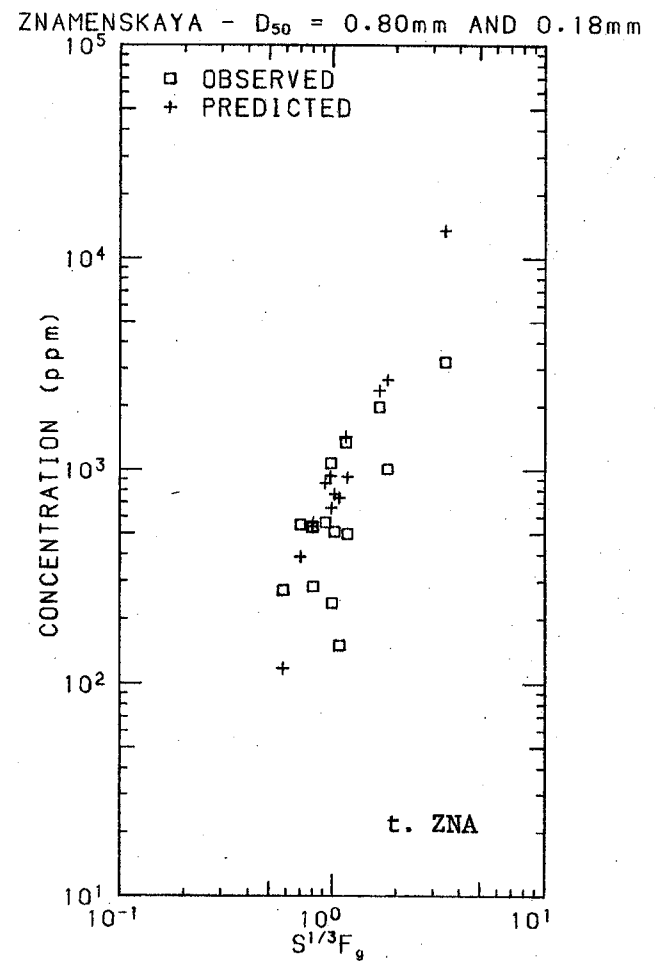
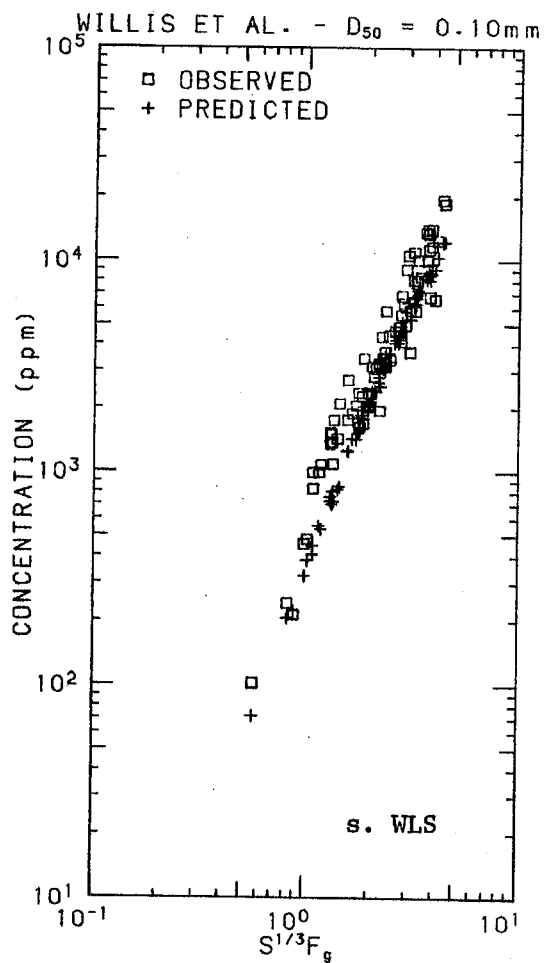


Figure 6.4 continued

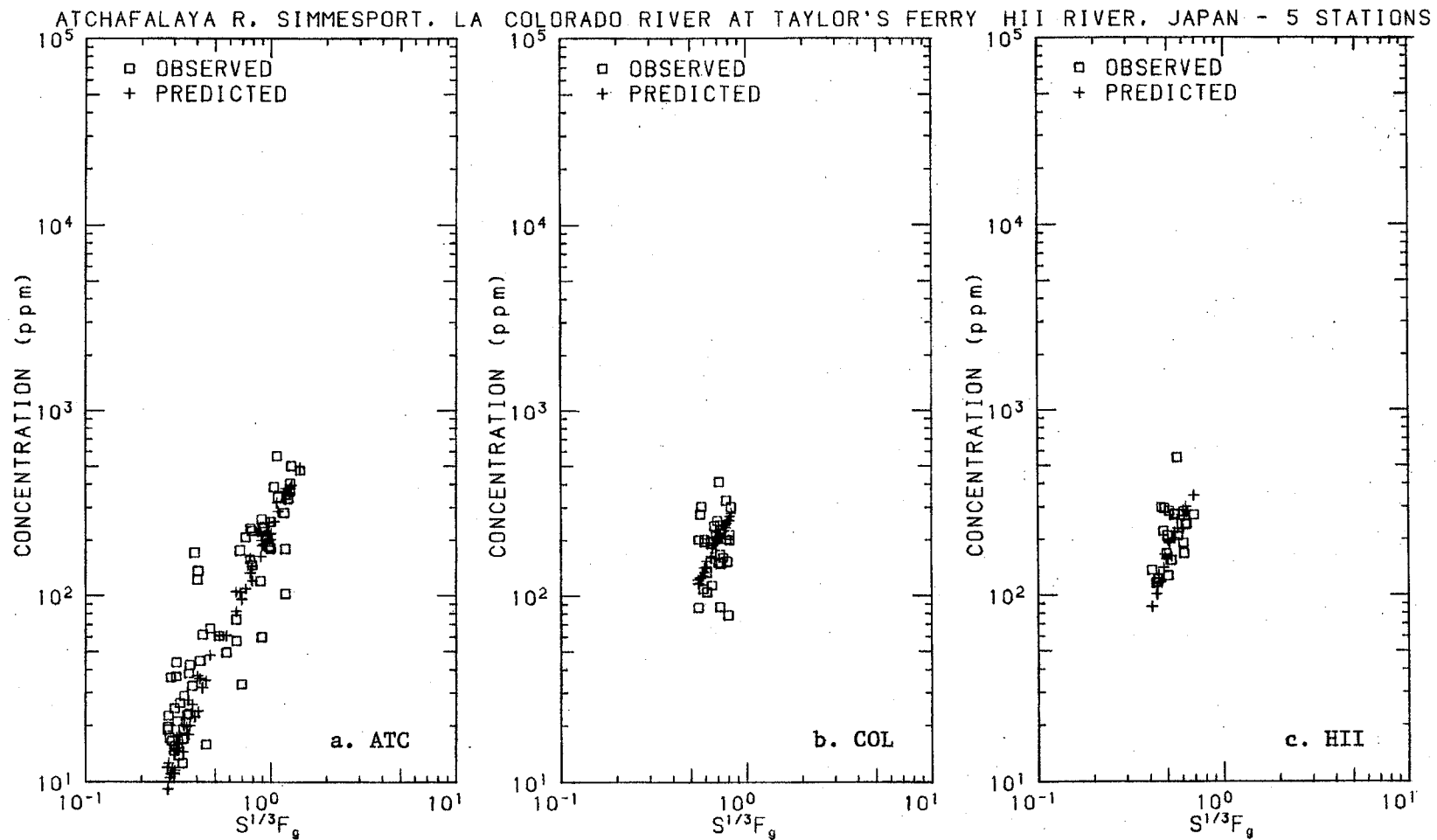


Figure 6.5 Field sediment concentration as observed and as predicted by Eq. 6.9, as a function of $S^{1/3}F_g$, where $F_g = v/\sqrt{gD_{50}(\rho_s - \rho)}/\rho$. Data set codes from Table 5.2 are given in the lower right corner of each plot.

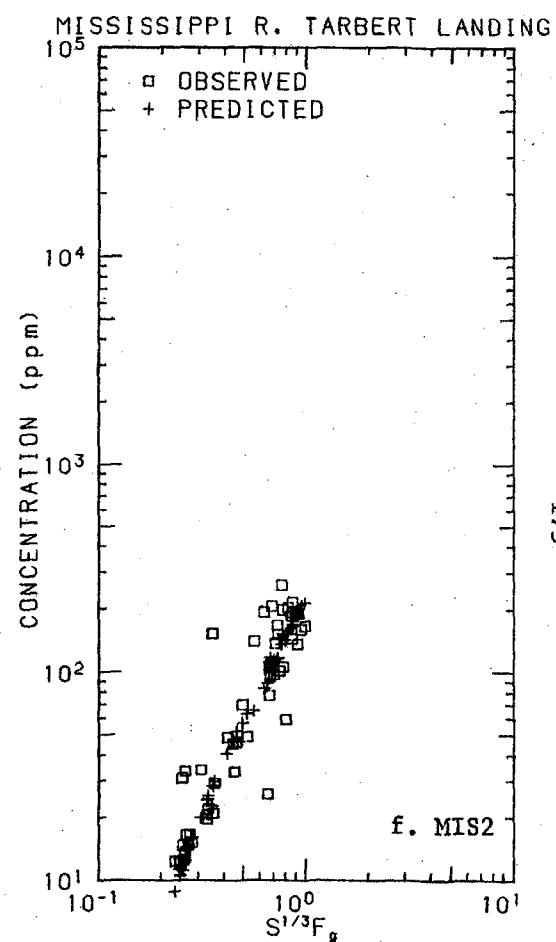
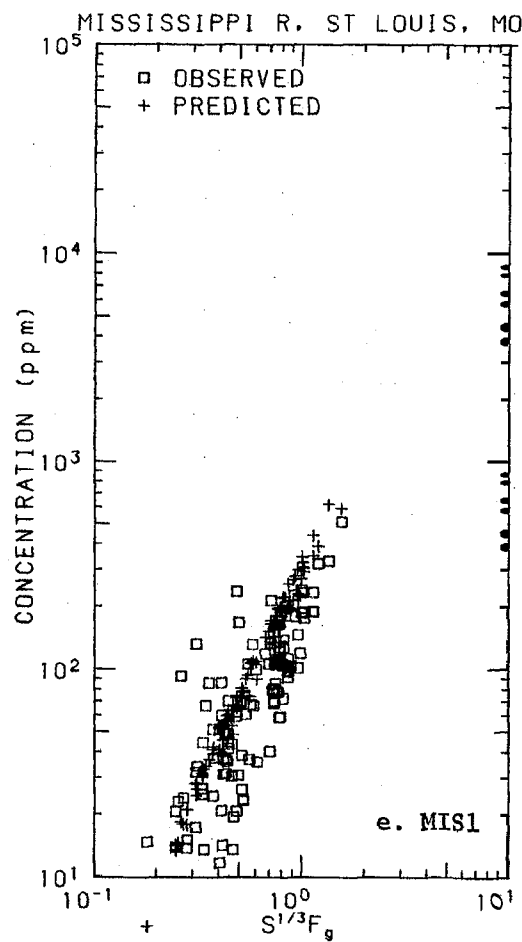
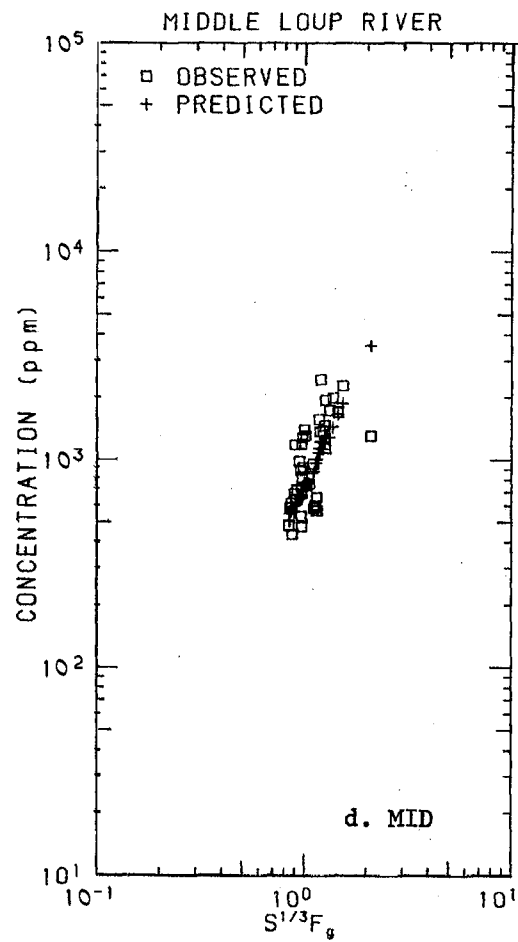


Figure 6.5 continued

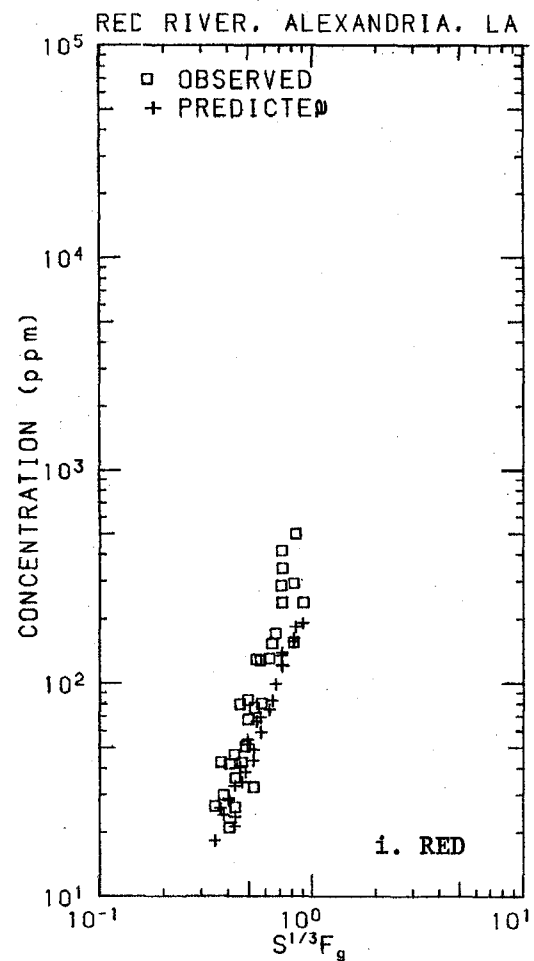
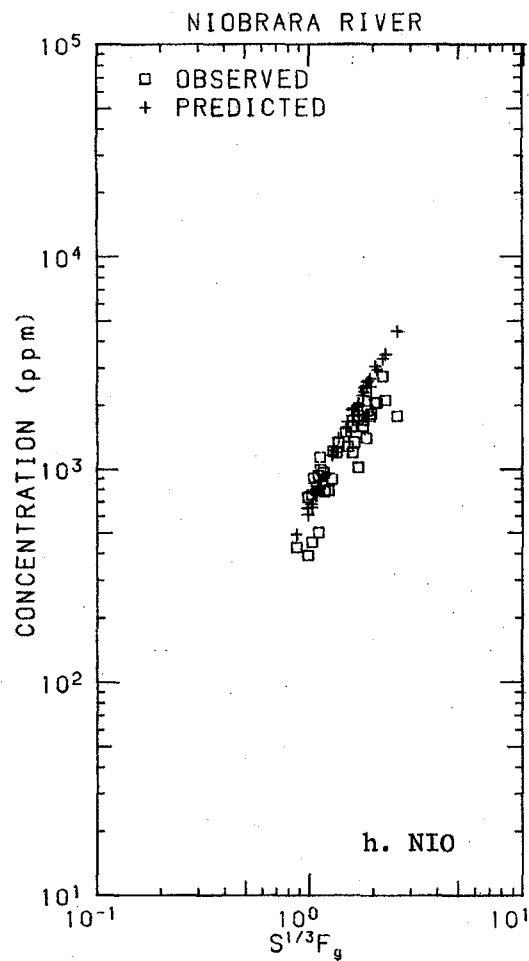
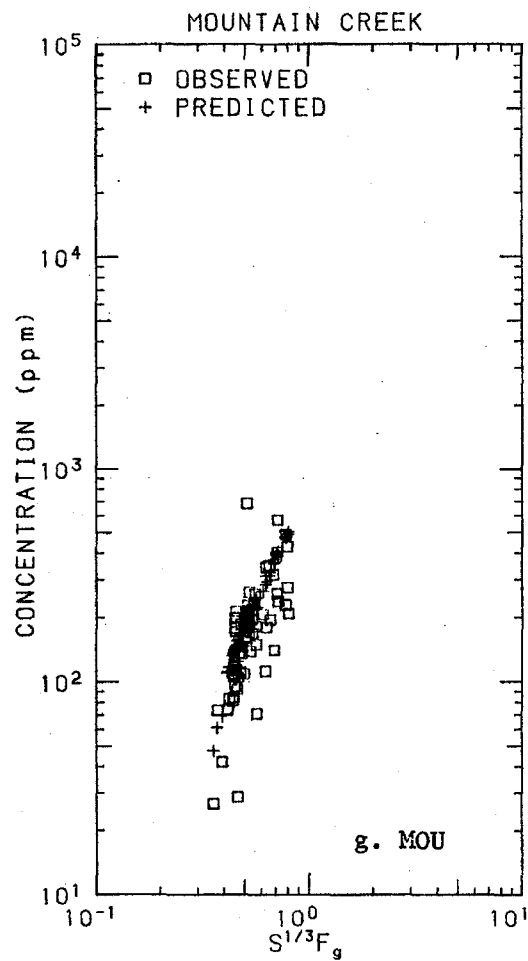


Figure 6.5 continued

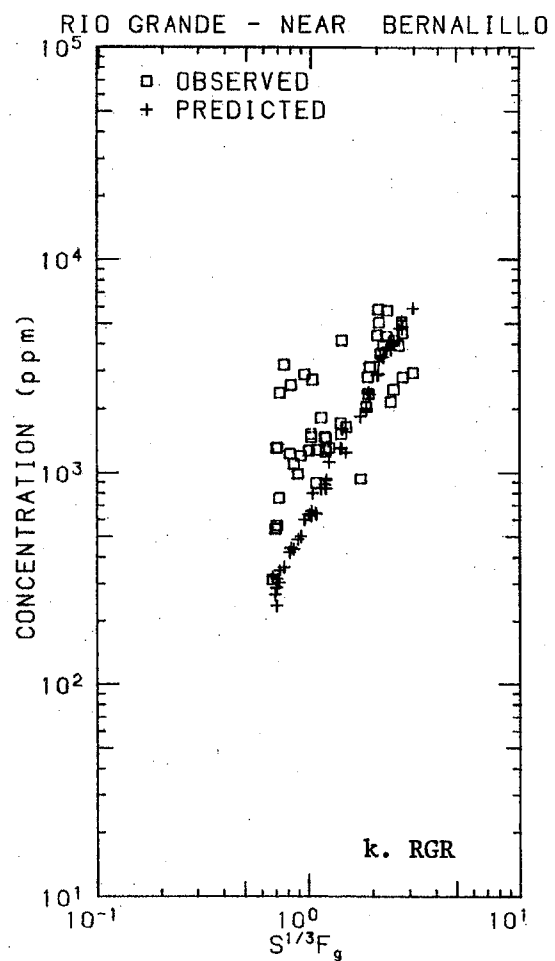
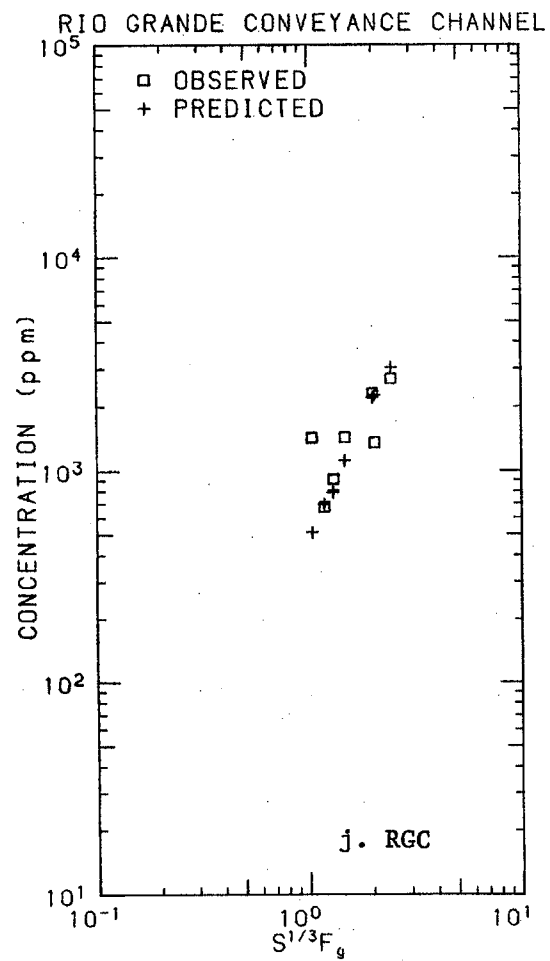


Figure 6.5 continued

Table 6.2

Ratio of Predicted to Observed Concentration for Proposed Method -- Lab Data

Data Set	Number	Geo.Mean	Geo.S.D.	Minimum	16 %ile	Median	84 %ile	Maximum
BAL	26	0.667	1.718	0.293	0.388	0.542	1.145	1.486
BRO	6	0.615	1.712	0.209	0.359	0.635	1.054	1.092
COS	11	1.278	1.715	0.499	0.745	1.497	2.191	2.364
DAV	69	1.213	1.670	0.325	0.727	1.103	2.026	3.428
FOL	9	1.069	1.261	0.803	0.847	1.101	1.348	1.554
GUY1	27	0.994	1.605	0.467	0.619	1.024	1.595	2.921
GUY2	47	1.256	1.627	0.496	0.772	1.147	2.043	6.178
NOR1	22	1.537	1.571	0.584	0.978	1.526	2.415	3.477
NOR2	11	1.102	1.288	0.713	0.856	1.090	1.420	1.976
OJK	14	1.177	1.800	0.263	0.654	1.126	2.119	3.491
PRA	25	1.205	1.446	0.647	0.833	1.128	1.742	2.384
SIN	20	0.695	1.236	0.516	0.562	0.625	0.859	1.157
STE	44	0.901	1.264	0.508	0.713	0.916	1.139	1.466
STR	21	0.888	1.470	0.335	0.604	0.943	1.306	1.667
TAY	12	1.232	1.272	0.856	0.968	1.220	1.507	2.053
VAB	14	0.738	1.769	0.301	0.417	0.723	1.305	2.028
VAH	6	0.995	1.664	0.422	0.598	0.879	1.656	2.109
WLM	5	0.986	1.099	0.903	0.897	0.962	1.083	1.178
WLS	77	0.761	1.304	0.404	0.584	0.777	0.992	1.453
ZNA	14	1.542	1.925	0.431	0.801	1.502	2.969	4.902
All	480	1.000	1.638	0.209	0.610	0.967	1.638	6.178

Table 6.3

Ratio of Predicted to Observed Concentration for Proposed Method - Field Data

Data Set	Number	Geo.Mean	Geo.S.D.	Minimum	16 %ile	Median	84 %ile	Maximum
ATC	63	0.812	1.792	0.131	0.453	0.821	1.455	3.336
COL	30	1.026	1.585	0.409	0.647	0.951	1.627	3.286
HII	22	0.883	1.435	0.394	0.615	0.932	1.267	1.607
MID	38	0.908	1.453	0.504	0.625	0.854	1.319	2.721
MIS1	111	1.405	1.740	0.199	0.807	1.553	2.444	3.590
MIS2	53	0.917	1.608	0.149	0.570	0.950	1.475	3.427
MOU	75	1.238	1.463	0.289	0.846	1.218	1.812	4.304
NIO	40	1.230	1.295	0.706	0.950	1.210	1.592	2.518
RED	29	0.642	1.394	0.332	0.461	0.622	0.895	1.370
RGC	8	0.890	1.501	0.358	0.593	0.886	1.336	1.661
RGR	50	0.608	1.917	0.112	0.317	0.657	1.166	2.005
ALL	519	1.000	1.746	0.112	0.573	1.029	1.746	4.304

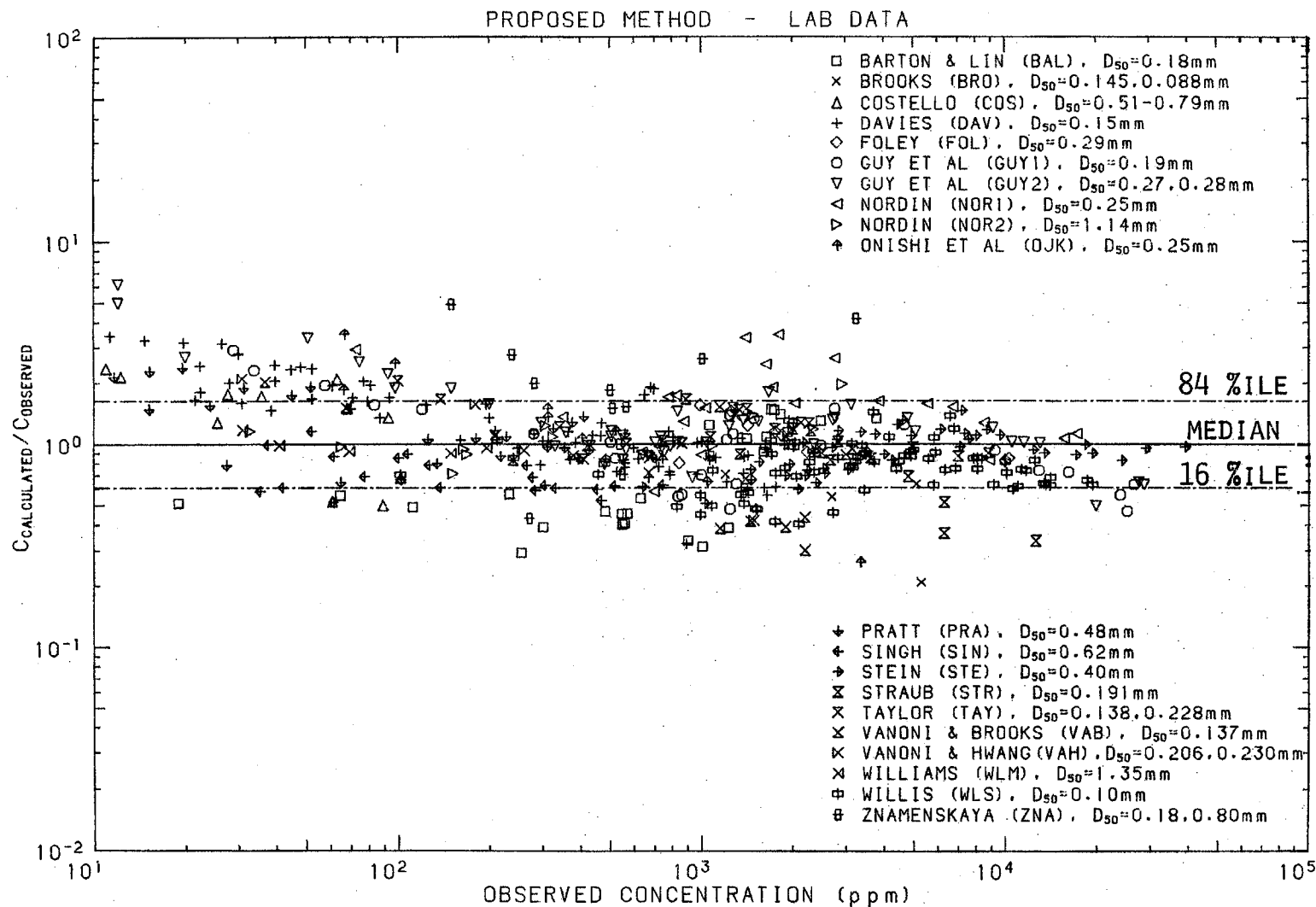


Figure 6.6a Ratio of concentration calculated from Eq. 6.8 or Eq. 6.9 technique to observed concentration as a function of observed concentration, for laboratory data.

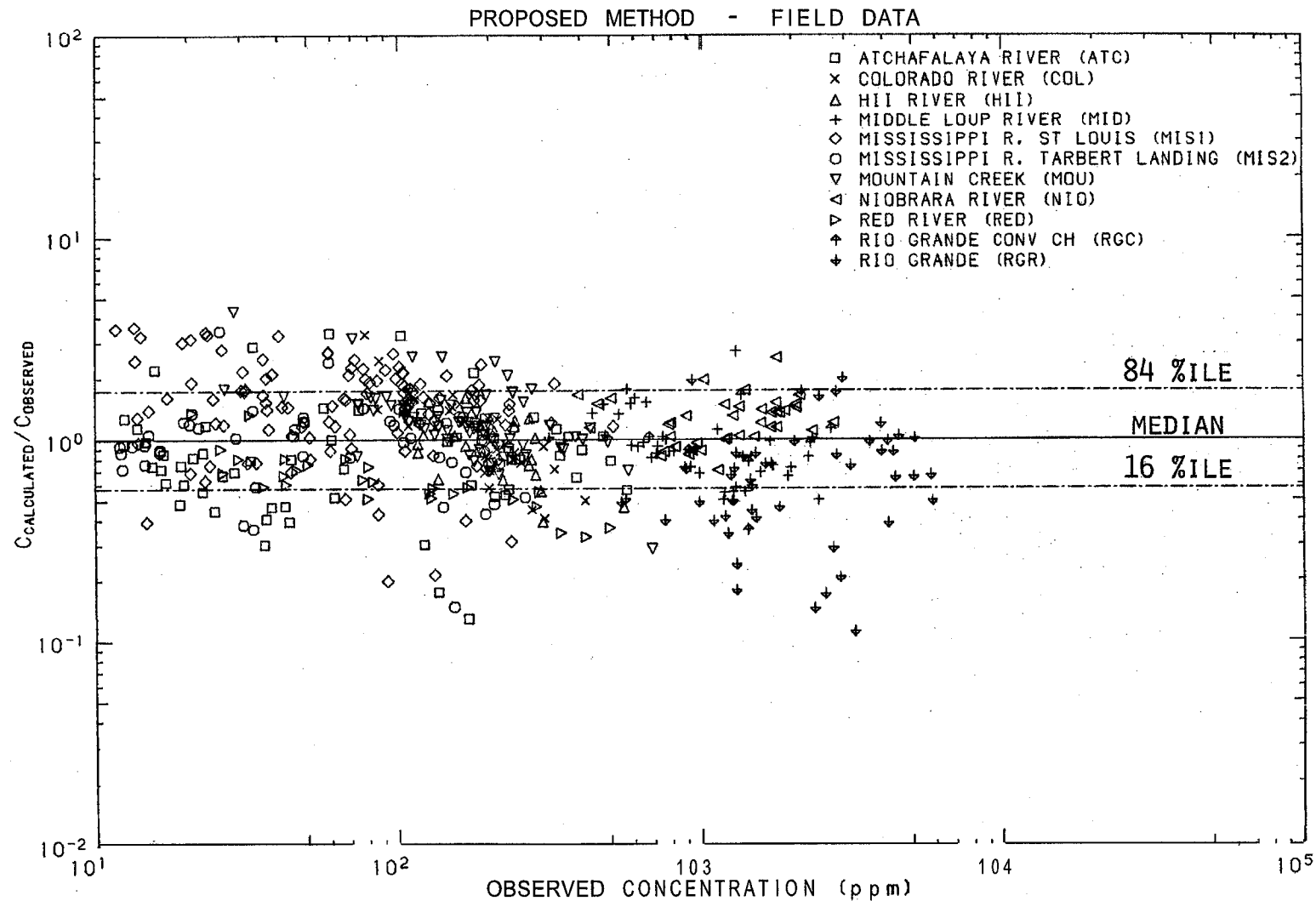


Figure 6.6b Ratio of concentration calculated from Eq. 6.8 or Eq. 6.9 technique to observed concentration as a function of observed concentration, for field data.

concentration computed from cross-sectional averaged hydraulic variables will be different from concentration calculated from local hydraulic properties and integrated over the cross-section. The analysis that follows was undertaken to explore the possible connection between the observed difference in laboratory and field observations of sediment concentration and the existence of irregular river cross-sections,

The problem is illustrated schematically in Fig. 6.7. In the derivation that follows, the subscript "i" is used to indicate values of velocity, depth, and concentration for the i^{th} element in the cross-section. All non-subscripted representations of these variables refer to cross-sectionally averaged values. The derivation that follows assumes that for a given channel the slope and bed-material properties are constant.

For a river with dunes, a depth-velocity relationship at any point in the cross-section should behave like Eq. 4.10a with r replaced by the local depth, d_i . Rearranging and incorporating slope, gravity and bed-material properties in the constant yields an expression for the local velocity:

$$v_i = a_1 d_i^{b_1} \quad (6.10)$$

where $b_1 = 0.53$, approximately.

If the flow velocity is considerably larger than the critical velocity, then a similar treatment of the concentration Eq. 6.8 yields:

$$c_i = a_2 v_i^{b_2} d_i^{b_3} \quad (6.11)$$

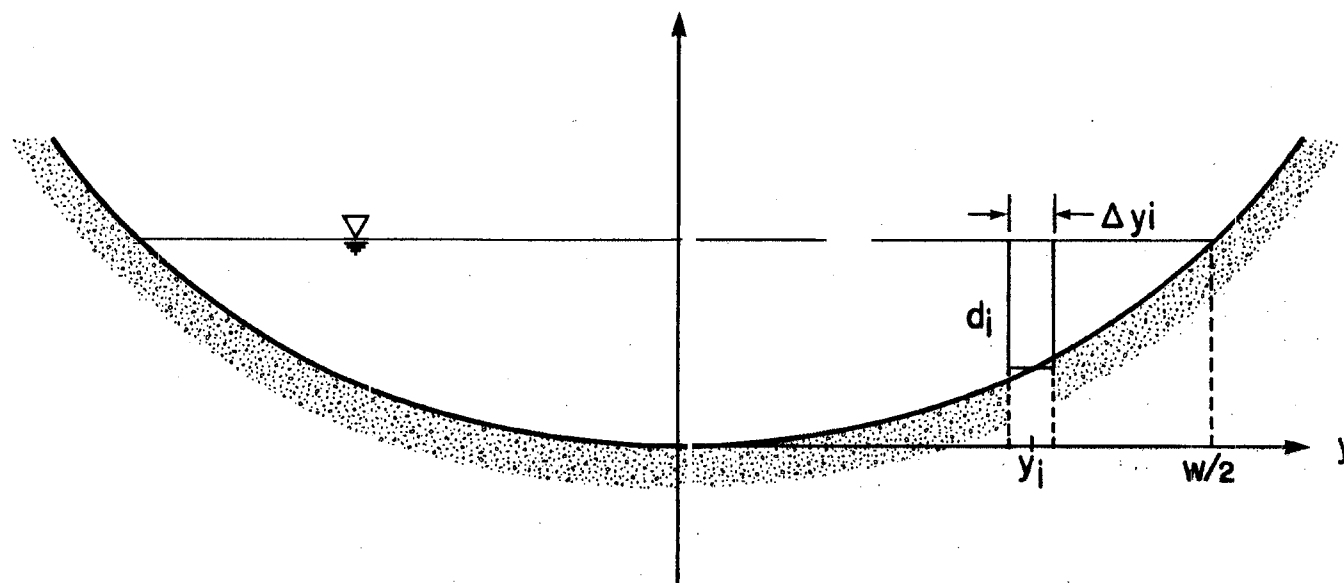


Figure 6.7 Idealized nonrectangular channel.

where $b_2 = 2.0$ and $b_3 = -0.33$, approximately. Here the critical velocity term has been neglected. Omission of the critical velocity term from Eq. 6.11 will cause an over-estimation of the local concentration, particularly near the sides of the cross-section. For rivers where a significant transport rate exists, such as many shown in Figs. 6.5a-j, this error will be small.

In order to explore the effect of an irregular cross-section, a certain cross-sectional shape is required. Leopold and Maddock (1953) have shown that relationships of the following form exist for most rivers:

$$w = aQ^b \quad (6.12)$$

$$\text{and } d = cQ^f \quad (6.13)$$

For observations at a station, they found the average values to be $b = 0.26$ and $f = 0.40$.

Elimination of Q from Eqs. 6.12 and 6.13 yields

$$d = Aw^B \quad (6.14)$$

where A is a general coefficient and $B = f/b$, and has the average value $B = 1.54$.

One cross-sectional depth distribution which satisfies Eq. 6.14 is

$$d_i = \left(\frac{B+1}{B} \right) A [w^B - (2y)^B] \quad \text{for } y > 0 \quad (6.15)$$

If $B=2$, then Eq. 6.15 provides for a parabolic cross-section. However, the actual shape of the cross-section is less important than the

integral properties of the depth distribution. Therefore, Eq. 6.15 should be satisfactory, since when integrated over the cross-section it satisfies Eq. 6.14.

The mean sediment concentration in the section can be calculated from

$$C = \frac{2 \sum_{i=1}^n C_i v_i d_i \Delta y_i}{2 \sum_{i=1}^n v_i d_i \Delta y_i} \quad (6.16)$$

Substituting Eqs. 6.10 and 6.11, and dividing by the concentration calculated from the mean depth gives

$$\frac{C}{C(d)} = \frac{\sum_{i=1}^n d_i^{1+b_1+b_1 b_2+b_3} \Delta y_i}{d^{b_1 b_2+b_3} \sum_{i=1}^n d_i^{1+b_1} \Delta y_i} \quad (6.17)$$

Substituting Eq. 6.15 gives

$$\frac{C}{C(d)} = \left[\left(\frac{B+1}{B} \right) \frac{A}{d} \right]^{b_1 b_2+b_3} \frac{\int_0^{w/2} \left[w^B - (2y)^B \right]^{1+b_1+b_1 b_2+b_3} dy}{\int_0^{w/2} \left[w^B - (2y)^B \right]^{1+b_1} dy} \quad (6.18)$$

The use of the transformation $u = 2y/w$ gives

$$\frac{C}{C(d)} = \left[\left(\frac{B+1}{B} \right) \frac{Aw^B}{d} \right]^{b_1 b_2+b_3} \frac{\int_0^1 (1-u^B)^{1+b_1+b_1 b_2+b_3} du}{\int_0^1 (1-u^B)^{1+b_1} du} \quad (6.19)$$

Finally, recalling Eq. 6.14, Eq. 6.19 can be reduced to

$$\frac{C}{C(d)} = \left(\frac{B+1}{B} \right)^{b_1 b_2+b_3} \frac{\int_0^1 (1-u^B)^{1+b_1+b_1 b_2+b_3} du}{\int_0^1 (1-u^B)^{1+b_1} du} \quad (6.20)$$

Simpson's Rule was used to calculate the integrals in Eq. 6.20 for a range of B values. From these values, $C/C(d)$ has been calculated and is plotted in Fig. 6.8. The average value of $B = 1.53$ from Leopold and Maddock (1953) yields $C/C(d) = 1.43$, which should be compared with the observed correction for field data, $c_F = 1.268$. These values are reasonably close, especially when one recalls that the omission of the critical velocity term from Eq. 6.11 will tend to cause an over-estimation of $C/C(d)$.

The analysis presented here suggests that the irregularity of river cross-sections could indeed be responsible for the observed higher values of Meld measurements of sediment concentration over laboratory measurements. Figure 6.8 shows that the amount of this factor will change from river to river based on the specific channel shapes. From the available data, the value $c_F = 1.268$ seems to be a reasonable average value of this multiplicative factor.

6.6 Comparison with Existing Methods

A statistical comparison of available methods for calculating sediment concentration is given in Table 6.4. The table gives the geometric mean and geometric standard deviation of the ratio of computed to observed sediment concentration for both laboratory and field observations. A graphical display of the statistics is presented in Fig. 6.9. The comparison is somewhat unfair in that the proposed method was fitted to the same data used to make the comparison. Of course,

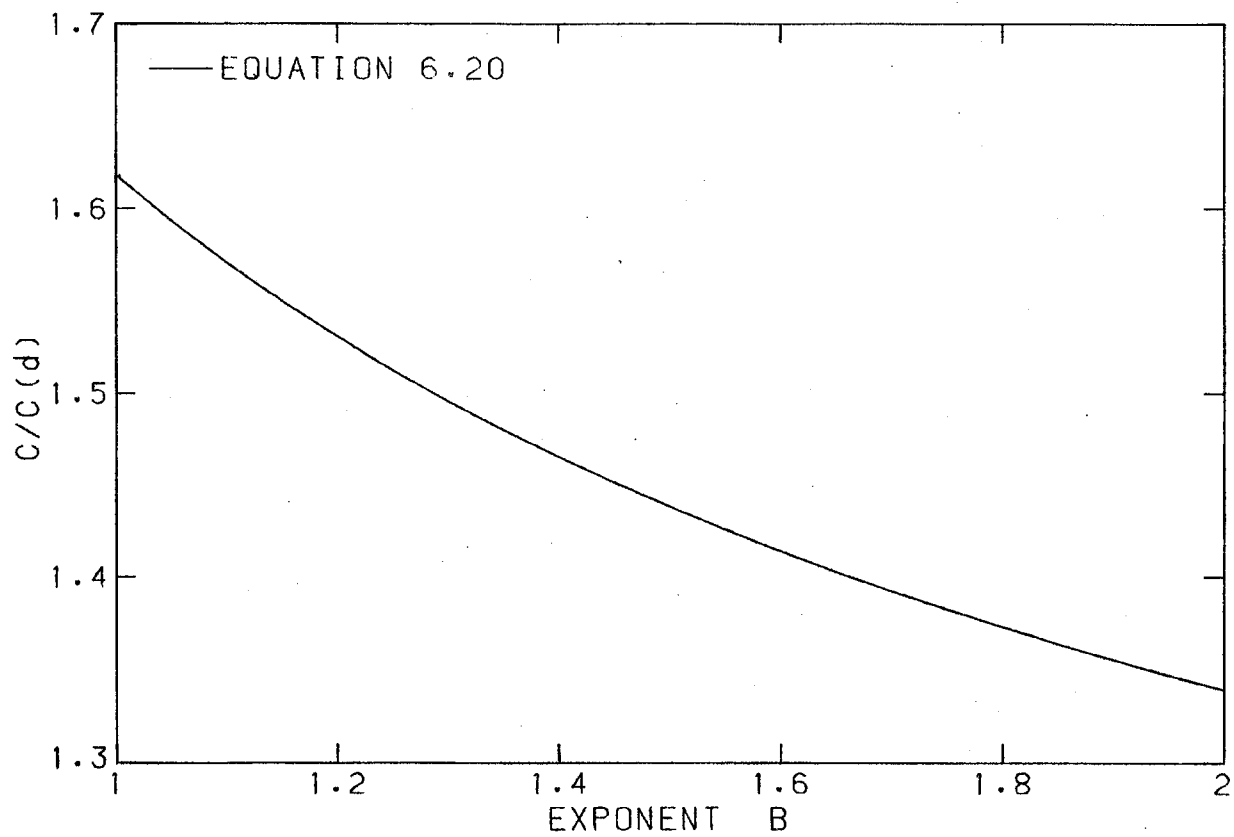


Figure 6.8 Ratio of cross-sectionally integrated concentration to concentration calculated from mean depth, as a function of the value of exponent B in Eq. 6.14.

Table 6.4

Geometric Mean and Geometric Standard Deviation of the Ratio
of Predicted to Observed Concentration for All Methods, for
Laboratory and Field Conditions

Investigator	Number	Laboratory		Field	
		Mean	S.D.	Mean	S.D.
Ackers and White (1973)	998	1.150	1.758	0.694	2.027
Bagnold (1966)	999	2.155	2.718	1.173	2.537
Bishop et al. (1965)	973	0.695	2.300	0.443	2.488
Einstein (1950)	950	0.628	4.059	0.420	3.719
Engelund and Fredsoe (1976)	825	1.274	2.972	3.179	14.026
Engelund and Hansen (1967)	999	1.236	2.064	0.916	1.997
Graf (1971)	999	1.360	3.696	1.005	3.124
Laursen (1958)	972	1.296	2.532	0.420	3.098
Ranga Raju et al. (1981)	833	1.160	1.882	0.333	2.813
Rottner (1959)	999	0.920	2.101	0.603	1.904
Shen and Hung (1971)	940	0.866	1.656	0.432	2.973
Toffaletti (1968)	995	1.166	2.749	0.854	2.572
Yang (1973)	993	1.215	1.710	0.471	3.077
Brownlie (1981)	999	1.000	1.638	1.000	1.746

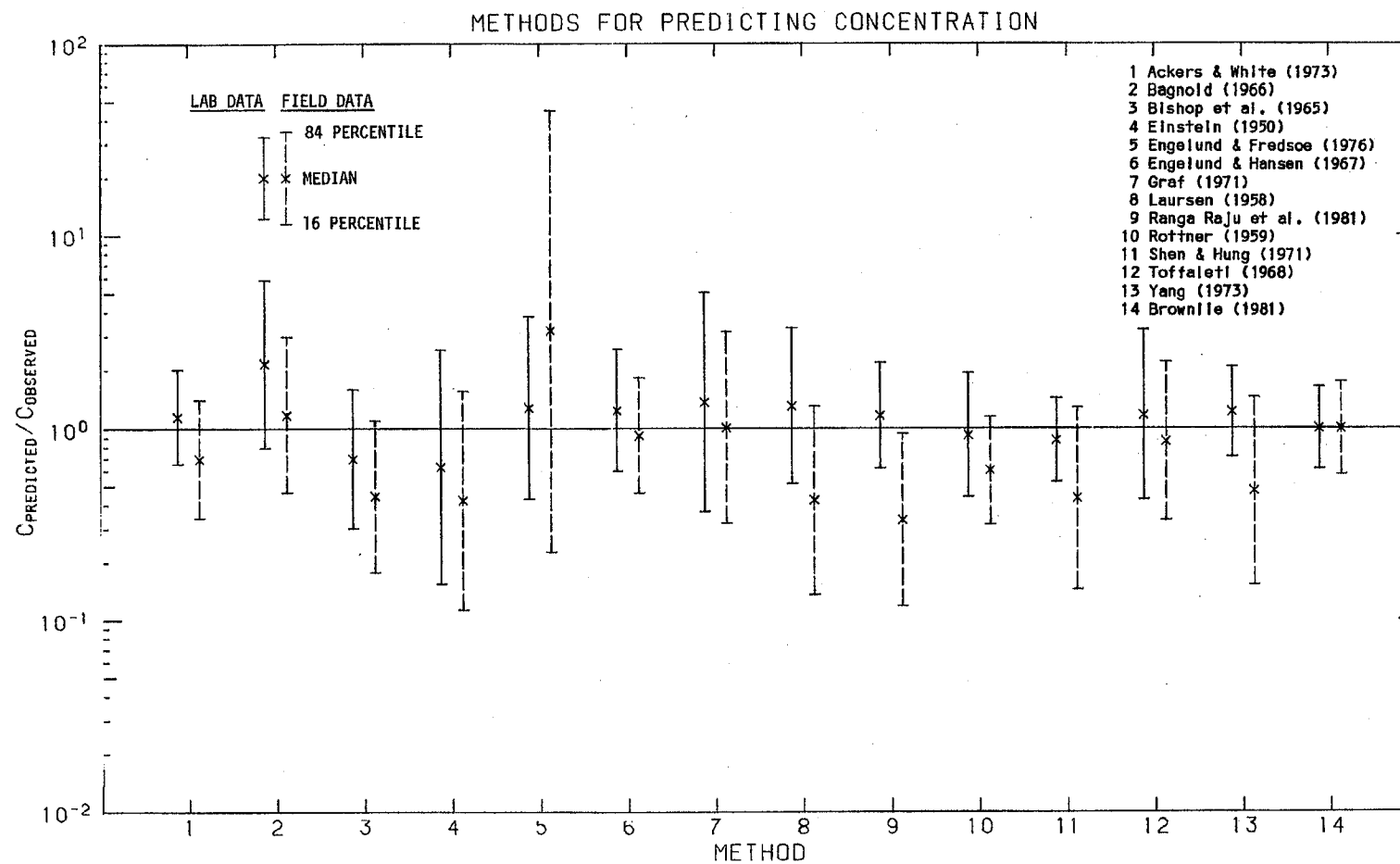


Figure 6.9. Comparison of methods for predicting sediment concentration. Median and 16 and 84 percentile values are based on the approximation of a log-normal distribution of errors.

some of these data were also used in the derivation of many of the existing methods,

The geometric mean and geometric standard deviation were calculated by taking the antilogs of the mean and standard deviation, respectively, of the logarithms of ratios of computed to observed concentration. As shown in Chapter 5, the errors tend to be log-normally distributed, and therefore these two parameters provide a good description of the distribution. Approximately 68 percent of the data can be found to lie in a range from the geometric mean divided by the geometric standard deviation to the geometric mean times the geometric standard deviation.

6.7 Summary

A method has been proposed for the calculation of the mean bed-material concentration in a channel. For the convenience of the reader, the necessary equations are repeated here. The method assumes that the bed-material properties, slope, and water temperature are known. The method also requires hydraulic radius and mean velocity, which if not known, can be calculated if the unit discharge is known, from the procedure described in Chapter 4.

First, critical shear stress is determined either from Fig. 6.3 or from Eq. 6.3:

$$\tau_{*c} = 0.22Y + 0.06(10)^{-7.7Y} \quad (6.3)$$

$$\text{where } Y = \left(\sqrt{\frac{\rho_s - \rho}{\rho}} R_g \right)^{-0.6}$$

Next, the critical grain Froude number is determined from Eq. 6.4 :

$$F_{g_o} = 4.596 \tau_{*o}^{0.5293} S^{-0.1405} \sigma_g^{-0.1606} \quad (6.4)$$

Finally, the bed-material concentration, in parts per million by weight, is determined from Eq. 6.8:

$$C = 7115c_F \left(F_g - F_{g_o} \right)^{1.978} S^{0.6601} \left(\frac{r}{D_{50}} \right)^{-0.3301} \quad (6.8)$$

where $c_F = 1$ for laboratory conditions and $c_F = 1,268$ for field conditions,

In the derivation of Eq. 6.8 concentration in parts per million by mass has been taken to be equivalent to concentration measured as milligrams per liter. For concentrations less than 16,000 ppm, this approximation will result in an error of less than 1 percent. The range of concentration for the input data used to develop Eq. 6.8 was from 10 ppm to 40,000 ppm. The ranges of the values of other parameters are given in Table 5.2a and 5.2b, and restrictions on the input data are summarized in Table 5.3.

CHAPTER 7

RECOMMENDATIONS FOR NUMERICAL MODEL DEVELOPMENT

A numerical solution to the set of Eqs. 1.1 through 1.5 is presented in this chapter. The proposed solution is not yet a working model, but rather a test of the possibility of using the new relations for flow depth and sediment concentration to define Eqs. 1.4 and 1.5, respectively. Later in the chapter recommendations are given for further development of the solution techniques.

7.1 Solutions to the Differential Equations

Implicit finite difference solutions to the set of Eqs. 1.1 through 1.5 have been given by Cunge and Verdreau (1973), Liggett and Cunge (1975), and Ponce et al. (1979). These solutions have been primarily concerned with the simplified case where time derivatives in the momentum and continuity equations, Eqs. 1.1 and 1.2, respectively, are neglected. The problem being attacked here is different in that the full equations are to be solved.

Equations 1.1 through 1.3 can be rearranged in the form

$$-\frac{\partial H}{\partial x} - \frac{1}{g} \frac{\partial u}{\partial t} = S \quad (7.1)$$

$$\frac{\partial q}{\partial x} + \frac{\partial h}{\partial t} = 0 \quad (7.2)$$

$$\frac{\partial q_s}{\partial x} + \frac{\partial h_s}{\partial t} = 0 \quad (7.3)$$

where

$$H = z + h + \frac{u^2}{2g}$$

$$S = \frac{fu^2}{8gh}$$

$$q = uh$$

$$q_s = Cuh$$

$$h_s = (1 - \lambda) \frac{\rho_s}{\rho} z + Ch$$

Equations 7.1, 7.2, and 7.3 each have the general form

$$\frac{\partial f_1}{\partial x} + \frac{\partial f_2}{\partial t} + f_3 = 0 \quad (7.4)$$

where f_1 , f_2 , and f_3 are functions of h , z , and u .

Using the standard finite difference representation, **sometimes** attributed to **Preissmann (1965)**, the terms in Eq. 7.4 can be approximated by

$$\frac{\partial f_1}{\partial x} \approx \frac{1}{\Delta x} (f_{1,j+1} - f_{1,j}) + \frac{\theta}{\Delta x} (\Delta f_{1,j+1} - \Delta f_{1,j}) \quad (7.5)$$

$$\frac{\partial f_2}{\partial t} \approx \frac{1}{2\Delta t} (\Delta f_{2,j+1} + \Delta f_{2,j}) \quad (7.6)$$

$$f_3 \approx \frac{1}{2} (f_{3,j+1} + f_{3,j}) + \frac{\theta}{2} (\Delta f_{3,j+1} + \Delta f_{3,j}) \quad (7.7)$$

where $0 \leq \theta \leq 1$ is a weighting coefficient, and the delta (Δ) in front of functions f_1 , f_2 , and f_3 refers to the change in the value of the function over a time step, as illustrated in Fig. 7.1. The **incremental** value of any function at any point can be represented as shown here for the function f_1

$$\Delta f_{1,j} = \left(\frac{\partial f_1}{\partial h} \right)_j \Delta h + \left(\frac{\partial f_1}{\partial z} \right)_j \Delta z + \left(\frac{\partial f_1}{\partial u} \right)_j \Delta u \quad (7.8)$$

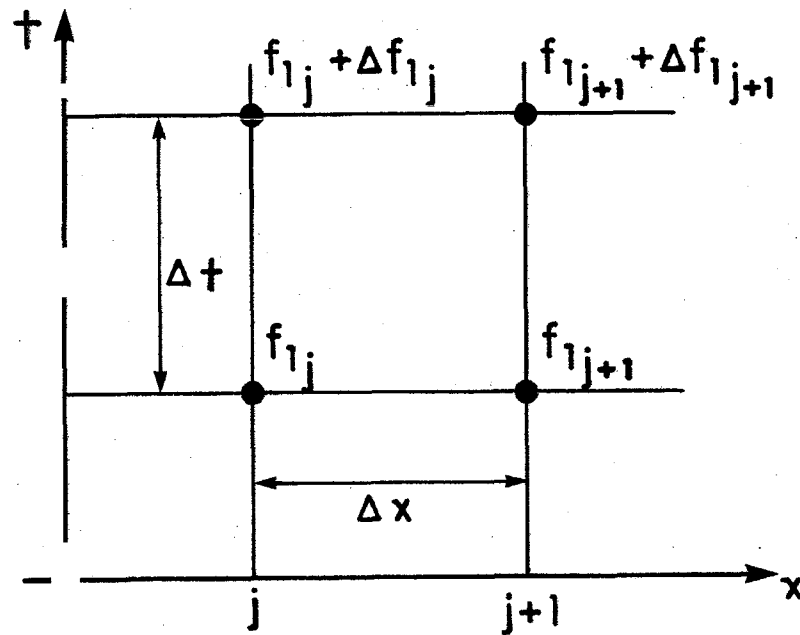


Figure 7.1 Definition sketch for four-point implicit finite difference scheme.

Given expressions for the friction factor, f , and the concentration, C , a set of linear finite difference equations can be established and solved for the incremental values Δh , Δz , and Δu at all points along the channel. Here the solution of the finite difference equations was accomplished through the use of Gauss elimination with pivotal condensation and back substitution (McCracken and Dorn, 1968).

A definition of f for the lower flow regime can be obtained by a rearrangement of Eq. 4.10a, and for the upper flow regime by a rearrangement of Eq. 4.10b. Rearrangements of Eqs. 4.10a and 4.10b solving for several dimensionless quantities are given in Table 7.1. When flows are entirely in one flow regime or the other, the definition of f is therefore easily accomplished. However, for situations involving both flow regimes, a transition mechanism will be required. Such a mechanism has not yet been developed.

The concentration can be determined from Eq. 6.8 after first determining the critical grain Froude number from Eqs. 6.3 and 6.4. Equation 6.8 gives an equilibrium solution for steady flow conditions. If a sudden change in flow conditions occurs, a non-equilibrium value of concentration may exist. Dobbins (1944) has developed a transient solution for the sediment concentration profile after a change in turbulence intensity. The first eigenvalue of the transient solution given by Dobbins (1944) has been used to adjust the equilibrium value of concentration. The resulting equation provides for an exponential decay or growth from one equilibrium condition to another,

Using this approximation, the concentration at point j , C_j , can be

Table 7.1

Rearrangement of Flow Depth Predictors
Equation 4.10a and Equation 4.10b

<u>Regime</u>	<u>Relative Roughness</u>		
Lower	$\frac{r}{D_{50}} = 0.05761(s-1)^{0.9447} F_g^{1.889} S^{-0.7345} \sigma_g^{0.3034}$		(7.9a)
Upper	$\frac{r}{D_{50}} = 0.03478(s-1)^{0.8326} F_g^{1.665} S^{-0.7668} \sigma_g^{0.2136}$		(7.9b)
	<u>Slope</u>		
Lower	$S = 0.02054(s-1)^{1.286} F_g^{2.572} \left(\frac{r}{D_{50}}\right)^{-1.361} \sigma_g^{0.4130}$		(7.10a)
Upper	$S = 0.01252(s-1)^{1.086} F_g^{2.172} \left(\frac{r}{D_{50}}\right)^{-1.304} \sigma_g^{0.2785}$		(7.10b)
	<u>Grain Froude</u>		
Lower	$F_g = \frac{v}{\sqrt{(s-1)gD_{50}}} = 4.530(s-1)^{-0.5} S^{0.3888} \left(\frac{r}{D_{50}}\right)^{0.5293} \sigma_g^{-0.1606}$		(7.11a)
Upper	$F_g = \frac{v}{\sqrt{(s-1)gD_{50}}} = 7.515(s-1)^{-0.5} S^{0.4605} \left(\frac{r}{D_{50}}\right)^{0.6001} \sigma_g^{-0.1283}$		(7.11b)

Table 7.1
-Continued-

<u>Regime</u>	<u>Friction Factor</u>		
Lower	$f = \frac{\tau}{\rho v^2} = 0.164(s-1)$	$0.286 F_g^{0.572} \left(\frac{r}{D_{50}}\right)^{-0.361} \sigma_g^{0.413}$	(7.12a)
Upper	$f = \frac{8grS}{v^2} = 0.100(s-1)$	$0.086 F_g^{0.172} \left(\frac{r}{D_{50}}\right)^{-0.304} \sigma_g^{0.279}$	(7.12b)
	<u>Froude Number</u>		
Lower	$F = \frac{v}{\sqrt{gr}} = 4.53$	$s^{0.389} \left(\frac{r}{D_{50}}\right)^{0.0293} \sigma_g^{-0.161}$	(7.13a)
Upper	$F = \frac{v}{\sqrt{gr}} = 7.52$	$s^{0.461} \left(\frac{r}{D_{50}}\right)^{0.100} \sigma_g^{-0.128}$	(7.13b)

- Notes:
1. For use with the differential equations velocity "v" should be replaced by the x component of velocity "u," and "r" should be replaced by "d".
 2. $s = \rho_s / \rho =$ specific gravity.
 3. For statistical reasons three or four significant figures are retained in the coefficients and exponents, although the accuracy of the computed results cannot be considered to be more than about two significant figures.

determined from the equilibrium concentration at j , C_{ej} , (from Eq. 6.8) and the concentration at upstream point $j + 1$, C_{j+1} , from

$$C_j = C_{ej} + e^{-\epsilon (\alpha^2 + \beta^2) t} (C_{j+1} - C_{ej}) \quad (7.14)$$

where $\beta = \frac{w}{2\epsilon}$

and $2 \cot(h\alpha) = \frac{\alpha}{\beta} - \frac{\beta}{a}$

and w is the fall velocity of the particles and ϵ is the turbulent diffusion coefficient. The concentration at the top of the reach is necessarily assumed to be at **equilibrium**. In test runs the adjustment of the equilibrium concentration in this manner had only a small (on the order of 10 percent) influence on the concentration. When the equilibrium value of concentration changes abruptly from one location to another, the effect may be much greater,

In developing Eq. 7.14, only the first eigenvalue of the Dobbins (1944) solution was used. This simplification will be valid for large enough time steps. However, more research is needed both experimentally and analytically to verify the use of Eq. 7.14.

For the test runs, the boundary conditions consisted of one downstream condition and two upstream conditions. The downstream condition is a constant water surface elevation, expressed in finite difference form as

$$\Delta h_1 + \Delta z_1 = 0 \quad (7.15)$$

The upstream conditions are

$$u_n \Delta h_n + h_n \Delta u_n = Aq - \Delta h_n \Delta u_n \quad (7.16)$$

$$\Delta z_n = 0 \quad (7.17)$$

The term A_q in Eq. 7.16 is the change in the inflow over a time step for some given inflow hydrograph. Since the quantities Δh_n and Δu_n appear as a product on the right side of Eq. 7.16, an iterative procedure is required to solve for the upstream depth and velocity. This second order correction, applied only at the upstream boundary, allows for an exact representation of the inflow hydrograph. Equation 7.17 implies that the bed at the upstream end of the reach is fixed, which agrees with the assumption that the inflow concentration is at equilibrium,

Some test results are shown in Figs. 7.2 through 7.5." Water surface elevations at 15 minute intervals along a 6 kilometer test reach are shown in Fig. 7.2. The inflowing flood wave has a duration of 1 hour. The channel has a bed slope of 0.001 and a uniform sand bed with a particle size of $D_{50} = 0.4$ mm. The model parameters are as follows: $\Delta x = 100$ meters, $\Delta t = 9$ seconds and the weighting factor for the implicit scheme, $\theta = 0.5$. The initial condition is derived from a steady-state backwater calculation.

The passage of the flood wave through the reach is illustrated in Fig. 7.3. The figure illustrates how the wave is attenuated by friction losses as it passes through the reach. Although the bed elevation is not fixed, its changes are imperceptible on this time scale.

An unusual aspect of this type of numerical simulation is the ability to examine hysteresis effects. The term "hysteresis" in hydraulic applications refers to situations where properties such as flow depth or sediment concentration have different values for a given discharge during rising and falling stages. Figure 7.5 shows how the

*The lower regime Eq. 7.16a has been used in this example; transition between regimes has not been included (see p. 204 for further discussion).

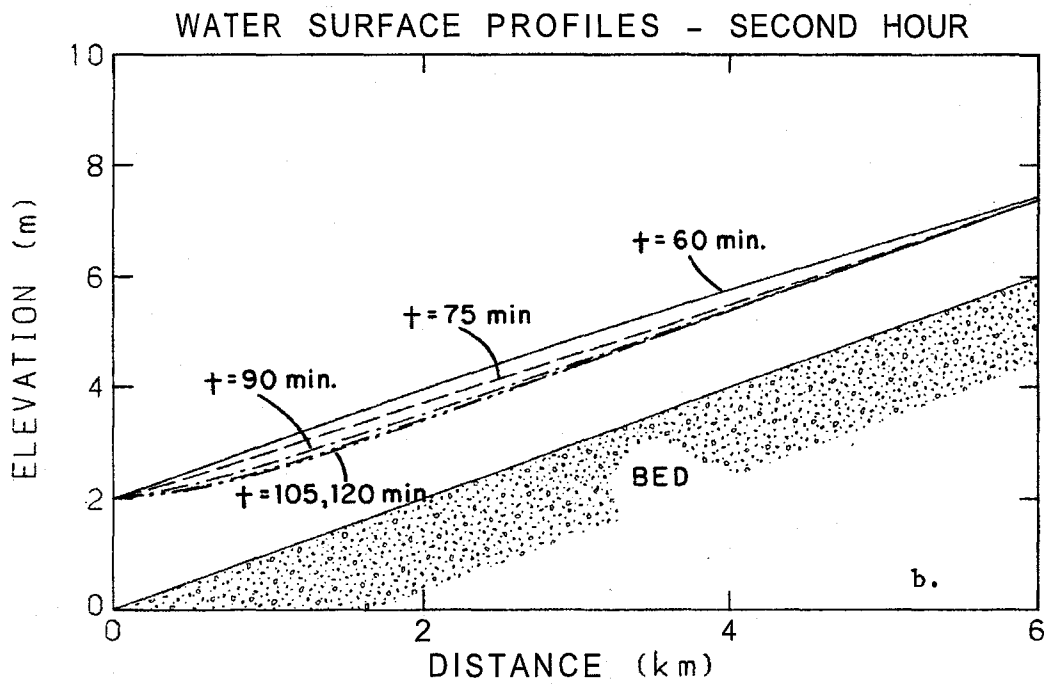
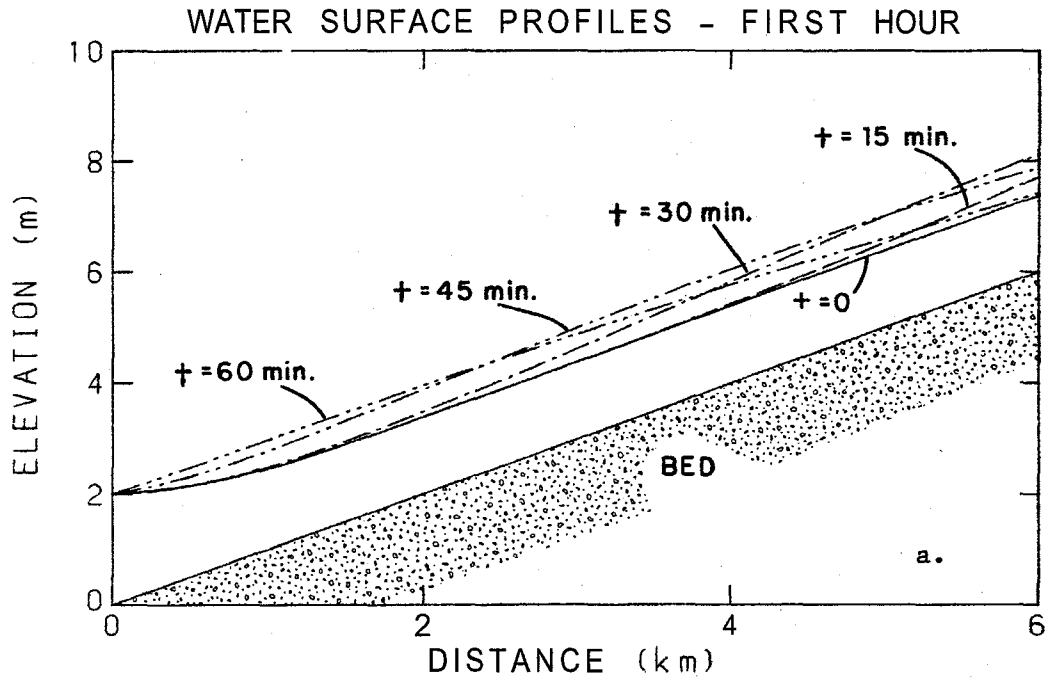


Figure 7.2 Water surface profiles for model test reach for: (a) $t = 0$ to 60 minutes, and (b) $t = 60$ to 120 minutes.

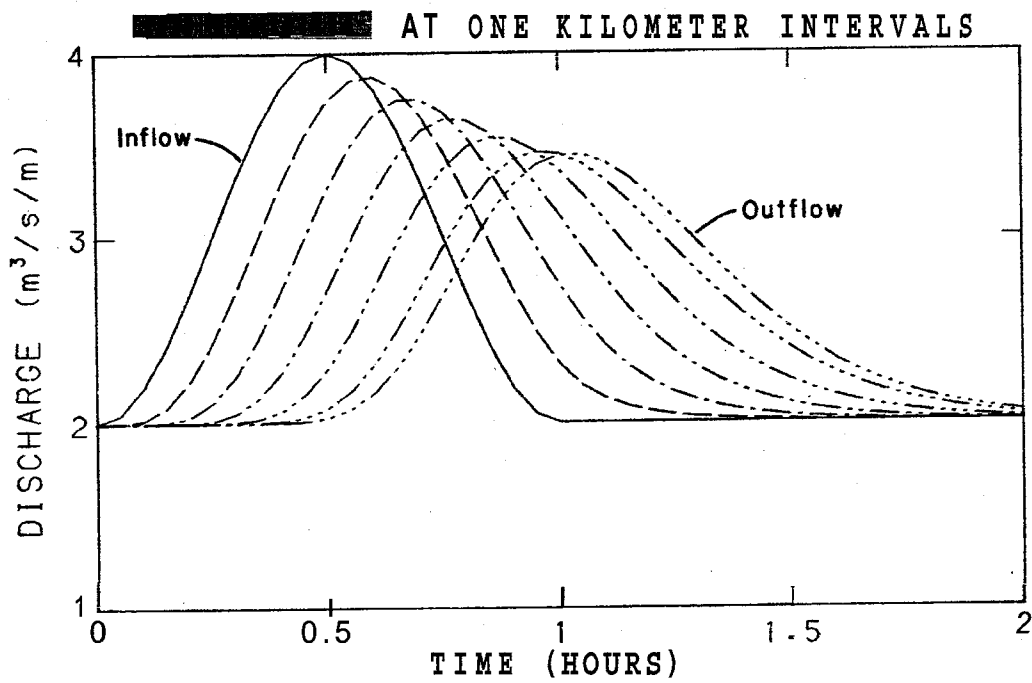


Figure 7.3 Attenuation of inflow hydrograph; hydrographs shown at a one kilometer interval.

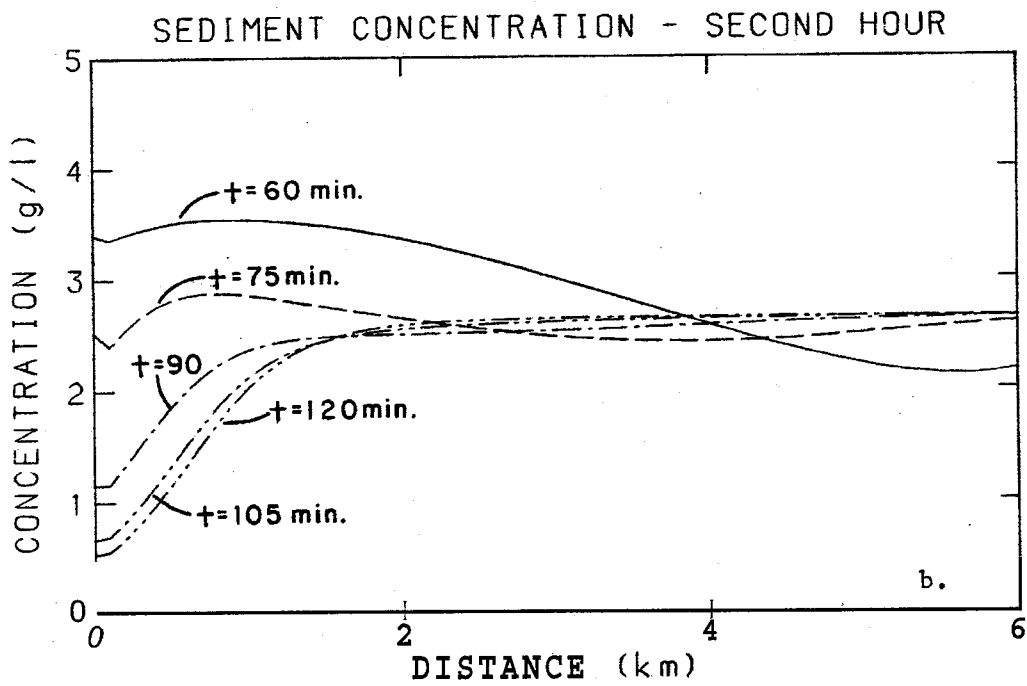
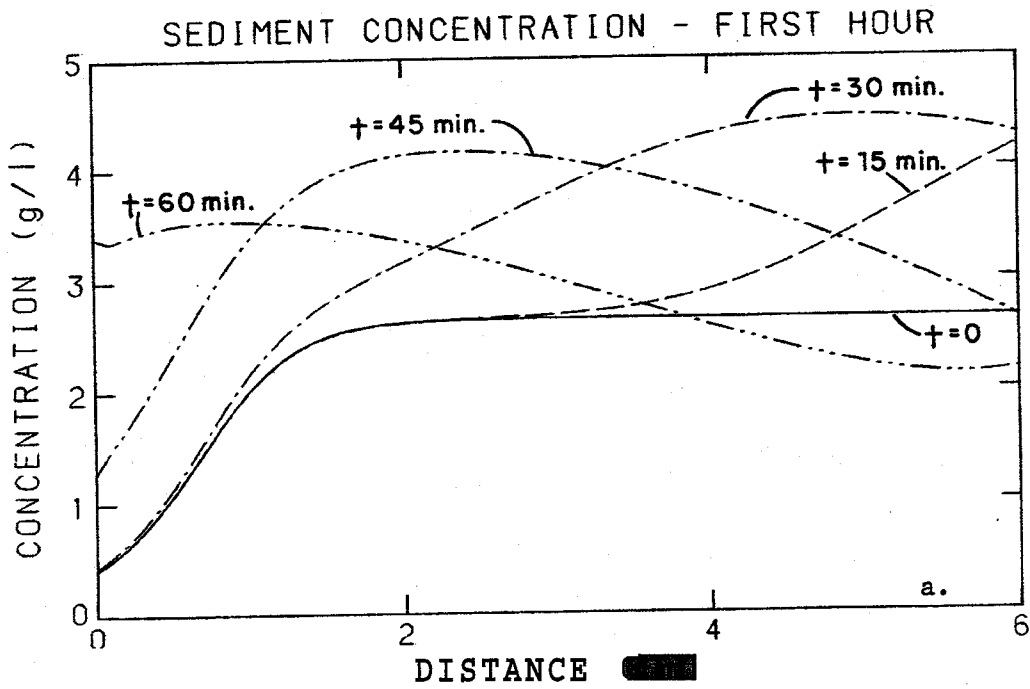


Figure 7.4 Sediment concentrations along test reach for:
 (a) $t = 0$ to 60 minutes, and (b) $t = 60$ to 120 minutes.

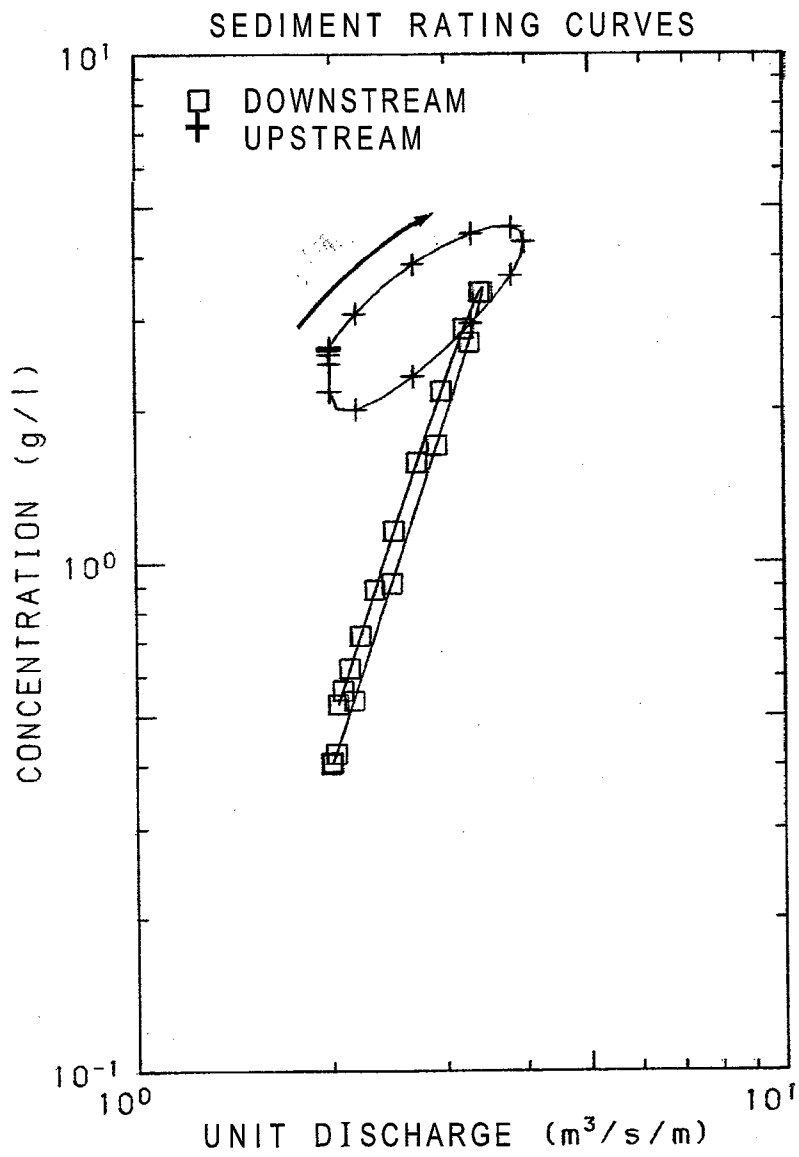


Figure 7.5 Sediment concentration rating curves.

sediment concentration may be higher during the rising limb of a flood wave than during the falling limb, for a given discharge. The effect is very noticeable at the top of the channel reach, and negligible at the downstream end where flow depth is controlled by the boundary condition.

7.2 Recommendations for Future Work

In Chapter 1 five problems that one might encounter when applying the HEC-6 model to situations involving rapidly changing flows were discussed. All five of these problems have been addressed to some extent in this report. The first two points involved simplifications to the basic differential equations which have been avoided in the implicit solution. The third point dealt with the definition of slope or friction factor, and was considered in Chapters 3 and 4. The fourth point concerned the selection of a concentration relationship and was addressed in Chapters 5 and 6. The final point dealt with the fact that sediment concentration would not always be at an equilibrium value. While this point has been addressed to some extent, clearly more work is needed, as mentioned previously. Additional improvements are discussed here,

Probably the most important next step in the development of the model would be the implementation of a **function** describing the transition between the upper and lower flow regimes. Static or slowly changing transition was discussed in Section 4.3. "Static" transition refers to a steady flow in the transition regime. During an actual

transition, the time scale of bed form changes may be significantly longer than the time scale of the changes in the hydraulic variables.

One approach to the development of a function which describes the transition from one flow regime to the other would be to describe the behavior of the effective bed roughness, k_d in Eq. 4.4. Gee (1973) and Wijnbenga and Klaassen (1981) have performed experiments on the transient behavior of dunes. Allen (1978) and Fredsøe (1979) have presented analytical expressions for the transition from one dune height to another. Wijnbenga and Klaassen (1981) have suggested that the present theoretical expressions are not totally satisfactory.

More work is needed both analytically and experimentally on the behavior of dunes during transition. If an analytical expression were developed, there would still be the problem of adapting it to numerical modeling applications,

Another aspect of the problem which requires more research is the phenomenon of armoring or grain sorting. Gessler (1971) proposed a probabilistic approach to the bed armoring process which may provide a satisfactory mechanism in a numerical model. This method allows for an increase in the median particle size of the bed material as the bed undergoes degradation. This method has been adapted for use in the HEC-6 model, but little work has been done which would verify its accuracy.

7.3 Discussion

The regression procedure used to develop the flow depth equation was based on the assumption that errors occur in the depth measurements, and that discharge and slope are known accurately. The resulting errors are on the order of 10 percent in the prediction of depth. The values of the exponents of Eqs. 4.10a and 4.10b are such that when they are rearranged to solve for other variables, as done in Table 7.1, different values of error can be expected. If one considers that velocity and depth are known accurately, then errors in predicting observed slope may be on the order of 33 percent.

The depth predictor and concentration predictor were developed with the notion of solving the equations using the set of initial conditions and boundary conditions as prescribed in the example given here. The initial conditions are based on a backwater calculation which utilized the flow depth predictor to obtain the normal depth (asymptotic upstream condition). Accuracy problems associated with the predictor of flow depth, as discussed above, may cause an ill-conditioned system with other sets of boundary conditions and initial conditions.

If the relationship between depth, slope, and velocity is known for a particular river station, then the coefficients and exponents given in Table 7.1 can and should be adjusted to satisfy that relationship. As is, the coefficients represent values fitted to a large body of data, which can be adjusted for any particular river as suggested by the errors given in Table 4.1.

For the lower regime, f can be expressed as:

$$f = 0.390 s^{0.222} \left(\frac{r}{D_{50}} \right)^{-0.0586} \sigma_g^{0.322} \quad (7.17)$$

indicating that f is nearly constant for a given slope and bed material. (A value of $x = 0.667$ in Fig. 4.1 would have produced a constant f .) For the upper regime, Manning n (metric units) can be expressed as:

$$n = 0.133 \frac{D_{50}^{0.100}}{\sqrt{g}} r^{0.0667} s^{0.0390} \sigma_g^{0.128} \quad (7.18)$$

indicating that n is nearly constant for a given slope and bed material. (A value of $x = 0.6$ in Fig. 4.2 would have produced a constant n .)*

So far the discussion has been confined to the one-dimensional problem. To model real river systems lateral and perhaps even vertical, dimensions will need to be considered as well as the longitudinal dimension. The additional complications will include meandering and changes in channel width. In future pursuits, the **writer's** approach would be first to develop a satisfactory one-dimensional model and then increase its sophistication to include the second and third dimensions.

For applications involving rapidly varying flow conditions, it may be necessary to abandon the computational simplifications inherent in many engineering river models such as the **HEC-6** model. The techniques presented in this chapter appear to have promise for the **future** development of a numerical **model** for unsteady flow conditions. However, a river is in fact a complex system, and it is the **writer's** belief that the development of a reliable, widely applicable river model is still somewhat in the future.

*Note: for upper regime $f = 0.141s^{0.088} \left(\frac{r}{D_{50}} \right)^{-0.200} \sigma_g^{0.256}$

CHAPTER 8

SUMMARY AND CONCLUSIONS

8.1 Summary

In recent years attempts have been made to numerically model unsteady flows in channels with sediment transport. The HEC-6 program is the most widely used engineering model. The HEC-6 program is useful in the analysis of slowly varying processes, such as long-term reservoir sedimentation, but less useful when rapidly varying processes are important.

The present research has been undertaken to study two elements which are **fundamental** to the development of an accurate model for unsteady flows in sand-bed channels. These elements are the relation between the hydraulic variables (energy slope, depth, and velocity) and the predictor of sediment concentration. The following approach has been used to study these relationships:

1. The large data base given in Appendix B has been created to analyze both the hydraulic relationship and the sediment relationship. The data base contains 7027 records (5263 laboratory records and 1764 field records) in 79 data files.
2. An examination of existing techniques for prediction of flow depth has suggested that a wide ranging **solution** which can easily be adapted to numerical modeling applications does not exist.

3. Relying heavily on dimensional analysis, a new relationship (Chapter 3) has been developed. The proposed new method solves for flow depth for upper regime flow and lower regime flow and provides a method for determining which flow regime one might expect. A statistical analysis indicates that the one standard deviation errors in predicting flow depth are 9.5 percent for upper regime and 12.1 percent for lower regime, as shown in Table 4.1. More work is needed to define a function describing the transition between lower and upper regime. Table 7.1 contains rearrangements of the equations.
4. A graphical and statistical analysis has been presented for 13 existing methods for predicting sediment concentration. Several methods performed reasonably well in the prediction of laboratory concentrations, but most drastically underestimated the concentration for field conditions. The Ackers and White (1973) and the Englund and Hansen (1967) methods provided the best results when analyzed with a carefully screened data set containing about 1000 records.
5. A new method for predicting concentration has been developed, which is easy to use and more accurate. The new method, based on dimensional analysis, suggests that complicated procedures, such as those required for the Einstein (1950) procedure, are not warranted. The geometric standard deviation of the ratio of predicted to observed concentration is 1.64 for laboratory data and 1.75 for field data. No other method had both of these indicators under two. The method is summarized in Section 6.7.

6. A four-point implicit finite difference scheme has been presented to demonstrate the feasibility of applying the new hydraulic and sediment relationships to a numerical solution of the differential equations. A proposed time lag has been included to provide for non-equilibrium values of sediment concentration.

A discussion of the general purpose HEC-6 model was presented in Chapter 1. Five possible problems associated with the model were discussed, each of which can be related to a simplification or an approximation involved in solving the basic set of one-dimensional equations (Eqs. 1.1 to 1.5). A new model has ~~not~~ been presented which would replace the HEC-6. Instead, the intention of this work was to pursue a course of research which would ultimately lead to an improved solution of the one-dimensional equations. Problems such as bank erosion and meandering, which are not treated by the HEC-6 program, have not been considered here.

It is hoped that the present work will lay the foundation for the future development of an accurate model for engineering applications. As discussed in Section 7.3, there are still several problems to be resolved before a satisfactory general purpose model can be developed.

8.2 Conclusions

1. None of the existing methods for prediction of friction factor adequately predict uniform flow depth from given unit discharge, bed slope, and bed-material properties, for a wide range of data.

2. For depth calculations of engineering design accuracy, it is satisfactory to classify bed-form regimes simply as either lower regime (dunes and ripples) or upper regime (flat bed and antidunes).
3. Flow depth can be predicted to an accuracy on the order of 10 percent for either regime by the method proposed here.
4. Given slope and bed-material properties, friction factor, f , varies only slightly for the lower regime, while Manning n varies slightly for the upper regime. This implies that the measure of bed-form roughness is nearly proportional to the depth for the lower regime.
5. Transition between flow regimes, for a constant slope, appears to take place over a narrow range of depth.
6. Neglecting viscous effects, transition values of velocity can be determined from slope and median bed-particle size.
7. Of the 13 existing techniques for predicting sediment concentration, the Ackers and White (1973) and the Engelund and Hansen (1967) methods give the most satisfactory results for a wide range of lab and field data (see Fig. 6.9). This conclusion is in agreement with the results of the White, Milli, and Crabbe (1973) comparison.
8. Large scatter in the data causes an inevitable accuracy problem in the prediction of sediment concentration. In the laboratory data, the scatter may be partly the result of differences between experimental techniques. In the field data, the scatter is probably a result of short sampling times compared to the time

scales of the large scale turbulent and sediment concentration fluctuations.

9. The proposed new technique for predicting sediment concentration is easy to use and at least as good or better than any of the other techniques tested. The geometric standard deviation of the ratio of predicted to observed concentration is 1.64 for the available lab data and 1.75 for the available field data.
10. The methods for predicting sediment concentration that give the best results, including the new method, are fairly simple regression equations, while in general the more complex procedures give poorer results, within the range of data tested.
11. The HEC-6 program has the capability of using either the Laursen or Toffaleti technique for predicting sediment transport, or a user defined rating curve. Figure 6.9 suggests that the performance of the model could be improved by simply using the proposed new method.

REFERENCES

- ASCE Task Force, "Friction Factors in Open Channels," Journal of the Hydraulics Division, ASCE, Vol 89, No. HY2, March 1963, pp. 97-143.
- Ackers, P. and White, W. R., "Sediment Transport: New Approach and Analysis," Journal of the Hydraulics Division, ASCE, Vol. 99, No. HY 11, November 1973, pp. 2041-2060.
- Alam, A. M. Z., Cheyer, T. F. and Kennedy J. F., "Friction Factors for Flow in Sand Bed Channels," Hydrodynamics Laboratory Report No. 78, Massachusetts Institute of Technology, Cambridge, Massachusetts, June 1966.
- Alam, A. M. Z. and Kennedy, J. F., "Friction Factors for Flow in Sand Bed Channels," Journal of the Hydraulics Division, ASCE, Vol. 95, No. HY6, November 1969, pp. 1973-1992.
- Allen, J. R. L., "Computational Models for Dune Time-lag: An Alternative Boundary Condition," Sedimentary Geology, Vol. 16, 1978, pp. 255-279.
- Bagnold, R. A., "An Approach to the Sediment Transport Problem from General Physics," U.S. Geological Survey, Professional Paper 422-1, U.S. Government Printing Office, Washington, D.C., 1966.
- Bayazit, M., "Free Surface Flow in a Channel of Large Relative Roughness," Journal of Hydraulic Research, Vol. 14, No. 1, 1976, pp. 115-126.
- Bishop, A. A., Simons, D. B. and Richardson, E. V., "Total Bed Material Transport, Proc. ASCE, Vol. 91, HY2, February 1965.
- Brownlie, W. R., "Re-examination of Nikuradse Roughness Data," Journal of the Hydraulics Division, ASCE, Vol. 107, No. HY1, January 1981, pp. 115-119.
- Chang, H. H., "Flood Plain Sedimentation and Erosion," San Diego County Department of Sanitation and Flood Control, 1976.
- Chang, N. H. and Hill, J. C., "A Case Study for Erodible Channel Using a Mathematical Model," March 1981.
- Chu, H. and Mostafa, M. G., "A Mathematical Model for Alluvial Channel Stability," Proceedings of Engineering Workshop on Sediment Hydraulics, California State University, Long Beach, February 3, 1979, pp. 130-150.

- Colby, B. R., "Discontinuous Rating Curves for Pigeon Roost Creek and Cuffawa Creeks in Northern Mississippi," Report ARS41-36, Agricultural Research Service, April 1960.
- Cunge, J. A. and Verdreau, N., "Mobile Bed Fluvial Mathematical Models," *La Houille Blanche*, No. 7-1973, pp. 561-580.
- Dawdy, D. R., "Depth-Discharge Relations of Alluvial Streams -- Discontinuous Rating Curves," Water-Supply Paper 1948-C, U.S. Geological Survey, Washington, D.C. 1961.
- Dobbins, W. E., "Effect of Turbulence on Sedimentation," *Transactions, ASCE*, Vol. 109, Paper No. 2218, 1944, pp. 629-678.
- Einstein, H.A., "Estimating Quantities of Sediment Supplied to Streams to a Coast," Coastal Engineering Conference Proceedings, 1950, pp. 137-139.
- Einstein, H. A. and Barbarossa, N., "River Channel Roughness," Transactions, ASCE, Vol 117, 1952, pp. 1121-1146.
- Engelund, F., Closure to "Hydraulic Resistance of Alluvial Streams," Journal of the Hydraulic Division, ASCE, Vol. 93, No. HY4, July 1967, pp. 287-296.
- Engelund, F. and Fredsoe, J., "A Sediment Transport Model for Straight Alluvial Channels," Nordic Hydrology, Vol. 7, 1976, pp. 293-306.
- Engelund, F., and Hansen, E., "A Monograph on Sediment Transport in Alluvial Streams," Teknisk Vorlag, Copenhagen, Denmark, 1967.
- Fredsoe, J., "Unsteady Flow in Straight Alluvial Streams: Modification of Individual Dunes," Journal of Fluid Mechanics, Vol. 91, Part 3, 1979, pp. 497-512.
- Garde, R. J. and Ranga Raju, K. G., "Resistance Relationships for Alluvial Channel Flow," Journal of the Hydraulics Division, ASCE, Vol. 92, HY4, July 1966, pp. 77-100.
- Garde, R. J. and Ranga Raju, K.G., Mechanics of Sediment and Alluvial Stream Problems, Wiley Eastern Limited, New Delhi, 1977, 483 pp.
- Gee, D. M., "Sediment Transport in Non-steady Flow," University of California, Berkeley, California, Report 4EC 22-3, 1973.
- Gessler, J., "Critical Shear Stress for Sediment Mixtures," Proc. of Fourteenth Congress of International Association for Hydraulic Research, Vol. 3, 1971, C1-1 - C1-8.
- Graf, W. H., Hydraulics of Sediment Transport, McGraw-Hill Book Company, 1971.

- Henderson, F. M., Open Channel Flow, Macmillan Publishing Company, Inc., New York, 1966, 522 pp.
- Hydrologic Engineering Center, "HEC-6 Scour and Deposition in Rivers and Reservoirs," U.S. Army Corps of Engineers, Computer Program 723-G2-L2470, 1976.
- Jansen, P. P., et al., Principles of River Engineering: The Non-Tidal River, Fearon Pitman Publishers, Inc., Belmont, California, 1979, 509 pp.
- Jordan, P. R., "Fluvial Sediment of the Mississippi at St. Louis, Missouri," U.S. Geological Survey, Water-Supply Paper 1802, Washington, D.C., 1965.
- Lane, E. W. and Carlson, E. J., "Some Factors Affecting the Stability of Canals Constructed in Coarse Granular Materials," Proceedings, Minnesota International Hydraulics Convention, September 1953, pp. 37-48.
- Leopold, L. B. and Maddock, T., Jr., "The Hydraulic Geometry of Stream Channels and Some Physiographic Implications," Geological Survey Professional Paper 252, U.S. Department of the Interior, U.S. Government Printing Office, Washington, 1953, 57 pp.
- Liggett, J. A. and Cunge, J. A., "Numerical Methods of Solution of the Unsteady Flow Equations," Unsteady Flow in Open Channels, K. Mahmood and V. Yevjevich, eds., Water Resources Publications, Fort Collins, Colorado, 1975, pp. 89-182.
- Limerinos, J. T., "Determination of the Manning Coefficient from Measured Bed Roughness in Natural Channels," Studies of Flow in Alluvial Channels, U.S. Geological Survey, Water-Supply Paper 1898-B, 1970, 47 pp.
- McCracken, D. D. and Dorn, W. S., Numerical Methods and Fortran Programming With Applications in Engineering and Science, John Wiley and Sons, Inc., New York, 1968, 457 pp.
- Mostafa, M. G. and McDermid, R. M., Discussion of "Sediment Transport Mechanics: Hydraulic Relations for Alluvial Streams," ASCE Task Committee, Journal of the Hydraulics Division, ASCE, Vol. 97, No. HY10, October 1971, pp. 1777-1780.
- Nakato, T., "Evaluation of Several Existing Sediment-Transport Formulas for the Sacramento River," Final Report, unpublished, March 1981, 21 pp.

- Nikuradse, J., "Laws of Flow in Rough Pipes," (translation of "Stromungsgesetze in rauhen Rohren," 1933), National Advisory Committee for Aeronautics Tech Memo 1292, Washington, D.C., 1950, 62 pp.
- Ponce, V. M., Indlekofer, H. and Simmons, D. B., "The Convergence of Implicit Bed Transient Models," Journal of the Hydraulics Division, Vol. 105, HY4, April 1979, pp. 351-363.
- Preissmann, A., "Difficultés Recontrées dans la Calcul des Ondes de Transition à Front Raide," Congress of the International Association for Hydraulic Research, Seminar, Leningrad, U. S. S. R., 1965.
- Ranga Raju, K. G., "Resistance Relation for Alluvial Streams," La Houille Blanche, No. 1, 1970, pp. 51-54.
- Ranga Raju, K. G., Garde, R. J. and Bhardwaj, R., "Total Load Transport in Alluvial Channels," Journal of the Hydraulics Division, ASCE, Vol. 107, No. HY2, February 1981, pp. 179-191.
- Rottner, J., "A Formula for Bed-Load Transport," La Houille Blanche No. 3, May 1959, pp. 301-307.
- Shen, H. W. and Hung, C. S., "An Engineering Approach to Total Bed-Material Load by Regression Analysis," Symposium to Honor H. A. Einstein, 1971.
- Streeter, V. L., Fluid Mechanics, Fifth Edition, McGraw-Hill Book Company, Inc., New York, New York, 1971, 755 pp.
- Strickler, A., "Contributions to the Question of Velocity Formula and Roughness Data for Streams, Channels and Closed Pipelines," 1923, translation by T. Roesgen and W. R. Brownlie, W. M. Keck Laboratory Translation T-10, California Institute of Technology, Pasadena, California, January 1981, 104 pp.
- Vanoni, V. A., "Data Used to Develop Shields Diagram," W. M. Keck Laboratory of Hydraulics and Water Resources, Technical Memorandum 65-2, Division of Engineering and Applied Science, California Institute of Technology, Pasadena, California, April 1965, 8 pp.
- Vanoni, V. A., "Factors Determining Bed Forms of Alluvial Streams," Journal of the Hydraulics Division, ASCE, Vol. 100, HY3, March 1974, pp. 363-377.
- Vanoni, V. A., ed., Sedimentation Engineering, ASCE Manuals and Reports on Engineering Practice, No. 54., New York, 1975.

- White, W. R., Paris, E and Bettess, R, "A New General Method for Predicting the Frictional Characteristics of Alluvial Streams," Report No. IT 187, Hydraulics Research Station, Wallingford, England, July 1979.
- White, W. R., Milli, H. and Crabbe, A. D., "Sediment Transport: An Appraisal of Available Methods, Vol. 2, Performance of Theoretical Methods when Applied to Flume and Field Data," Report No. INT 119, Hydraulics Research Station, Wallingford, Berkshire, England.
- Wijbenga, J. H. A and Klaassen, G. J., "Changes in **Bedform** Dimensions Under Unsteady Flow Conditions in a Straight Flume," Second International Conference on **Fluvial** Sediments, University of Keele (U.K.), September 1981.
- Yang, C. T., "Incipient Motion and Sediment Transport," Journal of the Hydraulics Division, ASCE, Vol. 99, No. HY10, October 1973, pp. 1679-1704.

Data Sources

- Abdel-Aal, Farouk, M., "Extension of Bed Load Formula to High Sediment Rates," **PhD** thesis presented to the University of California, at Berkeley, California, December 1969.
- Barton, J. R., and Lin, P.N., "A Study of the Sediment Transport in Alluvial Channels," Report No. CEF 55JRB2, Colorado State University, Fort Collins, Colorado, 1955, 41 pp.
- Borgardi, J., and Yen, C. H., "Traction of Pebbles by Flowing Water," **PhD** thesis presented to the State University of Iowa, 1939, 66 pp.
- Casey, H.J., "Uber Geschiebebewegung," Preuss. Versuchsanst. fur Wasserbau und Schiffbau, Berlin, Mitt., Vol. 19, 1935, 86 pp. (Translation on file at U.S. Soil Conservation Service, Washington, D.C.).
- Chaudhry, H. M., Smith, K. V. H and Vigil H, "Computation of Sediment Transport in Irrigation Canals," Proc. Institution of Civil Engineers, Vol. 45, Paper 7241, 1970, pp. 79-101.
- Chitales, S. V., "Hydraulics of Stable Channels," Tables 13 and 17, Government of India, Ministry of Irrigation and Power, Central Water and Power Commission, 1966.

- Chyn, S.D., "An Experimental Study of the Sand Transporting Capacity of the Flowing Water on Sandy Bed and the Effect of the Composition of the Sand," thesis presented to the Massachusetts Institute of Technology, Cambridge, Massachusetts, 1935, 33 pp.
- Colby, B. R., and Hembree, C. H., "Computations of Total Sediment Discharge Niobrara River Near Cody, Nebraska," Water-Supply Paper 1357, U. S. Geological Survey, Washington, D.C., 1955.
- Costello, W.R., "Development of Bed Configuration in Coarse Sands," Report 74-1, Department of Earth and Planetary Science, Massachusetts Institute of Technology, Cambridge, Massachusetts, 1974.
- Culbertson, J.K., Scott, C. H. and Bennett, J. P., "Summary of Alluvial-Channel Data from Rio Grande Conveyance Channel, New Mexico, 1965-69," Professional Paper 562-J, United States Geological Survey, Washington, D.C. , 1972, 49 pp.
- Da Cunha, L. V., "River Mondego, Portugal," Personal Communication, Laboratório Nacional De Engenharia Civil, Lisboa, 1969.
- Daves, T. R. , "Summary of Experimental Data for Flume Tests over Fine Sand," Department of Civil Engineering, University of Southampton, 1971.
- East Pakistan Water and Power Development Authority, "Flume Studies of Roughness and Sediment Transport of Movable Bed of Sand," Annual Report of Hydraulic Research Laboratory for 1966, 1967, 1968-1969, Dacca.
- Einstein, H.A., "Bed Load Transportation in Mountain Creek," U.S. Soil Conservation Service, SCS-TP-55, 1944, 50 pp.
- Einstein, H. A and Chien, N., "Effects of Heavy Sediment Concentration near the Bed on Velocity and Sediment Distribution," MRD Series No. 8, University of California, Institute of Engineering Research and U.S. Army Engineering Division, Missouri River Corps of Engineers, Omaha, Nebraska, August 1955.
- Foley, M. G., "Scour and Fill in Ephemeral Streams," W. M. Keck Laboratory Report No. KH-R-33, California Institute of Technology, Pasadena, California, 1975.
- Franco, John J., "Effects of Water Temperature on Bed-Load Movement," Journal of Waterways and Harbors Division, ASCE, Vol. 94, No. WW3, Proc. Paper 6083, August 1968, pp. 343-352.

- Gibbs, C. H., and Neill, C. R., "Interim Report on Laboratory Study of Basket-Type Bed-Load Samplers," Research Council of Alberta in association with Department of Civil Engineering, University of Alberta, April 1972, Number REH/72/2.
- Gilbert, G. K., "The Transportation of Debris by Running Water," U. S. Geological Survey, Professional Paper 86, 1914.
- Guy, H. P., Simons, D. B. and Richardson, E. V., "Summary of Alluvial Channel Data from Flume Experiments, 1956-61," U.S. Geological Survey, Professional Paper 462-1, 1966, 96 pp.
- Hill, H. M., Srinivasan, V.S. and Unny, T. E., Jr., "Instability of Flat Bed in Alluvial Channels," Journal of Hydraulics Division, ASCE, Vol. 95, No. HY5, September 1969, pp. 1545-1558.
- Ho, Pang-Yung, "Abhängigkeit der Geschiebebewegung von der Kornform und der Temperature," Preuss. Versuchsanst. für Wasserbau und Schiffbau, Berlin, Mitt., Vol. 37, 1939, 43 pp.
- Hubbell, D. W. and Matejka, D. Q., "Investigation of Sediment Transportation, Middle Loup River at Dunning, Nebraska," U.S. Geological Survey, Water Supply Paper No. 1476, 1959.
- Johnson, J. W., "Laboratory Investigations on Bed-Load Transportation and Bed Roughness," U.S. Soil Conservation Service, SCS-TP-50, 1943.
- Jorissen, A. L., "Etude Experimentale du Transport Solide des Cours d'Eau," Revue Universelle des Mines, Belgium, Vol. 14, No. 3, 1938, pp. 269-282.
- Kalinske, A. A., and Hsia, C. H., "Study of Transportation of Fine Sediments by Flowing Water," Iowa University Studies in Engineering, Bulletin 29, 1945, 30 pp.
- Kennedy, J. F., "Stationary Waves and Antidunes in Alluvial Channels," Report KH-R-2, W. M. Keck Laboratory of Hydraulics and Water Resources, California Institute of Technology, Pasadena, California, 1961.
- Kennedy, J. F. and Brooks, N. H., "Laboratory Study of An Alluvial Stream of Constant Discharge," Proceedings, Federal Inter-Agency Sediment Conference, Misc. Pub. 970, U.S. Department of Agriculture, 1963, pp. 320-330.
- Knott, J.M., "Sediment Discharge in the Trinity River Basin, California," Water-Resource Investigations 49-73, U.S. Geological Survey, 1974, 62 pp.

- Laursen, E. M., "The total Sediment Load of Streams," ASCE, Journal of the Hydraulics Division, Vol. 84, No. HY1, Proc. Paper 1530, February 1958, 36 pp.
- Leopold, L. B., "Personal Communication, "Sediment Transport Data for Various U.S. Rivers," 1969.
- MacDougall, C. H., "Bed-Sediment Transportation in Open Channels," Transactions of the Annual Meeting 14, American Geophysical Union, 1933, pp. 491-495.
- Mahmood, K., et al., "Selected Equilibrium-State Data from ACOP Canals," Civil, Mechanical and Environmental Engineering Department Report No. EWR-79-2, George Washington University, Washington, D.C., February 1979, 495 pp.
- Mavis, F. T., Liu, T., and Soucek, E., "The Transportation of Detritus by Flowing Water -- II," Iowa University Studies in Engineering, Bulletin 11, 1937, 28 pp.
- Meyer-Peter, E., and Muller, R., "Formulas for Bed Load Transport," Proceedings, Second Meeting of International Association for Hydraulic Structures Research, Stockholm, 1948, 26 pp.
- Milhaus, R.T., "Sediment Transport in a Gravel-Bottomed Stream," PhD thesis, Oregon State University, 1973, 232 pp.
- Mutter, Douglas Gerald, "A Flume Study of Alluvial Bed Configurations," Masters thesis submitted to the Faculty of Graduate Studies, University of Alberta, 1971.
- NEDECO, "Rio Magdalena and Canal del Dique Project, Mission Tecnica Colombo-Holandesa," NEDECO Report, NEDECO, the Hague, 1973.
- Neill, C. R., "Laboratory Study of Scour of Coarse Uniform Bed Material," Personal Communication, Research Council of Alberta, 1967.
- Nordin, C. F., Jr., "Flume Studies with Fine and Coarse Sands," Open File Report 76-762, U.S. Geological Survey, Washington, D.C., 1976, 18 pp.
- Nordin, C. F. and Beverage, J. P., "Sediment Transport in the Rio Grande, New Mexico," Professional Paper 462-F, U.S. Geological Survey, Washington, D.C. 1965, 35 pp.
- O'Brien, M. P., "Notes on the Transportation of Silt by Streams," Transactions of the Annual Meeting 17, American Geophysical Union, 1936, pp. 431-436.

- Onishi, Y., Jain, S. C. and Kennedy, J. R., "Effects of Meandering in Alluvial Channels," Journal of the Hydraulics Division, ASCE, Vol. 102, No. HY7, July 1976, pp. 899-917.
- Paintal, A. S., "Concept of Critical Shear Stress in Loose Boundary Open Channels," Journal of Hydraulic Research, No. 1, 1971, pp. 90-113.
- Peterson, A. W., and Howells, R. F., "A Compendium of Solids Transport Data for Mobile Boundary Channels," Report No. HY-1973-ST3, Department of Civil Engineering, University of Alberta, Canada, January 1973.
- Pratt, C. J., "Summary of Experimental Data for Flume Tests over 0.49 mm Sand," Department of Civil Engineering, University of Southampton, 1970.
- Samide, G. W., "Sediment Transport Measurements," Masters thesis presented to the University of Alberta, June 1971.
- Sato, S., Kikkawa, H. and Ashida, K., "Research on the Bed Load Transportation," Journal of Research, Public Works Research Institute, Vol. 3, Research Paper 3, Construction Ministry, Tokyo, Japan, March 1958, 21 pp.
- Seitz, H. R., "Suspended and Bedload Sediment Transport in the Snake and Clearwater Rivers in the Vicinity of Lewiston, Idaho," File Report 76-886, U.S. Geological Survey, Boise, Idaho, 1976, 77 pp.
- Shen, H. W., Mellema, W. J. and Harrison, A.S., "Temperature and Missouri River Stages Near Omaha," Journal of the Hydraulics Division, ASCE, Vol. 104, No. HY1, January 1978, pp. 1-20.
- Shinohara, Kinji and Tsubaki, Toichiro, "On the Characteristics of Sand Waves Formed Upon Beds of the Open Channels and Rivers," Reprinted from Reports of Research Institute of Applied Mechanics, Kyushu University, Vol. VII, No. 25, 1959.
- Simons, D. B., "Theory of Design of Stable Channels in Alluvial Materials," PhD thesis, Colorado State University, May 1957.
- Singh, B., "Transport of Bed-Load in Channels with Special Reference to Gradient Form," PhD thesis presented to the University of London, London, England, 1960.
- Soni, J. P., "Short Statistical Analysis of Total Load Concentration," Journal of the Hydraulics Division, ASCE, Vol. 106, No. HY8, August 1980, pp. 1383-1389.

- Stein, R. A., "Laboratory Studies of Total Load and Apparent Bed Load," Journal of Geophysical Research, Vol. 70, No. 8, 1965, pp. 1831-1842.
- Straub, L. G., "Transportation Characteristics Missouri River Sediment," M.R.D. Sediment Series No. 4, St. Anthony Falls Hydraulic Laboratory, Minneapolis, Minnesota, April 1954.
- Straub, L. G., Anderson, A. G. and Flammer, G. H., "Experiments on the Influence of Temperature on the Sediment Load," M.R.D. Sediment Series No. 10, St. Anthony Falls Hydraulic Laboratory, Minneapolis, Minnesota, January 1958.
- Taylor, B. D., "Temperature Effects in Alluvial Streams," W. M. Keck Laboratory of Hydraulics and Water Resources Report KH-R-27, California Institute of Technology, Pasadena, California, August 1971, 204 pp.
- Toffaletti, F. B., "A Procedure for Computation of the Total River Sand Discharge and Detailed Distribution, Bed to Surface," Technical Report No. 5, Committee of Channel Stabilization, Corps of Engineers, U.S. Army, November 1968.
- United States Department of the Interior, Bureau of Reclamation, "Interim Report, Total Sediment Transport Program, Lower Colorado River Basin," January 1958, 175 pp.
- United States Army Corps of Engineers, U.S. Waterways Experiment Station, Vicksburg, Mississippi, "Studies of River Bed Materials and Their Movement with Special Reference to the Lower Mississippi River, Paper 17, 1935A, 161 pp.
- United States Army Corps of Engineers, U.S. Waterways Experiment Station, Vicksburg, Mississippi, "Effect of Turbidity on Sand Movement," unpublished report of experiments, 1935B.
- United States Army Corps of Engineers, U.S. Waterways Experiment Station, Vicksburg, Mississippi, "Flume Tests Made to Develop a Synthetic Sand Which Will Not Form Ripples When Used in Movable-Bed Models," Technical Memorandum 99-1 (unpublished), 1936A, 21 pp.
- United States Army Corps of Engineers, U.S. Waterways Experiment Station, Vicksburg, Mississippi, "Flume Tests of Synthetic Sand Mixture (Sand No. 10)," Technical Memorandum 95-1 (unpublished), 1936B, 21 pp.

- United States Army Corps of Engineers, U.S. Waterways Experiment Station, Vicksburg, Mississippi, "Studies of Light-Weight Materials, with Special Reference to their **Movement** and use as Model Bed Material," Technical Memorandum 103-1 (unpublished), 1936C, 56 pp.
- Vanoni, V. A., and Brooks, N. H., "Laboratory Studies of the Roughness and Suspended Load of Alluvial Streams," M.R.D. Sediment Series No. 11. California Institute of Technology Sedimentation Laboratory, 1957, 121 pp.
- Vanoni, V. A., and Hwang, Li San, "Relation Between Bed **Forms** and Friction in Streams," Journal of the Hydraulics Division, ASCE, Vol. 93, No. HY3, Proc. Paper 5242, May 1967, pp. 121-144.
- West Bengal, **Government** of, "Study on the Critical Tractive Force Various Grades of Sand," Annual Report of the River Research Institute, West Bengal, Publication No. 26, Part I, 1965, pp. 5-12.
- Williams, G. P., "Flume Width and Water Depth Effects in Sediment Transport Experiments," U.S. Geological Survey, Professional Paper 562-H, 1970.
- Willis, J. C., Coleman, N. L. and Ellis, W. M., "Laboratory Study of Transport of Fine Sand," Journal of Hydraulics Division, ASCE, Vol. 98, HY3, Proc. Paper 8765, March 1972, pp. 489-501.
- Willis, J.C., "Suspended Load from Error-Function Models," Journal of the Hydraulics Division, ASCE, Vol. 105, No. HY7, July 1979, pp. 801-816.
- Znamenskaya, N. S., "Experimental Study of the Dune Movement of Sediment," Transactions of the State Hydrologic Institute (Trudy GGI) No. 108, 1963, pp. 89-111. Translated by L. G. Robbins.

LIST OF SYMBOLS

A, c, m, n	Coefficients in Ackers and White (1973) technique.
A, B, n	Coefficients in Eq. 3.25,
A, B	Coefficients in Eq. 6.14.
a	Coefficient in Manning-Strickler equation.
$a_0 \dots a_6$	Coefficients.
b	Coefficient in Eq. 3.20.
$b_1 \dots b_3$	Coefficients in Eq. 6.10 and Eq. 6.11.
C	Chezy coefficient.
C	Mean sediment concentration (see p. 9).
C_a	Reference concentration at elevation a in Eq. 5.1.
c_b	Volumetric bed concentration in Eq. 5.10.
C_e	Equilibrium concentration.
c_f	Coefficient for field data, Eq. 6.8.
C_M	Dimensionless Planning coefficient.
D	Pipe diameter.
d	Mean flow depth.
D_{gr}	Dimensionless particle size, Eq. 5.6.
D_s	Arbitrary particle-size diameter.
D_{si}	Mean particle diameter of size fraction P_i .
D_{35}, D_{50} D_{65}, D_{84}	Particle sizes in a distribution, for which 35, 50, 65, and 84 percent, by weight, respectively, are finer.
e_b	Bagnold bed load transport efficiency,
F	Froude number, v/\sqrt{gr} .

f, f', f''	Friction factor, friction factor due to grain resistance, and due to form resistance, respectively,
$f_1 \dots f_3$	General functions,
F_D, F_R	Modified Froude Number, see pp. 36, 133.
F_g	Grain Froude number, see p. 164.
F_{go}	Critical grain Froude number , see p. 164.
F_{gr}	Mobility Number, defined by Eq. 5.4.
g	Gravitational acceleration.
H	$z + h + u^2/2g$
h	Flow depth.
h_s	$(1 - \lambda) \rho_s z + Ch$
I_1, I_2	Einstein integrals in Eq. 5.12.
i, j	Integer indices.
K_1, K_2	Coefficients determined from Fig. 3.8.
k	von Karman's constant,
k_d	Measure of bed-form roughness.
k_s	Roughness height,
m	Ranga Raju et al, parameter in Eq. 5.22.
n	Manning coefficient.
P_i	Size fraction of bed material,
Q	Water discharge.
q	Discharge per unit width,
q_s	Sediment discharge per unit width.
q_*	Dimensionless unit discharge, $q/\sqrt{gD_{50}^3}$.
R	Reynolds number, $4rv/\nu$.
r, r', r''	Hydraulic radius, hydraulic radius due to grain resistance, and due to form resistance, respectively.

R_g	Grain Reynolds number, see p. 164.
s, s', s''	Slope, slope due to grain resistance, and due to form resistance, respectively,
s	Specific gravity of bed particles.
T	Temperature.
$t_g \psi_0$	Bagnold measure of dynamic friction.
u	Component of velocity in x-direction, averaged over depth.
u_*, u_*'	Shear velocity and shear velocity due to grain resistance.
V, v	Mean flow velocity.
v_{cr}	Critical velocity for Yang (1973) technique.
w	Channel width.
w	Fall velocity of median sediment particle.
w, x, y, z	Coefficients in Eq. 4.6.
w_i	Fall velocity for size fraction P .
w_m	Mean fall velocity of bed particles.
Y_c	Laursen parameter in Eq. 5.17.
z	Bed elevation,
α, β	Dimensionless groups defined by Eq. 3.11.
δ	Laminar sublayer thickness, $11.6 \nu/u_*'$.
Δf	Change in a function over a discrete time step.
Δh	Change in depth over a discrete time step.
Δq	Change in discharge over a discrete time step.
Δt	Time step
Δu	Change in velocity over a discrete time step.
Δx	Space step.

Δy_i	Width of i^{th} element of a cross-section.
Δz	Change in bed elevation over a discrete time step.
	Turbulent diffusion coefficient.
	Weighting factor for the implicit scheme.
	Porosity of bed sediment.
	Kinematic viscosity.
	Dimensionless transport rate.
ϕ_B	Dimensionless bed load transport rate.
ϕ_S	Dimensionless suspended transport rate.
ρ	Density of water.
ρ_S	Density of sediment.
σ_g	Geometric standard deviation of bed-particle sizes.
τ	Mean shear stress.
τ_*, τ_*'	Dimensionless shear stress, and dimensionless shear stress due to grain resistance, see pp. 28-36.
τ_{*0}	Critical dimensionless shear stress for initiation of motion.
τ_{*S}	Dimensionless shear stress based on D_s , see p. 46.

APPENDIX

HY1

TECHNICAL NOTES

115

RE-EXAMINATION OF NIKURADSE ROUGHNESS DATA

By William R. Brownlie,¹ A. M. ASCE

INTRODUCTION

Two sets of flow resistance data are commonly used in the evaluation of friction factors for pipes and open channels. The data compiled by Colebrook and White for commercial pipes were used by Moody to construct his well known friction factor diagram (3, Fig. 5.32). A similar diagram based on the data of Nikuradse (1) for sand-roughened pipes appears in most texts of fluid mechanics (2, Fig. 108 and 3, Fig. 5.31), however, with a much more limited range of relative roughness and Reynolds number than the Moody diagram. While the Colebrook and White data are appropriate for commercial pipe applications, the Nikuradse data, with its sand roughness, may be more applicable for problems involving open channels with uniform-sand beds for which grain friction factor is required. This note describes an inconsistency in the original presentation of some of the Nikuradse data and provides a Moody-type diagram with some engineering applications for a range of the data believed to be valid. The data are reviewed here because they appear in many classical texts of fluid mechanics for engineers (e.g., 2, 3).

ORIGINAL DATA

The experiments reported by Nikuradse were conducted using pipes with diameters of 2.474 cm, 4.94 cm, and 9.94 cm. Roughness was created by gluing uniform sands to the pipes. In all, five sands were used, with mean diameters ranging from 0.01 cm-0.16 cm, to give six values of relative roughness (grain diameter over pipe diameter). Uniformity of sand grains was created by sieving, resulting in a typical geometric standard deviation of 1.02 for the grain-size distributions. Measurements in the pipes were taken using an approach length of approximately 40 pipe diam.

The data has traditionally been presented graphically in two different forms following the original presentation of Nikuradse (1). In the Moody-type form, friction factor is plotted against Reynolds number on a log-log scale with a different curve and set of data points for each of the six values of relative roughness. In the alternate form, by transforming the dotting coordinates, the

¹Grad. Research Asst., W. M. Keck Lab. of Hydr. and Water Resources, Calif. Inst. of Tech., Pasadena, Calif. 91125.

Note.—Discussion open until June 1, 1981. To extend the closing date one month, a written request must be filed with the Manager of Technical and Professional Publications, ASCE. Manuscript was submitted for review for possible publication on April 25, 1980. This paper is part of the Journal of the Hydraulics Division, Proceedings of the American Society of Civil Engineers, © ASCE, Vol. 107, HY1, January, 1981. ISSN 0044-796X/81/0001-0115/\$01.00.

six curves are collapsed to one curve as in Fig. 1.

Fig. 1 shows data from 90 runs randomly selected from the 362 that are published. The figure also shows the Colebrook transition function upon which the Moody diagram is based. Since the equivalent sand roughness of the Colebrook and White data was calibrated to the Nikuradse data in the fully rough regime, the two curves converge to the same asymptote on the right side of Fig. 1.

An inconsistency in the original data presentation can be seen by comparing the two plot types (1, Figs. 9 and 11) with the data tables. The data in the tables cover the range of parameters shown in Fig. 1; however, all points plotted on the original diagram do not appear in the tables. Conversely, all of the data in the tables are not shown in the original diagram, but they do conform closely to the curve in Fig. 1. On the other hand, the Moody-type diagram shows data with Reynolds numbers as low as 500 whereas the lowest Reynolds

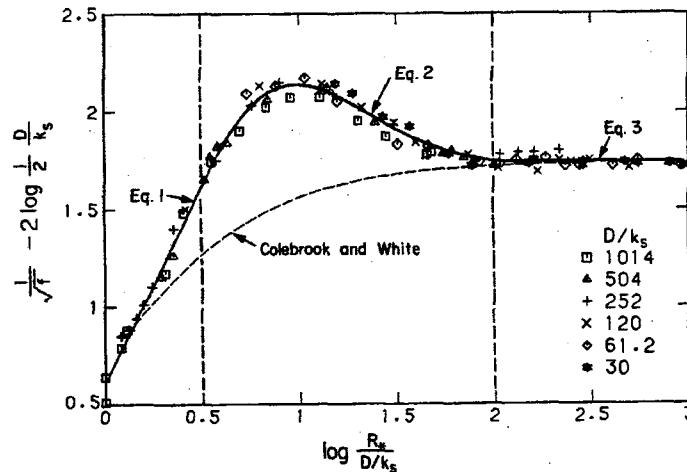


FIG. 1.—Comparison between Nikuradse Resistance Data and Colebrook and White Transition Function (about 25 percent of Published Data are Shown)

number given in the tables is 4,300. Furthermore, the two diagrams are consistent only for Reynolds numbers greater than 10,000. Finally, the unpublished data are somewhat suspect because they show a smooth transition from turbulent to laminar flow occurring at a Reynolds number of about 2,000, for all given values of relative roughness. Such a condition seems unlikely due to the nature of the physical transition.

FLOW RESISTANCE CHART

The Moody-type flow resistance chart shown in Fig. 2 was derived from the curve fitted to the data points in Fig. 1. Although there are inconsistencies in the original diagrams, the experiments appear to have been carefully conducted and the data in the tables are reasonable. Reynolds numbers lower than 10,000 have been omitted.

It is hoped that Fig. 2 will be a useful and accurate tool for engineers. The chart can be used for side-wall corrections as well as for separating total resistance into grain resistance and form resistance. For open channel flow calculations, pipe diameter D should be replaced by 4r in which r = hydraulic radius.

Fig. 2 is based on three equations which apply to different domains along the abscissa of Fig. 1:

$$\frac{1}{\sqrt{f}} - 2 \log \frac{1}{2} \frac{D}{k_s} = 0.705 + 2 \log \frac{R_* k_s}{D} \dots \text{for } \log \frac{R_* k_s}{D} < 0.5 \dots (1)$$

$$\frac{1}{\sqrt{f}} - 2 \log \frac{1}{2} \frac{D}{k_s} = \sum_{i=0}^6 A_i \left(\log \frac{R_* k_s}{D} \right)^i \dots \text{for } 0.5 \leq \log \frac{R_* k_s}{D} \leq 2.0 \dots (2)$$

$$\frac{1}{\sqrt{f}} - 2 \log \frac{1}{2} \frac{D}{k_s} = 1.74 \dots \text{for } \log \frac{R_* k_s}{D} > 2.0 \dots (3)$$

in which $R_* = \sqrt{f/8} R$; f = friction factor; D = pipe diameter; k_s = the sand grain roughness (equivalent to grain diameter); R = Reynolds number;

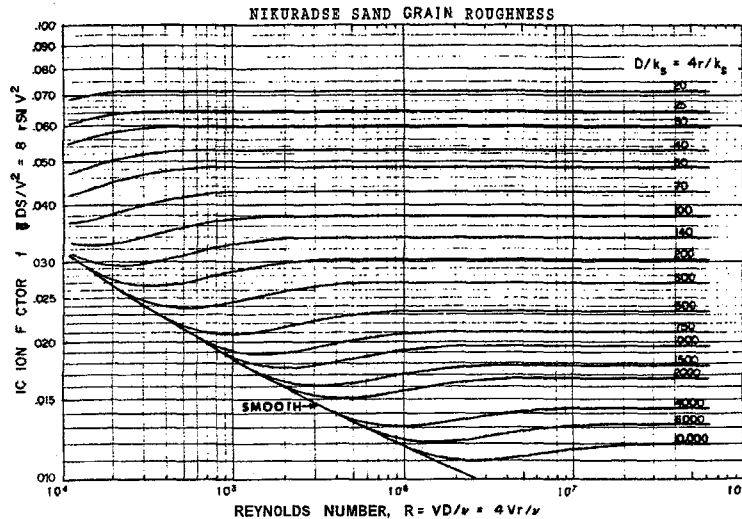


FIG. 2.—Friction Factor Diagram, for Pipes of Diameter, D, or Channels of Hydraulic Radius, r

and A_i = empirical constants. Eq. 1 is for smooth pipes, and relative roughness can be removed by factoring both sides of the equation. Eq. 2 was fitted by the writer to the transition data from the smooth to the rough regime, with the coefficients A_0 through A_6 , defined as 1.3376, -4.3218, 19.454, -26.480, 16.509, -4.9407, 0.57864, respectively. Eq. 3 describes the fully rough regime where friction factor is a function of relative roughness only.

SIDE-WALL CORRECTION

Fig. 2 can be used to perform a side-wall correction for flow at a given R , in flumes with a known friction factor, f , and roughness, k_s , using a procedure analogous to the smooth-wall procedure described by Vanoni and Brooks (4). From the derivation given in Ref. 4, the following equations can be obtained:

$$R_w = \frac{R}{f} f_w \dots \dots \dots (4)$$

$$r_w = \frac{r}{f} f_w \dots \dots \dots (5)$$

$$f_b = f + \frac{p_w}{p_b} (f - f_w) \dots \dots \dots (6)$$

$$r_b = \frac{r}{f} f_b \dots \dots \dots (7)$$

in which p = wetted perimeter; the subscript b denotes bed, and the subscript w denotes wall.

The procedure for using Fig. 2 to calculate r , and r_b is as follows:

1. Plot Eq. 4 on Fig. 2 as a straight line with a slope of 1 in log units, and an intercept of $0.01R/f$ at $f = 0.01$. The desired values of f , and R , will lie on this line.
2. Pick a trial value of r_w and compute $4 r_w / k_{sw}$ and determine f , from Fig. 2.
3. Compute a new value of r_w from Eq. 5, return to step 2. The solution should converge after two or three iterations.
4. The quantities f_b and r_b can now be calculated directly from Eqs. 6 and 7.

FORM AND GRAIN RESISTANCE

In some open channel flow problems it is often desirable to separate grain resistance from bed-form resistance. Two procedures are possible for separating the bed shear stress into its two components. Either the slope may be broken into components or the hydraulic radius of the bed may be broken into components. Vanoni and Brooks (4) have presented a graphical solution of the Einstein-Barbarosa approach which divides the hydraulic radius into two components. Fig. 2 could also be used to carry out this procedure by applying a technique similar to that of the side-wall correction procedure just described. However, a more convenient and perhaps more conceptually reasonable approach is to divide the energy slope into two components.

The following equations can be used with Fig. 2 to perform this procedure:

HY1

TECHNICAL NOTES

119

$$S' = \frac{f'_b V^2}{8gr_b} \dots \dots \dots (8)$$

$$S'' = S - S' \dots \dots \dots (9)$$

$$f''_b = f - f'_b \dots \dots \dots (10)$$

in which S' and f'_b = the energy slope and bed friction factor, respectively, resulting from grain resistance; and S'' and f''_b = those quantities resulting from form drag, for a flow with a given velocity and bed hydraulic radius. The quantity f'_b can be determined directly from Fig. 2, given R_b and $4r_b/k_s$. The remaining quantities can be calculated from Eqs. 8, 9, and 10.

ACKNOWLEDGEMENTS

The preparation of this note was suggested by Norman H. Brooks and based upon work supported by the National Science Foundation, under Grant CME 79-20311. Special thanks to A. Massengale.

APPENDIX.—REFERENCES

1. Nikuradse, J., "Laws of Flow in Rough Pipes," (translation of "Stromungsgesetze in rauhen Rohren," 1933), *National Advisory Committee for Aeronautics Tech Memo 1292*, Washington, D.C., 1950, 62 pp.
2. Rouse, H., *Elementary Mechanics of Fluids*, John Wiley and Sons, Inc., New York, N. Y., 1946.
3. Streeter, V. L., *Fluid Mechanics*. 5th ed., McGraw-Hill Book Co., Inc., New York, N.Y., 1971.
4. Vanoni, V. A., and Brooks, N. H., "Laboratory Studies of the Roughness and Suspended Load of Alluvial Streams," *Sedimentation Laboratory Report No. E68*, California Institute of Technology, Pasadena, Calif., 1957, 121 pp.